The linking of angiogenesis to contractile performance and substrate metabolism in the hypertrophied and failing heart.

By

James Winter

A thesis submitted to The University of Birmingham for the degree of DOCTOR OF PHILOSOPHY

School of Clinical and Experimental Medicine

College of Medical and Dental Sciences

The University of Birmingham

September 2010

Abstract

It has been suggested that a failure of angiogenesis (capillary growth) to keep pace with myocyte expansion is the driving force which pushes hypertrophied hearts into a state of failure marked by contractile dysfunction and alterations in the mechanisms governing energy production. The aims of this study were to investigate how alterations in ventricular capillarity affect contractile performance and substrate metabolism in the isolated rat heart. It was hypothesised that, if cardiac contractile performance and substrate utilisation are directly related to ventricular capillarity then methods to alter the number and distribution of capillaries within the ventricle could be utilised to demonstrate this relationship. Treatment regimes were split into those aimed at inducing new capillary growth (e.g. chronic bradycardia and exposure to cold environments) and those aimed at reducing ventricular capillarity (e.g. hypertension and β-adrenoceptor stimulation). In contrast to previous reports, capillary growth within the ventricle was very limited in animals exposed to a chronic increase in energy demand (e.g. cold environments) and those subjected to extended periods of mechanical stimulation (e.g. bradycardia). Ventricular remodeling appears to accommodate for alterations in the load and/or energy demand without the need for an expansion of the existing capillary network. Experiments conducted in β-adrenoceptor mediated hypertrophy demonstrate that capillary rarefaction has little effect on cardiac contractile performance and experiments with hypertensive animals show no capillary growth despite the dramatic increase in energy demand placed on the heart in these conditions. In conclusion these data demonstrate surprising plasticity in the response of the myocardium to a number of physiological and pathological stimuli and indicate that adequate compensation occurs without the need for expansion of the existing capillary bed. The limited angiongenic capacity of the myocardium may therefore indicate that the capillary supply of the ventricle is not limiting to the function of the heart.

Acknowledgments

Firstly I extend my thanks David Hauton and Stuart Egginton for allowing me to come and study with them and for all the time they have taken over the last 4 years in molding me into a better scientist. I also owe a huge debt of gratitude to Clare Ray, Andy Coney and Katie Glen for advice given and the support they have shown me at Birmingham. I feel indebted to many people not in the least to my friends and family but especially to Kate. Thank you everyone.

Publications

Winter, J., Egginton S. and Hauton D. Do current estimates of coronary capillary recruitment reflect a significant capillary reserve? ABSTRACTS OF THE 59th MEETING OF THE BRITISH MICROCIRCULATION SOCIETY 30th - 31stMarch, 2009, The Medical School, University of Birmingham, UK. Microcirculation. 16 (5): 444-486.

Table of Contents

Chapter One: Introduction 15

Preload and afterload 15

Catecholamines, calcium and excitation contraction coupling 3

Adenosine triphosphate (ATP) and the energetics of cardiac function 4

Cross-bridge cycling 4

SERCA 4

Energy consumption – Contractile state and the Frank-Starling mechanism 5

Cardiac work and oxygen consumption 9

Molecular mechanisms linking ATP and oxygen consumption 10

Uptake of carbon substrates 11

Glycolysis and glucose oxidation 11

Beta-oxidation 13

The citrate cycle, oxidative phosphorylation and the oxygen cost of metabolism 14

Phosphotransfer networks 15

Endogenous energy stores 16

Cardiac responses to chronic stress 21

Pathological hypertrophy and heart failure 22

Contractile dysfunction 22

Energy metabolism during hypertrophy and heart failure 23

Myocardial hypoxia as a potential cause of hypertrophic de-compensation and cardiac failure 29

Thesis aims and layout 36

Chapter Two: Material and Methods 41

Animal welfare and regulations 41

Treatment regimes 41

Experiments in the rat 41

Surgical Procedures 41

Assessment of LV contractile performance 43

Histological Procedures 55

Assessment of SERCA2a protein expression 62

Statistical analysis 67

Chapter Three: Effects of reduced capillarity on cardiac performance and metabolism. Part 1: Microspheres 68

Coronary Flow Reserve 69
Microvascular dysfunction 69
Chapter aims 71
Materials and methods 73
Protocol 1: Assessment of the effects of acute micro-vascular blockade on left ventricular contractile performance 73
Protocol 2: Assessment of the effects of acute micro-vascular blockade on left ventricular substrate metabolism 74
Histological methods 75
Coronary flow reserve and myocardial oxygen consumption 76
Statistical analysis 77
Results 78
Coronary flow reserve and myocardial oxygen consumption 78
Histological findings 78
Ventricular performance during micro-vascular blockade 78
Ventricular metabolism during micro-vascular blockade 79
Discussion 80
Arteriolar occlusion and LV contractile performance 80
Arteriolar occlusion and substrate oxidation 80
Arteriolar occlusion and coronary flow 83
Methodological considerations and future work 84
Conclusion 84
Chapter Four: Effects of reduced capillarity on cardiac performance and metabolism. Part 2: Isoprenaline 91
Chapter Aims 93
Material and methods 94
Treatment regime 94
Results 95
Animal mortality 95
Physiological parameters 95
Capillary supply 95
Ex vivo contractile performance 96
Dobutamine challenge 97
Discussion 98
Subcutaneous dosing and animal mortality 98

Isoprenaline and hypertrophy 98
Isoprenaline, LV contractile performance and ventricular phenotype 99
Role of oxygen diffusion in isoprenaline induced contractile dysfunction 101
Future work and methodological considerations 102
Conclusion 102
Chapter Five: Effects of reduced capillarity on contractile performance and metabolism in the left ventricle. Part 3: L-NAME 112
NO, vascular tone and blood vessel growth 113
NO and hypertrophy 114
Chapter Aims 115
Material and methods 116
Treatment regime 116
Results 117
Studies in the rat 117
Studies in the mouse 118
Discussion 120
Chronic L-NAME and LV remodeling 120
Chronic L-NAME and contractile performance 122
Conclusion 124
Chapter Six. Effects of increased capillarity on cardiac performance and metabolism. Part 1: Cold acclimation 135
Physiological adaptation to chronic cold exposure 135
Cold acclimation of young animals 137
Chapter Aims 137
Materials and Methods 138
Cold acclimation protocol 138
Results 139
Studies in the rat 139
Studies in the mouse 140
Discussion 141
Cold acclimation induced LV remodeling 141
Cold cclimation and LV capillarity 142
Cold acclimation and LV contractile performance 143
Conclusion 144

Chapter Seven. Effects of increased capillarity on cardiac performance and metabolism. Part 2: Atenolol 154
Chapter Aims 155
Materials and methods 156
Treatment regime 156
Equations 156
Modifications of metabolism protocol 156
Results 157
Experiments in the rat 157
Experiments in the mouse 160
Discussion 162
Bradycardia and capillarity 162
Bradycardia and LV contractile performance 164
Bradycardia and substrate metabolism 166
Caveats and future work 168
Conclusion 168
Chapter Eight: Modifying capillary supply and substrate selection in the hypertrophied heart. ... 182
PART A. Modifying capillarity in the hypertrophied heart 182
PART B. Modifying substrate selection in the hypertrophied heart 183
Summary 184
Material and methods 184
Treatment regimes 185
Control data 185
Chapter Legend 185
Results 186
PART A. Modifying capillarity in the hypertrophied heart 186
PART B. Modifying capillarity in the cold acclimated heart 188
Discussion 189
PART A. Modifying capillarity in the hypertrophied heart 189
PART B. Modifying substrate selection in the hypertrophied heart 193
Conclusions 195
Chapter Nine: General Discussion 210
Summary of findings 210
Methodological considerations 212

SERCA activity 212
Capillary Length 212
Statistical power 213
Future work 213
Alternative models for capillary growth in the rat 213
Alternative models of hypertrophy in the rat 214
References 215

List of Figures

Figure 1.1. Excitation-contraction coupling in the heart. 7

Figure 1.2. The theory of cross-bridge cycling in the heart. 8

Figure 1.3. Glucose uptake, glycolysis and oxidation in the heart. 18

Figure 1.4. FA uptake and oxidation in the heart. 19

Figure 1.5. Oxidative phosphorylation of the mitochondria. 20

Figure 2.1. Factors measured during assessment of left ventricular contractile performance. 45

Figure 2.2 Example raw data trace following addition of dobutamine (150nM) to the perfusate of a Langendorff isolated beating rat heart preparation. 46

Figure 2.3 Calculation of intraventricular volume and ventricular chamber stiffness from the diastolic pressure-volume relationship. 47

Figure 2.4 Systolic stress-strain relationship. 48

Figure 2.5. Example of lectin stain and counting procedure. 60

Figure 2.6. Capillary distribution analysis. 60

Figure 2.8. Example of BSA standard curve and calculations used to quantify sample protein concentration. 61

Figure 3.1. Representative image of epicardium demonstrating the α-smooth muscle actin staining and microsphere blockade. 85

Figure 3.2. High magnification images of microsphere blockade. 86

Figure 3.3. High magnification images of large vessel blockade. 86

Figure 3.4. Relationships between ventricular performance and the degree of arteriolar blockade. 87

Figure 3.5. Mean relationship between ventricular performance (RPP), oleate metabolism and glucose metabolism before and after microsphere infusion. 88

Figure 3.6. Relationships between ventricular performance, rates of metabolism, coronary flow and the degree of arteriolar blockade. 89

Figure 3.7. Relationships between rates of metabolism per unit external (observed work) and the degree of arteriolar blockade. 90

Figure 4.1. Effect of Isoprenaline on LV capillarity and myocyte morphology in the rat. 105

Figure 4.2 Effect of isoprenaline treatment on LVDP-volume relationship (A) and LVEDP-volume relationship (B). 106

Figure 4.3 Effect of isoprenaline treatment on +dPdt (A) and -dPdt (B). 107

Figure 4.4 Effect of isoprenaline treatment on estimated LV systolic stress-strain. 108

Figure 4.5. Effect of isoprenaline treatment on HR (A) and CF (B). 109

Figure 4.6. Representative western blots of SERCA2a and acylated tubulin. 110

Figure 4.7. Representative images of LV subendocardial collagen content. 110

Figure 5.1. Effect of L-NAME on LV capillarity and myocyte morphology in the rat. 128

Figure 5.2 Effect of L-NAME treatment on LVDP-volume relationship (A) and peak systolic pressure (B).....129

Figure 5.3 Effect of L-NAME treatment on +dPdt (A) and -dPdt (B). 130

Figure 5.4 Effect of L-NAME treatment on LVEDP-volume relationship (A) and estimated LV systolic stress-strain (B).....131

Figure 5.5. Effect of L-NAME treatment on HR (A) and CF (B).....132

Figure 5.6. Representative western blots of SERCA2a and acylated tubulin.....133

Figure 5.7. Representative images of LV subedocardial collagen content. 133

Figure 6.1. Schematic of changes in ambient temperature and hours of light per day over the 31 day cold acclimation process.....145

Figure 6.2. Effect of cold acclimation on LV capillarity and myocyte morphology in the rat. 147

Figure 6.3. Effect of cold acclimation on LVDP-volume relationship (A) and peak systolic pressure (B).....148

Figure 6.4. Effect of cold acclimation on +dPdt (A) and -dPdt (B). 149

Figure 6.5. Effect of cold acclimation on estimated LV systolic stress-strain. 150

Figure 6.6. Effect of cold acclimation on HR (A) and CF (B).....151

Figure 6.7. Representative western blots of SERCA2a and acylated tubulin. 152

Figure 6.8. Representative images of LV subendocardial collagen content. 152

Figure 7.1. Effect of atenolol treatment on LV capillarity and myocyte morphology in the rat. 170

Figure 7.2 Effect of atenolol treatment on LVDP-volume relationship (A) and LVEDP-volume relationship (B). 171

Figure 7.3 Effect of atenolol treatment on +dPdt (A) and -dPdt (B). 172

Figure 7.4 Effect of atenolol treatment on estimated LV systolic stress-strain. 173

Figure 7.5 Effect of atenolol treatment on HR (A) and CF (B). 174

Figure 7.6. The influence of a change in ventricular compliance on pressure development at different end diastolic pressures 175

Figure 7.7. Representative western blots of SERCA2a and acylated tubulin. 176

Figure 7.8. Representative images of LV subendocardial collagen content. 176

Figure 7.9. Left ventricular performance during the metabolism protocol. 177

Figure 7.10. Raw data plots of oleate oxidation against time. 178

Figure 7.11. Raw data plots of glucose oxidation against time. 179

Figure 7.12. Ex vivo left ventricular substrate oxidation rates in control and atenolol treated hearts at 'low' and 'high' workloads. 180

Figure 7.13. Ex vivo left ventricular metabolism in control and atenolol treated hearts at low and high workloads. 181

Figure 8.1. Effect of cold acclimation + treatment on LV capillarity and myocyte morphology. 198

Figure 8.2 Effect of cold acclimation + treatment on LVDP-volume relationship (A) and LVEDP-volume relastionship (B). 199

Figure 8.3 Effect of cold acclimation + treatment on +dPdt (A) and -dPdt (B). 200

Figure 8.4 Effect of cold acclimation + treatment on LVEDP-volume relationships (A) and estimated LV stress-strain (B). 201

Figure 8.5 Effect of cold acclimation + treatment on HR (A) and CF (B). 202

Figure 8.6. Raw data plots of oleate oxidation against time. 204

Figure 8.7. Raw data plots of glucose oxidation against time. 205

Figure 8.8. Ex vivo left ventricular substrate oxidation rates in control, cold acclimated, fenofibrate and cold acclimation + fenofibrate treated rats. 206

Figure 8.9. Ex vivo left ventricular metabolism in CON, FEN, CA and CAF treated hearts. 208

Figure 8.10. Left ventricular performance during the metabolism protocol. 209

List of Tables

Table 1.1. Summary of studies looking at the effects of models of cardiac hypertrophy and failure on contractile performance and rates of metabolism in the heart. 27

Table 1.2. Expression of key glucose and FA enzymes in human and experimental heart failure. .. 28

Table 3.1. Histological data from microsphere studies. 86

Table 4.1 Effects of isoprenaline treatment on cardiac mass and in vivo physiological parameters. 104

Table 4.2. Effects of isoprenaline treatment on ventricular phenotype. 110

Table 4.3. Effect of dobutamine (150 nM) addition on cardiac performance of control and isoprenaline treated hearts. 111

Table 5.1. Studies demonstrating hypertrophic growth in the hearts of rats exposed to chronic L-NAME dietary supplementation. 125

Table 5.2. Studies demonstrating a non-hypertrophic growth in the hearts of rats exposed to chronic L-NAME dietary supplementation. 126

Table 5.3. Effects of L-NAME treatment on organ mass and in vivo physiological parameters. 127

Table 5.4. Effects of L-NAME treatment on ventricular phenotype. 133

Table 5.5. Effect of dobutamine (150nM) addition on cardiac performance of control and L-NAME treated hearts. 134

Table 6.1. Effects of cold acclimation on organ mass and in vivo physiological parameters. 146

Table 6.2. Effects of cold acclimation on ventricular phenotype. 152

Table 6.3. Effect of dobutamine (150nM) addition on cardiac performance of control and cold acclimated hearts. 153

Table 7.1. Effects of atenolol treatment on cardiac mass and in vivo physiological parameters. .. 169

Table 7.2. Effects of atenolol treatment on ventricular phenotype. 176

Table 8.1 Effects of treatment on in vivo physiological parameters and cardiac phenotype hearts from the cold acclimation + treatment study. 196

(n=5-6) 196

Table 8.2 Summary of effect of treatment regimes on in vivo parameters and ventricular phenotype. 197

Table 8.3. Effect of dobutamine (150nM) perfusion on cardiac performance of control and cold + treatment hearts. 203

Table 8.4. Effect of cold acclimation and fenofibrate treatment on endogenous energy stores and labelled tracer incorporation during the 60-minute perfusion protocol. 207

List of Common Abbreviations and Definitions

ACC = Acetyl Coa carboxylase

ADP = Adenosine monophosphate

ATP = Adenosine triphosphate

bFGF = Basic fibroblast growth factor

C:F = Capillary-to-fibre ratio

CA = Cold acclimation

CD = Capillary denisty

CF = Coronary flow

CFR = Coronary flow reserve

CK = Creatine kinase

CPT = Carnitine palmitoyltransferase

CSA = Cross-sectional area

DAG = Diacylglycerol

dP/dt = Rate of change of pressure

FA = Fatty acids

FAD = Flavin adenine dinucleotide

GLUT = Glucose transporter

HF = Heart failure

HIF = Hypoxia inducible Factor

HSL = Hormone sensitive lipase

ISO = isoprenaline

LAL = Lysosomal lipase

LCAD = Long chain acyl dehydroganse

L-NAME = N (G)-nitro-L- arginine methyl ester

L-NNA =NG-Nitro-L-arginine

LVDP = Left ventricular developed pressure

LVEDP = Left ventricular end diastolic pressure

MCAD = Medium chain acyl dehydrogenase

MCD = Malonyl CoA decarboxylase

mean NN = mean nearest neighbour distance

NAD^+ = Nicotinamide adenine dinucleotide

NCX = Sodium calcium exchanger

PCr = Phosphocreatine

PDH = Pyruvate dehydrogenase

PFK = Phosphofructokinase

PKA = Protein kinase A

PLB = Phospholamban

RPP = Rate systolic pressure product

RyR = Ryanodine receptor

SERCA = sarcoplasmic reticulum Ca^{2+}-ATPase

SHR = Spontaneously hypertensive rat

SR = Sarcoplasmic reticulum

TAG = Triacylglycerol

TCA = Tricarboxylic acid cycle

VEGF = Vascular endothelial derived growth factor

Chapter One: Introduction

In simple physical terms the heart provides the hydraulic energy required to circulate blood around the body. The performance of the heart, be it as a measure of output or of contractile strength, is dependent upon physical factors (preload and afterload), hormonal and neuronal influences and upon the availability of oxygen and oxidisable substrates to provide the chemical energy for contraction. This Introduction will give an overview of how basic cardiac mechanics links to energy and oxygen consumption within the myocardium and how metabolic mechanisms regulate energy supply during changes to cardiac workload. Finally the focus will shift to the remodelling response to a chronic increase in stress, the contractile and metabolic dysfunction associated with heart failure and the possible role that impaired oxygen delivery plays in this pathological process.

Preload and afterload

The concept of preload and afterload is an important principle governing myocardial performance and cardiac output. Preload describes the load present before contraction provided by the venous return of blood to the atrium and ventricles. Preload is related to the stretch of the cardiac myocytes in response to this loading and so is related to sarcomere length (the contractile unit of the myocytes). Increases in preload will result in ventricular filling and will dramatically affect stroke volume through the Frank-Starling mechanism of the heart. These length induced increases in the force of contraction occur in the absence of altered calcium release but increased Ca^{2+} sensitivity.

Preload is affected by a number of factors including central venous pressure, heart rate, atrial contractility, ventricular compliance and aortic pressure.

- Increased central venous pressure: acting through either decreased venous compliance (mediated through sympathetic venoconstriction) or increased venous return (augmented

by increased respiratory and skeletal muscle pump activities or gravity), results in a greater preload. Increases in venous return can also activate stretch receptors in the atrium activating parasympathetic neurons which reduce heart rate (the Bainbridge reflex).

- Decreases in heart rate will increase ventricular filling time and so increase preload.
- Sympathetic stimulation of atrial contractility or increased atrial filling will pump more blood into the left ventricle per beat.
- Ventricular compliance describes the relationship between the change in pressure and the resulting change in ventricular lumen size, conditions such as ventricular fibrosis will reduce compliance and therefore reduce preload.
- Preload is elevated by increases in aortic pressure which reduce ejection from the left ventricle as a result of the increased afterload it now has to overcome.

Afterload describes the load which the heart must eject blood against. Simply afterload can be related to the aortic pressure, however more precisely it is related to ventricular wall stress (σ), which describes the amount of force experienced per unit area of tissue.

$$\sigma = \frac{P \times r}{W}$$

This relationship is known as the law of LaPlace, which states that wall tension is proportionate to the pressure (P) multiplied by the radius (r) for a thin walled sphere. Therefore, wall stress (σ) is wall tension divided by wall thickness (W). Afterload is increased when aortic pressure is greater, when there is an increase in systemic, or pulmonary, vascular resistance (SVR/PVR) and by ventricular dilation (an increase in ventricle lumen volume). In a closed system when afterload increases the heart has to generate a greater force per unit area of tissue in order to eject the same quantity of blood into the systemic or pulmonary circulation. Therefore in the absence of modification of the contractile state of the myocardium, change of preload or altered vascular resistance there will be a reduction in the volume of blood ejected per contractile cycle (stroke volume). Note; in this setting

incomplete emptying of the ventricle can indirectly elevate preload as the remaining volume of blood in the ventricle is added to the preload during diastole. We will see later that wall stress is a major determinant of the substrate metabolism and oxygen consumption of the heart. [1-3]

Catecholamines, calcium and excitation contraction coupling

The theory of excitation-contraction (E-C) coupling provides an understanding of how the movement of calcium ions between intracellular stores controls the contractile cycle of the myocardium. The illustration of this process in Figure 1.1 can be summarised as per the bullet points listed below.

1. During the cardiac action potential calcium ions (Ca^{2+}) enter the cell via depolarisation sensitive channels, primarily L-Type voltage sensitive channels in the myocyte. This is known as the inward calcium current (I_{Ca}) and is a major contributor to the action potential plateau. Ca^{2+} entry triggers calcium release from the sarcoplasmic reticulum (SR) through the ryanodine receptor (RyR).
2. The net result of both these initial processes in an increase in free intracellular calcium which through binding to troponin C switches on the contractile machinery.
3. For relaxation to occur intracellular calcium must decline allowing disassociation of calcium from the troponin complex. This involves the extrusion of calcium from the cytosol via the SR Ca –ATPase (SERCA), the sarcolemma Na^{+}/Ca^{2+} exchanger (NCX), the sarcolemma Ca^{2+}-ATPase and mitochondrial Ca^{2+} uniport. [4]

In the rat heart SERCA accounts for some 92% of calcium flux during cardiac relaxation, around 7% of calcium is extruded through NXC while the relatively slow sarcolemmal and mitochondrial ATPases account for the remaining 1%. [5] While detailed understanding of the mechanics of excitation-contraction coupling is beyond the scope of this thesis it is important to appreciate the energy dependent nature of this process and that of the contractile cycle.

Adenosine triphosphate (ATP) and the energetics of cardiac function

The hydrolysis of ATP to inorganic phosphate (Pi) and adenosine diphosphate (ADP) provides a release of stored chemical energy which is used to drive the muscular action of the cardiac contractile proteins as well as the various energy dependent ion pumps of the sarcoplasmic reticulum and sarcolemma. Two processes, 1) the contractile work of the myofilaments and 2) the active pumping of calcium ions through SERCA, account for the majority of ATP consumption in the myocardium.

Cross-bridge cycling

The theory of cross-bridge cycling forms the molecular basis for the production of movement and force within cardiac muscle and can be summarised in a number of steps (Figure 1.2 corresponds to the bullet points below). Note; prior to entering this cycle the rise in cytosolic calcium has removed the inhibitory effect of the troponin complex on myofilament interaction.

1. Hydrolysis of ATP primes the myosin head of the cross bridge for attachment to the thin filament (actin fibres).
2. Myosin binds to actin.
3. The products of ATP hydrolysis (ADP and Pi) are released resulting in a conformational change of structure in the myosin head. This process is thought to provide the force of contraction, often referred to as the 'power stroke'.
4. Myosin detaches from actin upon binding of ATP.
5. ATP is hydrolysed returning the cross bridge to its original formation.

SERCA

SERCA is the second major site of ATP utilisation within the myocardium. As with the cross-bridge cycle the transfer of phosphate groups from ATP to the pump results in a conformational change in

structure and a change in the affinity of the calcium binding sites promoting the release of calcium ions into the sarcoplasmic reticulum while preventing their dissociation back into the cell cytosol. There is a net movement of two calcium ions per mole of ATP consumed by the hydrolytic site of SERCA [5]. SERCA activity is regulated by prevailing intracellular calcium content and by the actions of its endogenous inhibitor protein phospholamban (PLB). The role for PLB in the control of SERCA activity is demonstrated by the enhanced contractile function of hearts from mice lacking the gene encoding for PLB [6]. SERCA-PLB interaction is modulated through adrenergic signalling representing an important mechanism relating an increase in neural sympathetic drive to an increase in cardiac output (see below).

Energy consumption – Contractile state and the Frank-Starling mechanism

The Frank-Starling mechanism describes how an increase in fibre stretch (lumen dilation), due to greater preload, can enhance contractile force and so elevates stroke volume. In order to generate more force there must be a greater number of 'power strokes' and therefore the ATP requirement of each contraction is increased. Changes in contractility can also occur in the absence to changes in cardiac preload and afterload either augmenting or depressing performance. The sympathetic nervous system represents one mechanism whereby inotropy, lusitropy and chronotropy can be increased in the myocardium. Where inotropy defines the force muscular contraction, lusitropy relates to the rate of muscular relaxation and chronotropy describes to the rate of contractile cycling. Noradrenaline released from sympathetic nerve terminals in the heart stimulates rapid changes in myocardial contractility under physiological conditions. In addition adrenaline released from the adrenal medulla can circulate in the blood and exert effects at the heart. Catecholamines (a term encapsulating both noradrenaline and adrenaline) exert their actions through binding to the α and β-adrenoceptors of the cell sarcolemma. The β-adrenoceptors can be further divided into three subtypes; two with similar functional roles (β1and β2) and one inhibitory isoform (β3). Binding to the β1 and β2 receptors results in increases in cardiac contraction, calcium transient amplitudes and rates of relaxation. These effects are mediated primarily through stimulation of adenylate

cyclase which elevates intracellular cyclic adenosine monophosphate (cAMP) in turn activating cAMP dependent protein kinase (PKA). PKA phosphorylates a number of key contractile proteins including 1) troponin I (reducing myofilament calcium sensitivity) 2) sarcolemma calcium channels (increased calcium entry), 3) phospholamban (reducing its inhibition of calcium reuptake into the SR through SERCA) and 4) SR calcium release channels (alterations in RyR gating). While the decreased sensitivity of the myofilaments to calcium appears counterproductive the dramatic increase in calcium transients more than compensates promoting an increase in contractility. Increases in cytosolic calcium concentrations will promote cross-bridge cycling and SERCA activity enhancing cardiac rate, inotropy and lusitropy and as such elevates myocardial ATP utilisation. $\beta 3$ activation produces negatively inotropic effects thought to be mediated through the production of nitric oxide from locally bound neuronal nitric oxide synthase (nNOS). The role of nitric oxide in the control of contractile function will be discussed in more detail in Chapter 5. The β-adrenoceptors represent the primary mechanism whereby catecholamines enhance force production in the heart however it is worth noting that binding of catecholamines to α_{1A} promotes calcium uptake through the sodium calcium exchanger elevating intracellular calcium and increasing contractile force. In addition activation of the alpha adrenergic signalling pathway increases myofilament calcium sensitivity. [3, 5]

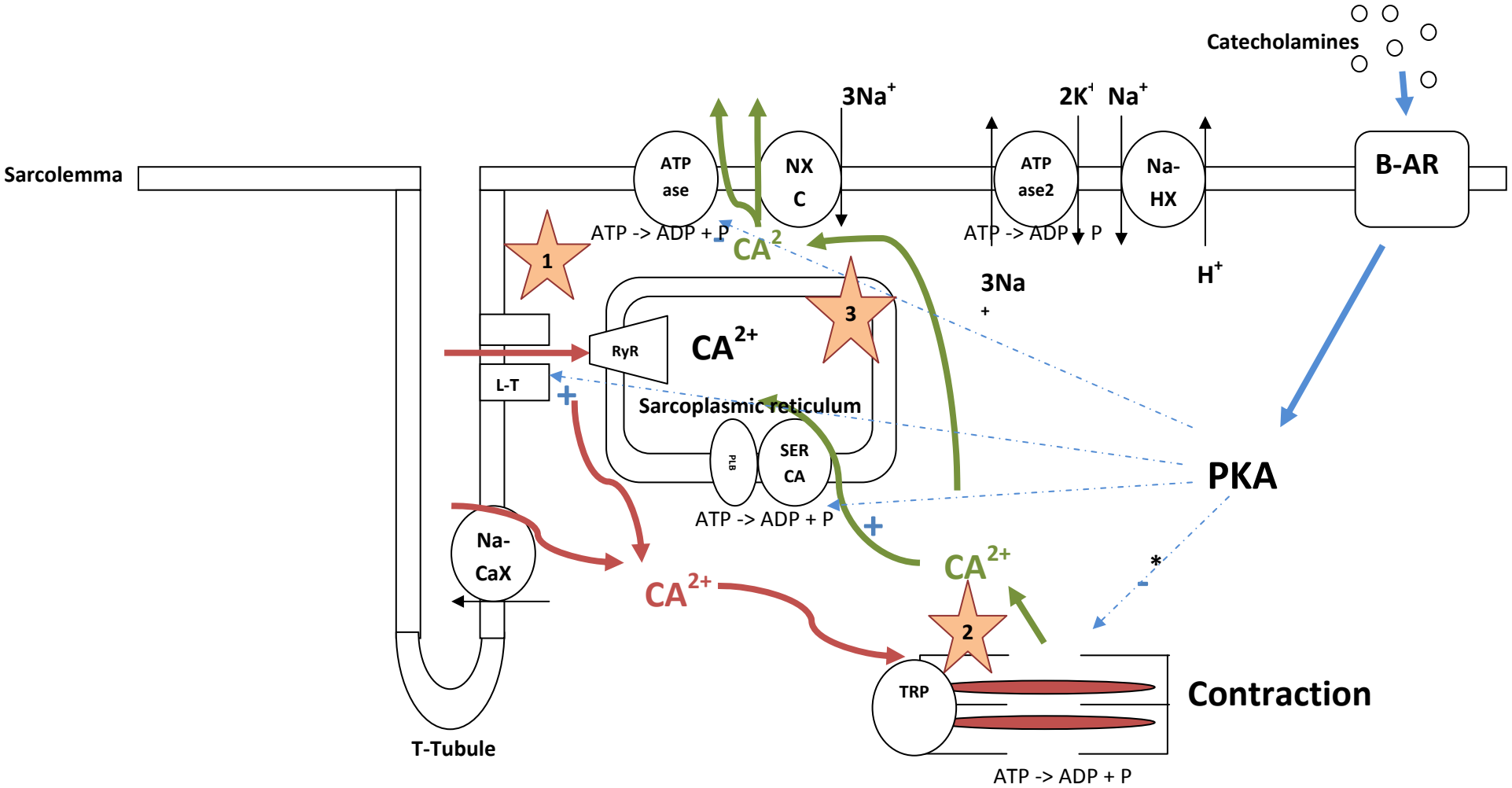

Figure 1.1. Excitation-contraction coupling in the heart. See main text for discussion. Legend: ATPase= sarcolemma Ca^{2+} ATPase, NXC=sarcolemma sodium potassium exchanger, ATPase2= sodium-potassium pump, NaHX=Sodium-hydrogen exchanger, B-AR=Beta-adrenoceptor, L-T=L-type calcium channel, SERCA=Sarcoplasmic reticulum Ca^{2+} ATPase, PLB=Phospholamban, TRPI- Troponin complex. Red lines represent calcium induced calcium release and resulting contraction. Green lines represent the active lowering of intracellular free calcium to bring about relaxation. Note the energy consuming processes indicated through ATP breakdown to ADP and inorganic phosphate. * Beta-adrenergic stimulation actually reduces the sensitivity of the myofilaments to calcium but inotropy is promoted through the significant rise in cytosolic calcium.

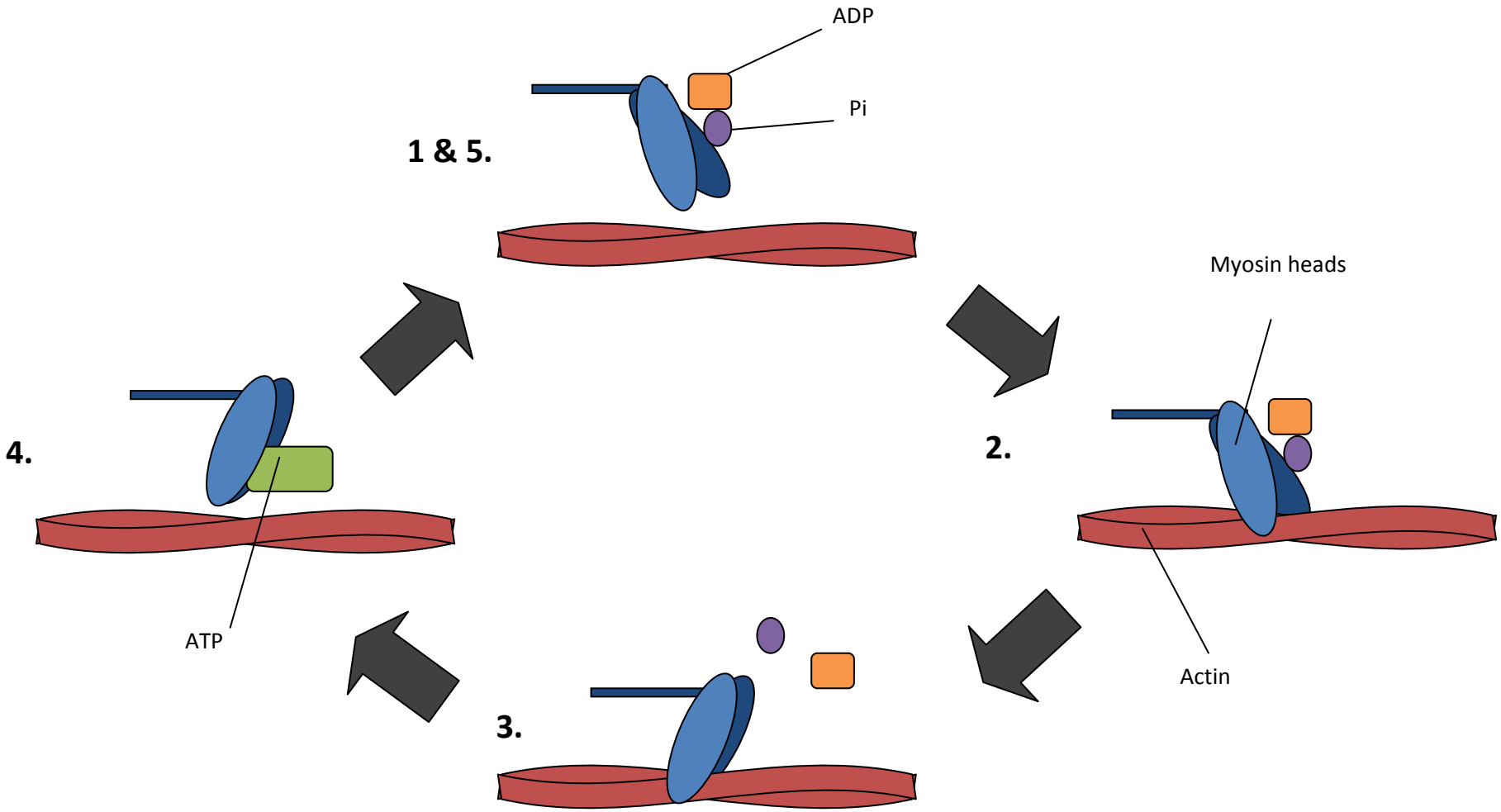

Figure 1.2. The theory of cross-bridge cycling in the heart. See main text for discussion. Legend: ADP= adenosine diphosphate, P_i=phosphate, ATP= adenosine triphosphate. In the absence of calcium this process is inhibited by the troponin complex. Binding of calcium to troponin I results in a conformational change in shape and allows cross-bridge cycling to occur.

Cardiac work and oxygen consumption

Cardiac contractile work is closely related to oxygen consumption and Sarnoff et al. In 1958 demonstrated a classic example of this relationship [7]. Sarnoff's preparation utilized a blood perfusion consisting of an isolated dog's heart supported by a second heart from a donor dog. Blood from the left ventricle of the isolated heart is ejected through an adjustable resistance tube and turbine flow meter into a reservoir which drains into the left atrium through a second adjustable resistance tube. Blood from the coronary circulation drains into the right ventricle which ejects blood into the jugular veins of the support dog. Re-oxygenated blood is returned to the reservoir from the support dog at the rate at which it was removed. This elegant method provided a heart with maintained cardiac performance and allowed the assessment of the effects of varying heart rate (through electrical stimulation), preload and afterload on cardiac oxygen consumption. Adjustment of outflow and inflow resistances allowed for precise modification of cardiac preload and afterload. O_2 and CO_2 contents of arterial and venous blood were estimated gasometrically and blood oxygen saturation was constantly measured through densitometry. Oxygen consumption was calculated by applying the Fick principle, whereby oxygen consumption is equal to the product of coronary blood flow and the difference between coronary arterial and venous oxygen content. Sarnoff *et al* demonstrated that pressure work (afterload) increased oxygen consumption in a manner that was paralleled by the increase in aortic pressure but with little or no change to cardiac output. During pressure work the increase in oxygen consumption results from the increase in internal tension development (wall stress) and the length of time in this state before ejection occurs. During volume work a small increase in oxygen consumption occurred along with an increase in cardiac output resulting from activation of the Frank-Starling mechanism. Volume work therefore improves cardiac efficiency (work per unit oxygen) whereas pressure work significantly decreases it. Increases in rate work (achieved through electrical pacing of the heart) were also associated with an increase in oxygen consumption relative to the increase in the peak systolic pressure-time integral.

These relationships were similarly described by Neely *et al* (1967) in experiments performed in the isolated beating rat heart [8].

Catecholamines, which enhance contractile force, lusitropy and rate, dramatically elevate myocardial oxygen consumption. Vasu *et al* (1978) showed in the donor supported dog heart (as described above) that a range of natural and synthetic catecholamines cause an increase in oxygen consumption that can be directly related to the increase in the peak systolic-time integral [9]. Therefore catecholamines do not alter the energetic cost of work but merely augment contractile force and heart rate. Feinberg and Katz (1958) utilised an open chest dog preparation to investigate the effects of noradrenaline and adrenaline on coronary flow rates, cardiac work and oxygen consumption. Treatment with both of these adrenergic agents resulted in a dramatic increase in myocardial oxygen consumption, cardiac output, coronary flow and coronary sinus oxygen content. The increase in sinus oxygen content implies that while oxygen delivery is improved through increased coronary flow rates the rate of oxygen extraction is reduced [10]. Note; at times of reduced oxygen availability and/or elevated vessel shear stress (see later definition), as occurs when hearts are perfused with oxygenated crystalloid buffer solutions instead of blood, the ability to increase coronary blood flow is reduced and in these circumstances there is greater extraction of oxygen per unit perfusate [11].

Molecular mechanisms linking ATP and oxygen consumption

The relationship between oxygen consumption and cardiac workload is directly linked to the oxygen dependent metabolism of FAs and glucose to provide the energy for mitochondrial synthesis of ATP, providing the energy for both the contractile cycle of the myofilaments and the movement of ions by various channels and pumps. These molecular mechanisms are well described and immensely intricate and complex. The balance and flux through these metabolic pathways closely links changes in myocardial energy demand to changes in substrate oxidation and energy production. The

following discussion provides an overview of the processes involved in myocardial glucose and FA uptake, oxidation and utilisation in the heart (Figure 1.3 and 1.4 respectively).

Uptake of carbon substrates

Glucose

Two transporters control the uptake of glucose from the blood stream across the sarcolemma into the cells of the heart: *GLUT 4* and *GLUT 1*. GLUT 1 is constitutively expressed in all cells and thought to control basal levels whereas GLUT 4 is recycled between cytosolic and plasma membrane pools as in response to changes in afterload [12], catecholamines [13, 14], oxygen availability and insulin [15]. The transport of glucose into the cardiac myocytes is regulated by the content of glucose transporters in the sarcolemma.

The first step of glucose metabolism

There is very little free glucose found within the cytosol of the cell as after its uptake glucose is rapidly converted to glucose-6-phosphate by hexokinase at the cost of one molecule of ATP. This rapid conversion effectively traps the phosphorylated glucose in the cell for entry in to citrate and glycogen cycles while preserving the inward glucose gradient across the sarcolemma [15].

Fatty Acids

As with glucose the uptake of long chain FA appears to be governed by specific transport proteins which can translocate the sarcolemmal membrane in response to alterations in workload [16]. FA translocase (CD36) is one important component of this process and hearts from mice engineered to lack the gene encoding for CD36 demonstrate a 50% reduction in FA uptake [17].

The first step in FA metabolism

The first step of FA metabolism results in the formation of long-chain Acyl-CoA (LCAC) maintaining cytosolic free FA at low concentrations.

Glycolysis and glucose oxidation

Glycolysis is the metabolic pathway that converts glucose into pyruvate. The free energy released in this process is used to form ATP and reduced nicotinamide adenine dinucleotide (NADH). NADH, along with FADH, acts as an electron donor in the electron transport chain (Figure 1.5). Raising cardiac mechanical workload by elevating afterload is associated with increased rates of glycolysis, a potential result of the accumulation of fructose-2,6-biphosphate (fru-2,6-Bi) in the cytosol [12, 18, 19]. Fru-2,6-Bi is synthesised by 6-phosphofruckto-2kinase (PFK-2) and stimulates 6-phosphofructo-2-kinase (PFK-1) a key regulatory enzyme of the glycolytic pathway. Mechanical work it thought to signal through a phosphatidylinositol 3-kinase dependent pathway resulting in the activation of protein kinase B (PKB) which mediates the phosphorylation of these target proteins [12]. Citrate acts as a negative allosteric regulator of PFK-2 activity linking changes in mitochondrial energy metabolism to glycolysis and provides a mechanism whereby accumulation of intracellular free FA inhibits this process [20]. PKA and protein kinase C (PKC) have also been shown to regulate glycolytic flux at PFK-2 (promoters) highlighting the importance of this site in the control of glycolytic flux [15].

Decarboxylation of the pyruvate formed during glycolysis is the key irreversible step of carbohydrate oxidation. Pryruvate dehydrogenase (PDH), located within the mitochondria, is responsible for catalysing this reaction. Phosphorylation of the PDH complex by a specific PDH kinase results in inactivation whereas dephosphorylation via a PDH phosphatase produces activation [15]. PDH activity is increased when the intracellular concentration of calcium ions increases such as during adrenergic stimulation. The net shift in kinase and phosphatase activity promotes the conversion of pyruvate to acetyl CoA and so provides a metabolic link between the energy demand of the myocardium and the metabolism of substrates for ATP production. FAs promote the activity of PDK and so are able to suppress glucose oxidation when circulating concentrations are high (the glucose-FA cycle) [21].

Excess pyruvate unable to enter the TCA cycle is converted to lactate by the reversible actions of lactate dehydrogenase. The oxidation of NADH to NAD^+ during this process is of importance in times

of reduced oxygen supply, such as ischaemia resulting from vascular occlusion. During the 6th reaction of the glycolytic pathway glyceraldehyde phosphate dehydrogenase (GADPH) catalyses the conversion of glyceraldehyde 3-phosphate to 1,3-biphosphoglycerate reducing 2 molecules of NAD+ to NADH in the process [22]. As the NADH/NAD^+ ratio is an important mechanism regulating GADPH (feedback inhibition) it is possible to envisage how when oxidative metabolism is unable to proceed (i.e. low oxygen availability) that the function of glycolysis would also cease. The conversion of pyruvate to lactate and the oxidation of NADH to NAD^+ provides a mechanism for the continuation of the glycolytic pathway allowing for the production of a small but limited amount of ATP (anaerobic). In the normal well-oxygenated myocardium the heart is able to import and oxidise lactate, in this situation lactate dehydrogenase catalyses the conversion of lactate back to pyruvate

Beta-oxidation

β-Oxidation occurs in the mitochondria and requires the transport of LCAC into the mitochondrial matrix. This is achieved through a carnitine-dependent transport system found within the inner and outer mitochondrial membranes. Carnitine palmitoyl-transferase I (CPT-I) catalyses the conversion of LCAC to long-chain acylcarnitine, which is shuttled into the inner mitochondrial space. Acyl carnitine crosses into the mitochondrial matrix via the carnitine/acylcarnitine translocase complex. Carnitine palmitoyl-transferase II (CPT-II), found bound to the inner mitochondrial membrane, catalyses the transesterification of fatty acyl carnitine to acyl CoA, which is an activated substrate for beta-oxidation. This system allows the separation of CoA and carnitine in the cytosol and mitochondria so the pathways can continue to function in unison.

Malonyl-CoA is the rate-limiting regulator of long chain FA entry into the mitochondria, an allosteric inhibitor of CPT-1. Acetyl-CoA carboxylase (ACC), in particular the beta isoform, is the enzyme responsible for the carboxylation of cytosolic acetyl-CoA to form malonyl-CoA. This system allows the switching off of FA metabolism in the face of excess acetyl-CoA in the cytosol. Importantly malonyl-CoA production appears to occur using only acetyl-CoA formed from glucose. This means

that malonyl CoA may act to inhibit FA oxidation in times when carbohydrates are in ready supply. The level of malonyl-CoA within the cell is regulated by the balance between its synthesis by ACC and its breakdown by malonyl-CoA decarboxylase (MCD). A study by Goodwin and Taegtmeyer (1999) investigated how malonyl-CoA regulates FA oxidation during contractile stimulation (adrenaline + 40% increase in afterload) in the isolated beating rat heart [23]. During contractile stimulation ACC activity was unaffected despite an increase in total FA oxidation (exogenous + endogenous). MCD activity was, however, some 55% greater than controls, suggesting that an increase in degradation of malonyl CoA occurs during an increase in workload and that this drives the higher rates of total β–oxidation noted in this and other studies [23, 24]. After entry into the mitochondria activated FAs (bound to coenzyme A) are cleaved into multiple two-carbon acetyl CoA units (removed from the carboxyl end of the FA chain). This produces one molecule of acetyl CoA, one molecule of NADH and one molecule of $FADH_2$ per turn of the cycle. Specific enzymes exist to hydrolyse FAs of varying chain length. The two carbon acetyl CoA fragments produced are free to enter the citrate cycle.

The citrate cycle, oxidative phosphorylation and the oxygen cost of metabolism

During the tricarboxylic acid cycle acetyl CoA from the glycolytic breakdown of glucose and β-oxidation of FAs is used to drive the reduction of nicotinamide adenine dinucleotide (NAD) and flavin adenine dinucleotide (FAD). These coenzymes act as electron donors taking electrons released in the citrate cycle and donating them to the electron transport chain where they are used to form ATP. The process of energy production through the five complexes of the mitochondria is known as oxidative phosphorylation. A simplified diagram of this process is presented in Figure 1.5 however detailed discussion of the mechanisms involved is beyond the scope of this thesis. It is important to note that oxygen acts as the final electron acceptor where it is converted with free H^+ to water. Each electron donated to the oxidative chain from reduced NAD (NADH) provides enough energy for the production of 2.5 ATP molecules. Each electron donated from reduced FAD ($FADH_2$) provides enough energy for the production of 1.5 ATP molecules. Therefore the classical yield of ATP for each

molecule of glucose is 38 (12 NADH=30 ATP, 4 NADH=6 ATP + 2 ATP from glycolysis). During β oxidation the breakdown of the 16 carbon FA palmitic acid produces 7 NADH, 7 $FADH_2$ and 8 acetyl-CoA molecules and uses 2 molecules of ATP in the activation of the FA. Therefore the net gain of ATP per molecule of palmic acid is 106 molcules of ATP [25]. In terms of ATP yield per mole of oxygen utilised glucose metabolism is relatively more efficient with a ratio of 3.17 compared to 2.83 for palmitate. Therefore the oxygen cost of ATP production from FAs is greater than that of glucose despite greater yields per mole of substrate. Oxygen consumption is elevated at all workloads when hearts are perfused with FAs [26, 27]. This idea of metabolic efficiency will be discussed later in terms of the late stage metabolic changes associated with heart failure [1].

Phosphotransfer networks

Optimal operation of the myocytes bioenergetic system requires that high energy phosphoryls are synthesised and delivered to the energy consuming processes of the myocardium at a rate comparable to their rate of degradation. Additionally the breakdown products of ATP hydrolysis (namely ADP, free Pi and H^+) require removal in order to prevent hindrance of ATPase activity. Diffusional exchange of adenine nucleotides has been shown to be kinetically inefficient requiring the existence of large concentrations gradients which do not exist in normal cells [28]. Inefficient transfer would result in an inability to sustain hydrolysis of ATP at the sites of energy production as well as a build up of ATP hydrolytic end products resulting in ATPase inhibition. It has been suggested that sequential rapidly equilibrating biochemical reactions provide a means whereby reaction ligands are able to transverse relatively large spaces quickly and without the need for a significant concentration gradient [28, 29]. According to this model, incoming ligands on one end of the system push adjacent molecules triggering a propagation of a signal flux through a network of rapidly catalysing enzymes. Therefore ligands do not travel the entire length of the pathway but rather the molecules arriving at the distal site are equivalent but not the same as the molecule generated at the site of origin. The phosphocreatine and adenylate kinase reactions of the myocytes represent two of these important phosphotransfer networks. In addition to its roles in NADH

reduction glycolysis is now often viewed as a phosphotransfer mechanism, whereby a series of interlinked reactions spread across the myocyte provide a system for rapid ATP regeneration from ADP and Pi. Detailed discussion of the phosphocreatine and adenylate kinase systems is perhaps beyond the scope of this introduction, but it is important to recognise the role of these systems in energy transfer and their potential theorised importance in maintaining local ATP concentrations during an increase in energy demand.

Endogenous energy stores

Glycogen

Cardiac glycogen is a polysaccharide molecule made up from a number of smaller glucose units. Stored in granules in the cell cytosol this molecule provides a reserve of energy shown to be of particular importance during times of cardiac stress (e.g. a jump in the work rate requirement of the heart or during β-adrenoceptor stimulation [15]). While acting as an energy store, glycogen is also thought to play an important role in normal glucose metabolism; acting as a thoroughfare for glucose 6-phosphate entering the glycolysis pathway (i.e. large turnover of the glycogen pool) [30]. The glycogen pool is in a constant state of flux, with variable rates of production and breakdown. Intracellular glycogen concentration is therefore determined by the balance between rates of synthesis and degradation. Glycogen production takes place through the actions of the enzyme glycogen synthase. Glycogen synthesis is known to increase by both the activity of insulin during the fed state and via depletion of the cardiac stores (as seen in periods of increased workload and ischaemia) [15]. In the fasted (low circulating glucose concentrations) state glycogen production still occurs but at a slower rate than that seen in the fed state. During these fasted periods glycogen synthase can be stimulated through increasing intracellular glucose 6-phosphate concentrations (allosteric activator) resulting from the free FA induced blockade of glycolysis. Breakdown of glycogen occurs through the actions of phophorylase and occurs during periods of increased need, as seen with beta-adrenergic stimulation. Increased calcium ion release and beta adrenergic

stimulation lead to the conversion of the inactive phosphorylase B to the active form phosphorylase A [31].

Triglycerides

Triacyglycerol (TAG) is formed of three FAs bound to a glycerol backbone and provides andimportant energy reserve in the heart. Studies in isolated rodent hearts have shown that turnover of the triglyceride pool is large even in hearts provided with high circulating free FA concentrations, contributing some 8 to 11% of the calculated oxidative ATP production [32]. Reductions in circulating FA concentrations results in a higher contribution of the TAG pool to ATP production (up to 50% during perfusion with glucose alone) with a depletion of intracellular TAG content over time. Synthesis of triglycerides is carried out by a series of enzymes in both the outer mitochondrial membrane and in the endoplasmic reticulum (the Kennedy pathway) [15, 33]. Glycerol 3-phosphate acyltransferase (GPAT) catalyses the rate limiting first step of this pathway. It has been speculated that the co localisation of GPAT with CPTI on the outer mitochondrial membrane represents a site of competition for acyl CoA substrates. Flux through either pathway may be regulated by energy demand but the experiments to look at this in the heart have not been performed.

Breakdown of intracellular triglycerides occurs through the actions of hormone sensitive lipase (HSL), lysosomal lipase (LAL), a microsomal diacylglycerol (DAG) hydrolase and a monoaacylglycerol (MAG) hydrolase. As the rates of breakdown of DAG and MAG dramatically exceed those of TAG it is thought that HSL and/or LAL regulate TAG content at the first step in the hydrolytic pathway [33]. Several studies have demonstrated that free FA and acyl-CoAs inhibit these lipases providing a link between energy demand and energy utilisation whereby lypolysis is promoted when intracellular concentrations of these substrates fall [34-36]. HSL may also be regulated through phosphorylation by cAMP dependent protein kinase during exposure to catecholamines.

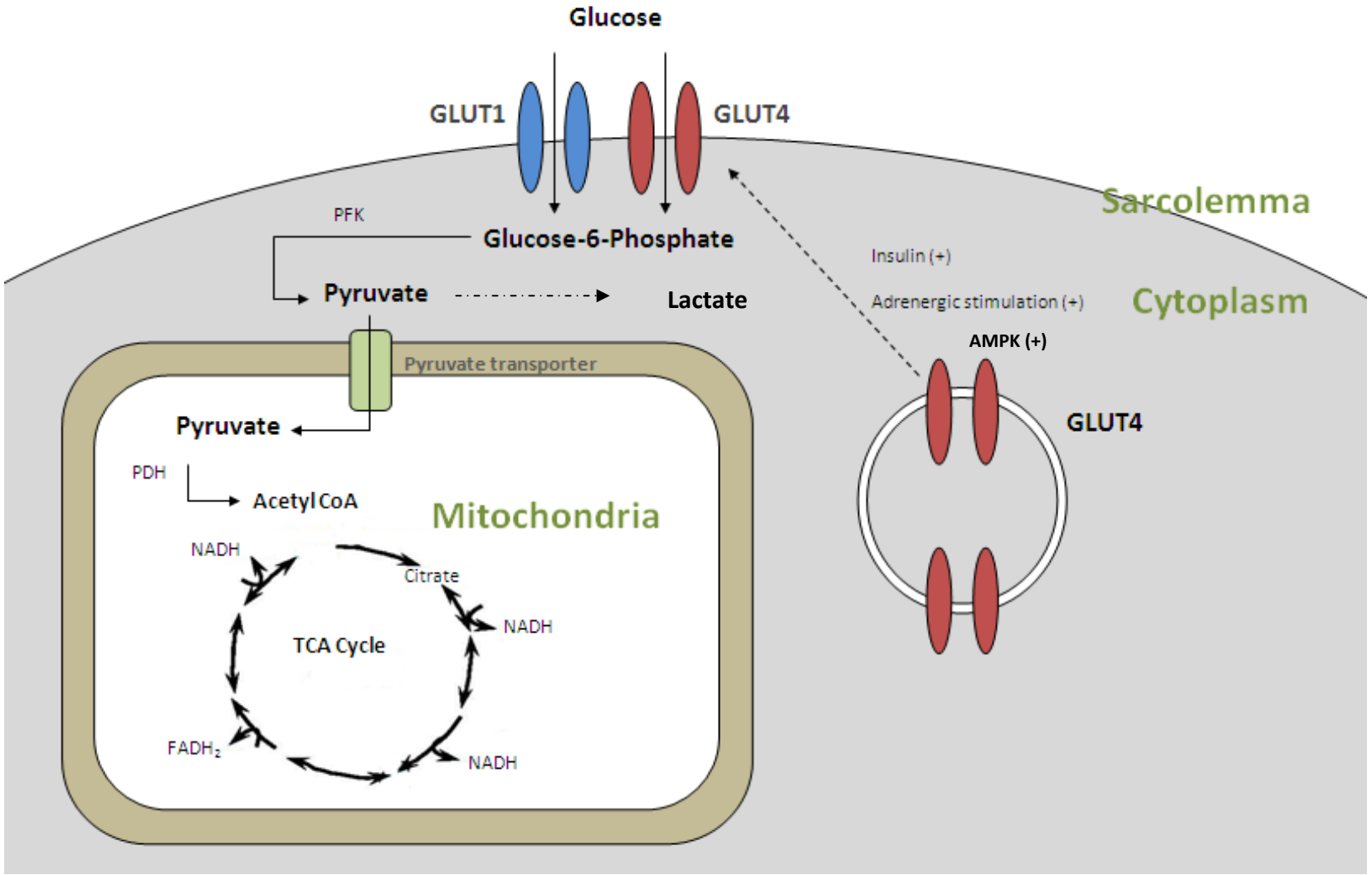

Figure 1.3. Glucose uptake, glycolysis and oxidation in the heart. See main text for discussion. Legend: NADH= Nicotinamide adenine dinucleotide, $FADH_2$= flavin adenine dinucleotide TCA= Tricarboxylic acid, PFK = Phosphofructokinase, PDH = Pyruvate dehydrogenase, GLUT=Glucose transporter.

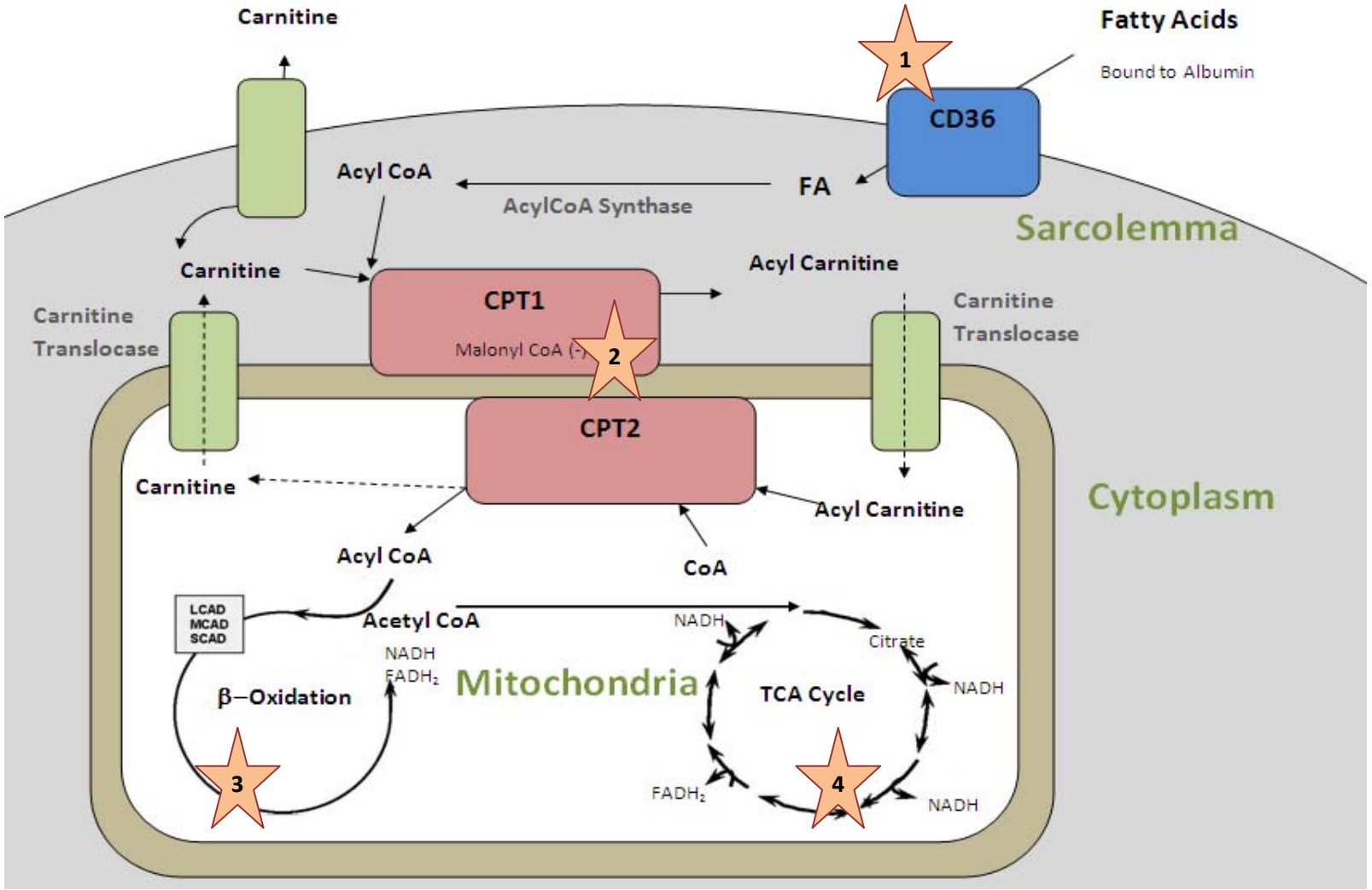

Figure 1.4. FA uptake and oxidation in the heart. See main text for discussion. Legend: LCAD = Long chain acyl-CoA dehydrogenase, MCAD= Medium chain acyl-CoA dehydrogenase, SCAD= Short chain acyl-CoA dehydrogenase, NADH= Nicotinamide adenine dinucleotide, $FADH_2$= Flavin adenine dinucleotide TCA= Tricarboxylic acid, FA= FAs. 1 = FA uptake, 2= Mitochondrial acyl-carnitine transport, 3= β-oxidation, 4=Tricarboxcylic acid cycle.

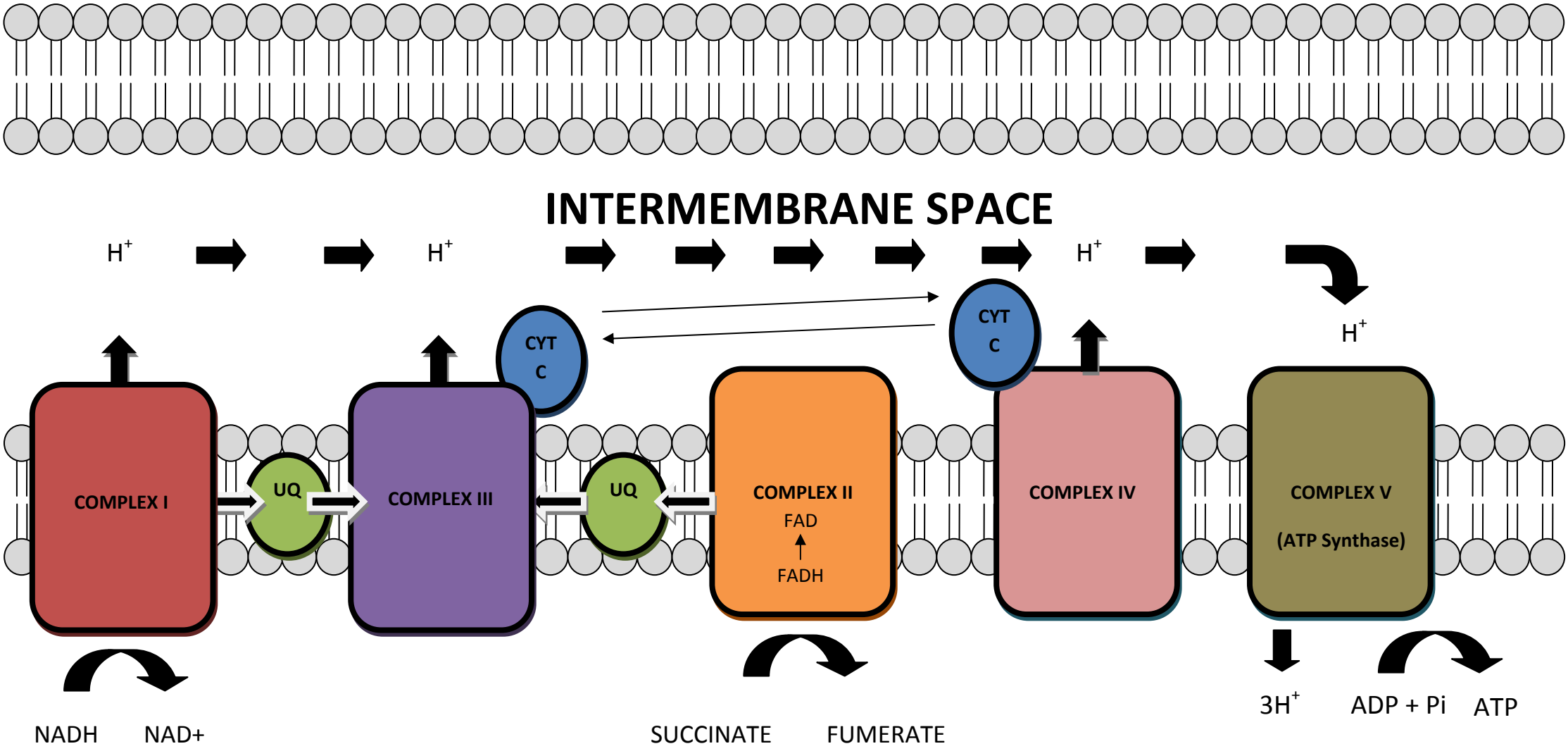

Figure 1.5. Oxidative phosphorylation of the mitochondria. During oxidative phosphorylation electrons are transferred from electron donors to electron acceptors. This series of redox reactions releases the energy required for the formation of ATP. Electron flow between the protein complexes of the oxidative chain provides the energy for pumping protons into the intermembrane space of the mitochondria. The potential energy produced during this process is utilised in the formation of ATP when protons flow back into the mitochondrial matrix through ATP synthase. Legend; NAD= nicotinamide adenine dinucleotide, UQ=Ubiquinone, CYTC= Cytochrome C.

Cardiac responses to chronic stress

Cardiac hypertrophy describes the process whereby the heart is able to respond to an increase in demand placed upon it by increasing muscle mass to normalise wall stress and maintain the rate and force of contraction. An increase of muscle mass in the heart must occur primarily through enlargement of the existing cell size as the myocytes of the adult myocardium are fully differentiated and unable to undergo hyperplasia (an increase in cell number mediated by splitting of existing cells). Cardiac hypertrophy is defined by increased cardiomyocyte size, enhanced protein synthesis and sarcomere reorganisation. The form of the inciting stress is a major determinant of the type of remodelling that occurs. Changes in pressure (as seen in aortic stenosis and hypertension) or volume (as seen in valvular insufficiencies) result in differential adaptations in cardiac geometry. Grossman et al (1975) first described how, in humans, examples of pressure and volume overload induce differential models of adaptive growth [37]. The increase in valvular or vascular resistance seen in patients with aortic stenosis and hypertension elevates ventricular afterload promoting a concentric model of hypertrophic growth. Parallel replication of the sarcomeres and an increase in the cross sectional area of the myocytes results in ventricular wall thickening. This can be viewed as an attempt to normalise ventricular wall stress and in this setting total cardiac oxygen consumption remains elevated while tension development and oxygen consumption are normalised per unit mass of tissue. Alternatively patients with mitral or aortic valvular insufficiency demonstrate myocyte fibre elongation; a result of blood flow back into the ventricles after ejection is complete. Volume overload promotes serial sarcomere replication, an increase in ventricular lumen volume and a modest increase in pressure development. Chamber enlargement also elevates systolic wall stress and so a small degree of wall thickening usually occurs normalising stress at the ventricular wall. These characteristics of human disease can be readily replicated in experimental animal models. Aortic banding (or transient aortic constriction), involving partial tie-occlusion of the descending aorta, increases vascular resistance and elevates cardiac afterload providing a model of pressure overload which reflects human states of hypertension or aortic stenosis. Aortic banding promotes

concentric left ventricular remodeling in a variety of animals, including rats and rabbits [38-41]. Experimental volume overload can be produced through the formation of a fistula between the descending aorta and vena cava. This opening allows oxygenated blood to flow directly into the venous circulation back to the heart. The harder the heart works to overcome the reduction in oxygen supply to other tissues the greater the return of oxygenated blood to the heart and the greater the increase in diastolic preload. This perpetual cycle results in rapid progression from a well adapted state to insufficiency and failure [42, 43].

Pathological hypertrophy and heart failure

Contractile dysfunction

Pathophysiological stimuli include mechanical forces (pressure or volume) and neurohumoral stimuli (e.g. renin-angiotensin II, endothelin, adrenergic). In general hypertrophy may be viewed as an adaptive process helping the heart deal with an increased workload through compensatory remodeling. At some point the compensation fails to meet the demands of the body and there is a progression to heart failure (HF). HF is defined as an inability to meet the metabolic demands of an organism due to insufficient cardiac output and is an increasing health problem in the western world with over 2 million reported cases per year in the U.S. alone. A certain part of the pathology of HF may ascribed to insufficient geometric remodeling which fails to adapt to the altered stress placed upon the heart. Again, using the law of LaPlace, we can see that an increase in arterial pressure or ventricular radius (dilation) must be met by a concurrent increase in wall thickness if cardiac output is to be maintained. Prolonged exposure to pressure overload, as with aortic banding or human hypertension, results in a decompensated form of hypertrophy with impaired contractile function. Incidentally prolonged exposure to a volume overload stimuli, as seen in the aortocaval fistula model of human valvular insufficiency, results in excessive myocyte lengthening and chamber dilation. In dilation, the ventricle volume is extremely large, but the cross sectional area of the myocytes has minimally increased and so pressure development and pump function can be severely impaired.

Geometric insufficiency does not however tell the whole story. Data accrued over the last 30 years suggests that molecular alterations are responsible for the contractile dysfunction associated with heart failure. Changes in calcium transient amplitudes appear to play a prominent role in the molecular mechanisms of heart failure. Bastie *et al* (1990) were the first to show that SERCA gene and protein expression is down-regulated in the pressure overloaded hypertrophied rat heart. Whole heart homogenates showed a reduction in the capacity for calcium uptake into the SR which could be directly related to a lower expression of SERCA2a [44]. Since this early report a tremendous number of studies have measured SERCA2a expression and function in models of pressure overload, pacing induced heart failure, volume overload and catecholamine exposure. It seems clear that SERCA expression is functionally decreased in heart failure [4, 5, 45-48]. There is also evidence that the phosphorylation state of PLB is altered in HF leading to a disproportionately high depression of SERCA activity. Schwinger *et al* (1999) published work showing impaired SERCA activity in human heart failure biopsies despite the preserved expression of SERCA and PLB [49]. It was found that patients with heart failure had a significant reduction in the phosphorylated form of PLB compared with controls. Adenoviral introduction of the SERCA2a gene into pressure overload (aortic banded) induced failing rat hearts has been used to completely restore the loss of contractile performance associated with these hearts [50]. Increased expression of the sodium calcium exchanger (NCX) has also been noted in a number of human and experimental studies of HF [51-53]. When combined with a down-regulation of SERCA these data suggest that there may be a shift in calcium handling away from the energy dependent processes of the sarcoplasmic reticulum to favour greter extrusion of intracellular calcium through the sarcolemmal NCX. Such changes may precipitate a reduction in SR calcium load resulting in reduced intracellular calcium transients and impaired myocyte contractility [4, 5].

Energy metabolism during hypertrophy and heart failure

Alterations in energy metabolism have been noted in both human experimental models of hypertrophic and dilated cardiac failure suggesting that changes in the pathways responsible for the

production, transfer and utilisation of ATP underlie the development of heart disease of several aetiologies. A time line of changes appears to occur in the pathways involved in ATP synthesis as hypertrophy develops from the compensated to decompensated form. Initially flux through the CK reaction falls as a demonstrable reduction in both total cellular creatine content and CK activity. Glucose uptake and utilisation are stimulated while FA metabolism is either suppressed or remains unchanged. Decompensated hypertrophy is marked by a further decrease in CK flux and a suppression of FA oxidation. At this stage increases in glucose utilisation (primarily occurring through increased glycolytic rates) is insufficient to meet the energy demands of the myocardium and ATP content falls. The fall in energetic reserve is thought to further impair cardiac contractile reserve (i.e. limited ATP supply when workload is elevated). The following headings will discuss in greater detail the metabolic alterations associated with HF.

High energy phosphates

Analysis of biopsy samples taken from humans with end stage heart failure has demonstrated a 25 to 30% reduction in ATP content [54]. Results confirmed by more recent ^{31}P nuclear magnetic spectroscopy measures of ATP content in patients with hypertensive heart disease, aortic stenosis and dilated cardiomyopathy [55] as well as longitudinal studies of pacing induced heart failure in the dog (demonstrating a progressive loss of both ATP and the total content of adenine nucleotides) [56]. Linear correlations have been demonstrated between tissue ATP content and measures of systolic and diastolic dysfunction in both experimental (62) and clinical (61) studies. Other investigators have reported correlations between diastolic dysfunction but not with systolic dysfunction in humans with end stage heart failure (60).

Dramatic reductions of intracellular creatine content in biopsies taken from patients with aortic stenosis [57] and severe heart failure [58] have been reported and confirmed in studies utilising nuclear magnetic spectroscopy techniques [59]. Given the rapidly equilibrating nature of the CK reaction these data tell us that PCr will be also be reduced in the failing heart and several ^{31}P NMR

studies in the early 1990's confirmed this and reported a fall in the PCr to ATP ratio in patients with HF [60, 61]. Interestingly the fall in PCR/ATP ratios occurs in well compensated hypertrophic models and as such may represent one of the earliest energetic abnormalities preceding the contractile dysfunction and later changes in ATP content and substrate metabolism [61]. Over the last decade the PCr to ATP ratio has proven to be a more accurate predictor of cardiovascular mortality than traditional indicators (the New York Heart Association Class and LV ejection fraction) [62]. Changes in the activity and expression of the CK enzymes co-localised to the myofibril and the mitrochondria and decreased numbers of creatine transporters may play a role in these changes in phophotransfer capacity [62].

Changes in the phosphorylation potential form the basis of arguments that the failing heart is energy 'starved' possibly through inadequate matching between ATP supply and ATP demand or by impairment in the systems through which energy transfer occurs.

Substrate metabolism

Table 1.1 summarises the major finding of a number of studies looking at rates of metabolism in the hearts with models of experimental hypertrophy and heart failure. The first conclusion from these data is that alterations in the metabolic profile of hypertrophic hearts are preceded by contractile dysfunction. For example Chandler *et al* (2004) showed no significant alteration in substrate oxidation despite a decrease in contractile performance in their model of micro-embolism induced cardiac failure [63]. These data are supported by time-course studies in pacing induced heart failure which show that alterations in metabolism occur around 20 days after the onset of decreased contractile performance [64]. Despite the impairment of contractile force in these models of early failure, cardiac metabolism is not concurrently depressed resulting in higher oxygen consumption per unit work. It is generally accepted that during the switch from compensated to de-compensated hypertrophy there is significant down-regulation of long-chain FA oxidation with a concurrent increase in the rates of glycolysis and glucose oxidation. Increased rates of glucose oxidation have

been reported at just 14 days in the rat aortic banding model suggesting that an increase in glucose utilisation is one of the earliest metabolic alterations [40]. Suppression of FA metabolism along with increased rates of glucose oxidation has been reported in spontaneously hypertensive rats [65] and in pacing induced failure in the dog [64, 66] and seems to represent a mid stage alteration in metabolic phenotype during heart failure, increasing the heart's reliance upon glucose metabolism to provide the energy for ATP synthesis. Referring back to the earlier discussion of metabolic efficiency this could normalise for the decrease in efficiency (less oxygen consumption per ATP molecule synthesised from glucose than FA). Late stage heart failure appears to be associated with an uncoupling of the glycolytic and glucose oxidative metabolic pathways. Allard *et al* (1994) have demonstrated that significant uncoupling occurs at just 8 weeks in the aortic banded rat [38]. In this study glycolytic rates of glucose utilisation were significantly higher in the hypertrophied hearts whereas glucose oxidation was comparable to controls (FA rates were also significantly depressed). In the rat aortic banding model, the uncoupling of glycolytic activity is marked by an elevation of pefusate lactate, suggesting an impaired ability to perform oxidative metabolism in these hearts [38, 67]. There are very few data on substrate metabolism in humans and the results of these studies are somewhat conflicting. Both increased [68] and decreased rates [69] of FA uptake have been reported in studies utilising positron emission tomography to compare heart failure patients to age matched healthy controls. It has been proposed that a similar temporal pattern relating metabolic alterations to disease severity can explain the conflict in these data [15]. Human studies suffer from their inability to assess glucose oxidation directly; relying instead upon the rate of uptake of tracer compounds.

Table 1.1. Summary of studies looking at the effects of models of cardiac hypertrophy and failure on contractile performance and rates of metabolism in the heart.

Investigators	Model	Perceived severity of model.	Performance/Contractility	Glucose metabolism	FA metabolism
Taegtmeyer *et al* (1988) [70]	Rabbit Unilateral nephrotemy and renal artery stenosis	Non failing. Slow developing hypertension. No hypertrophy.	↑ Pressure development	↑ Glucose utilisation	-
Allard *et al* (1994) [38]	Rat Aortic banding	Severe. Hypertrophy	↓ Pressure development at low workloads. Comparable to controls at high workloads.	↑ Glycolysis at low workloads. Comparable to controls at high workloads. Comparable rates of glucose and lactate oxidation between groups.	Suppressed FA oxidation
Chandler *et al* (2004) [63]	Dog. Microembolism induced failure.	Mild-Moderate. Hypertrophy	↓ Contractile performance	No change in rates of glucose metabolism.	No change in rates of FA metabolism.
Christe and Rodgers (1994) [65]	Spontaneously hypertensive rats	Moderate. Hypertrophy	-	↑ Glucose oxidation	↓ FA oxidation
Masie et al (1995)	Swine Aortic banding	Moderate. Hypertrophy	-	↑ Glucose oxidation ↑ Glycolysis	-
Lei *et al* (2004) [66]	Dog Pacing induced failure	Severe Dilated cardiomyopathy	↓ Pressure development and rate of force production. ↑ End diastolic volume	↑ Glucose oxidation	↓ FA oxidation
El Aloaoui-Talibi *et al* (1992) [42]	Rat Aortocaval fistula.	Moderate Hypertrophy	↓ Cardiac output and pressure work	-	↓ FA oxidation at high workloads (↑ afterload)
Recchia et al (1998) [64]	Dogs Pacing induced failure	-	↓ Contractility recorded from day 7 to day 28	↑ Glucose uptake seen after 26 days	↓ FA uptake seen after 22 days
Allard et al (2000) [39]	Rat Aortic banding	Severe hypertrophy			
Doenst et al (2001) [40]	Rat Aortic banding 14 Days	Mild-Moderate	Impaired baseline contractile performance. Preserved response	↑ Glucose oxidation at 14 days	FA oxidation rate comparable to controls at 14 days.

See main text for discussion. Severity was assessed from known indicators of the severity of cardiac failure (i.e. pulmonary edema, contractile dysfunction).

Table 1.2. Expression of key glucose and FA enzymes in human and experimental heart failure.

Study	Model	Molecular alterations
Razeghi *et al* (2001) [71]	Human end stage heart failure	Reduced expression of mRNA for: • GLUT1 and GLUT4 • LCAD and MCAD • CPT1b (muscle isoform) • PDK2 (liver isoform) and PDK4 (heart isoform)
Lei *et al* (2004) [66]	Pacing-induced heart failure (Dog)	Reduced mRNA encoding for GLUT1, GLUT4, PDK4, CPT1b.
Taegtmeyer (1988) [70]	Unilateral nephrotemy and renal artery stenosis (Rabbit)	Increased activity of PFK-1, hexokinase and lactate dehydrogenase. No change in the activity of enzymes involved in the citrate cycle.
Sack *et al* (1996) [72]	Human HF and spontaneously hypertensive rats.	Reduced mRNA and protein levels for MCAD in both failing human hearts and spontaneously hypertensive rats.
Osorio *et al* (2002) [73]	Pacing-induced heart failure (Dog)	40% decrease in MCAD espression and activity. 40% decreased CPT1 activity.

Legend: mRNA = messenger ribonucleic acid, GLUT= glucose transporter, PDK = pyruvate dehydrogenase kinase, CPT= carnitine palmitotransferase, LCAD = Long chain acyl dehydrogenase, MCAD = Medium chain acyl dehydrogenase.

Table 1.2 summarises the alterations in metabolic enzyme protein and gene expression associated with hypertrophy and heart failure. These data show convincing evidence that the pathways for FA oxidation are suppressed in the failing heart. Particularly convincing are the consistent findings of reduced expression of acyl dehydrogenases involved in the beta oxidative cycle. In contrast the data for an increase of enzymes involved in glucose metabolism is not so clear cut with a number of contradictory reports. Apparent paradoxical reports of an increase activity of PDK4 despite increase glucose oxidative rates add further confusion to the issue [66]. These data may well represent activation of glucose metabolism occurring secondary to the suppression of FA metabolism (through removal of the inhibitory actions of FAs upon the glucose metabolic pathways).

Myocardial hypoxia as a potential cause of hypertrophic de-compensation and cardiac failure

Despite the vast amount of data upon the issue of contractile and energetic impairment during heart failure little is known about the underlying causes of these dysfunctional processes. It has been hypothesised that this energetic and contractile remodelling represents a state of 'energy starvation' where the heart is unable to keep up with an increase in energy demand by an increase in energy supply. One potential cause of this paradigm is a low oxygen tension environment. Presented below are arguments both in support and against a theory of hypoxia in hypertrophy. Investigations into the potential hypoxic environment of the hypertrophied heart and its effects on contractility and metabolism will form the basis of this thesis.

Arguments for hypoxia in hypertrophy

Altered energy status, substrate utilisation and contractile remodelling

Changes in the PCr/ATP ratio infer that energy production is inhibited in some way and the suppression of FA metabolism in favour of glucose utilisation suggests that there is a significant drive to increase the oxygen efficiency of ATP production. Down-regulation of energy consuming contractile processes (i.e. SERCA) and up regulation of the energy independent systems (i.e. NCX) suggests mechanical remodelling has an oxygen sparing role.

Capillary growth and supply demand mismatch

Capillaries represent the point of oxygen delivery to the myocardium. The movement of oxygen from the blood to the myocytes occurs through diffusion. Diffusion can be simply described as:

$$Js = -DS\frac{\Delta y}{\Delta x}$$

This is known as Fick's law of diffusion and it describes how the mass of solute diffusion per unit time is related to concentration difference driving force (Δy) and the distance across which this

transfer is occurring (Δx). $\frac{\Delta y}{\Delta x}$ is known as the concentration gradient. The surface area for transfer (S) and diffusion coefficient (D) both impact on the rate of solute transfer. The diffusion coefficient depends on the viscosity and size of each solute as well as on temperature. As the concentration of coronary blood oxygen content changes little then diffusion distances become the primary determinant of oxygen diffusion in the heart. Histological assessment of capillary density (number of capillaries per mm^2) in cardiac tissue therefore gives an inverse representation of this relationship while the ratio of capillary number to myocyte number gives a true measure of changing capillary number even when there is a change in myocyte cross sectional surface area.

Evidence that capillary growth occurs in response to normal physiological stimuli is controversial with reports of modestly increased, unchanged and decreased ventricular capillary density following chronic exercise training [74-76] [77]. Several explanations have been proposed to underlie the differences between these studies. Firstly there appears to be an age dependent response in which young rats are able to increase capillary number during chronic treadmill training while this angiogenic response is lost in older animals [74-76]. Secondly the intensity of exercise may be of important with reports of capillary growth during moderate intensity but not vigorous training regimes [77]. Thirdly attempts to assess capillary growth in the heart without assessment of myocyte size may have introduced methodological errors to some of the studies by failing to account for any hypertrophic response in the myocardium. Some more direct evidence of angiogenesis following swim training in rats is provided by measures of DNA replication i.e. ^{3}H-Thymidine incorporation into ventricular endothelial cells and capillary pericytes [78]. Capillary growth has also been noted in animals exposed to low oxygen for extended periods of time and in animals raised in cold environments for generations (demonstrating right and left ventricular hypertrophy respectively) [79, 80]. If capillary growth does occur in the physiological model it most likely occurs in response to changes in the mechanical stress experienced on the luminal (shear stress and wall tension) and abluminal (capillary stretch) sides of the vessel. Shear stress (τ) describes the tangential drag force

experienced at the vessel wall during flow and is proportional the viscosity of the blood (n), the velocity of the blood (V) and inversely related to lumen vessel radius (r).

$$\tau = n\left(\frac{4V}{r}\right)$$

Chronic increases in coronary blood flow induced by long term administration of adenosine [81] or dipyridamole (which inhibits adenosine uptake into red blood cells potentiating its biological effects) [82, 83] result in a significant increase in both subepicardial and subendocardial capillary density in adult rabbit hearts. These vasodilators increase lumen radius and elevate luminal shear stress in accordance with the equation presented above. Chronic vasodilation in skeletal muscle through dietary supplementation of prazosin removes the pressor effect of alpha adrenergic signalling, elevates vessel shear stress and promotes new capillary growth [84]. These studies provide some insight into the process linking a change in shear with new vessel formation. Shear induces a form of blood vessel growth known as splitting angiogenesis which is marked by thickening of the capillary endothelium and protrusion of cytoplasmic processes down the centre of the lumen. These protrusions eventually fuse with the opposite end forming two individual vessels. Experiments to confirm the involvement of similar mechanisms in myocardial shear induced capillary growth have not yet been performed.

The most extensive increases in capillary numbers have been reported in studies of long-term bradycardial pacing. Wright and Hudlická (1981) demonstrated that electrical pacing of rabbit hearts to 60% their normal rate results in a significant increase in capillary number (20-40%) [85] and similar findings have been reported in electrically paced pigs [86] and during pharmacologically induced negative chronotropy in the rat [87]. These changes occur on a background of comparable coronary blood flow implying that changes in shear stress do not underlie this growth. Two factors have been proposed to underlie bradycardia induced angiogenesis; 1) changes in the intra-luminal

wall tension and 2) an increase in stretch of the vessel wall. Capillaries have been observed to be wider during the diastolic period of the cardiac cycle and while the velocity of red blood cell flow is reduced the pressure in these vessels does not change significantly. Therefore by applying LaPlace's law, which we have discussed previously in the context of ventricular wall stress, we can see that the tension acting at the capillary wall is much greater during diastole (increase in lumen radius).

$$\sigma = \frac{P \times r}{W}$$

Wall tension is proportionate to the pressure (P) multiplied by the radius (r) for a thin walled sphere. Wall stress (σ) is wall tension divided by wall thickness (W).

Therefore regimes which lower heart rate will increase the length of times spent in diastole and increase wall tension/stress. In addition a prolonged diastole will expose the capillaries to an increase in stretch, a result of an increase in end diastolic filling. The ensuing contraction will also be greater (Frank-Starling law) and may play a role in this form of capillary growth. Skeletal muscle experiments during which extirpation of the postural tibialis anterior muscle results in a stretch/load induced hypertrophy and hyperplasia of the extensor digitorum longus muscle provides an insight into how stretch-induced vessel growth may occur [88]. During so called sprouting angiogenesis, proteases cause the degradation of the basement membrane close to the site of extra vascular stimulus. Endothelial cell proliferation occurs in the surrounding matrix leading to the formation of sprouts connected to surrounding capillary vessels. These sprouts migrate towards the source of the extra vascular stimulus in tandem with endothelial cells. Blind-ended sprouts connect together forming a lumen through which blood can flow. Finally a pericyte layer forms beneath the endothelial cells and lays down a new basement membrane [88].

Importantly experimental evidence suggests a correlation between ventricular capillarity and cardiac performance. Chronic electrical bradycardia induced capillary growth in rabbits and pigs has been associated with an increase in the cardiac output [85, 86] while the pharmacological bradycardic

agents alinidine (inhibitor of I_f current) [89] and metropolol (a β1 selective adrenoceptor antagonist) attenuate the contractile dysfunction associated with myocardial infarction and HF respectively and this occurs on a background of increased capillary number (see Chapter 7).

There is evidence that during pathological hypertrophy growth of the capillary bed is unable to keep pace with the hypertrophy of the myocytes. According to Fick's law an increase in the size of the myocytes and the resulting decrease in capillary density would impact upon the diffusion of oxygen into the tissue. Reductions in capillary density have been noted in models of pressure overload induced by aortic banding and during prolonged exposure to adrenergic agonists, angiotensin II and endothelin. It has been hypothesised that the combination of increased oxygen demand and altered oxygen delivery may play a role in the contractile and metabolic dysfunction of heart failure. Pressure overload increases myocardial oxygen consumption and may result in inadequate coronary perfusion (due to vessel remodelling, myocyte expansion and increased intra-ventricular pressures). Greater demand for perfusion, an increase in vascular resistance and greater distances over which oxygen must diffuse may contribute to a mismatch between coronary perfusion and oxygen supply in the hypertrophied heart. Two studies in the mouse have highlighted a possible link between inadequate neovascularisation and heart failure in experimental models of heart failure. Shiojima *et al* (2005) induced hypertrophy in the mouse heart through transduction of an activated *Akt* (protein kinase B) gene [90]. Akt signalling is thought to be involved in the development of a number of models of hypertrophy including exercise and pressure overload. Shiojima *et al* found that in the acute stage of hypertrophy development there was a concurrent increase in new capillary growth which was associated with the up regulation of specific vascular growth factors known to be involved in angiogenesis (vascular endothelial growth factor (VEGF) and angiopoeitin (ANG-1)). Inhibition of angiogenesis through adenoviral insertion of a gene coding for a decoy receptor of VEGF prevented the increase in capillary number, retarded cardiac growth and resulted in contractile dysfunction during induction of *Akt* hypertrophy. Sano *et al* (2007) published data demonstrating how chronic pressure overload initially promotes angiogenesis and latter suppresses

capillary growth in the mouse [91]. The authors noted an increase in ventricular capillary growth in the first 14 days following banding associated with an increase in the expression of angiogenic factors (VEGF and ANG-1). In prolonged pressure overload this increase in vessel number was prevented by the accumulation of P53 a known inhibitor of hypoxia inducible factor 1 stabilisation (HIF1, see below). Conversely, promotion of angiogenesis through adenoviral mediated induction of VEGF and ANG-1 prevented the development of heart failure in treated mice.

Altered gene and protein expression

HIF1 is composed of one α and one β subunit and regulates the adaptation of cells to low oxygen environments (e.g. increased anaerobic metabolism and new blood vessel formation). In normoxic conditions specific proline residues in HIF1α are hydroxylated allowing its ubiqutination and resulting proteolytic degradation [92-94]. In hypoxia the lack of oxygen inhibits this process allowing for α and β subunit dimerisation and the resulting activation of hypoxia driven gene expression. Chronic pressure overload in rats is associated with an up-regulation of HIF1α protein content in homogenates of cardiac tissue [80]. HIF1α is known to increase the transcription of genes involved in the regulation of capillary and arteriolar growth and, as such tissue, VEGF content is up-regulated in homogenate extractions from aortic banded hypertrophied rat hearts [80]. The apparent drive to improve both capillary and arteriolar supply suggests that there is significant demand for improved oxygen delivery in the hypertrophied myocardium.

Arguments against hypoxia in hypertrophy

Markers of hypoxia

Reports from isolated myocytes suggest that the critical PO_2 below which mitochondrial oxidative phosphorylation will be impaired is between 1 and 2 mmHg. Measuring intracellular PO_2 in the whole heart is not feasible with modern methods and as such a number of alternative oxygen dependent markers are used in the assessment of oxygen tension. Perfusion of hypoxyprobe (pimonidazole hydrochloride), a histological marker of hypoxia, in the hearts of rats with an aortic

banding model of failure show no significant hypoxia in a study by Choi *et al* (2008) [80]. Hypoxyprobe detects any PO_2 below 10 mmHg and has been utilised to show the effects of exposure to environmental hypoxic environments on myocardial oxygenation. Nuclear magnetic resonance spectroscopy can measure the amount of deoxymyoglobin found within the heart. Deoxymyoglobin is formed when the intracellular PO_2 falls below 4 mmHg and studies in failing rat hearts have failed to show significant alterations in the state of this molecule even when hearts were stressed to high workloads with the β1 specific adrenoceptor agonist dobutamine [95]. These indirect measures of oxygen tension are supported by mathematical modelling studies of capillary oxygen supply in the heart. Rakushan *et al* (1984) showed that hypertrophic growth itself should not produce a hypoxic environment within the myocytes but rather changes in the distribution of capillaries towards a more heterogeneous state could produce focal areas of tissue hypoxia [96].

In contrast to the evidence in mice, Flanagan *et al* (1991) have shown that inhibition of angiogenesis during LV pressure overload in the lamb is not associated with any change in ventricular function, compared with sham operated or banded controls [97]. Flanagan *et al* (1991) reported that angiogenesis was important for the maintenance of maximal LV coronary flow, but did not find any change of *in vivo* contractile performance (using intra-ventricular catheter measurements) following the inhibition of of angiogensis with protamine (a reversible inhibitor of bFGF binding).

Net importer of lactate and the effect of workload on substrate uncoupling

Despite the increased rates of glycolysis noted in more severe models of hypertrophy there does not appear to be a concurrent suppression of glucose oxidation. Allard *et al* (1994) have shown that aortic banded hypertrophied hearts oxidise a comparable amount of lactate as controls suggesting that there is no suppression of oxidative metabolism as would occur in a hypoxic environment (due to inhibition of the citrate cycle and the oxidative chain) [38]. In addition Allard and colleagues found that an increase in cardiac afterload both elevates the rates of glucose oxidation and normalises rates of glycolysis between the groups. These data suggest that the uncoupling of glycolysis and

glucose oxidation is not related to low oxygen availability but rather reflect specific alterations to the glycolytic metabolic pathway. The role of various enzymes of glycolysis in the rapid equilibrating transfer of ATP and its hydrolytic products throughout the cell could reflect compensation for the loss of flux through the CK system not necessarily the result of hypoxia.

Non-hypoxic mechanisms drive changes to gene and protein expression

In addition to the oxygen dependent mechanisms regulating HIF-1 activity there is growing evidence of oxygen independent regulation. Of interest to the present study is the induction of HIF1α in response to changes in mechanical stress. Kim et al (2002) found that induction of an aortocaval shunt (volume overload) resulted in the ventricular accumulation of VEGF and HIF1α protein within 1 hour of the operation, changes which were preserved during the 48 hour follow up period [98]. Isolated hearts exposed to ex vivo stretch through the inflation of an intra-ventricular balloon also demonstrated increased expression of HIF1α and VEGF after 1 to 2 hours. Similar results were noted in the non ischemic border regions of rat hearts 2 to 48 hours following left anterior descending coronary artery ligation. In all three of these models these changes in expression appear to be regulated by degree of wall stretch rather than oxygen availability due to their prevention by the stretch activated channel inhibitor gadolinium. Therefore it cannot be assumed that the activation of HIF-1 in hypertrophy is directly related to low oxygen availability as mechanical factors may well underlie these changes.

Thesis aims and layout

The question of what process drives the de-compensation of hypertrophy to heart failure remains to be answered. Despite speculation that mechanical and metabolic remodelling in the heart is an attempt to reduce energy consumption, it is unclear whether this reflects poor oxygenation (a hypoxic environment). On the contrary cardiac oxygenation never appears to be reduced to the critical level which would impact upon mitochondrial oxidative phosphorylation [79, 95]. Despite this there appears to be a drive to increase capillary density during hypertrophy and there is evidence

that inhibition of this process drives well compensated geometric remodelling into a state of failure [90] [91]. This raises the possibility that alterations in oxygen diffusion and/or regional under-perfusion, resulting from the expansion of the myocytes without concurrent vessel adaptation, are responsible for the metabolic and contractile derangement associated with HF. However, no study to date has directly assessed whether modification of these parameters in normal animals can mimic the derangements associated with HF. Studies utilising methods to induce capillary growth in both normal and ischemic hearts also suggest there may be some relationship between cardiac performance and ventricular capillarity, though these studies suffer from their use of *in vivo* measures of performance which are influenced by homeostatic, hormonal and neuronal mechanisms and in which loading conditions cannot be controlled. This aims of the present study were to investigate the impact of alterations in ventricular capillarity on the functional and metabolic characteristics of the isolated perfused beating rat heart.

It was hypothesised that, if cardiac contractile performance and substrate utilisation are directly related to ventricular capillarity then methods to alter the number and distribution of capillaries within theventricle could be utilised to demonstrate this relationship.

This study utilised the Langendorff isolated rat heart. Rats were selected due to their availability, relatively low cost and, most importantly, the vast amount of literature published on the species. The Langendorff preparation allows for the isolation of the heart from confounding neuronal and hormonal factors and permits for strict control of substrate availability and of ventricular workload. The use of crystalloid buffers, which have a low oxygen carrying capacity in comparison to blood, limits the ability of the myocardium to increase oxygen delivery through greater coronary flow (CF) and provides optimal experimental conditions. Despite this it is important to note that oxygen availability exceeds oxygen consumption in these preparations and that the hearts are able to respond for prolonged periods of time to stimuli that dramatically elevate oxygen consumption (e.g. dobutamine). Data supporting these statements are presented in the following chapters. Alterations

in ventricular capillarity were achieved through both chronic pharmacological and/or environmental treatment regimes and acute arteriolar occlusion experiments. Quantification of capillary density and cardiac performance was carried out in the same hearts.

Hearts from the treatment groups were compared to controls over a range of different workloads achieved through modifications in the volume of a fluid filled intra-ventricular balloon (effectively preload and afterload) and also through adrenergic stimulation using dobutamine (a $\beta 1$ specific agonist). Stressing hearts at high workloads should highlight any differences between the treated and untreated groups.

Due to the apparent importance of SERCA down-regulation in heart failure a number of chapters utilised molecular techniques to investigate the impacts of alterations in capillary supply upon SERCA protein expression levels. Treatments were also investigated in terms of their effect on the variance of capillary spacing as mathematical modelling suggests that alterations in the uniformity of capillary spacing will have a greater impact upon oxygenation than uniform cellular growth [38]. Such heterogeneity may upset the carefully controlled balance of supply and demand in the heart whereby some areas of cardiac tissue will have poorer oxygenation than others (i.e. greater diffusion distances). Tissue collagen content has been assessed due to its influence on cardiac contractile performance through modifications of ventricular compliance. Additionally collagen accumulation may impair regional coronary blood flow impacting upon oxygen delivery. Metabolic rates have been assessed using radiolabelled tracer studies which allow accurate quantifiable measurement of substrate oxidation. Histological analysis of capillary supply in certain experiments was also performed in hearts isolated from mice on similar treatment regime and offer support to the primary findings in the rat.

Experimental chapters will be broken down:

- Effects of reduced capillarity on cardiac performance and metabolism. Part 1: Microspheres – This chapter provides evidence of the link between capillary perfusion, contractile performance and rates of metabolism. Acute capillary blockade was achieved through infusion of 15 μm microspheres in the isolated heart. Parameters of contractile performance and metabolic rate before and after microsphere infusion were compared retrospectively to the degree of terminal arteriolar blockade (assessed using histological methods). These experiments look at the relevance of using the crystalloid perfused isolated rat heart in meeting of the primary aims of this thesis.
- Effects of reduced capillarity on cardiac performance and metabolism. Part 2: Isoprenaline – This chapter presents data regarding the chronic effect of reduced capillarity on cardiac contractile performance. Rapid left ventricular hypertrophy was induced in rats through the injection of isoprenaline (a β adrenoceptor agonist). The rapid nature of this model allows for comparison of hearts from a short (3-day) and long term (10-day) treatment regimes before and after capillary growth has had time to occur.
- Effects of reduced capillarity on cardiac performance and metabolism. Part 2: L-NAME – Data is presented on the effects of supplementation of animal drinking water with N (G)-nitro-L- arginine methyl ester (L-NAME), a non-specific nitric oxide synthase blocker, on cardiac morphology and contractile performance.
- Effects of increased capillarity on cardiac performance and metabolism. Part 1: Cold acclimation – Data is presented on the effects of 4 weeks of cold acclimation on cardiac morphology and *ex vivo* contractile performance.
- Effects of increased capillarity on cardiac performance and metabolism. Part 2: Atenolol – In this chapter chronic β adrenoceptor blockade was utilised to promote capillary growth in the left ventricular wall of the rat heart. The impact of these changes on contractile function and metabolic rates at a number of workloads was investigated.

- Modulating substrate metabolism and capillary supply in the hypertrophied heart – This chapter presents data on attempts to modify substrate metabolism and ventricle capillarity in the cold acclimated model of hypertrophy and their effects on ventricular contractile function and substrate metabolism.

Chapter Two: Material and Methods

Animal welfare and regulations

Animals for this study were used in accordance with the animal welfare regulations of the U.K Animal (Scientific Procedures) Act of 1986. Experiments were performed on male Wistar rats (an albino strain of *Rattus novegicus*) or male C57/BL6 mice (Charles Rivers). All animals were provided with food pellets (SDS RM3 diet, Lillico) and water *ad libitum*. Cage temperature was maintained at 21 $\pm$ 2^{o}C. Photoperiod was maintained in a 12:12 light:dark cycle. Animal weights were recorded twice weekly during which cage cleaning took place.

Treatment regimes

Water dissolved treatments were based on an average water consumption of 10 ml water per 100 grams body weight per day [99, 100]. These values are applicable to both rats and mice. Details of specific treatments will be reported in the relevant chapters along with references to support dose selection. Sucrose was added to all water-based treatments at a concentration of 5g/L drinking water (0.5% w/v) in a bid to disguise the taste of the drugs used.

Experiments in the rat

Surgical Procedures

Anaesthesia

Animals were anaesthetised using Isoflurane® at a concentration of 5% in $O_{2.}$ Initial of anaesthesia gas chamber was carried out using flow rates of 4 l/min; this was reduced to between 1.5 and 2 l/min for the maintenance of anaesthesia on the mask.

Assessment of heart rate and arterial blood pressure (in vivo)

In vivo parameters of heart rate and arterial blood pressure were assessed through cannulation of the right femoral artery. The right femoral artery and vein were then located and isolated from one

another and the surrounding connective tissue. The right femoral artery was cannulated with a vinyl cannula (OD = 0.80 mm, ID = 0.40 mm, Portex) containing normal saline (0.9% NaCl w/v), which was inserted until the tip of the cannula lay at the bifurcation of the inferior vena cava. This cannula was used to allow direct measurement of arterial blood pressure via a pressure transducer (type 4-4222 Bell & Howell Ltd., UK). The blood pressure transducer was calibrated regularly with a mercury sphygmomanometer.

Thoracotomy

An initial incision was made from the midline, inferior to the sternum, to expose the diaphragm and abdominal cavity. Bilateral incisions were made in the diaphragm to allow access to the thoracic cavity. The thorax was opened by removing the rib cage from the level of the diaphragm to the level of the clavicle. Using the tissues of the lung and oesophagus as support the heart was excised the thoracic cavity and these tissues were quickly placed in ice-cold Kreb Hensleit solution (in mM, 120 NaCl, 4.8 KCl, 25 $NaHCO_3$, 1.2 $MgSO_4$, 1.2 KH_2PO_4, 1.3 $CaCl_2$, 11 mM glucose) for the remaining surgery. 0.5 ml of heparin sulphate (500 Units) was added to each 25 ml of buffer used. The tissues were dissected to remove the lungs, oesophagus and thymus exposing the heart and great vessel architecture.

Langendorff perfusion

The heart was isolated and any excess tissues (e.g. lungs) were trimmed away. In order to expose the underlying aorta arch the thymus was split in two and carefully removed from the heart. The aortic arch was de-roofed allowing the aorta to be cannulated. The heart was secured using clips and then suture material and was perfused, at a constant head of pressure (80 mmHg), with a warmed (37^oC) Krebs Hensleit buffer containing (in mM) 120 NaCl, 4.8 KCl, 25 $NaHCO_3$, 1.2 $MgSO_4$, 1.2 KH_2PO_4, 1.3 $CaCl_2$, 11 glucose and gassed with 95% O_2, 5% CO_2 (pH = 7.4). A small incision was made through the right ventricular wall in order to aid drainage. Adipose tissue was carefully trimmed away in order to uncover the left atrial appendage. The appendage was removed to allow the passage of a water filled balloon through the atrial-ventricular valve into the left ventricular (LV)

lumen. The balloon was attached to a solid-state pressure transducer and a bridge amplifier for recording of LV performance. Balloon volume was adjusted to give the minimum balloon volume required to record a left ventricular developed pressure (LVDP) of above 10 mmHg. Data from the pressure transducer was recorded at 1 kHz at a sensitivity of 10 mV using a 4 channel MacLab system in combination with the bundled Chart software (Version 5.0, ADI Instruments).

Assessment of LV contractile performance

For assessment of *ex vivo* cardiac performance at different workloads, the balloon volume was increased at 50 μL increments until a maximal systolic pressure of 200 mmHg was reached. Functional recordings were made until the trace had adjusted to a new baseline for a period of 1 minute (i.e. constant measures of diastolic and systolic pressure). Data from the pressure transducer allowed measurements of heart rate (HR), LV peak systolic pressure, LV end diastolic pressure (LVEDP), LV developed pressure (LVDP), rate-systolic pressure pressure product (RPP) and the rate of change of pressure (+dP/dt and -dP/dt). RPP is simply the product of the heart rate multiplied by the peak systolic pressure and is a measure of the total external work. The rate of change of pressure (dP/dt) can be calculated from the slope of the lines produced on the pressure traces (Figure 2.1). +dP/dt, being independent of changes in preload and afterload, provides information on the intrinsic contractility of the LV and is related to heart rate, developed pressure and ventricular compliance (Figure 2.1). –dP/dt can be used as a measure of the active relaxation component of the cardiac cycle, largely reflecting calcium handling, but also ventricular compliance. A minimum period of 30 seconds was used in the calculation of each functional parameter. Total coronary flow was estimated from the perfusate outflow from the heart and was calculated from the time taken to fill a known volume (0.93 ml). The curve produced from plotting diastolic pressure against balloon volume allows for the estimation of LV unstressed lumen volume, from the x intercept of the linear portion of this relationship (Figure 2.3) [101], as well as a measure of LV stiffness, Δpressure/Δvolume, from the same region (Figure 2.3) [5]. Values of unstressed ventricular volume utilising this method are similar to those obtained by serial cine-magnetic resonance imaging [102].

LV systolic stress-strain

By definition the Langendorff protocol measures LV chamber function and as such is affected by both the intrinsic contractility of the myocardium and also the geometric arrangement of the myocardial fibres. Systolic stress strain relationships allow for an estimate of the true contractile function of the myocardium normalizing for wall thickness and chamber dimension. Circumferential systolic wall stress (σ) and Langrangrian strain (ε) can be calculated from the following equations assuming a spherical geometry of the left ventricle.

$$\sigma = [1.36\ P\ V^{2/3}] / [(V + V_m)^{2/3} - V^{2/3}]$$

$$\varepsilon = \{[V^{1/3} + (V+V_m)^{1/3}] / [V_o^{1/3} + (V_o + V_m)^{1/3}]\}$$

[103]

Where V_m is equal to muscle volume (=0.943 LV mass), V is equal to intraventricular balloon volume and P to isovolumetric LVDP. Systolic function is assessed from the slope of this relationship (Figure 2.4).

Dobutamine inotropic challenge

Balloon volumes were adjusted to give a constant diastolic pressure (20mmHg) and performance was recorded. Perfusate was then switched to one containing dobutamine (final concentration 150 nM) and performance characteristics were again recorded until a steady state response was achieved. An example trace of the inotropic response to dobutamine simulation is shown in Figure 2.2. Following completion of the protocol hearts were frozen either for metabolic studies, protein analysis or histology (see relevant protocols).

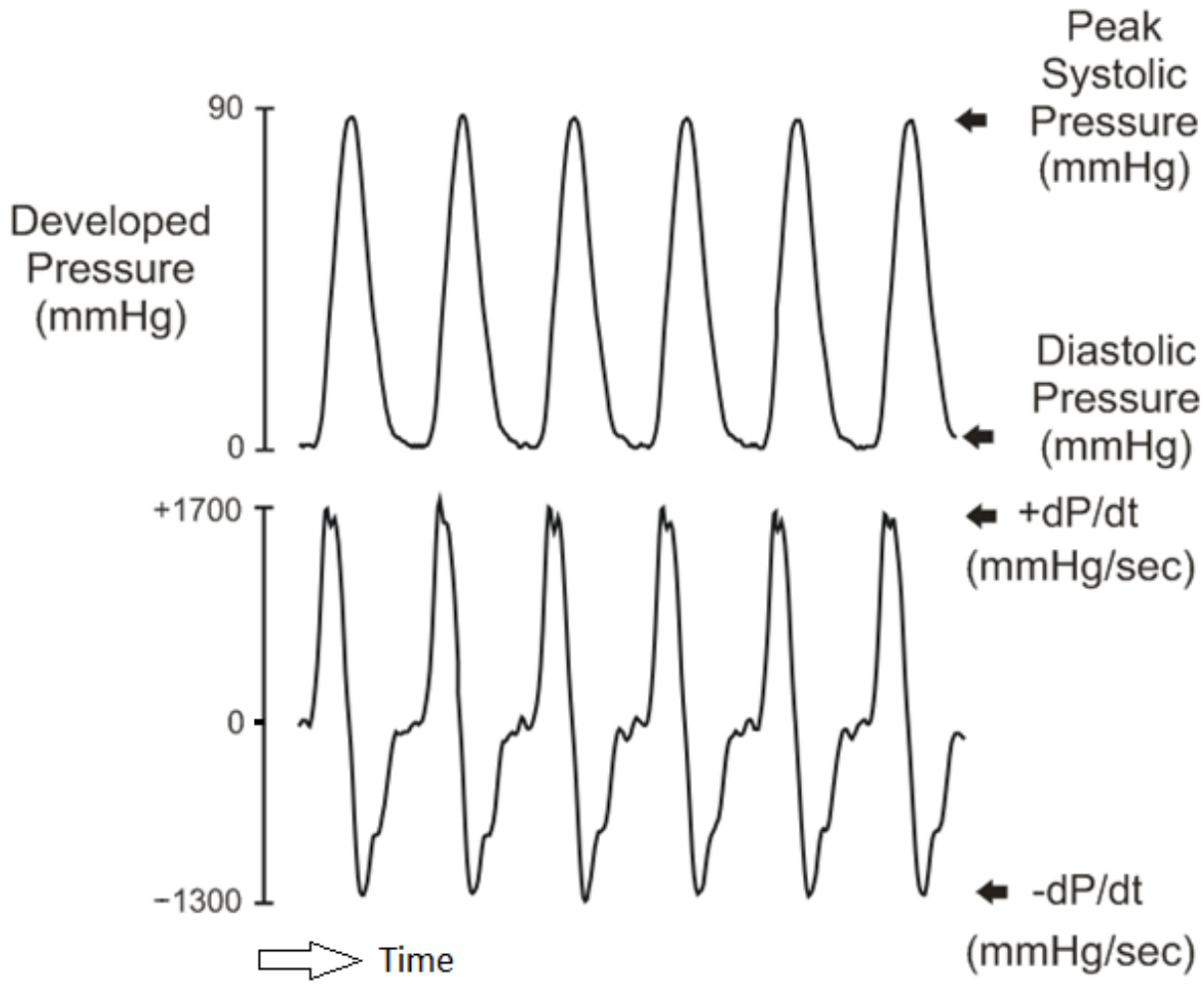

Figure 2.1. Factors measured during assessment of left ventricular contractile performance. The pressure trace was recorded directly from the transducer and allowed calculations of various variables. HR was assessed by mean average of the number of peaks in at least a 1-minute of trace. LVDP was measured difference between the diastolic and systolic pressures. Maximal (+dP/dt) and minimal (–dP/dt) rate of change of pressure was calculated from the first order derivative of the pressure wave.

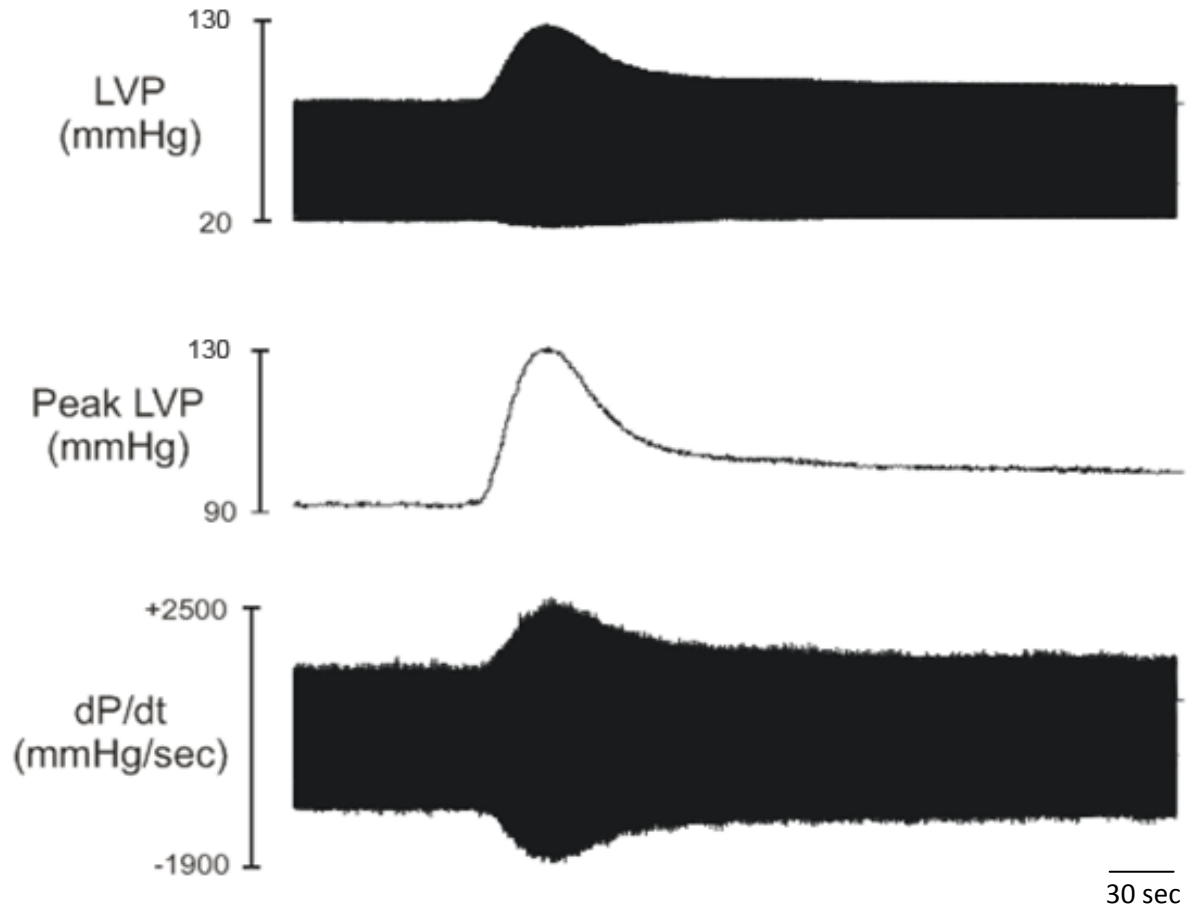

Figure 2.2 Example raw data trace following addition of dobutamine (150nM) to the perfusate of a Langendorff isolated beating rat heart preparation. Legend: LVP = Left ventricular pressure, dP/dt= rate of change of pressure.

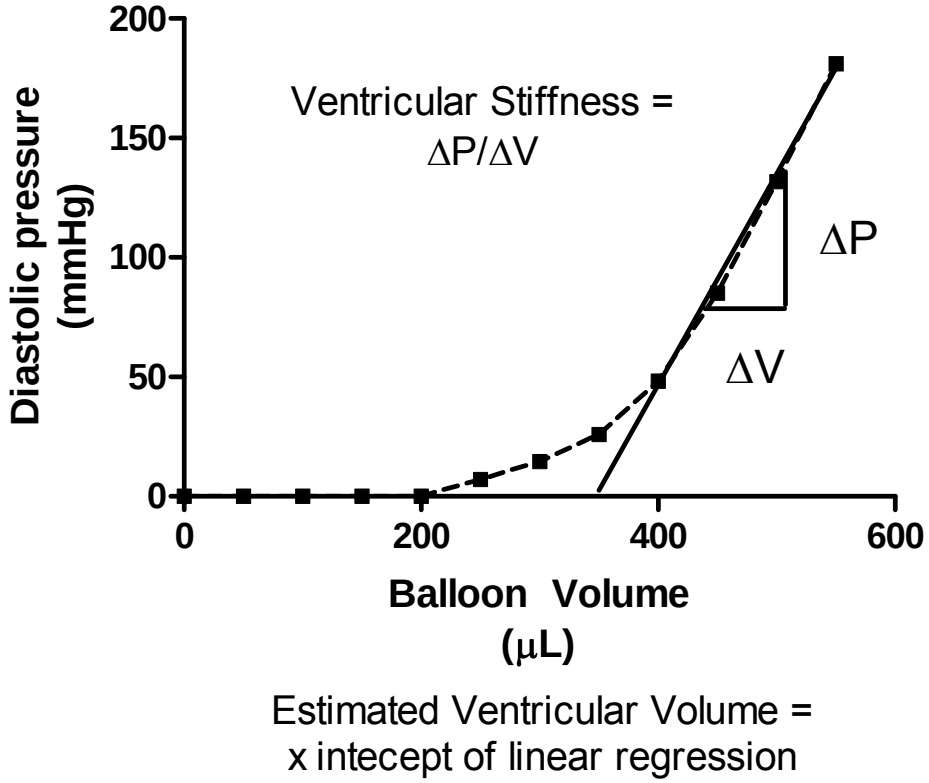

Figure 2.3 Calculation of intraventricular volume and ventricular chamber stiffness from the diastolic pressure-volume relationship. Ventricle volume is calculated from x intercept of the linear portion of this relationship and ventricular chamber stiffness as the change in pressure divided by the change in volume in the same region.

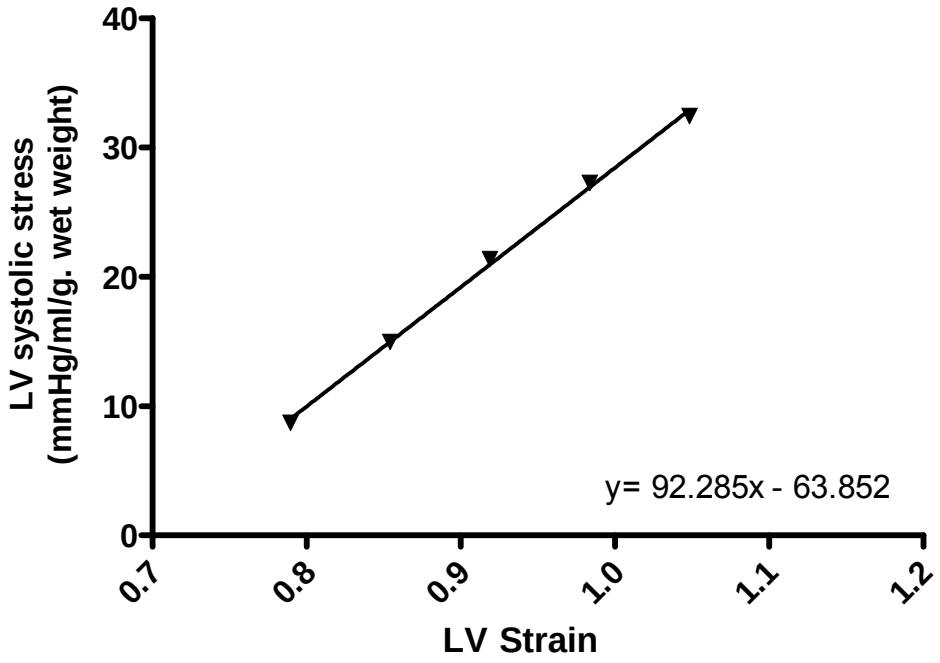

Figure 2.4 Systolic stress-strain relationship. Myocardial contractility is measured from the slope of this relationship.

Assessment of substrate metabolism

Assessment of rates of metabolism and tissue concentrations of specific metabolites have been carried out according to previously described methods [104-106] or using commercial available kits. Where kits have been used reference is made to the supplier, product code and protocol used.

Glucose and FA substrate preparation

In order to prevent cardiac toxicity the FAs used in this experiment were pre-bound to albumin. The following protocol explains the steps taken to prepare the glucose and FA substrates used for estimating metabolism in the isolated heart.

1) 1-gram of fatty-acid free bovine albumin (A6003, Sigma) was dissolved in 10 ml Krebs-Hensleit buffer.
2) 16.92 mg of Oleate FA sodium salt was added to 2 ml saline solution (0.9%w/v NaCl) and gently heated to solution (60^0C).
3) The albumin and heated FA were mixed together and left for 15 minutes to allow the albumin and FAs to bind.
4) 25 μL of radiolabelled FA (5.1 mCi) (^{3}H-oleic acid, Amersham) was transferred to a dry test tube and the solvent component allowed to evaporate. 200 μL alkali (0.1M potassium hydroxide) was added to the dry tube to saponify the FAs.
5) The FA labelled tracer component and the albumin-FA mixture were mixed and allowed to bind for 15 minutes.
6) 50 μL of radio-labelled glucose (D-[^{14}C)Glucose, Amersham (250 μCi)) was added to the solution.

This procedure provides a physiologically relevant final FA concentration of 0.4 mM (in 150 ml of perfusate). Glucose was provided in the Krebs Hensliet buffer at a concentration of 11 mM.

Experimental Protocol

Starting with a perfusate volume of 200 ml (Krebs Hensliet buffer containing 10 mM glucose/1.6 mM $CaCl_2$) the heart was perfused as described previously. A fluid filled balloon was inserted into the LV and its volume adjusted to give a stable resting diastolic pressure of 20 mmHg (stabilisation period of 10 to 20 minutes). Perfusate volume was then adjusted to 150 ml. A gas collection apparatus was set up to draw air out of the apparatus into the CO_2 trap, for sampling during the protocol. All entry and exit points in the apparatus were sealed to prevent gas exchange with the environment. The FA and labelled glucose were added to the reservoir and allowed to mix throughout the apparatus (5 to 10 minutes were allowed for adequate mixing).

Over the 60 min course of this experiment a number of different samples were taken (starting at time point zero and at 10 minute intervals for 60 minutes). At time point zero 3 x 0.5 ml samples of perfusate were transferred to individual scintillation vials and mixed with 5 ml of scintillation cocktail. These samples were used for the calculation of specific activity (SA) for both glucose and FA in the perfusate. Activity counts from each protocol described below were used in the calculation of total oleate and glucose oxidation at each time point with corrections for any dilution steps and for the reduction in perfusate volume. The slope of the linear regression of all time points over the 60-minute period gives the rates of oxidation for each sample.

Estimation of FA metabolism through the production of tritiated water

Complete oxidation of ^3H-labelled lipids during metabolism results in the production of tritiated water ($^3H_20$), and this can be used to determine rates of FA metabolism within the heart. Before this can be achieved it is vital to isolate the tritiated water from the remaining tritium-labelled lipids within the perfusate. This is achieved by use of a simple solvent extraction [38, 107, 108]

(1) At ten-minute intervals (starting at time point 0) 1 ml of perfusate is extracted to clean dry solvent tubes.

(2) A total of 20 ml of Folch reagent (choloroform:methanol, 2:1) was added to each sample and mixed vigorously.

(3) Following this 4 ml of distilled water were added to each sample and mixed vigorously to produce an emulsion that separated into two distinct stages.

(4) The aqueous layer (top) contained the tritiated water component and was decanted in 0.5 ml samples to scintillation vials. Scintillation cocktail was added to the vials at a ratio of 10:1 (5 ml).

(5) The activity of each sample was then analysed using a scintillation counter (BetaScint 2500, Perkin Elmer).

Estimation of glucose metabolism from ^{14}C-labelled substrates.

Measurement of the breakdown products from ^{14}C-labelled substrate in this experiment gave a direct measurement of glucose oxidation rate. Use of the aqueous perfusate presents a problem in that CO_2 can either be extracted as a gas or can be buffered in the perfusate to HCO_3^-. In order to properly estimate the amount of glucose metabolism that had occurred we therefore had to measure both components of this equilibrium. Total glucose metabolism can be calculated by addition of the bicarbonate values to the cumulative value produced for CO_2 extraction (see below). [38, 108]

Measurement of glucose metabolism from gaseous effluent

Over the course of the 60 min experiment exhaust gas was extracted and bubbled through 150 ml of CO_2 trapping agent (ethnolamine/ethelene glycol mixture (2:1)). Two 0.5 ml samples of CO_2 trapping agent were taken at 10 min intervals (starting at time point zero) and added to 5ml of scintillation cocktail. Analysis of these vials using a scintillation counter allows quantification of the CO_2 production during the experiment, and directly related to the metabolic breakdown of radiolabelled glucose. As the total starting glucose concentration was known, we used these scintillation counts and the SA to estimate the oxidation of glucose at various time points.

Measurement of glucose metabolism from aqueous HCO3-

Seven Erlenmeyer flasks were prepared for each experiment; these are conical flasks with a separate central well. The central well was filled with 1 ml of CO_2 trapping agent and the area outside the well with 2.0 ml of 7M H_2SO_4. The Erlenmeyer flasks were sealed from the external environment using a rubber septum. Starting at time point zero, and at proceeding 10 min intervals, 1 ml of perfusate was rapidly transferred from the Langendorff preparation into the acid surrounding the central well. This leads to acidification of the perfusate and the conversion of any $H^{14}CO_3^-$ to $^{14}CO_2$ which diffuses into the trapping solution. Following completion of the experiment, the Erlenmeyer flasks were incubated for at least two hours (37^oC) before recovering the trapping agent from the central well. This solution was transferred to a scintillation vial and mixed with 10 ml of scintillation cocktail and analysed for its radioactive content.

Tissue grinding (for tissue lipids)

Sample preparation

- Using a pestle and mortar, pre-cooled with liquid nitrogen, an aliquot of the tissue was ground into a fine powder.
- Between 100 and 150 mg of this powder were decanted into a glass extraction tube and mixed vigorously with 20 ml Folch solvent (chloroform/methanol 2:1).
- To ensure adequate breakdown of the tissue each sample was homogenised using a Polytron blade homogeniser. The blade was washed in Folch solution following each sample to prevent contamination.
- A total of 5 mls of water were then added to each of the samples. The resulting solution was vigorously mixed and left to stand until it had separated into 2 phases.
- The lower solvent fraction was then recovered and transferred to a clean dry test tube. This solvent layer was allowed to evaporate off leaving the dried sample at the bottom of the test tube.

Preparative Thin Layer Chromatography (TLC) [107]

Preparing and running the plate

- Solvent with a composition of: hexane/diethyl ether/acetic acid (70:30:1.6) was prepared and left to equilibrate with the atmosphere in the TLC tank.
- Silica gel chromatography plates (thickness 250 μm) (Whatman, Cat. 4860-820) were scored to provide 7 lanes. 6 samples and a final lane for the TLC standard.
- Samples were re-suspended in 200 μL chloroform and spotted across the entire width of one lane, 2 cm from the bottom of the plate.
- Each sample was further washed with 200 μL of chloroform and spotted again on the appropriate sample lane.
- A total of 20 μL of standard consisting of diacylglycerol, FA, triacylglycerol and cholesterol esters at a concentration of 0.1mg/ml was transferred to the final empty lane.
- The completed plate was placed in the TLC tank such that the sample spots remained above the level of the solvent layer, preventing dissipation of loaded fats into the solvent. The solvent was allowed to elute up the plate.
- The plate was removed from the tank when the solvent had travelled ¾ of the length of the plate and allowed to dry in a fume cupboard.

Recovery of separated lipids from TLC plate

- Each TLC plate was then minimally sprayed with pre-prepared rhodamine B solution.
- Once dry, each plate was moved to a darkened room where a UV light source allowed visualisation of the lipids.
- TLC standard was used to identify lipids in the samples. These bands were found in the order (from the origin upwards) phospholipids, diacylglycerol, FAs, triacylglycerol, and cholesterol esters.

- Using a single sided razorblade each of the lipid fractions were mechanically recovered and transferred to pre-labelled scintillation vials.
- Then 10 ml of scintillation cocktail was added to each vial. These samples were shaken and transferred to the liquid scintillation counter for analysis.
- The incorporation of ^{3}H-oleate into each of the lipid components was calculated using the SA for each sample with corrections for mass and for any dilution steps.

Total tissue triglyceride assay

- Samples were prepared by the pre-described tissue grinding protocol and the extracted lipids were evaporated to dryness. To the dry tubes 100% (v/v) ethanol was added to a final tissue concentration of 100mg/ml of ethanol.
- A commercial kit (Trinder method) was used for the estimation of total tissue triglyceride concentration with minor alterations to the instructions provided (TR210, Randox, Ireland). The assay was initiated with the enzymatic hydrolysis of the triglycerides by lipase to produce glycerol and free FAs. The glycerol released was subsequently measured by a coupled enzymatic reaction system with a colorimetric readout at 540 nm.

- A total of 200 μL of TAG reagent was added to each well of the 96-well plate along with 10 μL of sample, blank or standard (provided in the kit).
- The plate was then incubated at room temperature for 10 minutes. Absorbance was measure on the plate reader at 500 nm with reference to standard.

Total tissue glycogen assay

- Between 25 to 50 mg of frozen tissue sample was alkali digested at 70^{o}C in 200 μL of 30% KOH for two hours.
- Then 4 volumes of absolute ethanol were added to each sample and left over night in the fridge to allow the glycogen precipitation.

- Samples were centrifuged at 10000 rpm for 10 min.
- The resulting supernatant was discarded. The pellet was re-dissolved in 200 μL distilled water. 4 further volumes of absolute ethanol were added and the samples again left to precipitate in the fridge before spinning the next day. This process was repeated 3 times to remove all low weight molecular metabolites, leaving glycogen.
- After the final wash the air-dried pellet was re-dissolved in 200 μL of distilled water. An aliquot (50 – 100 μL) of this was counted directly for radioactivity in order to assess the 1 hour incorporation of ^{14}C-glucose into glycogen.
- The remaining sample was digested into glucose units through the addition of alpha-amylo-glucosidase enzyme dissolved in sodium acetate solution (2000 U/ml and 50 μL per sample, pH 4.5). These samples were left to digest over night.
- Total glucose concentration, and thus glycogen, was estimated using a commercial kit (Glucose oxidase kit, Thermo-Electron, Australia), following the protocol as described.

Histological Procedures

Tissue Sampling

Following completion of the Langendorff protocol, hearts were perfused with KCl solution (200 mM) to invoke contracture and the whole heart was cleaned of excess connective tissues and weighed. The left ventricular free wall was excised and weighed. A segment of muscle from the LV free wall (containing both endocardium and epicardium) was then taken and embedded on a pre-labelled cork disk using an inert mounting medium (Tissue-Tek, OCT) and frozen in isopentane (2-methylbutane) followed by cooling in liquid nitrogen (-190^{o}C). For studies in the mouse the thoaracic cavity was opened and the entire heart removed, weighed and embeded base down on a cork disk. All tissues were stored at -80^{o}C until they were used for histological analysis. Cryostat sections of 10 μm thicknesses were cut at -20^{o}C using a Bright 5030 microtome and were placed onto polylysine

coated microscope slides. Sections were collected at 200 μm intervals through the LV free wall providing 8 to 10 slides per animal.

Histochemistry, staining procedures and image collection

Lectin

Lectins are plant proteins that bind to specific sugar residues, in this case to galactose residues, which are found at high concentrations on the proteoglycans in the glycocalyx that lines the blood vessels. Therefore fluorescent conjugated lectins can be used to assess capillary numbers in left ventricular sections. The sarcolemma of muscle fibres is also faintly stained which allows quantification of myocyte number and size. Lectin staining is visible as fluorescence when stimulated by ultra violet light. [109]

Slides were left to dry for 30 min before being fixed in ice-cold acetone for 1 minute. A total of 10 μL of 1 M calcium solution was added to 100 ml of phosphate buffered saline (PBS) solution (Sigma). Fluorescence-conjugated *Giffonia simplicifolica* lectin (RL-1102, Vectorlabs, Ireland) was added to this stock buffer at a ratio of 1:100. The slides were stained in this solution for one hour before being rinsed in three times in PBS solution. Slides were mounted in Vectashield (H-1000, Vectorlabs, Ireland) and sealed with a coverslip. Care was taken to avoid any unnecessary exposure to light during and after this technique, due to the fluorescent nature of the stain. Pictures of the subendocardial (n=8-10) and subepicardial (n=8-10) regions of the heart were captured digitally on a Zeiss microscope system using the built in software (Axiovision v.4) at a total magnification of x500 (eyepiece x10, objective x40, and drawing arm x1.25). Images were only taken from areas cut in good cross section.

Massons trichrome with aniline blue

Massons trichrome is a combination of four different stains which has been used in the present study for the quantification of ventricular collagen content. Weigert's iron haemotoxylin stains for nuclei, picric acid for erythrocytes, a mixture of acid dyes highlight the cytosol and aniline blue

allows visualization of the connective tissues. A pre-prepared kit (010902, Bio Optica, Italy) was purchased and used according to the supplied instructions.

Sections were briefly submerged in distilled water. Equal amounts of hematoxylin solutions A and B (3 to 4 drops of each) were added to each slide and left to act for 10 minutes. Without washing slides were drained and covered with 3 to 4 drops of picric acid alcoholic solution (left for 4 minutes). The slides were quickly washed in distilled water and covered with 3 to 4 drops of ponceau acid fuchsin solution (4 minutes). The slides were quickly washed in distilled water and covered with 3 to 4 drops of phosphomolybdic acid solution (10 minutes). Without washing slides were drained and covered with 3 to 4 drops of aniline blue solution (left for 5 minutes). Slides were washed and rapidly dehydrated through ascending alcohols (70, 80, 90, 95, and 100%). Slides were cleared in xylene (x2) and mounted in histomount (xylene based mounting solution). Pictures of the subendocardial (n=6-8) regions of the heart were captured digitally on a Zeis microscope system using the built in software (Axiovision v.4) at a total magnification of x125-250 (eyepiece x10, objective x10 or x20, and drawing arm x1.25).

Quantification of images

Blinding of counts

Images were randomised before quantification in an attempt to reduce possible bias within the sample populations.

Capillary density, capillary-to-fibre ratio and myocyte cross-sectional area

A square lattice of known area (calculated using a slide graticule) was superimposed on each image (Figure 2.5). Capillaries and myocytes were counted within this region excluding those touching the pre-defined bottom and left hand side of the lattice. This histological process is known as Gundersens rule and is a useful correction when calculating the area of constituents within a counting frame (this rule also reduces the possibility of double counting bias when serial images are taken across the length of a tissue sample) [110]. A point count method was applied to correct for

gaps in the section when appropriate and was performed on phase contrast images captured from the same region as the fluorescent lectin stain. Capillary density (CD) defined as the number of capillaries per unit area of tissue (capillaries/mm^2) was calculated as...

$$CD = \frac{n}{A(1-(\frac{Ce}{Ct}))}$$

Where n is the number of capillaries, A the area of the counting lattice, Ct the total number of points in the lattice (excluding the left and bottom edge) and Ce the number of points of the lattice touching empty space. Myocyte cross-section area (CSA) was estimated as...

$$CSA = \frac{A(1-(\frac{Ce}{Ct}))}{f}$$

Where f is the number of myocytes. Given that hyperplasia does not occur in the adult myocardium the ratio of the number of capillaries to the number of myocytes was used in each section and gives an indication of true capillary growth/regression. CD will be influenced by both changes in capillary number and alterations in myocyte CSA.

Morphometric analysis of the capillary bed

In addition to the aforementioned histological techniques morphometric analysis was used to look at the heterogeneity of capillary spacing within the ventricle and was carried out on in house software (Oxygentransport, GA Gaffney, Oxford University). Binary images of capillary numbers were produced from the digital images captured previously. The shortest point between each given capillary and its surrounding capillaries were measured producing a Delaunay triangulation (Fig 2.6B) and a value of mean nearest neighbour distance (mean NN). By taking the average squared deviation of each NN distance from the mean we can get an estimated of how spread out a distribution is (i.e. variance). Comparisons of the variance within a population of animals were used to estimate the uniformity of capillary spacing and so compare the effects of treatment on this parameter.

Ventricular collagen content

A coherent square lattice of known area was superimposed on each image and a point count methodology utilised to assess the percentage of each sample occupied by collagen (Figure 2.7). Collagen content (FIB) was calculated as...

$$FIB\ (\%) = \left(\frac{Cf}{Ct - Cs}\right)100$$

Where Cf is the number of lattice points touching collagen.

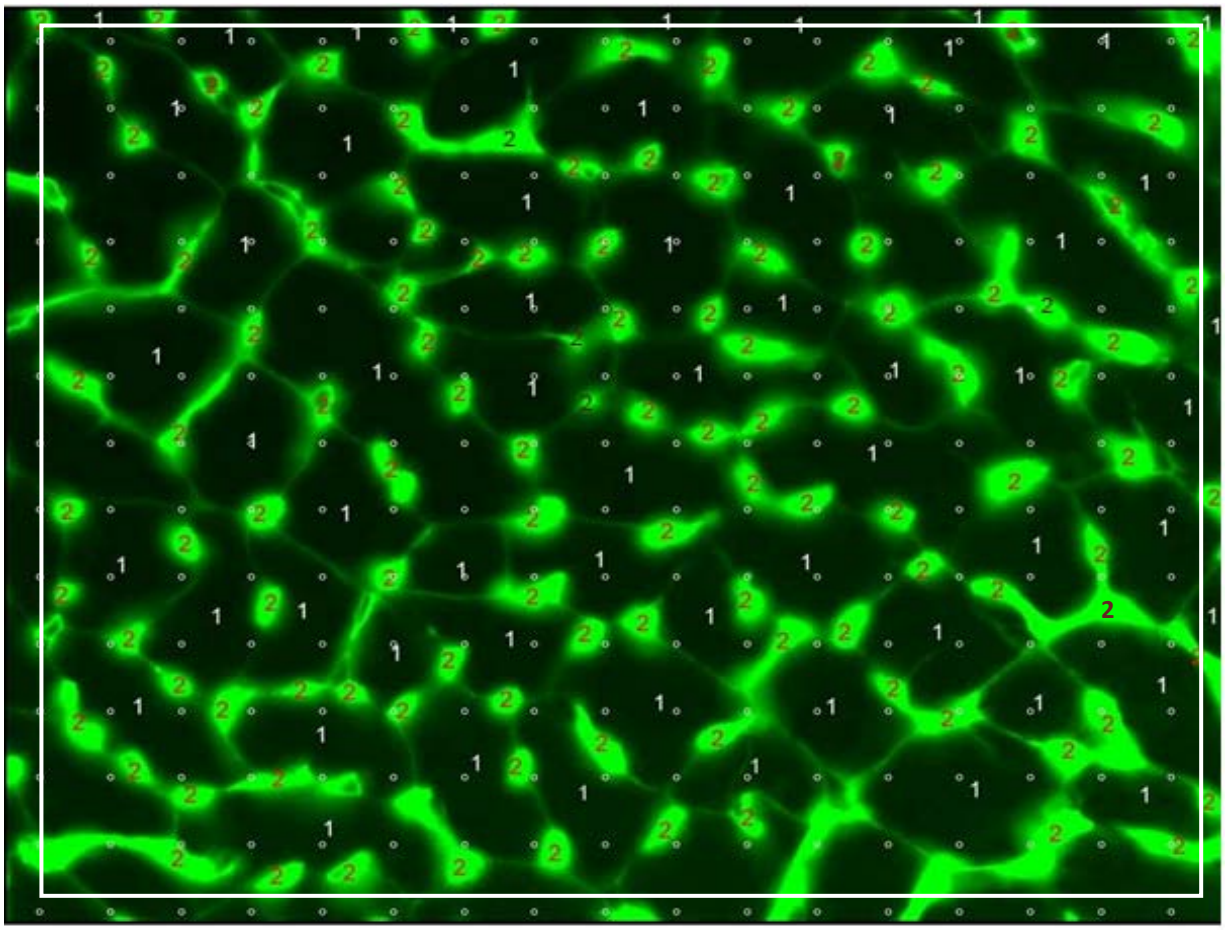

Figure 2.5. Example of lectin stain and counting procedure. Legend: 1=Myocyte, 2=Capillary. Region of interest is defined by the white border. Capillaries and myocytes which interact with the bottom and left hand border were excluded from counts in keeping with Gundersen's edge-counting rule. Magnification=x500.

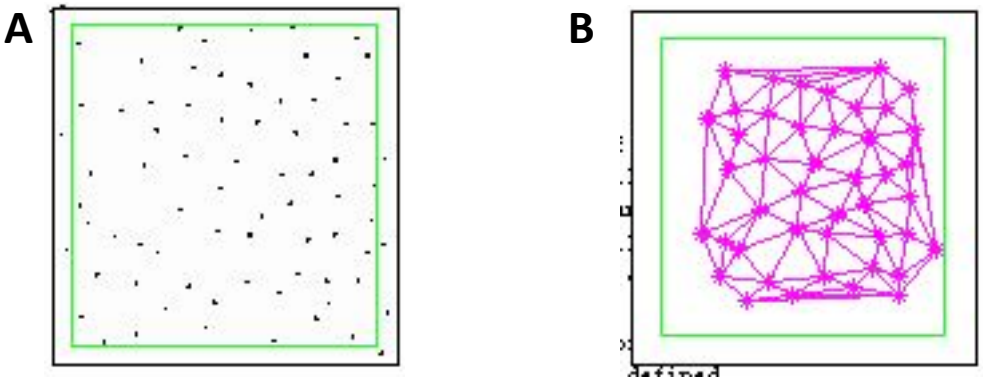

Figure 2.6. Capillary distribution analysis. Example binary capillary count (A) and nearest neighbour calculations (Delaunay triangulation) (B).

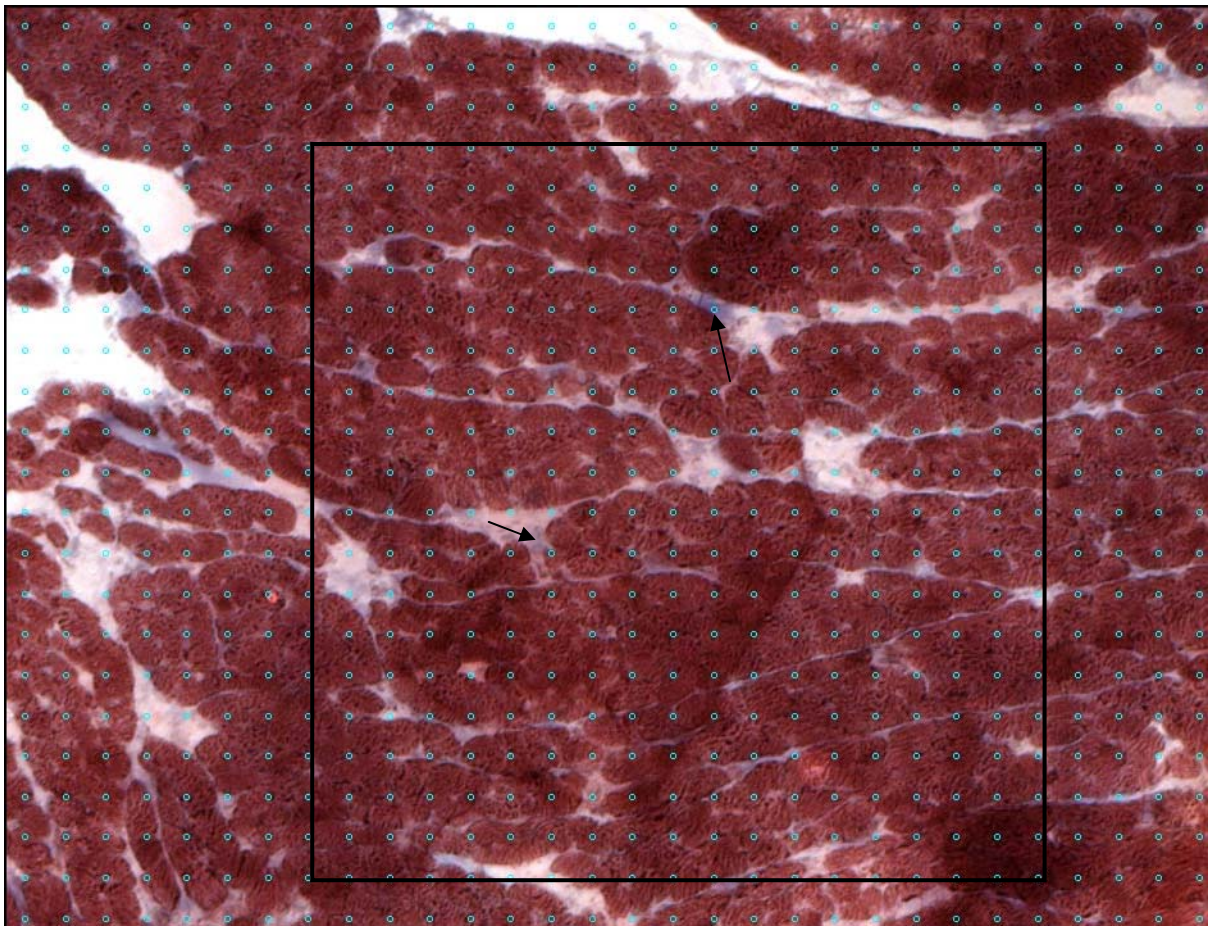

Figure 2.7. Example of Massons trichrome stain and counting procedure. Region of interest is defined by the black border. Collagen is shown in blue (see arrows) and the myocytes in red. Magnification=x125.

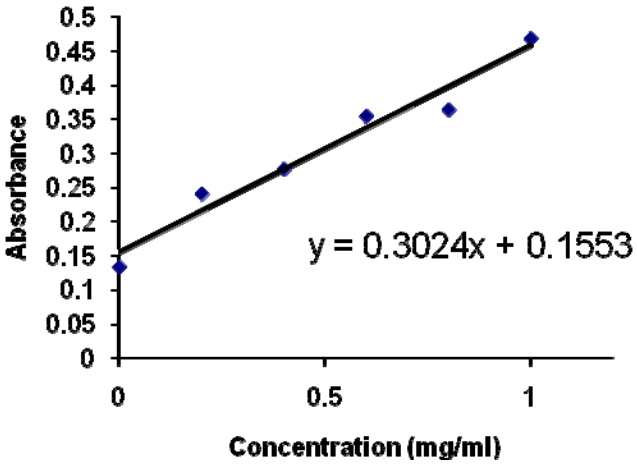

Calculations:

Absorbance of sample = 0.417

0.417 = 0.3024x + 0.1553

0.417 – 0.1553 = 0.2617

0.2617/0.3024 = 0.87 mg/ml

1 in 8 dilution so 0.87 x 8 = 6.92 mg/ml

Figure 2.8. Example of BSA standard curve and calculations used to quantify sample protein concentration.

Assessment of SERCA2a protein expression

Gel electrophoresis was utilised to separate proteins based upon their molecular weight and western immuno blotting was used to visualise the expression of SERCA2a with specific antibodies to that protein. The methods used are described in detail below.

Protein extraction

Frozen tissue samples were ground to a fine powder on liquid nitrogen cooled metal block and transferred to scintillation vials containing 1ml of sample buffer. This buffer contains a number of salts (TRIS 25mM, NaCl 50 mM) and detergents (NP-40 1% (w/v), deoxycholate 1% (w/v), SDS 1% (w/v)) employed to encourage lysis of cells and solubise the proteins. Also included in the buffer was phenylmethanesulfonyl fluoride (PMSF, P7626, Sigma) a protease inhibitor which prevents degradation of the proteins by the tissue's own enzymes. Samples were quickly homogenised and centrifuged for 10 minutes at 16000g (4^{o}C). The supernatant was recovered and transferred to a clean eppendorff before being frozen and stored at – 80^{o}c. By performing all these steps on ice protein denaturation should be kept to a minimum.

Protein concentration determination

Protein concentration determination is required to ensure that equal concentrations of protein are loaded into the polyacrylamide gel. The bicinchonicinic acid (BCA) assay is an extremely sensitive colorimetric assay used for this purpose. The first step of which is the chelation of copper with proteins in an alkaline environment forming a light blue complex (known as the Beirut reaction). Secondly BCA reacts with the reduced copper cation formed in step one to form a purple colored reaction product. The BCA/copper complex is water-soluble and exhibits a strong linear absorbance at 562 nm with increasing protein concentrations. Bovine serum albumin at concentrations of 0-0.5 mg/ml was added to a 96 well plate producing a standard curve of absorbance against concentration. Then 10 μL of each protein sample was loaded into the plate in triplicate; these samples were diluted to concentrations found within the linear portion of the BSA protein assay (a 1

in 8 dilution from the stock concentration). Samples of protein extraction buffer blanks were also quantified. A total of 200μL of working buffer were added to each well (1:50 copper sulphate solution (4%):BCA), mixed gently and stored at 37^{o}C for 30 minutes. Absorbance was read at a wavelength of 562nm. Sample concentrations were calculated from the BSA standard curve using absorbance values (taking into account any dilution factors) (Fig 2.8). Aliquots of sample were prepared at a concentration of 2 mg/ml and frozen at -80^{o}c until further use.

Gel electrophoresis

Gel selection

The range of separation of proteins that occurs in the SDS-polyacrylamide gels depends upon the concentration of acrylamide used and so the number of cross-links formed. These factors affect the size of the pore through which the protein complexes are passed. The size of the pore decreases as the polyacrylamide:bis ratio increases meaning choosing the correct gel for a given polypeptide length is very important. The gels used in this study were discontinuous, consisting of stacking and resolving gel components (see gel preparation).

Gel preparation

The gels were mixed and poured into 1 mm plastic cassettes (NC2010, Invitrogen) with the following composition (7.5% gel; Tris HCL 375 μM (Stock 1 M, pH 8.8), Tetramethyllethylenediamine (TEMED) 5.6 μM, Acrylamide/Bis-Acrylamide (ACR/BIS) 7.5 % (w/v), Ammonium persulfate (APS) 0.1 % (w/v), Sodium dodecyl sulfate 0.1 % (w/v)). This gel mixture allows for adequate separation of proteins assessed in this work. Gels were topped with isopropanol and left to polymerise for 45 minutes. Isopropanol does not mix with the gel and produces a smooth surface free of imperfections at the point the proteins will enter the resolving gel. Once the resolving gel had fully polymerised the isopropanol was poured off and replaced with a 5% stacking gel (Tris HCL 130 μM, TEMED 8.6 μM, ACR/BIS 5%, APS 0.1% (w/v), SDS 0.1% (w/v)), combs for the loading lanes were inserted before the acrylamide completely polymerised.

Loading and running the gels

Prior to assembly into the electrophoresis tank the combs were carefully removed. Two cassettes were then assembled into the tank, which was filled with electrophoresis running buffer. Prior to loading 10 μL of sample was added to 5 μL of loading buffer (TRIS 60mM, Glycerol 25% (v/v), SDS 2% (v/v), β1-mercaptoethanol 14.4mM, bromophenol blue). SDS an anionic detergent denatures the secondary and non–disulfide–linked tertiary protein structures, and applies a negative charge to each protein in proportion to its mass (allowing for a linear relationship between migration and mass during electrophoresis). β-mecaptoethanol is included to reduce any disulphide bonding within the sample. Glycerol increases the density of the sample ensuring it sinks to the bottom of the well. Samples were then mixed and heated at 95^{o}C for 3 minutes to restore the proteins to their primary structure of discrete polypeptide chains. Samples were then transferred to ice and loaded into the wells of the stacking gel (10 μL). One well in each gel was loaded with 10 μL of pre-prepared standard containing proteins of known molecular weight. A voltage was then applied across the gel: 100V through the stacking gel and then 150V in the resolving gel until the bromophenol dye reaches the bottom of the gel.

Protein transfer

While the gels were running a polyvinylidene difluoride (PVDF) membrane (pore size 0.4 μm, Millipore, Fisher) was cut to the dimensions of the gel and soaked in 100% methanol for 15 seconds. Methanol is used as it promotes the adhesion of proteins to the PVDF membrane. The membranes, scotch brite pads and filter paper were then equilibrated in the transfer buffer. When the running of the gels was complete the plates were carefully separated and the stacking gel was gently removed leaving on the resolving gel. The gel sandwich was then prepared. The blotting cassette was opened and the negative cathode was placed down in the solution, one of the pre-soaked fibre pads were placed down on this cassette and a sheet of filter paper was laid upon this. The gel was then carefully placed on the filter paper and the PVDF membrane layered across the gel. A final piece of filter paper was placed upon this and the cassette was further filled up with pre-soaked fibre pads

until the cassette could be firmly closed. After the addition of every layer a pipette tip was rolled across the surface in order to remove and air bubbles. The transfer tank was constructed, filled with transfer buffer (TRIS 25 mM, Glycine 192 mM, methanol 20% (v/v)) and the whole apparatus was placed in ice. The proteins were then transferred from the gel to the PVDF membrane at 25V for 12 hours. Once the transfer was complete the tank was dismantled and the membrane was used for antibody incubation and immuno-detection (see below). The efficiency of the transfer process was assessed using a Comassie stain on the remaining resolving gel. The remaining resolving gel was stained for 30 minutes in Comassie blue staining solution (Comassie blue 300mM, glacial acetic acid 7.5% (v/v), ethanol 50% (v/v)). This gel was then soaked in de-stain solution (glacial acetic acid 7.5% (v/v), methanol 10% (v/v)) for 10 to 30 minutes allowing visualisation of any remaining protein as an indication of the quality of protein transfer.

Antibodies and immunodetection

Antibodies are generated when a host species is exposed to the protein of interest (or a part thereof). Antibody production is part of the normal immune response and they can be harvested and used as sensitive and specific detection tools that bind the protein directly. Commonly secondary antibodies are raised against a species-specific portion of the primary antibody. These secondary antibodies are conjugated to either horseradish peroxidise enzymes or fluorescent tags depending upon their application. Secondary antibodies are raised in a different species of animal to that of the primary antibody.

The SERCA2a antibody used in this study was bought from Santa Cruz (sc-8095) and raised in goats. Mouse anti-goat conjugated with horseradish peroxidise was bought from Sigma-Aldrich (A9452). Primary and secondary antibodies were diluted in blocking solution (TRIS 20mM, NaCl 20mM, Tween 20 0.05% (v/v), dry milk powder 5% (w/v)) and wash cycles also took place in this buffer. The blocking buffer is used to reduce the amount of non-specific binding and improve the quality of the blot. The initial primary SERCA2a antibody was diluted in blocking solution to a ratio of 1 in 2000.

Membranes were exposed over night at 4^{o}Cin a cold room and were placed on a rocking platform to promote even binding. Following primary incubation membranes were washed three times for ten minutes in blocking solution. Secondary incubation was carried out room temperature for 4 hours at a dilution factor of 1 in 5000. Membranes were then washed again for three times in blocking solution.

Signals were detected using an enhanced chemo luminescence (ECL) system (ECL detection system, Roche). 1 ml of solution A was added to 10 µl solution B (Kit instructions). The membrane was covered in this solution for 1 minute. The ECL fluid was drained off and the membranes were placed in the plastic holder of an autoradiography cassette. The membranes were exposed to autoradiography film (SIS, United Kingdom) for increasing time periods (from 30 seconds) to visualise the protein bands. The film was then developed using a Kodak GBX developer and fixer (Sigma-Aldritch, United Kingdom).

To correct for errors in protein loading, all blots must be compared to a highly expressed control protein (i.e. one expressed at a constant level in all treatment groups). For this purpose an aceylated α–tubulin primary antibody and the appropriate secondary antibody were purchased from Sigma – Aldrich (Primary T4026, Secondary A4789, United Kingdom). Before the membranes were re-probed the previous antibodies were stripped off through immersion for 10 minutes in NaOH (25 mM). The stripped membranes were washed in blocking buffer three times for a period of 10 minutes per wash. Membranes were immersed in blocking solution containing the tubulin primary antibody at a concentration of 1 in 3000 for 4 hours at room temperature. Secondary incubation following the wash stages was carried out for 2 hours at room temperature (1 in 5000). After a final set of wash stages the membranes were developed as described above.

Analysis of films

The images were scanned (Scan snap 121, AGFA, Fujitsu) at 300 dpi using the Scanwise programme (AGFA, Fujitsu) and saved as tagged image file formats (TIFF). The band densities were quantified

using the public domain ImageJ application (developed at the U.S. National Institute of Health). Templates of the same shape were drawn around the individual bands of the blot and used to measure the integrated density. The product of peak area and peak intensity was estimated to quantify protein loading. The density of each band was presented in graphical form and the area under each peak was calculated to give a numerical representation of protein expression. Each antigen band was expressed as a ratio of the corresponding tubulin band or total protein loaded; this provides a way of normalising for loading errors and provides accurate representation of protein expression.

Statistical analysis

Two-way analysis of variance (ANOVA) was used in the comparison of contractile performance between treatment groups over a range of balloon volumes. Statistical significance between groups was computed using Fisher least significant difference (FLSD) post hoc tests. Simple comparisons such as heart weight or ventricular volume were made with unpaired Student t-tests or one way ANOVA with FLSD if more than 2 groups were included. Comparisons between treatment groups and regions of the myocardium in histological studies were carried out with one way ANOVA and FLSD. All data represent mean ± SEM unless otherwise stated.

Chapter Three: Effects of reduced capillarity on cardiac performance and metabolism. Part 1: Microspheres

Oxygen consumption is directly related to oxygen demand in the beating myocardium and any increases in cardiac workload are met through greater oxygen provision. The heart has a limited ability of extract more oxygen from the coronary blood and as such greater oxygen delivery is achieved through increases in coronary blood flow [111]. Large coronary conduit vessels and small arteries extend into the epicardial portion of the myocardium and offer little resistance to blood flow. As such these large vessels do not play an important role in the response of the coronary circulation to changes in oxygen demand within the myocardium, such as that which occurs during exercise. Control of coronary blood flow primarily occurs at the level of the coronary microcirculation in vessels which offer significant vascular resistance. Small resistance arterioles (100 to 500 μm diameter) represent a second mechanistically distinct population of blood vessels. The function of these vessels is to maintain pressure at the site of origin of the arterioles [112, 113]. When coronary flow changes, shear stress is normalised by endothelium dependent dilatation (this process also occurs in the arterioles themselves). Increases in coronary flow elevate shear stress and result in the release of nitric oxide, a potent vasodilator which acts to reduce vessel shear stress. Increases in aortic pressure result in myogenic contraction of the distal pre arterioles which maintains a constant perfusion pressure at the level of the arterioles [112, 113]. The arterioles represent vessels smaller than 100 μm in diameter and play a fundamental role in matching coronary blood flow to cardiac oxygen consumption through metabolic regulation. These vessels have a high resting tone and dilate in response to the release of metabolites (e.g. adenosine) from the myocardium when rates of oxygen consumption increase. Dilatation of the arterioles in response to workload or ischaemia will increase shear stress in larger pre-arterioles, resulting in nitric oxide mediated dilatation of these vessels. This is the proposed mechanism whereby the arterioles

regulate coronary blood flow through the entire coronary tree and allows the matching of oxygen supply and demand [112, 113].

Coronary Flow Reserve

Coronary flow reserve (CFR) describes the magnitude of the increase in coronary blood flow from a baseline state to a state of maximal coronary vessel dilatation. As coronary flow appears to be regulated at the level of the microvasculature this measure provides some insight into the ability of the microvasculature to respond to a given stimulus. Clinically, CFR is assessed by taking measurement of myocardial blood flow at rest and then during 'maximal' hyperaemia induced through infusion of either adenosine or dipyridamole – two potent coronary vasodilators [112, 114, 115]. Experimentally CFR can be estimated through the infusion of these and other vasodilators (e.g. nitric oxide donors [116]) and through a comparison of CBF before and after transient complete occlusion of the coronary vessels (around 10 to 30 seconds of occlusion are required) [117]. Assessment of CFR in the latter manner shows the true capacity for flow accommodation in the coronary tree (i.e. maximal flow) but may not truly reflect flow which can be recruited in normal physiological circumstances (e.g. exercise).

Microvascular dysfunction

Microvascular dysfunction represents abnormalities in the function and structure of the coronary microciriculation exhibited clinically by a reduction in CFR. Alterations in CFR have been noted in clinical and experimental studies of hypertension, cardiac hypertrophy and HF. Strong correlations have been demonstrated between the degree of micro-vascular dysfunction and the progression of HF indicating that poor oxygen delivery or supply/demand mismatch during times of increased demand may an important role in the development of HF.

Systemic arterial hypertension

Abnormalities in CFR have been noted in patients with systemic arterial hypertension with or without cardiac hypertrophy. Positron emission tomography (PET) imaging of the coronary

microvasculature in clinical studies suggests that coronary flow can be either globally impaired (reduced CFR in response to dipyridamole) or that patients exhibit a heterogeneous pattern of regional micro-vascular dysfunction [118]. The latter appears to be closely associated with an increase in ventricular mass, suggesting that non-uniform perfusion plays an important role in the pathology of hypertensive heart disease. A reduction in CFR has been noted in several experimental models of hypertension, including spontaneously hypertensive rats (SHR) [119] and chronic nitric oxide synthase inhibition [120]. Hypertension induced microvascular dysfunction is often associated with a reduction in diameter of the coronary vessels, occurring through hyperplasia of the smooth muscle cells. SHR demonstrate a significant increase in intramyocardial pre-arteriolar wall thickness compared with normotensive control animals [119]. Treatment with the angiotensin converting enzyme inhibitor, lisinopril, normalised the arterial wall thickness/lumen ratio (a potential result of a decrease in arterial wall stress and/or vessel shear stress). Intra-luminal hyperplasia appears to represent an attempt to normalise arterial wall stress in response to an increased hemodynamic load. A reduction in arteriolar density (vessel size; < 20 μm) has been demonstrated in the SHR model, despite normal measures of density for larger coronary vessels [120]. It has been proposed that impaired flow through the pre-arterioles occurs as a result of intra-luminal hyperplasia, and that this reduced flow drives remodelling of the arteriolar bed and may contribute to the reduction of CFR associated with systemic arterial hypertension. Hypertension is known to be an important clinical risk factor for HF, probably due to its pronounced effects on cardiac oxygen consumption (elevated afterload). It seems likely that the combined effect of increased oxygen consumption and poor coronary perfusion could play a role in the progression of HF.

Aortic stenosis

Aortic stenosis dramatically elevates left ventricular wall stress and is associated with a compensatory hypertrophic remodelling. Patients with aortic stenosis demonstrate impaired CFR despite normal coronary arteries (as assessed by angiography) [121]. Aortic stenosis is associated with high left ventricular pressure development which may limit coronary flow through compression

of the intra-ventricular vessels. The high pressures developed in the left ventricle are much greater than coronary perfusion pressure and so the time during which flow can occur may also be significantly reduced. Experimental studies in isolated hearts from aortic banded rats show impaired CFR in response to adenosine infusion [122]. Impairment of the CFR in aortic banded hearts was associated with remodelling of the resistance arteries (< 150 μm diameter) resulting in a significant increase in medial wall thickness with comparable lumen diameters (therefore representing a drive to normalise vessel wall stress). Though this model represents some characteristics of clinical aortic stenosis (i.e increased cardiac workload) it also elevates coronary perfusion pressure, and thus discrimination between the effects of perfusion pressure and the effects of LV hypertrophy on coronary flow is difficult to discern. As with hypertension, aortic banding dramatically elevates oxygen consumption due to an increase in cardiac afterload. The contractile and metabolic remodelling associated with the aortic banding model is well described (e.g. impaired performance and a switch toward oxygen sparing metabolic pathways) and be a result of regional myocardial hypoxia occurring due to supply/demand mismatch (i.e. microvascular dysfunction plus elevated oxygen consumption).

Chapter aims

Micro-vascular dysfunction is closely correlated to the risk of serious cardiac events (i.e. atrial and ventricular fibrillations) and to patient mortality in clinical studies [123]. Additionally, microvascular dysfunction may play an important role in the progression from compensated hypertrophy to heart failure, perhaps through regional tissue hypoxia at high workloads. Despite this, there has been no direct assessment of the impact of microvascular occlusion on cardiac performance and rates of metabolism. The principle aim of this chapter was to assess the acute influence of micro-vascular blockade on the contractile performance and metabolic rates of the isolated rat heart. Current literature has focussed upon models of macrovascular blockade where a large and predictable portion of muscle is occluded through ligation of one of the coronary arteries. We describe a novel model of microvascular blockade where isolated hearts are perfused with a known volume of 15

micron diameter polyethylene microspheres. By altering the number of beads infused into the heart we are able to measure cardiac performance and rates of substrate metabolism at varying degrees of microvascular blockade. Given the potential role of microvascular dysfunction in the progression of heart failure these data may have important clinical relevance. Especially important is the random distribution of microvascular blockade that is achieved in this model perhaps representing the heterogeneous nature of micro-vascular dysfunction in models of hypertrophy. This work provides evidence that acute modification of oxygen delivery can directly influence cardiac contractile performance as well as rates of glucose and FA metabolism in the isolated rat heart. Additionally, data from this chapter regarding coronary reserve and oxygen consumption will provide supportive evidence for the utilisation of the Langendorff isolated heart in the meeting of the primary aims of this thesis.

Materials and methods

The following protocols outline the steps taken to assess ventricular performance and metabolism during micro-vascular blockade in the isolated hearts of age matched Wistar rats. Micro-vascular blockade was induced by infusion of 15μm diameter polyethylene microspheres into these hearts. Differing degrees of blockade were achieved through the infusion of numbers of microspheres ranging from 1 $x10^6$ to 10 x 10^6 per heart (see protocol 1). Ventricular performance and rates of metabolism (where applicable) were assessed in the same hearts before and after microsphere infusion. Histological assessment of the frozen tissue from these perfusions provided evidence of the degree of micro-vascular blockade achieved.

Protocol 1: Assessment of the effects of acute micro-vascular blockade on left ventricular contractile performance

An initial volume-response curve was performed in accordance with the protocols outlined in the General Materials and Methods chapter. In all experiments the final balloon volume was limited to 350 μL to prevent mechanical injury to the hearts. Following completion of the initial volume-response curve balloons were deflated to 0 μL (developed pressure of 10-20 mmHg) and hearts were divided into 1 of 4 groups.

Group 1: Hearts were infused with 1% bovine serum albumin dissolved in Krebs Hensleit buffer solution (300 μL). This group represents control conditions and provides evidence of the repeatability of volume-response relationship. (Total 5 hearts)

Group 2: Hearts were infused with $1x10^6$ microspheres suspended in 300 μL 1% bovine serum albumin solution. (Total 4 hearts)

Group 3: Hearts were infused with $3x10^6$ microspheres suspended in 300 μL 1% bovine serum albumin solution. (Total 4 hearts)

Group 4: Hearts were infused with $5x10^6$ microspheres suspended in 300 μL 1% bovine serum albumin solution. (Total 5 hearts)

Group 5: Hearts were infused with $3x10^6$ microspheres suspended in 300 μL 1% bovine serum albumin solution. 1 ml coronary effluent was collected from these hearts directly after infusion and centrifuged at 10,000 RPM for 2 minutes. The supernatant was discarded and the remaining microsphere pellet was re-suspended in 300 μL 1% bovine serum albumin solution. Hearts were then infused with this second bolus of microspheres (Total 3 hearts)

Following a 5-minute acclimation period volume-response curves were repeated for all hearts. Hearts were then frozen for histological analysis (see general materials and methods).

Analysis of protocol 1

Data are presented in terms of the absolute values of ventricular performance following blockade and as ratios of performance before and after micro-vascular blockade. The second of these methods allows for normalisation of data and the removal of a source of variability. All data are plotted against micro-vascular blockade which is calculated from those protocols outlined under the *histological methods* heading of this chapter.

Protocol 2: Assessment of the effects of acute micro-vascular blockade on left ventricular substrate metabolism

Initial rates of glucose and FA oxidation were assessed over a 45-minute period in accordance with the methods outlined in the general materials and methods. For these experiments samples of effluent were collected at 7.5-minute intervals. Workload was kept constant at a set end diastolic of 20 mmHg. Following completion of this initial phase hearts were infused with $3x10^6$ microspheres suspended in 300 μL of 1% bovine serum albumin solution (w/v). Following a 5 minute acclimation period rates of metabolism were again assessed over a 45 minute period. Hearts were snap frozen for histological analysis following completion of this protocol (see general materials and methods). Experiments were carried out in 8 hearts.

Analysis of protocol 2

All performance data are presented as RPP as this was found to be the best correlate with micro-vascular blockade during protocol 1. CF rates were estimated from the collection of coronary effluent and the time taken to collect a known volume of perfusate. Rates of FA and glucose oxidation were calculated in accordance with the protocols outlined in the General Materials and Methods chapter (Chapter 2).

Histological methods

Tissue sampling was carried out as described in the general materials and methods (Chapter 2).

α-Smooth muscle actin

The α-smooth muscle actin stain (C6198, Sigma) is a monoclonal antibody that binds to the specific isoform of actin found in smooth muscle and as such allows imaging of the arteriolar bed in cardiac muscle sections. α-smooth muscle actin is visible as fluorescence when stimulated by ultra-violet light. Slides were left to dry for 30 min before being fixed in ice-cold acetone for 1 minute. A volume of 10 μL of 1 M calcium solution was added to 100 ml of phosphate buffered saline (PBS) solution (Sigma). Fluorescence-conjugated α-smooth muscle actin stain (C6198, Sigma) was added to this stock buffer at a ratio of 1:100. The slides were stained in this solution for one hour before being rinsed in three times in PBS solution. Slides were mounted in Vectashield (H-1000, Vectorlabs) and sealed with a coverslip. Care was taken to avoid any unnecessary exposure to light due to the fluorescent nature of the stain.

Arteriolar densities and diameters were assessed from images captured digitally on a Zeis microscope system using the built in software (Axiovision v.4) at a total magnification of x125 (eyepiece x10, objective x10, and drawing arm x1.25). Terminal arterioles were defined as those 20 μm in diameter or less. Diameter was measured from the outer edges of the arterial walls. Larger vessels (> 20μm), indiscriminate, venule or pericyte like structures were excluded from counts (Figure 3.1). Arteriolar density (capillaries/mm^2) was calculated using the same methods outlined for

CD in the General Materials and Methods chapter (Chapter 2). Counts were performed in the subendocardial, subepicardial and midwall regions of the left ventricle free wall (18-24 images in total per animal). In 8 hearts CD was calculated (see Chapter 2) in the subepicardial and subendocardial region of the LV and used to assess the total number of capillaries supplied by each terminal arteriole.

The degree of arteriolar blockade was assessed as a ratio of the total number of arterioles and the number of arterioles occluded by microspheres. Figures 3.1 and 3.2 are representative images of the counting protocol applied to an image of the epicardial region and high magnification images of arteriolar blockade.

Coronary flow reserve and myocardial oxygen consumption

CFR was assessed in four Langendorff hearts through the addition of sodium nitroprusside (SNP (10 μM)) to the perfusate. This concentration was selected as one that influences CF without significantly affecting contractile performance. Coronary flow and ventricular performance were assessed before and during SNP mediated vasodilatation (following a 5 minute acclimation period). Myocardial oxygen consumption was assessed in the same hearts prior to SNP perfusate supplementation. CFR was estimated in a total of 4 hearts.

Oxygen partial pressure was measured from samples of perfusate using a GEM 4000 Premier Blood Gas Analyzer (Instrumentation Laboratory, USA). In crystalloid perfusions oxygen partial pressure and oxygen content are related in a linear manner. The oxygen content of the perfusate can therefore be calculated from...

$$C_aO_2 = 0.0031 \times P_aO_2$$

Where C_a0_2 is the oxygen content, and Pa02 the partial pressure of oxygen. The constant 0.0031 represents the amount of oxygen dissolved in plasma at 1 atmosphere (ml/100ml perfusate). Samples of 1 ml of perfusate were taken from the upper reservoir of the sealed Langendorff

preparation and provided a measure of 'arterial' oxygen content. Samples of coronary effluent (1 ml) were collected for calculation of 'venous' oxygen content. Myocardial oxygen consumption (MVO_2) was calculated according to Fick's principle (MVO_2 = (Arterial O_2 content – Venous O_2 content) x Coronary flow (ml/min/g. Wet weight). MVO_2 was estimated in a total of 4 hearts.

Statistical analysis

Where applicable linear regression analysis was applied to data sets allowing the calculation of R^2 values. R^2 gives an estimate how well the data points fit a specific regression curve. Non-linear regression (polynomial second order) was used in some situations where the data points seemed to warrant such analysis. In these circumstances statistical comparisons (sum of squares test) were made between linear and non-linear regressions whereby the simpler model (linear) was accepted unless a P value of less than 0.05 was generated. All statistical analyses were carried out using the Graphpad Prism software package (Graphpad Software Inc.)

Results

Coronary flow reserve and myocardial oxygen consumption

Addition of SNP (10 μM) to the perfusate resulted in a significant 20% increase in the rate of coronary flow (11.8 ± 0.2 vs. 14.2 ± 0.3 ml/min/g. wet weight, P<0.01). Cardiac performance demonstrated as RPP, was comparable before and after addition of SNP (14800 ± 300 vs. 14200 ± 200). 'Arterial' oxygen content was 1.67 ± 0.02 ml O_2/100 ml of perfusate while 'venous' oxygen content was 0.59 ± 0.07 ml O_2/100 ml. Oxygen extraction was therefore 64.7 ± 4.24 % of total oxygen availability. MVO_2 was 0.14 ± 0.01 ml O_2/min/g wet weight.

Histological findings

Capillary and terminal arteriolar densities were significantly greater in the subepicardial region compared with the subendocardial region (Table 3.1). The number of capillaries supplied by each terminal arteriole was comparable in both cardiac regions (78 ± 5 vs. 78 ±9 capillaries/arteriole). Infusion of an increasing numbers of microspheres achieved a degree of micro-vascular blockade no greater than 33%. A second infusion of microspheres (Group 5) was required to achieve degrees of blockade between 33 and 50 %. Some occlusion of larger coronary vessels (50-100 μm) was noted in hearts infused with greater numbers of microspheres (Figure 3.3).

Ventricular performance during micro-vascular blockade

Increasing arteriolar blockade was linearly related to declining left ventricular developed pressure (R^2=0.44 P=0.001, Figure 3.4C), RPP (R^2=0.82 P=<0.0001, Figure 3.4A), +dP/dt (R^2=0.53 P=0.0002, Figure 3.4E) and –dP/dt (R^2=0.52 P=0.0002, Figure 3.4F). HR decreased in a non-linear manner when plotted against increasing arteriolar blockade (R^2=0.54, Figure 3.4 D). Increasing degrees of arteriolar blockade were related in a curve-linear manner to normalised cardiac performance (ratio RPP before/ratio RPP after) (Figure 3.4B, R^2=0.91).

Ventricular metabolism during micro-vascular blockade

Mean RPP, oleate and glucose oxidation rates were significantly lower after bead infusion (Figure 3.5). RPP was linearly related to CF in all preparations (R^2=0.71 P=<0.0001, Figure 3.6A), both before and after arteriolar occlusion. RPP declined in a linear manner when plotted against increasing degrees of arteriolar blockade (R^2=0.89 P=0.0004, Figure 3.6B). RPP was linearly related to the rate of total oleate oxidation (R^2=0.56 P=0.0009, Figure 3.6C) and unrelated to the rate of total glucose oxidation (Figure 3.7D). Increasing degrees of arteriolar blockade was linearly related to a decrease in the rates of total oleate oxidation (R^2=0.87 P=0.0005, Figure 3.6E). Total glucose oxidation rates were unrelated to the degree of arteriolar blockade (Figure 3.6F). Rates of oleate and glucose oxidation expressed per unit external (observed) work were unrelated to the degree of arteriolar blockade (Figure 3.7).

Discussion

Arteriolar occlusion and LV contractile performance

This study is the first of its kind look at the impact of microvascular occlusion on ventricular performance and metabolism in the isolated beating rat heart. Results from this study show that left ventricular cardiac function is directly related to the degree of microvascular perfusion. The impact of relatively low degrees of arteriolar blockade upon left ventricular contractile function demonstrates the importance of adequate coronary perfusion in the maintenance of cardiac viability. Studies of ischemic injury, where coronary flow is reduced in a pre-selected region through coronary artery ligation or to the whole heart, demonstrate similar impairment of contractile function [124-126]. The best correlate with arteriolar blockade was found to be product of systolic pressure and rate (RPP) which has previously been demonstrated to be a reflective measure of myocardial oxygen consumption and therefore total cardiac work [7]. The impairment of cardiac contractile performance after microvascular blockade therefore reflects the proportion of under-perfused poor and non-contractile tissue. Poor oxygen delivery to these regions will inhibit oxidative ATP production. A lack of ATP and build up of hydrolytic bi-products (ADP,Pi and H^+) impairs the ATPases of myosin heavy chain and the activity of the energy dependent ion pumps.

Arteriolar occlusion and substrate oxidation

Total rates of myocardial substrate oxidation were reduced in keeping with a reduction in oxygen delivery to the myocardium. The rate of FA oxidation was found to reflect both the contractile performance of the myocardium and was inverse to the proportion of arteriolar blockade (and so the proportion of perfused myocardium). Similar trends were not demonstrated with glucose indicating that glucose oxidation is independent of work and CF in this setting. These data may reflect 1) the spatial arrangement of oxygen supply and its effects on substrate selection in the myocardium or 2) a potential limitation of the substrate only perfused heart to utilise exogenous glucose. These ideas are discussed in detail below.

1) Spatial influence of oxygen supply and substrate selection

The capillaries of the heart do not run parallel with the muscle fibres but weave a tortuous interconnected path [127]. Therefore it seems a reasonable assumption that the blockade of a single arteriole will not result in the blockade of 78 adjacent capillaries but rather in a random distribution of fully and partially occluded capillaries. Oxygen diffuses into the myocytes from several capillaries surrounding the myocytes and as such oxygen supply in the myocardium is defined by the spatial arrangement of the capillary bed rather than a situation where a single myocyte is supplied by a single capillary (i.e. oxygen diffuses in all directions from each capillary). The random occlusion of capillaries from a uniform capillary bed results in regions of the myocardium that will be normoxic, hypoxic or anoxic. Hypoxia increases the rate of glucose uptake (GLUT4 translocation [128]), increases flux through the glycolytic pathway (increased PFK2 activity [129]) and promotes the breakdown of glycogen into glucose (decreased glycogen synthase activity and enhanced phosphorylase activity [15]). Many of these effects are mediated through adenosine monophosphate kinase (AMPK) which senses alterations of intracellular AMP and PC content and modifies energy consumption in the myocardium. The relative contribution of glycogen to total glucose oxidation may shift in regions of the myocardium where there is still sufficient oxygenation for some oxidative metabolism to occur. There is evidence from studies in isolated hearts that glucose from glycogen is preferentially oxidised over imported exogenous glucose [130]. Therefore in regions of low oxygenation may redirect exogenous glucose to anaerobic glycolysis while simultaneously promoting the breakdown of glycogen which will contribute a greater proportion of glucose for oxidation. Studies in low flow ischaemia have demonstrated that exogenous FAs still contribute to the majority share of oxidative ATP production. AMPK activation also increases rates of FA uptake (through CD36 translocation [131]), increases flux through the beta oxidative cycle (inhibition of ACC [132]) and suppresses triglyceride breakdown to free FA (potentially through modification of HSL [133]). The use of FA for ATP production, unlike glucose, is completely dependent upon oxygen availability which in the present study is related to the degree of

microvascular occlusion, coronary perfusion and LV contractile performance. Hypoxia may modify the fate of exogenous glucose and alter the contribution of intracellular glycogen to oxidative ATP production. Therefore accumulation of $^{14}CO2$ and $H^{14}CO^{3-}$ may not directly reflect contractile performance.

2) A limitation in glucose utilisation

Doenst *et al* (2001) have previously demonstrated that FA oxidation and not glucose oxidation is related in a linear manner to cardiac power (the product of flow output and systemic arterial pressure) in experiments performed in normal, hypertrophied and failing hearts lending support to the present findings [46]. Interestingly, in the same study, perfusions containing insulin or adrenaline demonstrate linear relations between cardiac power and both oleate and glucose oxidation rate. Insulin and adrenaline both stimulate glucose uptake (GLUT4 translocation), increase flux through the glycolytic pathway (increase PFK2 and so PFK1 activity) and allow for greater entry of glucose into the citrate cycle (through phosphorylaton of the PDH complex). These data imply that glucose oxidation in perfusions containing glucose alone are limited at some point in the metabolic pathway (uptake, glycolysis or oxidation) and in the present study the rate of glucose oxidation may reflect the capacity for glucose oxidation in each heart rather than the energy demands of the myocardium. There is some controversy as to whether this increase in energy consumption is met by increased rates of glucose or FA metabolism. In several studies Neely and various cohorts demonstrated that glucose uptake [27] and oxidation[26, 108] is elevated in response to greater workloads when provided as the sole substrate, a finding prevented by the addition of palmitate to the perfusate. In dual substrate studies (glucose plus palmitate) Neely *et al* demonstrated that increases in workload were met through an increase in palmitate uptake [27] and oxidation[26, 108]. Contrary to this Allard *et al* (1994) demonstrated a significant increase in exogenous glucose oxidation but not palmitate oxidation when cardiac afterload was elevated in isolated beating heart preparations [38]. The latter differs from the earlier studies by Neely and cohorts in that insulin was included in the

perfusate. Several studies using adrenaline have also shown increased exogenous glucose uptake and oxidation occured to meet the increased energy demand of the myocardium [24, 134].

In the present study we have made no estimation of sarcolemmal glucose transporter density, PFK1, PFK2 or PDH activity or of total glycolytic rate which would give insights into the operation of the individual components of the glucose metabolic pathway.

Arteriolar occlusion and coronary flow

Linear relationships were demonstrated between the degree of arteriolar blockade and coronary flow demonstrating that no significant recruitment of coronary flow occurs in this model. The ability of the crystalloid buffer perfused Langendorff rat heart to recruit coronary flow in response to nitric oxide was also relatively limited when compared to data from *ex* vivo blood perfused rat hearts. Mouren *et al* (2010) demonstrated a 257 % increase in coronary flow after supplementation with SNP (10 μM) in isolated rat hearts perfused with blood [116]. The limited CFR of the crystalloid perfused isolated heart is well described and likely results from the low oxygen carrying content of crystalloid buffers as well as the high shear rate attributable to its low viscosity. Significantly greater measures of recruitable flow are demonstrated in studies of Langendorff hearts perfused with blood lending support to this [116, 117]. The Langendorff isolated rat heart is therefore ideal for meeting the primary aims of this thesis. This model will allow investigation of the impacts of alterations of capillarity on ventricular function and metabolism in a setting where the ability to increase oxygen delivery is severely impaired. It should be mentioned that although the oxygen content in this buffer is low there is still adequate oxygenation to support normal contractile function. Only 65% of total perfusate oxygen was extracted showing a significant oxygen reserve within the preparation. IN addition as demonstrated in later chapters and in many other studies [134-136] these hearts are able to respond for prolonged periods of time to the positively inotropic and chronotropic effects of β_1-adrenoceptor agonists.

Methodological considerations and future work

Occlusion of larger coronary vessels

While blockade was assessed in terms of arteriolar occlusion there was evidence that occlusion also occurred in larger coronary vessels. The most likely explanation for this finding is the backing up of microspheres from the site of occlusion to the distal lumens of larger pre-arterioles. This 'daisy chain' effect was demonstrated in a number of images from the histological studies. It is unclear how these factors might influence any results. Additionally arteriolar estimates were made in this experiment without perfusion fixation of the vasculature. A possible consequence of this is the inaccurate assessment of arteriolar densities. Despite this potential source of error the arteriolar densities were comparable to other studies of the coronary microvasculature [137, 138]. Such errors were inherent in all the samples and as such all data are internally consistent.

Lactate and glycolysis

No assessment of lactate production was made in this study which is a source of potential error in the expression of rates of glucose oxidation. It would be interesting to see what happens to global rates of glycolysis during micro-vascular blockade. This could be achieved through estimation of $^{3}H_2O$ production from [5-^{3}H] radio-labelled glucose. Catabolism of the glucose molecule during glycolysis results in the release of hydrogen in form of water (phosphate pentose and enolase reactions) [108]. ^{13}C-nuclear magnetic spectroscopy could also be used to measure real time flux through the glycolytic pathway.

Conclusion

The Langendorff isolated heart is an ideal model to study the effects of capillarity on LV contractile performance and substrate oxidation. The limited ability to increase CF in the Lagendorff heart can be utilised to demonstrate the existence, or lack thereof, of direct relationships between oxygen diffusion, contractile performance and metabolic rate in the treatment groups utilised in this thesis.

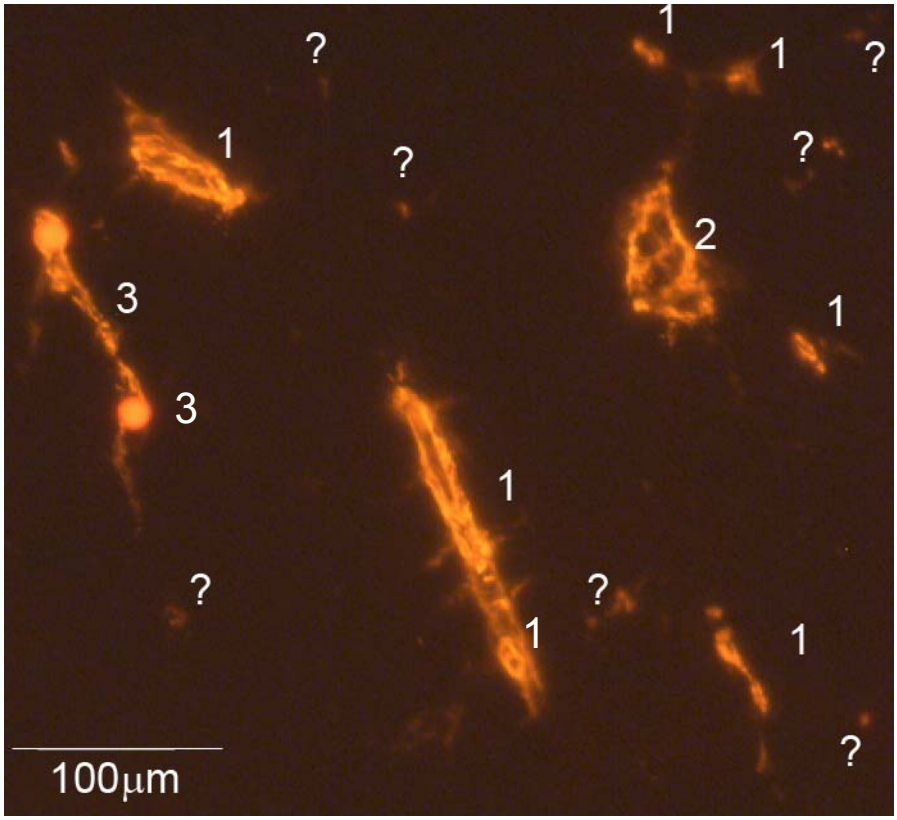

Figure 3.1. Representative image of epicardium demonstrating the α-smooth muscle actin staining and microsphere blockade. 1=Unblocked arterioles, 2=Large coronary vessels 3=Arterioles blocked by microspheres, ?=Excluded vessels (indiscriminate, venule or pericyte like structures). X125

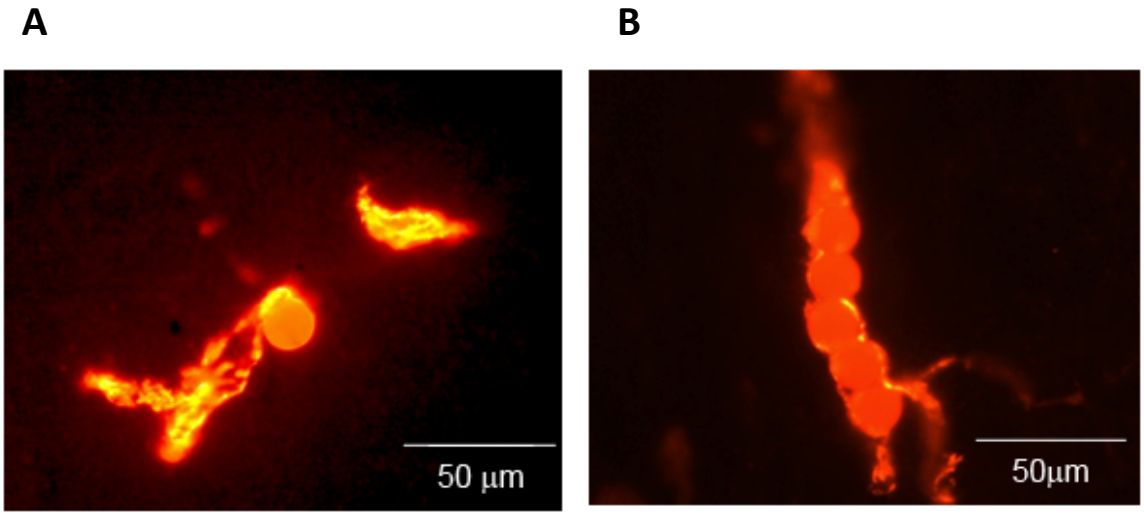

Figure 3.2. High magnification images of microsphere blockade. A= Single microsphere in arteriole lumen, B= Multiple beads in lumen of single arteriole. X1250

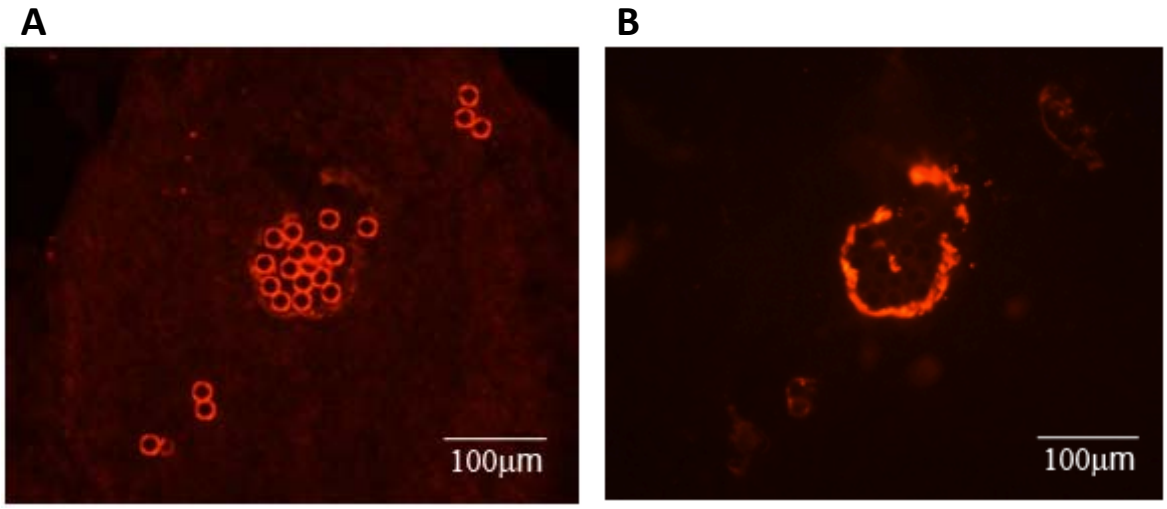

Figure 3.3. High magnification images of large vessel blockade. A= Light microscopy, B= Fluorescent microscopy. X500

Table 3.1. Histological data from microsphere studies.

	Arteriolar density (capillaries / mm^2)	**Capillary density (capillaries / mm^2)**	**Capillaries per terminal arteriole**
Endocardium	25 ± 2	1852 ± 82	78 ± 5
Epicardium	29 ± 2*	2092 ±61**	78 ± 9

N=8 hearts (6 fields of view per region per heart). Epicardium vs. endocardium; *P<0.05, P<0.01.

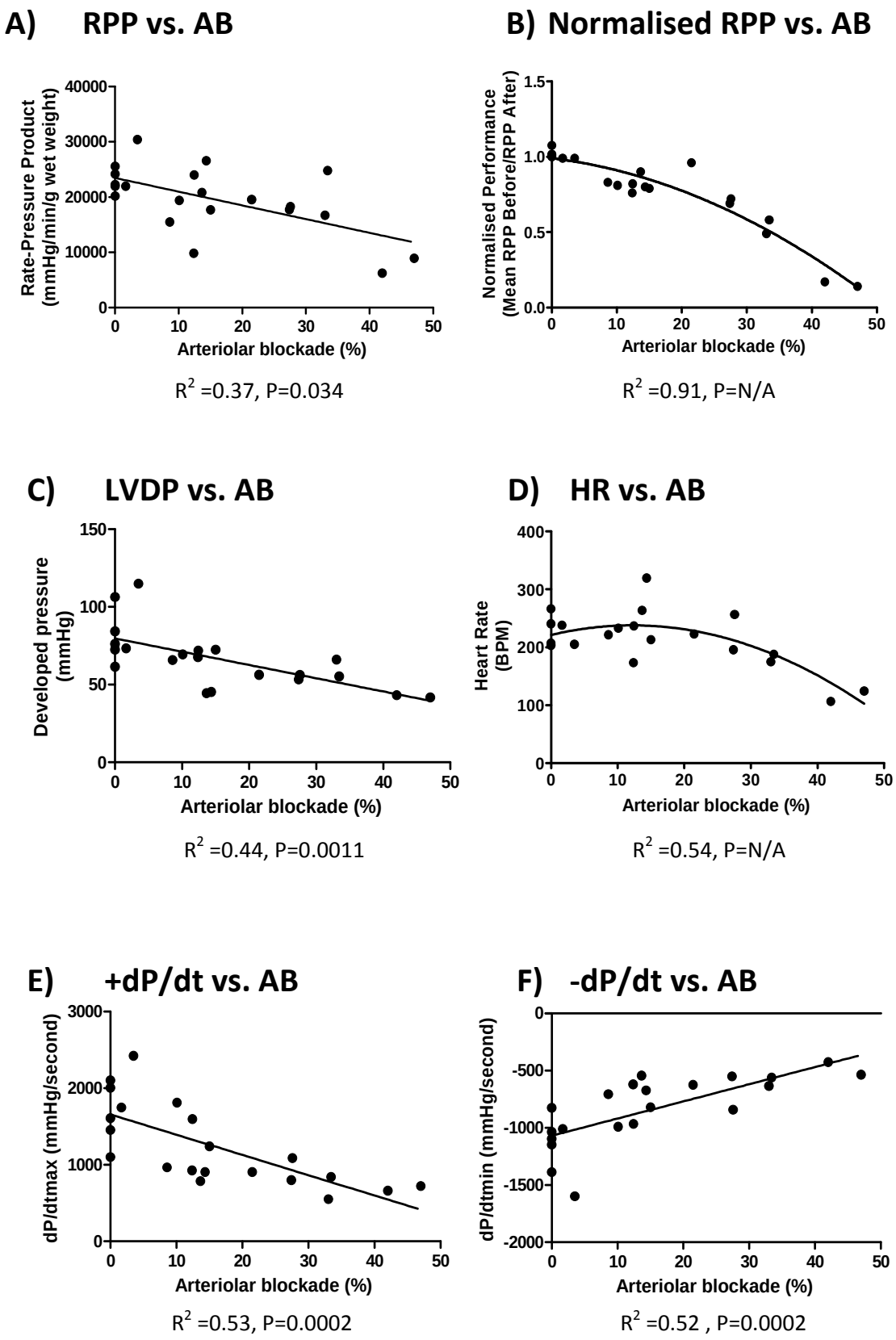

Figure 3.4. Relationships between ventricular performance and the degree of arteriolar blockade. Data from 21 experiments. Legend: RPP=Rate-Pressure Product, AB=Arteriolar Blockade, dP/dt=rate of change of pressure, N/A=Not applicable.

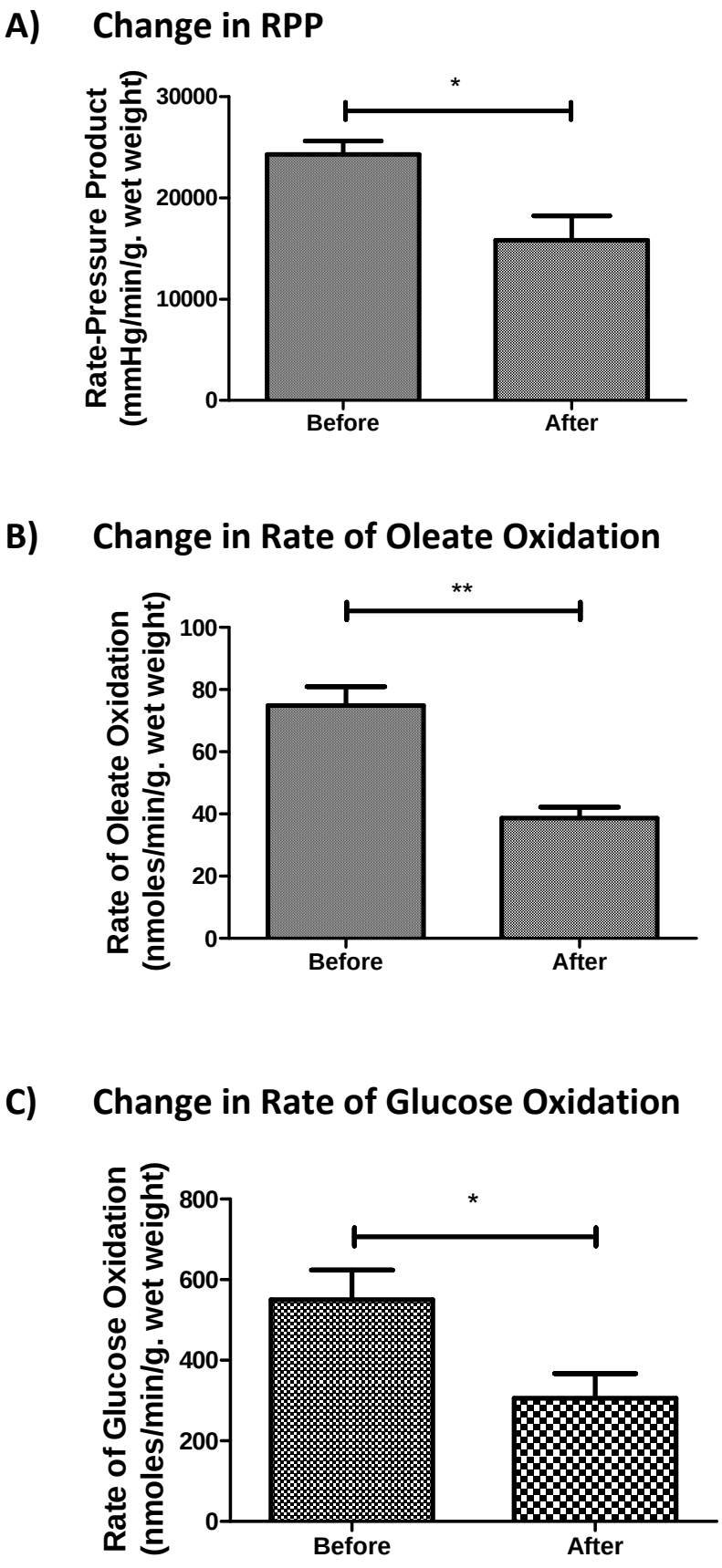

Figure 3.5. Mean relationship between ventricular performance (RPP), oleate metabolism and glucose metabolism before and after microsphere infusion. Data from 7 experiments (excluded experiment 8 was a control and was not perfused with any microspheres). Statistical analysis was carried out using a paired Student's T-Test.

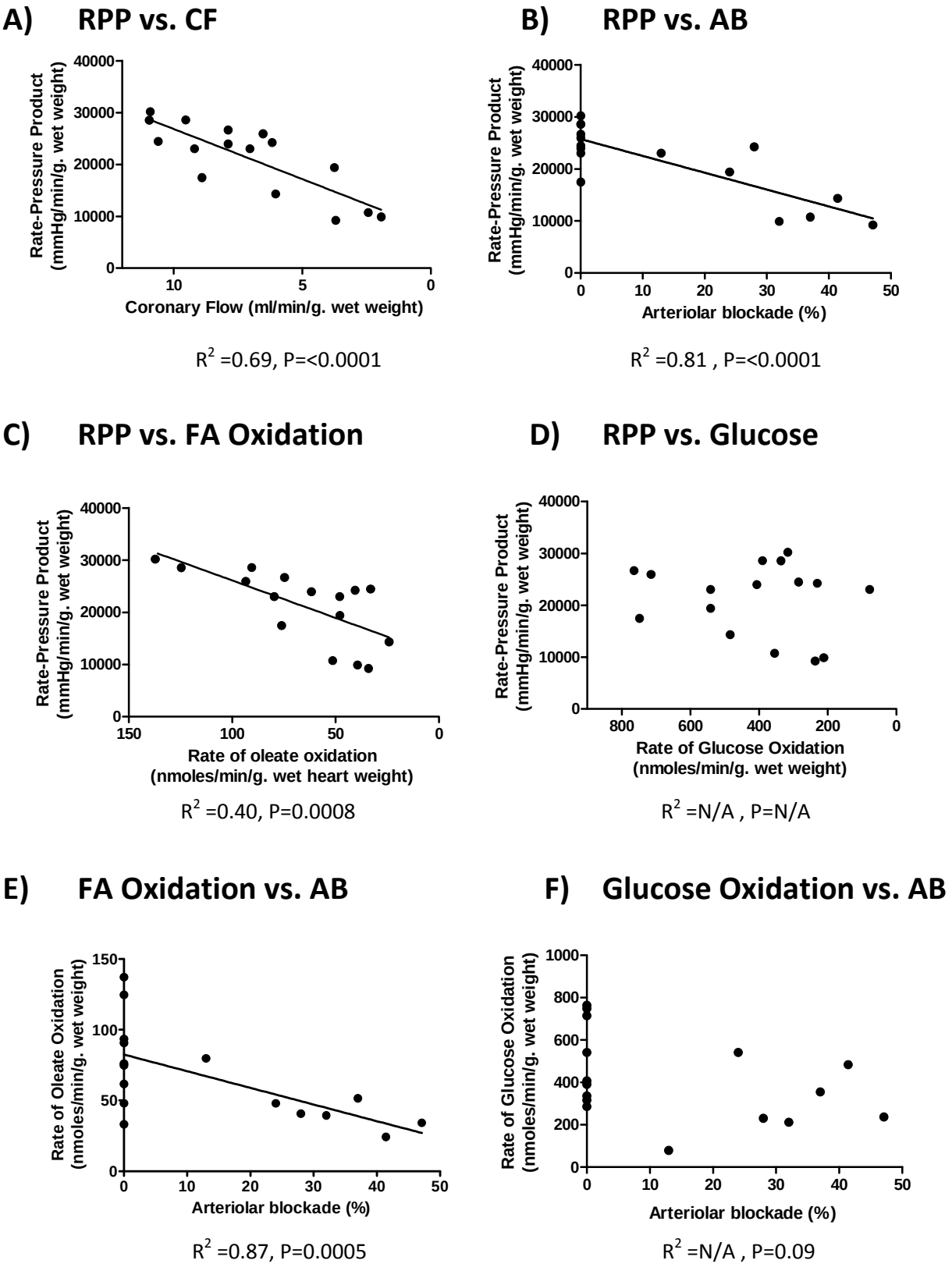

Figure 3.6. Relationships between ventricular performance, rates of metabolism, coronary flow and the degree of arteriolar blockade. Data from 8 experiments. Legend: RPP=Rate-Pressure Product, AB=Arteriolar Blockade, FA=FA, N/A=Not applicable.

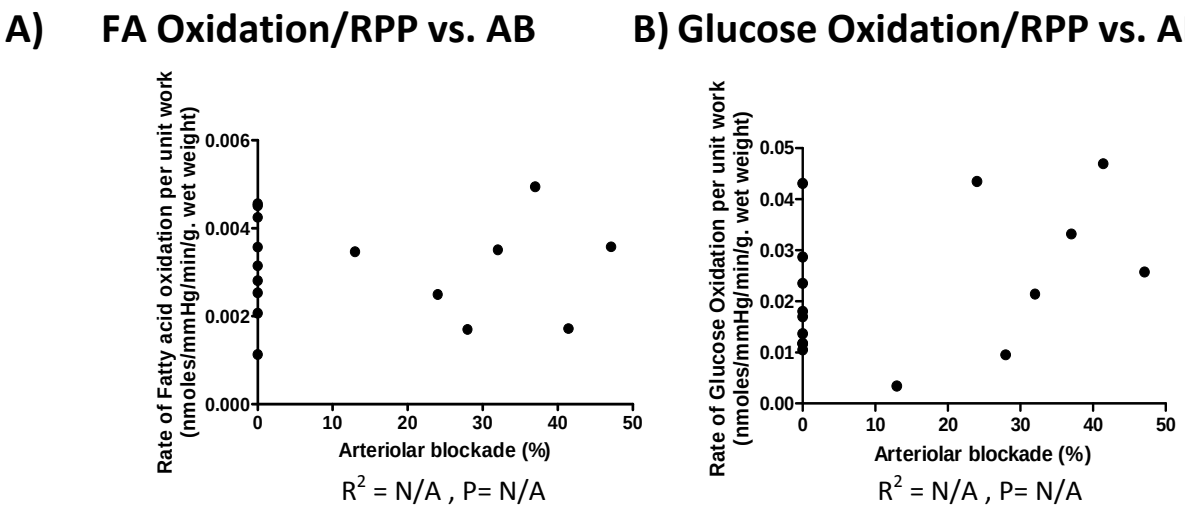

Figure 3.7. Relationships between rates of metabolism per unit external (observed work) and the degree of arteriolar blockade. Data from 8 experiments. Legend: N/A=Not applicable.

Chapter Four: Effects of reduced capillarity on cardiac performance and metabolism. Part 2: Isoprenaline

Catecholamines are important stimulators of cardiac contractility when there is an acute change in the physiological state of an organism such as during the 'fight or flight' response, during exercise and during exposure to a change in the local environment (e.g. a reduction in ambient temperature). In the acute setting catecholamines promote inotropy, lusitropy and chronotropy in the heart allowing an increase cardiac output to meet the changing demands of the body [9, 10]. These actions occur primarily through the activation of the β adrenergic signalling pathway resulting in an elevation of intracellular calcium ions (see Introduction). Prolonged exposure to catecholamines, seen physiologically during endurance and strength training [139] or the exposure of euthermic animals to low temperature environments [140], drives hypertrophic growth of the myocardium. Synthetic β adrenergic agonists are also able to promote cardiac remodelling. Isoprenaline induced hypertrophy is the best described model of this type of cardiac growth and previous studies suggest that distinct remodelling phenotypes are produced in response to differences in dosing regimes. Subcutaneous doses of isoprenaline in the range of 10 to 100 mg/kg are often utilised as a model of non-coronary myocardial necrosis. Dosing of this order of magnitude produces pronounced 'infarct like' areas of cell death in the hearts of a diverse number of animals including rats [141, 142], hamsters [143] and monkeys [144]. The cause of cell death during isoprenaline treatment is not clear but may involve calcium overload [145], non-esterified FA accumulation in the myocytes [146, 147] and/or a oxygen supply-demand imbalance (resulting elevated work rate (β1) and coronary vessel under perfusion (β2 mediated arterial dilation).

Traditionally, cardiac hypertrophy resulting from high dose isoprenaline was viewed as a secondary reparative process compensating for an impairment of systolic function. However, more recent evidence of hypertrophic growth in cell cultures of cardiac myocytes suggests that β-adrenergic signalling has direct trophic actions [148].Dosing of rats [141, 149-154], rabbits [155] and guinea pigs

[156] with isoprenaline at daily doses of 1 to 10 mg/kg for between 3 days and 4 weeks causes increases in cardiac weight of between 30 and 70%. Isoprenaline treatment at these concentrations, a whole magnitude lower than the infarct model, is associated with an increase in LV wall mass corresponding to an increase in myocyte cross-sectional area. Focal regions of myocyte necrosis have been reported by a number of investigators along with both perivascular and interstitial fibrosis indicating a stimulation of collagen production. Collagen deposition may be related to the direct actions of β-adrenergic signalling in cardiac fibroblasts [157] or alternatively a compensatory response to myocyte cell death [152]. Fibrosis appears to be limited to the endocardial regions where it may impact upon diastolic relaxation, limit the stretch and systolic response of myocytes to increases in preload and impair regional coronary blood flow [153, 158]. Interestingly in exposures to isoprenaline of relatively short nature (3 to 8 days) cardiac hypertrophy and fibrosis rapidly regress to control levels at the cessation of dosing. Kitagawah *et al* (2004) found that short term isoprenaline (3 days) induced hypertrophy and fibrosis regressed 2 days after the cessation of dosing [154]. Golomb *et al* (1994) similarly found that cardiac hypertrophy induced by dosing animals with isoprenaline for 7 days (2.5 to 10 mg/kg/day) reverted within 11 to 14 days of the cessation of dosing [159].

'Low' (1.0 to 5.0 mg/kg/day) dose delivery of isoprenaline to rats has been associated with impaired ventricular relaxation both *in vivo* and in *ex vivo* isolated heart preparations [151, 154, 160]. These findings are supported by the alterations in the expression of contractile proteins. Of particular interest to the present study are the effects of subcutaneous isoprenaline delivery on the expression of SERCA and the expression and phosphorylative state of phospholamban. Numerous studies have demonstrated that SERCA2a protein expression is down-regulated in the rat following chronic isoprenaline infusion via osmotic mini-pump [151, 154, 160, 161]. These changes appear to occur early, with reports of reduced expression after 3 and 7 days of infusion. Linck *et al* (1998) demonstrated that SERCA expression alterations may follow a specific time course noting reduced expression at 3 to 4 days and normalised values at 8 days onwards (up to 28 days) [161]. Reductions

in the expression of phospholamban, the allosteric regulator of SERCA activity, of a similar magnitude to the changes seen in SERCA expression have been noted in several studies of chronic isoprenaline exposure implying that the functionality of remaining transporters in preserved [151, 161]. However other investigators have noted a decrease in phosphorylated-Ser^{16}PLB after exposure (3 to 7 days) to isoprenaline in the rat [162], suggesting inhibition of the SERCA driven uptake of calcium into the sarcoplasmic reticulum.

Chapter Aims

The rapid nature of isoprenaline-induced hypertrophy has two major advantages in this study, the first being the absence of long-term structural remodelling seen in other models of hypertrophy. Secondly, it provides an opportunity to investigate a role for new capillary growth in hearts with significantly altered oxygen supply. Time course analysis of capillary growth in skeletal muscles following extirpation (stretch-induced angiogenesis) suggests that new capillaries do not appear until 7 days. [163, 164] Therefore, dosing animals for either 3 or 10 days will allow comparison of capillary supply and contractile performance between groups where in the latter regime capillary growth has had ample time to occur. The apparent time-dependent alterations in SERCA2a expression during isoprenaline treatment lends support to our study design and may reflect the delay in new capillary development. The aims of this study were to investigate the relationship between capillary density and performance in the isolated beating hypertrophic rat heart. Previous investigators have suggested that inotropic enhancement with the β1 adrenoceptor agonist dobutamine promotes new capillary growth as a result of abluminal forces acting on the vessel walls [165]. Therefore it was hypothesised that by 7 days significant capillary growth would have occurred and that if oxygen diffusion is limiting in the model this would be reflected in measures of ventricular contractile performance. The contribution of cell death to any alterations in contractile performance was assessed indirectly through staining for fibrosis.

Material and methods

Treatment regime

Animals were injected with isoprenaline (5 mg/kg/day i.p., 1.0 mg/kg/day or 0.2 mg/kg/day s.c.) for up to 10 days. [151, 153] Isoprenaline solutions were prepared in normal saline (0.9% NaCl) and frozen until the day of use. Due to the short nature of the protocol injection site injuries were deemed unlikely. As a result of this, and in the interest of animal welfare control, animals were not dosed with vehicle injections.

Results

Animal mortality

Isoprenaline treatment was not well tolerated, leading to significant loss of body mass and failure to grow normally. Moreover, unexplained nocturnal mortality occurred in 20% of animals treated through intraperitoneal injection. Subcutaneous injection resulted in a 100% mortality rate for both concentrations.

Physiological parameters

Heart to body mass ratios were greater in both groups when compared to control animals, but did not vary significantly between treatment regimes (Control 3.56 $\pm$ 0.23 vs. 3day 4.32 $\pm$ 0.11, 10 day 4.54 $\pm$ 0.35 mg/g, compared with controls $P<0.05$, Table 4.1). Recordings of mean arterial blood pressure show no difference between all groups (Table 4.1). Resting *in vivo* heart rate was significantly reduced in animals dose for 3 days (411 $\pm$ 8 vs. 380 $\pm$ 8 bpm, Table 4.1), but comparable to controls at 10 days.

Capillary supply

Capillary density (number of capillaries per mm^2) was significantly decreased in the subendocardial zone of hearts treated for 3 days (2500 $\pm$ 27 vs. 2081 $\pm$ 58 capillaries/mm^2, $P<0.01$, Figure 4.1B). This reduction in capillarity was not due to a lower number of capillaries in the ventricle (as assessed by capillary to fibre ratio) and can be attributed to an increase in myocyte size (553 $\pm$ 19 vs. 646 $\pm$ 15 μm^2, $P<0.01$, Figure 4.1A). A similar pattern of reduced capillarity and increased myocyte size was seen in the subepicardial zone though the latter of these did not reach statistical significance (Figure 4.1A and 4.1B). Delaunay triangulation assessment of capillary supply (Figure 4.1E and 4.1F) shows that in the endocardial zone both nearest neighbour (NN) distances (21.4 $\pm$ 0.1 vs. 23.6 $\pm$ 0.5 μm, $P<0.01$, Figure 4.1D) and the average area supplied by each capillary (veronoi cell) (297 $\pm$ 3 vs. 344 $\pm$ 18 μm^2, $P<0.01$) were elevated in the treatment group. The distribution of capillaries (variance) was less homogeneous in the subendocardial region of hearts treated with isoprenaline (7.6 $\pm$ 0.09 vs.

8.46 ± 0.08, P<0.01, Figure 4.1D). Similar assessment in the epicardial region did not show significant alterations in capillary supply. Mean NN distances (20.97 ± 0.45 vs. 21.84 ± 0.33 μm) and measures of capillary uniformity (7.36 ± 0.18 vs. 7.61 ± 0.14) were comparable with control sections.

LV capillary number and distribution was comparable between animals dosed for 3 and 10 days. Capillary density (2500 ± 27 vs. 2064 ± 72 capillaries/mm^2, Figure 4.1B), myocyte size (553 ± 19 vs. 661 ± 25 μm^2, Figure 4.1A) and mean NN capillary distance (21.4 ± 0.1 vs. 23.6 ± 0.3 μm, P<0.01, Figure 4.1D) were significantly different in the subendocardial region of 10-day isoprenaline treated animals vs. control..

Ex vivo contractile performance

Intrinsic heart rates were comparable in both control and all isoprenaline treated hearts (Figures 4.5A). LVDP increased proportionally with balloon volume until peak pressure development was reached at 350 μL in control hearts (Figure 4.2A). Further increases in balloon volume resulted in a decline in pressure development. Hearts dosed with isoprenaline for 3 days demonstrated similar LVDP-volume and LVEDP-volume relationships as control hearts (Figure 4.2A and 4.2B). Extended dosing for 10 days caused a significant systolic dysfunction with a preserved LVEDP-volume relationship (Figures 4.2A & 4.2B respectively). The ability to develop pressure in response to increased ventricular volume was severely inhibited in treated hearts – showing a 40% reduction in peak LVDP compared to controls (P<0.001). Similarly +dP/dt and –dP/dt were reduced following 10 days of isoprenaline dosing (Figure 4.3A and B respectively). LV systolic stress-strain was comparable between control and 3 day isoprenaline hearts (Figure 4.4), while longer term dosing resulted in a significant reduction in the slope of this relationship (93 ± 11 vs. 51 ± 5 mmHg/ml/g. wet weight, Figure 4.4). Ventricular chamber stiffness and unstressed LV lumen volume were comparable between all treatment groups (Figure 4.2B and Table 4.2). LV systolic dysfunction was unrelated to changes in CF rate as values were comparable between all groups and at all intraventricular balloon volumes (Figure 4.2C). No differences were noted in inter-ventricular collagen content between

either of the treatment groups and control animals (Table 4.2 & Figure 4.7). SERCA2a expression was comparable to controls in all treatment groups (Table 4.2 & Figure 4.6).

Dobutamine challenge

Addition of dobutamine to the perfusate resulted in a significant increase in LVDP (51 ± 9 vs. 86 ± 12 mmHg, P<0.01, Table 4.3), peak SP (65 ± 9 vs. 96 ± 11 mmHg, P<0.01, Table 4.3), +dP/dt (953 ± 105 vs. 1450 ± 225 mmHg/second, P<0.01, Table 4.3) and RPP (13500 ± 1900 vs. 20200 ± 2400 mmHg/min, P<0.001, Table 4.3) in control hearts. Similar responses were noted in hearts from animals dosed with isoprenaline for 3 days (Table 4.3). Contractile responses to dobutamine in hearts from the 10 day treatment group were reduced as demonstrated by a significant reduction in the % change in RPP following dobutamine perfusion (48.9 ± 5.9 % vs. 34.9 ± 2.4 % 10 day, P<0.05, Table 4.3).

Discussion

Subcutaneous dosing and animal mortality

The adverse effects following subcutaneous injection of isoprenaline were unexpected. Dosing regimens were similar to those used in a number of other studies. Single subcutaneous injections up to 150mg/kg/day have been utilised in studies to investigate the effects of isoproterenol on myocardial necrosis (over days and weeks) and none have reported the high mortality rates demonstrated in the present study [152, 166, 167]. One possible explanation for the discrepancy between the findings of this study and of other investigators is the preparation of isoprenaline in ascorbic acid which has been used previously to prevent the toxic breakdown of this drug on exposure to light. As we did not prepare our doses in this manner it seems probable that the breakdown of isopreanline contributed significantly to the high mortality rate seen in the present study

Isoprenaline and hypertrophy

Repeated dosing of isoprenaline resulted in rapid hypertrophic growth of the myocardium. The role of catecholamine stimulation on myocyte growth has been clearly described in a number of studies using intra-peritoneal injection [153, 168] and subcutaneous infusion [149, 150, 162, 169]. Estimations of end diastolic volume in both treatment groups, as assessed from x intercept of the LVEDP-volume relationship, shows that lumen volume is preserved and that the increase in mass occurs primarily through thickening of the ventricle wall (concentric hypertrophy) rather that geometric expansion. The histological finding of increased myocyte size in the transverse plane supports this hypothesis. A number of investigators have reported thickening of the ventricular walls following both subcutaneous [151] and intra-peritoneal isoprenaline delivery [153]. Extended dosing for 10 days did not produce an additional increase in cardiac mass or expansion of myocyte CSA in either the subendocardial or subepicardial regions of the LV. It is not clear whether this represents a maximal dose response (i.e. maximal expansion of the cardiomyocyte) or a desensitization of the tissue to β-adrenergic stimulation due to chronic over exposure to isoprenaline.

Isoprenaline, LV contractile performance and ventricular phenotype

While short-term treatment was not associated with changes in cardiac contractile performance, prolonged isoprenaline treatment resulted in pronounced systolic dysfunction. There is significant controversy as to the type of remodelling and dysfunction associated with isoprenaline treatment; possibly reflecting differences in the mode of drug delivery, the length of the treatment regime and the dose of isoprenaline utilised. Ferreira et al (2007) demonstrated that dosing of Wistar rats with isoprenaline through intraperitoneal injection (2 mg/kg/day for 7 days) results in a similar degree of systolic dysfunction to that seen in the present study (e.g. a 40% reduction in both +dP/dt and –dP/dt) [170]. Whereas numerous studies using identical treatment regimes, show that subcutaneous infusion of isoprenaline at doses between 1.2 and 3.2 mg/kg/day for between 3 days and 2 weeks results in cardiac hypertrophy associated with a decreased stroke volume, impaired ventricular relaxation and reduced cardiac output [151, 154, 160]. Despite impaired relaxation, systolic function appears to be preserved in these animals as evidenced by normal ejection fractions and rates of fractional shortening. Similar dosing regimens over 4 weeks or more are associated with an impairment of ventricular ejection fraction indicating hypertrophy with systolic dysfunction. Heather *et al* (2009) demonstrated that mini-pump delivery of higher doses of isoprenaline (5mg/kg/day for 7 days) resulted in a significant impairment of ventricular ejection fraction and chamber dilation on assessment of contractile performance by echocardiography [171]. Left ventricular dilation had been shown to accompany a reduction in chamber function in a number of human cardiac conditions [172, 173] and can be seen experimentally in a models of chronic pressure overload [101], volume overload [174], tachycardia induced HF [175], isoprenaline induced hypertrophy [101] and following ischemic injury [176]. We discussed earlier (Chapter 1), through the law of LaPLace, how geometric expansion without wall thickening increases ventricular wall stress and negatively impacts upon chamber function. In the present study isoprenaline treatment was not associated with any expansion of the LV lumen and therefore geometric insufficiency does not contribute to the systolic

dysfunction seen at 10 days. Therefore *ex vivo* myocardial function is impaired at this time point as evidenced by the decreased slope of the estimated LV stress-strain relationship. Isoprenaline had no effect on SERCA2a protein expression in either treatment group suggesting that impairment of calcium handling does not play a role in the altered contractile function at 10 days. Studies utilizing subcutaneous infusion have repeatedly shown that SERCA2a expression is suppressed following short term isoprenaline treatment [151, 154, 160]. It therefore seems a reasonable assumption that the chronic activation of adrenergic signalling required to alter SERCA2a expression is not achieved during intra-peritoneal delivery however these observations do not rule out alterations in SERCA activity. Previous investigators have noted a decrease in phosphorylated-Ser^{16}PLB after prolonged exposure to isoprenaline [162], suggesting inhibition of the SERCA-driven uptake of calcium into the sarcoplasmic reticulum has an important role in isoprenaline induced contractile dysfunction. In addition there are several other molecular level alterations which could contribute to these changes including shifts in myosin heavy chain expression (from adult to fetal) [177], decreased in calsequestrin expression [45, 178] and an increase in sarcolemmal NCX content [51-53]. The effects of isoprenaline on myocyte survival have been extensively studied and it is probable that myocyte necrosis and apoptosis contribute significantly to the systolic dysfunction noted at 10 days. While tissue fibrosis may give some in-direct indication of cell death more precise methods could be employed (i.e. DNA strand breaks or caspase activation). Assessment of the degree of myocyte necrosis would be a necessary pre-requisite in future studies to confirm its contribution to LV systolic dysfunction.

Suprisingly there was no evidence of an increase in interstial fibrosis following isoprenaline treatment for either 3 or 10 days. An increase in the collagen content of hypertrophied hearts has been reported in studies utilizing both intra-peritoneal and subcutaneous isoprenaline delivery in the ranges of 0.2 to 5 mg/kg/day [150-154, 160, 161, 171, 179]. The degree of collagen deposition in the ventricles of treated hearts varies significantly between 1.6 and 10 fold and these data do not appear to reflect either the dose of isoprenaline or the method of delivery utilised. Heather *et al*

(2009) found that dosing of Wistar rats for 7 days with isoprenaline (5 mg/kg/day) resulted in a dramatic 7 fold increase in collagen content in apical, but not in basal, regions of treated hearts [171]. Therefore, it is possible that the methodology employed in the present study fails to account for this regional variability in fibrosis. It may also be possible that the lack of fibrosis in this study reflect the bolus delivery method utilised. By delivering isoprenaline through intraperitoneal injection the chronic activation of adrenergic signalling seen in the subcutaneous mini-pump method does not occur. Given the conflict in the literature such a hypothesis would require careful investigation taking into account regional heterogeneity of response, delivery method and dosing regimen. Collagen distribution should be assessed at various depths (apex to base) through the LV wall to confirm any regional differences in isoprenaline mediated fibrosis. Measuring total hydroxyproline content (following acid hydrolysis of tissue samples) would provide a more accurate quantification of changes in total LV collagen (this hydroxylated form of proline (amino acid) is found in few proteins other than collagen [180]).

Evidence from models of β_1 adrenoceptor over-expression in the hearts of mice demonstrates an initial hypertrophic growth with increased cardiac contractility (assessed by time resolved magnetic resonance imaging) developing with time to a state of contractile dysfunction and heart failure [181]. This study lends support to the progression to systolic dysfunction during intraperitoneal isoprenaline injection. The controversy between different studies utilising isoprenaline appears to reflect the critical dose of isoprenaline required to induce early contractile dysfunction perhaps as a result of necrotic injury.

Role of oxygen diffusion in isoprenaline induced contractile dysfunction

Oxygen availability appears not to play a causative role in the cardiac dysfunction associated with this model. No differences were seen in capillary density between the 3 and 10-day groups, despite the significant differences in *ex vivo* contractile performance. Coronary flow rates were also comparable over all workloads and between all groups. Preservation of SERCA2a expression in both the 3 day and 10 day treatments suggests that the increase in oxygen diffusion distances does not

drive changes to protein expression in this model. The artificially low oxygen content of the perfusions buffer used in this experiment is not directly comparable to the *in vivo* situation where increases in demand can be met by dramatic increase in coronary blood flow. The use of a Krebs Hensleit buffer, with its low oxygen carrying capacity, instead of blood was aimed at promoting a state of maximal cardiac performance where capillary density becomes the major limitation on oxygen delivery. The ability of the isoprenaline treated hearts to respond to dobutamine shows that even in a situation of reduced oxygen availability the heart is not oxygen deprived and can draw on significant energetic reserves.

Future work and methodological considerations

Avoiding high animal mortality rates

The high rates of mortality seen in this study could be overcome through use of the subcutaneous minipump or utilization of cardiac specific β_1 adrenoceptor over-expressing mice. The receptor over expression models develop hypertrophy from the low-endogenous levels of catecholamines in their blood stream and so do not require any supplementation with harmful synthetic agonists.

Methodological considerations

Models of hypertrophy are commonly associated not only with an increase in myocyte dimensions but with a prolonged increase in systolic stress. Isoprenaline induced hypertrophy may therefore be a simplification of true hypertrophy without a chronic increase in cardiac work (e.g. afterload). It would be interesting to see if the addition isoprenaline to a model of well adapted chronic stress, such as cold acclimation, would result in failure that could be attributed to an oxygen supply/demand imbalance. (Note: Metabolic studies were not performed with this model due to home office restrictions due to animal fatalities).

Conclusion

In conclusion, short-term isoprenaline treatment resulted in a hypertrophic response with preserved contractile performance despite an increase in the distance over which oxygen must diffuse. Extended dosing resulted in systolic impairment at 10 days. Contractile dysfunction occurred in the

absence of alterations in SERCA2a expression and may be attributed to mycoyte necrosis and/or alterations in contractile protein expression. Limitations in oxygen diffusion do not play a causative role in the contractile dysfunction associated with chronic isoprenaline dosing.

Table 4.1 Effects of isoprenaline treatment on cardiac mass and in vivo physiological parameters.

	Control	***3 day Isoprenaline***	***10 day Isoprenaline***
Body Mass (g)	322 ± 13	256 ± 7**	285 ± 8*
Heart Mass (g)	1.16 ± 0.05	1.10 ± 0.02	1.32 ± 0.11
Heart mass / Body Mass (mg/g)	3.56 ± 0.23	4.32 ± 0.11*	4.54 ± 0.35 *
In vivo heart rate (bpm)	411 ± 8	380 ± 8*	369 ± 23
Mean arterial blood pressure (mmHg)	95 ± 4	94 ± 1	88 ± 2

(Control n=6, 3 Day n=4, 10 Day n=5). The effects of isoprenaline treatment *P<0.05, **P<0.01.

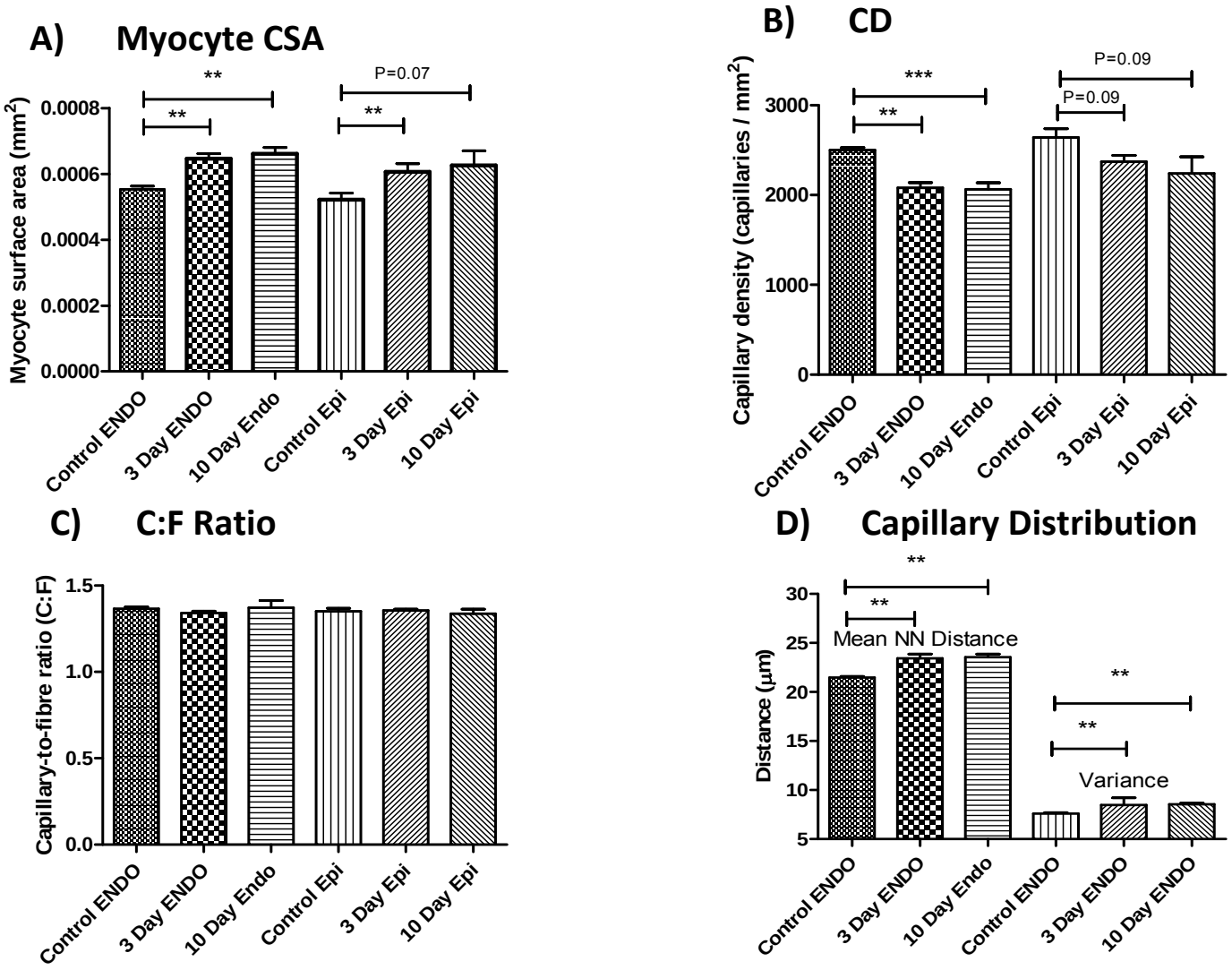

Figure 4.1. Effect of Isoprenaline on LV capillarity and myocyte morphology in the rat. (Control n=6, 3day n=4, 10day n=4). Treatment vs. Control; **P<0.01, ***P<0.001

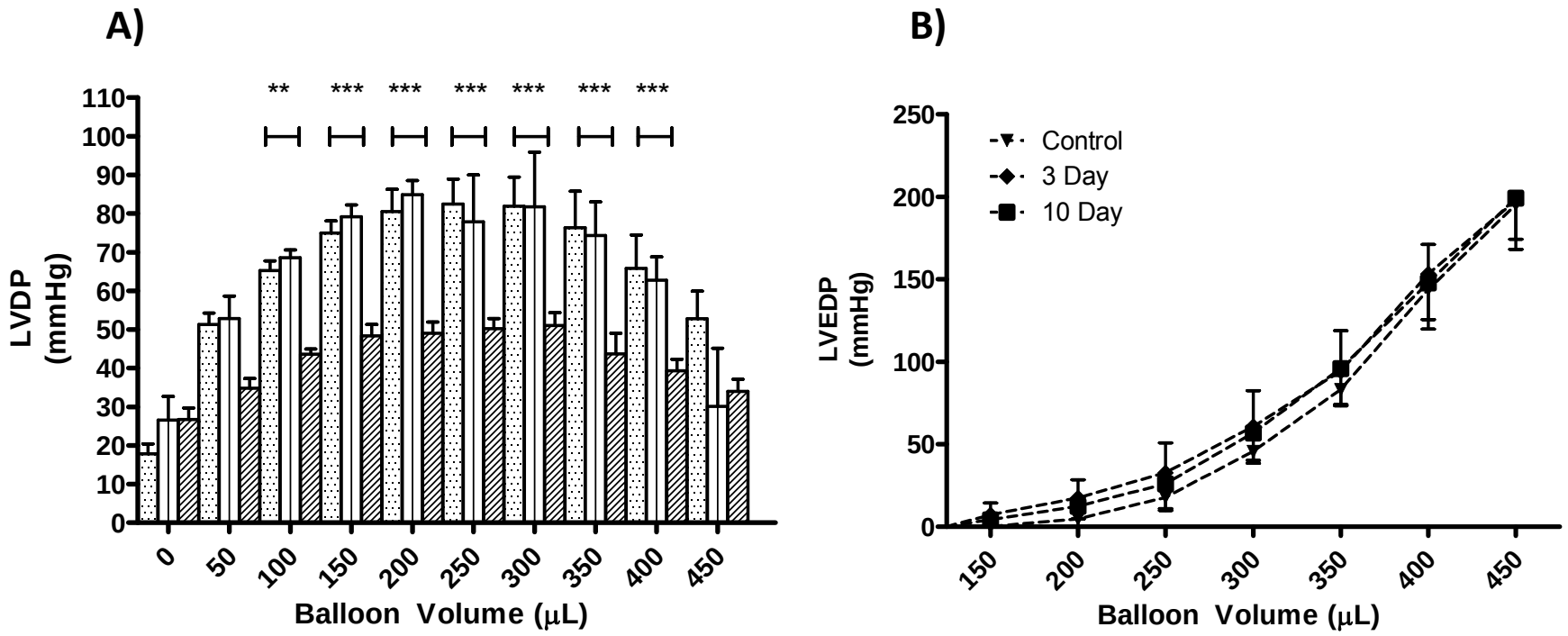

Figure 4.2 Effect of isoprenaline treatment on LVDP-volume relationship (A) and LVEDP-volume relationship (B). (Control n=6, 3day n=4, 10day n=4) The effects of isoprenaline treatment; **P<0.01, ***P<0.001. LEGEND: Dots = Control, Vertical stripes = 3 Day, Diagonal stripes = 10 day.

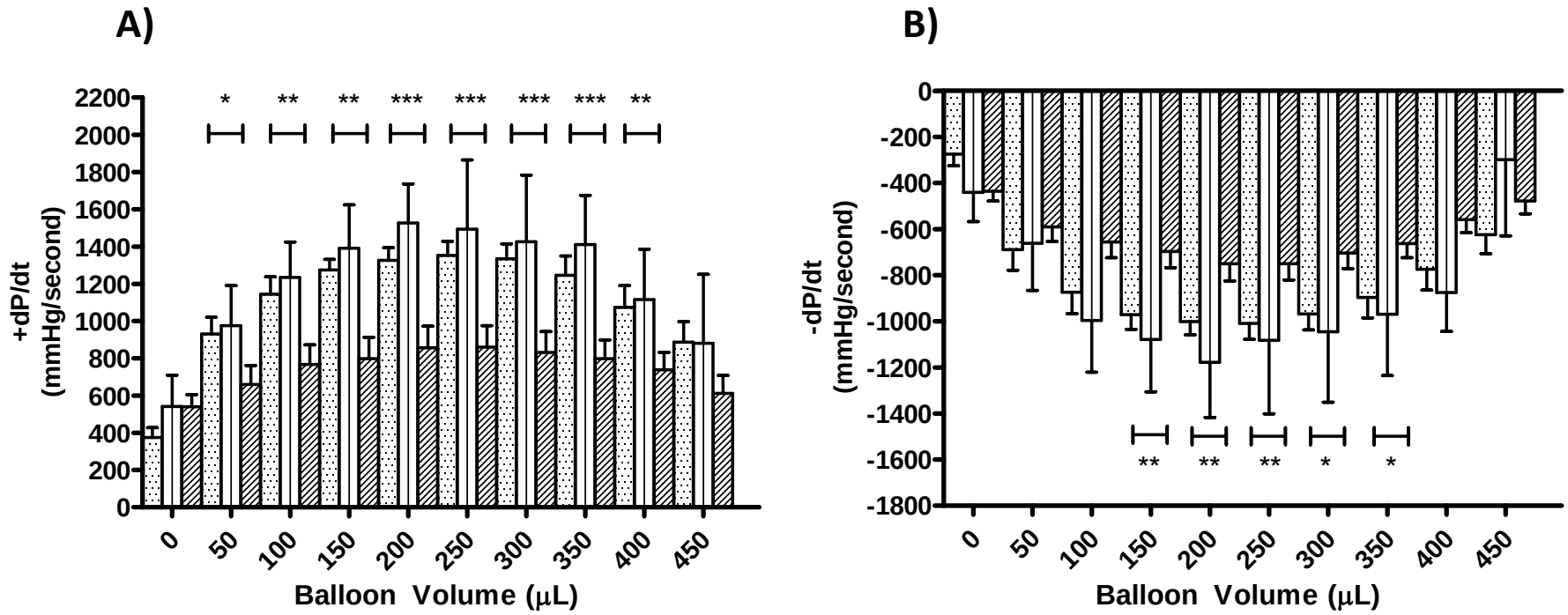

Figure 4.3 Effect of isoprenaline treatment on +dPdt (A) and -dPdt (B). (Control n=6, 3day n=4, 10day n=4) The effects of isoprenaline treatment; *P<0.05, **P<0.01, ***P<0.001. LEGEND: Dots = Control, Vertical stripes = 3 Day, Diagonal stripes = 10 day.

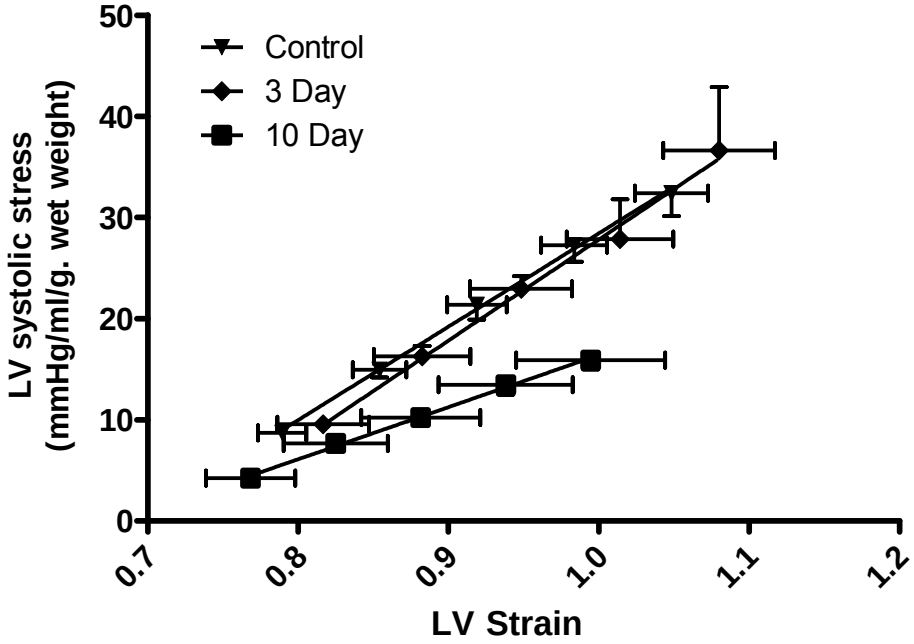

Figure 4.4 Effect of isoprenaline treatment on estimated LV systolic stress-strain. (Control n=6, 3day n=4, 10day n=4).

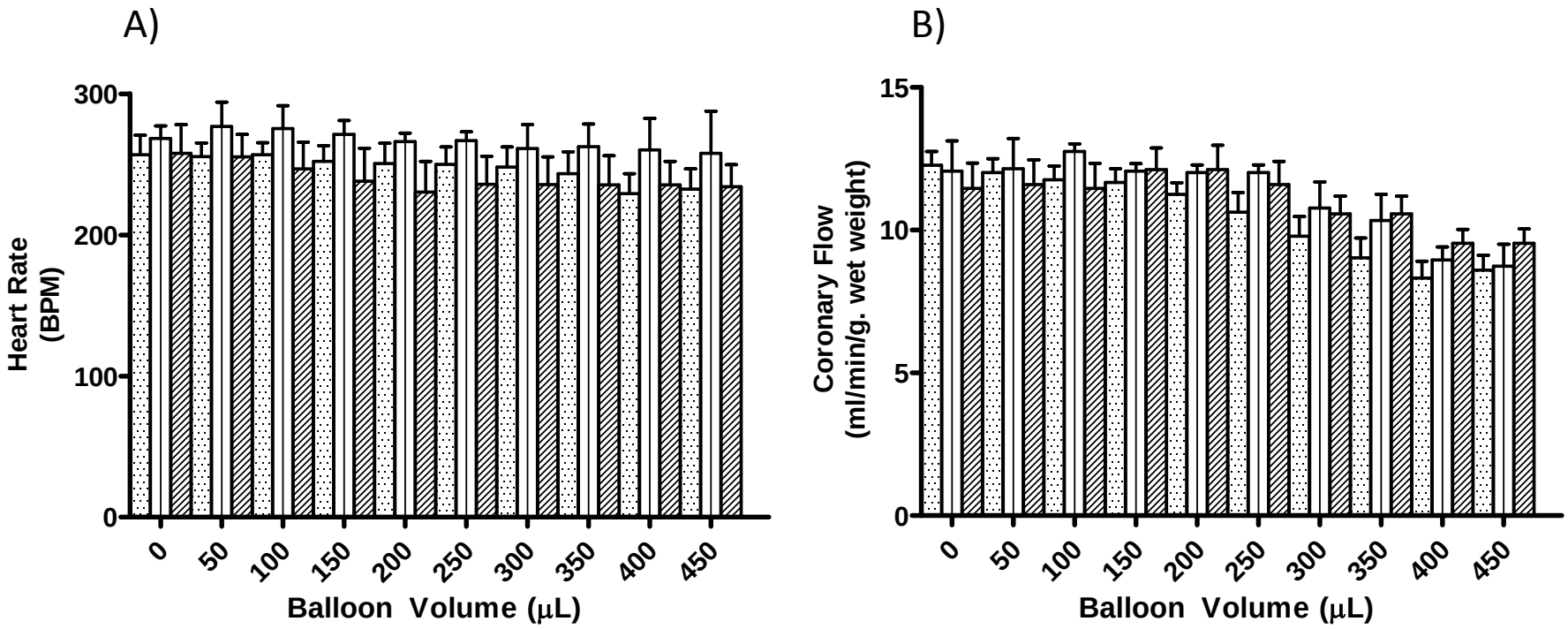

Figure 4.5. Effect of isoprenaline treatment on HR (A) and CF (B). (Control n=6, 3day n=4, 10day n=4) LEGEND: Dots = Control, Vertical stripes = 3 Day, Diagonal stripes = 10 day.

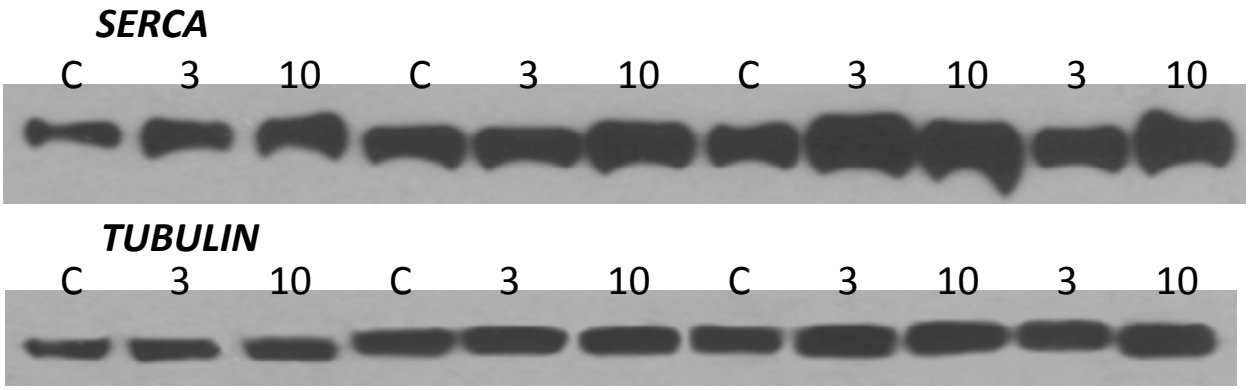

Figure 4.6. Representative western blots of SERCA2a and acylated tubulin. C = Control, 3=3 Day, 10=10 Day.

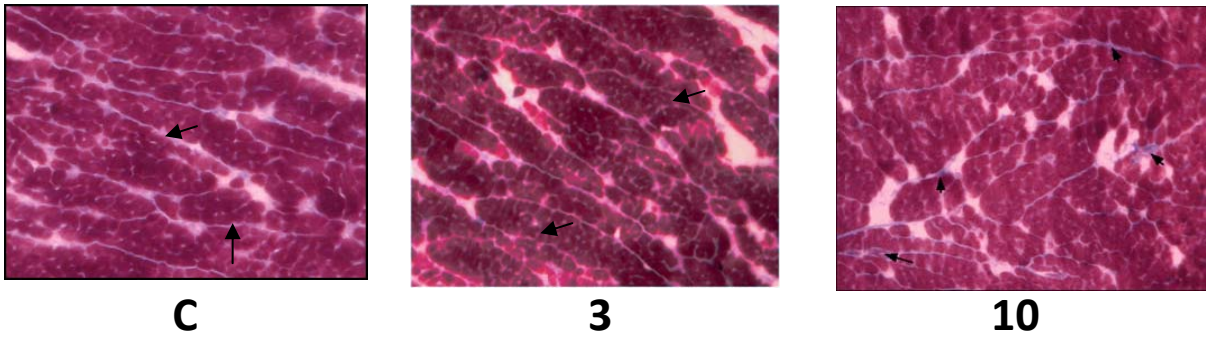

Figure 4.7. Representative images of LV subendocardial collagen content. Areas of collagen are shown in blue (see arrows). Magnification x125

Table 4.2. Effects of isoprenaline treatment on ventricular phenotype.

	Control	***3 Day***	***10 Day***
Estimated ventricular volume (μL)	273 ± 13	248 ± 42	243 ± 26
Ventricular chamber stiffness (mmHg/μL)	0.92 ± 0.15	0.90 ± 0.06	1.02 ± 0.08
Myocardial contractility (mmHg/ml/g. wet weight)	93 ± 11	98 ± 17	51 ± 5*
Ventricular collagen content (%)	2.34 ± 0.25	2.03 ± 0.32	3.01 ± 0.18
SERCA2 expression (A.U)	1.00 ± 0.05	1.15 ± 0.05	1.23 ± 0.10

(n=4-6) Estimated ventricular volume and chamber stiffness are assessed from the x intercept and slope of the linear portion of the LVEDP-volume relationship respectively. Myocardial contractility is assessed from the mean slope of the stress strain relationship. 10 day vs. Control; *P<0.05.

Table 4.3. Effect of dobutamine (150 nM) addition on cardiac performance of control and isoprenaline treated hearts.

	Control		*3 Day Isoprenaline*		*10 Day Isoprenaline*	
	Untreated	Dobutamine (150nM)	Untreated	Dobutamine (150nM)	Untreated	Dobutamine (150nM)
Heart Rate (bpm)	225 ± 2	218 ± 5	222 ± 11	225 ± 15	258 ± 18$^{\&}$	229 ± 21
Peak SP (mmHg)	65 ± 9	96 ± 11**	77 ± 5	101 ± 8**	64 ± 5	75 ± 5*
LVDP (mmHg)	51 ± 9	86 ± 12**	55 ± 8	86± 9***	31 ± 1$^{\&\&}$	47 ± 2*** $^{\&\&}$
+dP/dt (mmHg/sec)	953 ± 105	1450 ± 225***	1117 ± 181	1912 ± 214***	696 ± 45$^{\&\&}$	921 ± 65*** $^{\&\&\&}$
-dP/dt (mmHg/sec)	-720 ± 114	-1061 ± 217**	-903 ± 155	-1454 ± 198**	-526 ± 24$^{\&}$	-822 ± 123**
RPP (mmHg/min)	13500 ± 1900	20200 ± 2400***	15300 ± 1500	22600 ± 2000***	8100 ± 500$^{\&\&}$	10900 ± 900** $^{\&\&\&}$
Change in RPP (%)	-	48.9 ± 5.9	-	47.8 ± 4.28	-	34.9 ± 2.4$^{\&}$

(Control n=6, Treatment n=4). The effects of dobutamine; *P<0.05, **P<0.01, ***P<0.001. The effects of isoprenaline treatment; $^{\&}$P<0.05, $^{\&\&}$P<0.01, $^{\&\&\&}$P<0.001.

Chapter Five: Effects of reduced capillarity on contractile performance and metabolism in the left ventricle. Part 3: L-NAME

Nitric oxide (NO) is an important signalling molecule which influences many aspects of cardiac function including excitation-contraction coupling, oxygen consumption, substrate metabolism and hypertrophic growth. Endogenous NO plays an important role in the regulation of vascular tone and may be implicated in the development of new blood vessels. NO is synthesised from L-Arginine via the actions of nitric oxide synthase (NOS). Three isoforms of NOS have been demonstrated in the heart to date. NOS1 (or neuronal NOS) is the first of two constitutive (although expression is regulated) enzymes which appear to regulate contractility in the myocardium. Barouch *et al* (2002) demonstrated the co-localisation of NOS1 to the ryanodine receptor of the sarcoplasmic reticulum [182]. In keeping with this location NOS1 appears to regulate calcium handling and contractility. Knockout of NOS1 gene expression in transgenic mice results in a depression of basal contractile function and a reduced responsiveness to β adrenergic stimulation suggesting NO produced via NOS1 promotes cardiac inotropy [182]. Similar results are demonstrated when NOS1 activity is acutely inhibited by specific pharmacological blockade [183]. It should be noted that other studies have reported conflicting improvements in contractility in NOS1 knockout mice though technical differences between the studies have been proposed to underlie such differences [184, 185]. NOS3 (or endothelial NOS) is expressed in both the cardiac myocytes and in the endothelial cells lining the coronary blood vessels. In the myocytes NOS3 is co localised to the calveoli where it is proposed to regulate calcium influx through voltage sensitive L-type channels [185]. In contrast to the actions of NOS1, NO produced from NOS3 appears to depress contractility [182, 186]. The role of NO release from endothelial cells in the regulation of vascular tone is discussed in more detail later in this Introduction. The final NOS isoform NOS2 (inducible) normally absent in the myocardium is expressed during inflammatory response and produces large amounts of NO. This isoform is localised to the cytosol and its over-expression may be implicated in the patho-physiology of HF

[185]. Presented below is a discussion of the roles of NO in the regulation of vascular tone, blood vessel growth and hypertrophy.

NO, vascular tone and blood vessel growth

NO is a potent vasodilator which is released from the endothelium of blood vessels, namely arteries ranging from 100 to 500 micrometers in diameter, in response to changes in shear stress allowing for strict control of perfusion pressure at the site of origin of the arterioles [112, 113]. The endothelium dependent nature of shear stress induced vessel dilatation has been known for a number of years. Experiments where endothelial function was chemically denuded demonstrate a complete inhibition of flow induced dilatation in isolated blood vessels [187]. The role for NO in the regulation of vascular tone is evidenced by the increase in systemic arterial blood pressure when NOS activity is inhibited by pharmacological agents [188-190]. Elevated systemic blood pressure has been noted in mice engineered not to express the NOS3 gene while mice lacking NOS1 are comparable to controls [188, 189]. These gene knockout experiments demonstrate that NO derived from NOS3 is primarily responsible for modulating vessel tone.

Nitric oxide appears to play an important role in the growth of new capillaries. Experiments in skeletal muscles have demonstrated that pharmacological blockade of NOS activity prevents angiogenesis in response to increases in blood flow [163]. Studies in cultured human umbilical venous endothelial cells (HUVEC) have demonstrated an increase in nitric oxide release and an up-regulation in the expression of NOS in response to treatment with vascular endothelial derived growth factor (VEGF) implicating NO in the mechanism of pathway of angiogenic growth [191, 192]. In 3D fibrin gel assays, HUVEC's are able to form capillary like structures when stimulated by angiogenic growth factors (i.e. basic fibroblast growth factor and VEGF) [193]. The formation of these structures is prevented through pharmacological blockade of NOS, findings supported by the antagonism of VEGF induced blood vessel growth in the cornea of experimental rabbits dosed with L-NAME [194]. NO may play a critical role in capillary growth within the myocardium. Significantly

fewer capillaries have been noted in the left ventricle of neonatal mice lacking the gene for NOS3 [195]. 3D fibrin tube formation was significantly less in cardiac endothelial cells extracted from NOS3 knockout mice, a finding reversed through the addition of a nitric oxide donor compounds (DETA-NO). Attenuated expression of VEGF in whole heart homogenates from the neonatal mice suggests that NO regulates VEGF expression. Jozkowicz *et al* (2001) demonstrated that exogenous NO donors and transfection of genes encoding for NOS3 and NOS1 into cultured human and rat vascular smooth muscle cells up-regulates the expression of VEGF [196]. It is therefore probable that NO is both the downstream regulator of VEGF's pro-angiogenic actions and an upstream promoter of VEGF expression. Interestingly NOS3 gene knockout adult mice demonstrate similar cardiac capillary densities as control animals suggesting that other compensatory mechanisms are activated to normalise capillarity in these animals [195].

NO and hypertrophy

Cardiac hypertrophy has been demonstrated in response to chronic pharmacological inhibition of NOS activity by L-arginine analogues (Table 5.1). N (G)-nitro-L- arginine methyl ester (L-NAME) induced hypertrophy appears to occur independently of the increase in arterial blood pressure (afterload) due to its prevention with hydrazaline (a potent vasodilator) [197]. Therefore NO may have a direct role in regulating cellular growth. Cardiac hypertrophy is controlled by the complex interaction of stimulatory and counter regulatory signalling pathways. NO profoundly limits growth factor induced hypertrophy in isolated myocytes suggesting that it is an upstream activator of the anti-hypertrophic signalling. Further evidence for the anti-hypertrophic influence of NO can be found in studies of NOS gene deletion in mice. Barouch *et al* (2002) found that NOS1 and NOS3 gene knockout mice develop spontaneous cardiac hypertrophy [182]. This study is supported by the work of several other investigators reporting cardiac hypertrophy in mice lacking the gene which encodes NOS3 [189, 190]. Moreover cardiac hypertrophy appears to precede hypertension in this model [190].

Chapter Aims

This chapter addresses the suitability of using chronic nitric oxide synthase blockade to induce hypertrophy without concurrent angiogenic growth. To date no study has assessed the effect of L-NAME induced hypertrophy on ventricular capillarity. Given the potential role of NO in the growth of new blood vessels within the myocardium it was hypothesised that chronic exposure to L-NAME would induce ventricular myocyte hypertrophy without compensatory capillary growth providing a model of hypertrophy with impaired oxygen delivery.

Material and methods

Treatment regime

Wistar rats were treated with L-NAME, a non-reversible competitive NO synthase inhibitor, *ad libitum* in drinking water at a concentration of 400 mg/L for 4 weeks. This concentration gave doses of 40mg/kg body weight/day [198]. C57/Bl6 mice were treated with NG-Nitro-L-arginine (L-NNA), a reversible competitive NO synthase inhibitor, *ad libitum* in drinking water at a concentration of 100 mg/L giving a dose of 10 mg/kg body weight/day.

Results

Studies in the rat

Physiological parameters

Animals treated with L-NAME failed to thrive. Body masses were significantly lower in L-NAME treated animals compared with controls (268 ± 4 vs. 224 ± 11 g. wet weight, P<0.01, Table 5.3). Heart mass and heart/body mass ratios were found to be similar in both groups (Table 5.3). LV mass ratios were comparable between groups (1.08 ± 0.07 vs. 1.18 ± 0.09, Table 5.3)**.** *In vivo,* HRs were unaffected by L-NAME treatment (Table 5.3). Mean arterial blood pressure was significantly greater in animals dosed with L-NAME (95 ± 4 vs. 132 ± 5 mmHg, p<0.05, Table 5.3).

Capillary supply

CD was unaffected by L-NAME treatment in either the subendocardial (2378 ± 29 vs. 2298 ± 112 capillaries/mm^2, Figure 5.1A) or subepicardial (2898 ± 201 vs. 2767 ± 126 capillaries/mm^2, Figure 5.1A) regions of the left ventricle. C:F ratios and myocyte CSA were comparable between groups in both ventricular regions studied (Figure 5.1B & Figure 5.1C). Delaunay triangulation assessment of capillary supply shows that NN distances were comparable between control and L-NAME treated animals in the endocardial (20.8 ± 0.7 vs. 21.6 ± 0.7, Figure 5.1D) region of the left ventricle. The distribution of capillaries (variance) was also similar between treatment groups (Figure 5.1D). Terminal arteriole densities were comparable in epicardial (18.4 ± 1.3 vs. 18.0 ± 2.0 capillaries/mm^2) and endocardial regions (17.9 ± 1.0 vs. 17.1 ± 1.3 capillaries/mm^2).

Ex vivo contractile performance

Estimated ventricular volume was significantly less in L-NAME treated hearts (248 ± 34 vs. 137 ± 16 μL, P<0.001, Table 5.4) resulting in an earlier rise in the LVEDP-volume relationship when compared to controls (Figure 5.4A). Peak systolic pressure was greater in hearts from the L-NAME group (Figure 5.2B) and LVDP-volume relationship was similar in both treatment groups (5.2A). LV contractility

(+dP/dt) was similar at balloon volumes ranging from 0 to 150 μL but significantly lower in treated hearts at a balloon volume of 200μL (1326 ± 67 vs. 1081 ± 105 mmHg/sec, P<0.05, Figure 5.3A). LV relaxation (-dP/dt) was comparable to controls at all balloon volumes (Figure 5.3B). LV stress-strain was unaffected by L-NAME dietry supplementation (92.3 ± 2.22 vs. 84.5 ± 2.07 mmHg/ml/g. wet weight, Figure 5.4B). LV chamber stiffness was greater in the L-NAME group (0.85 ± 0.19 vs. 1.61 ± 0.24 mmHg/μL, P<0.05, Table 5.4). CF rates were impaired by 22 to 29 percent in L-NAME hearts when compared to controls at all balloon volumes (Figure 5.5B) and *ex vivo* HR was comparable between groups (Figure 5.5A). Histological analysis with Masons trichrome demonstrated a comparable degree of fibrosis in both control and L-NAME treated hearts (2.47 ± 0.21 vs. 2.95 ± 0.36 %, Table5.4). SERCA2a protein expression relative to acetylated tubulin was unaffected by chronic exposure to L-NAME (Figure 5.5 & Table 5.4)

Dobutamine challenge

Addition of dobutamine to the perfusate resulted in a significant increase in LVDP (23 ± 3 %), peak systolic pressure (20 ± 2 %), +dP/dt (57 ± 8 %), -dP/dt (5 ± 8 %) and RPP in control hearts (29 ± 2%). Similar findings were noted in hearts treated with L-NAME for 4 weeks (Table 5.5). Values of contractility did not differ between groups however the percentage increase in heart rate (5 ± 1 vs. 12 ± 3%, P<0.05) and RPP (29 ± 2 vs. 43 ± 3 %, P<0.05) was significantly greater in L-NAME treated hearts (All data table 5.5).

Studies in the mouse

Mice treated with L-NNA failed to thrive demonstrating lower body masses (28.8 ± 0.3 vs. 25.3 ± 0.8 g. wet weight, P<0.01) when compared to controls. Heart mass (0.14 ± 0.01 vs. 0.14 ± 0.01 g. wet weight) and heart to body mass ratios were comparable between both groups (5.03 ± 0.35 vs. 5.53 ± 0.15 mg/g. wet weight). Similar to the studies with L-NAME in the rat there was no alteration in myocyte CSA, CD or C:F ratio in either the subendocardial (CD: 3257 ± 20 vs. 3339 ± 147 capillaries/mm^2, C:F:1.73 ± 0.03 vs. 1.77 ± 0.03, CSA: 546 ± 10 vs. 538 ± 29 μm^2) or subepicardial (CD:

3360 ± 172 vs. 3210 ± 219 capillaries/mm^2, C:F: 1.80 ± 0.02 vs. 1.77 ± 0.04,CSA:552 ± 24 vs. 578 ± 42 μm^2) regions of the LV free wall. Data taken from a total of 5 animals per group.

Discussion

Chronic L-NAME and LV remodeling

Prolonged administration of L-NAME to rats resulted in a significant increase in systemic arterial blood pressure at 4 weeks. Since L-NAME is a specific inhibitor of NOS, these data support the role for NO release in the maintenance of systemic vascular tone [187-190]. Despite this elevation in blood pressure, cardiac mass was not increased in hearts from L-NAME treated animals. This finding is in contrast to other models of chronic systolic stress, such as aortic banding, where dramatic hypertrophic growth occurs within 1 week [40] and also conflicts with several reports utilising L-NAME dietary supplementation at comparable doses and lengths of exposure to those used in the present study [195, 200, 201]. Instead, the heart appears to accommodate a chronic increase in afterload by reducing LV lumen volume. The conservation of LV mass and the finding of normal subendocardial and subepicardial myocyte CSA suggest that there is a relative increase in the ratio of LV wall thickness to lumen volume. These observations are in keeping with the studies of Mandarim-de-Lacerda *et al* (2004), Matsubara *et al* (1998) and Bartunek *et al* (2000) who reported a decrease in LV lumen volume in the absence of ventricular hypertrophy and the conservation of total cardiac and LV mass [199, 200]. Arnal *et al* (1993) have demonstrated that both non-hypertrophic and hypertrophic remodeling can occur within a study population [201]. In their study of 25 rats dosed chronically with L-NAME (50 mg/kg body weight/day) just 6 developed left ventricular hypertrophy. Significant correlations were demonstrated between the activity of the renin-angiotensin system and cardiac mass suggesting a role for this known pro-hypertrophic signaling pathway in L-NAME induced hypertrophy. Moreover L-NAME induced hypertrophy is prevented through treatment with angiotensin receptor II blockers or angiotensin converting enzyme inhibitors [202, 203]. It is possible that luminal remodeling represents a transitional stage before the development of hypertrophy which may provide an argument for extending the length of the dosing protocol in future studies. However the evidence to date is conflicted with investigators reporting both hypertrophic and non-hypertrophic phenotypes at 4 weeks and 8 weeks of treatment. Vandsburger *et al* (2006)

demonstrated a reduced ventricular lumen volume in NOS1 knockout mice studied at 8 weeks (with preserved in vivo contractile performance) [204] suggesting that this NOS isoform is responsible for the LV remodeling seen during L-NAME treatment in the present study. This however contrasts with the work of Barouch *et al* (2002) who demonstrated a hypertrophic phenotype in both NOS1 and NOS3 gene knockouts [182]. Specific NOS1 antagonists are available and could be used in combination with gene deletion to investigate the potential differential role of NOS isoforms in LV remodelling. The morphological indices of ventricular dimensions (i.e. chamber radius and wall thickness) are defined by 1) the number of myocytes across the wall, 2) the average myocyte cross-sectional diameter and length and 3) the volume composition of the myocardium [205]. Therefore there are a number of potential mechanisms whereby chamber volume could be reduced. Firstly there could simply be fewer myocytes in the LV free wall. This is unlikely in L-NAME treated animals as LV free wall mass was comparable to controls. Secondly there could be a reduction in myocyte cell length which is again unlikely as CSA was conserved in both the subendocardial and subepicardial regions of the LV wall and therefore a reduction in myocyte length would be reflected as a reduction of cardiac or LV mass. Thirdly, there could be a reduction in the composition of the myocardium (i.e. less interstitial tissue) allowing for the compaction of the muscle fibres into a smaller volume Fourthly, transmural reorganisation of the fibres and other constituents (e.g. connective tissues and blood vessels) of the LV could alter LV diameter. Evidence from models of chamber dilation demonstrates how individual of groups of fibres can 'slide' in a lateral manner to alter ventricular geometry without significantly affecting ventricular mass. This myocyte slippage results in a thinning of the ventricle wall in order to accommodate an increase in chamber diameter. Chamber dilation occurs in models of ischemic injury [205], chronic pressure [206] and chronic volume overload [207]. If the reverse is true in L-NAME induced hypertension then there should be a significant increase in wall thickness associated with an increase in the number of myocytes across the LV wall. Light microscopy does not provide the resolution for counting myocytes at a magnification which could capture the entire LV free wall and as such previous investigators have

utilised low power electron microscopy to describe the transmural myocyte distribution associated with chamber dilation. These methods could be applied to hearts from L-NAME treated hearts. Previous investigators have however reported little change in absolute LV wall thickness reporting an increase in only wall thickness relative to LV lumen volume [199, 200]. Similar high resolution imaging techniques could be used to assess the volume composition of the myocardium (i.e. myocyte spacing and interstitial tissue makeup).

Chronic L-NAME and contractile performance

L-NAME hearts demonstrated a significant increase in systolic pressure development which was related to the early rise in the LVEDP-relationship and not associated with any change in the intrinsic contractile function of the myocardium (as evidenced by comparable stress-strain relationships). Both Bartunek *et al* (2000) and Matsubara *et al* (1998) demonstrated similar enhancement of LV systolic pressure development *in* vivo (echocardiography assessment) and in isolated heart preparations respectively [199, 200]. Matsubara *et al* (1998) also demonstrated no alteration in the intrinsic contractility of the myocardium (stress-strain relationships) in keeping with the findings of the present study. These data contrast with that of Moreno *et al* (1996) who found reduced isovolumetric pressure development in hearts from L-NAME treated animals - though there is no information on the loading conditions at which these values were obtained and only a single pressure is described [208]. In another study Jover *et al* (1993) reported a reduction in cardiac output in long-term L-NAME treated rats [202]. Cardiac output is however a measure of pump function and does not reflect the intrinsic contractility of the myocardium (i.e. the ability to generate force independent of loading conditions). In both these studies, L-NAME treatment was also associated with ventricular hypertrophy rather than geometric chamber remodeling (as seen in the present study and in that of Bartunek *et al* (2000) and Matsubara *et al* (1998)). Hypertrophy has been traditionally thought of as a compensatory mechanism however there is increasing suggestion that this process is maladaptive leading to contractile dysfunction and eventually HF [209]. Hearts in which the development of hypertrophy is prevented during chronic pressure overload (aortic

banding) with a calcineurin inhibitor demonstrate preserved haemodynamic function with no sign of deterioration over a period of several weeks [210]. The preservation of SERCA2a expression in L-NAME treated hearts suggests that there are no alterations in sarcoplasmic reticulum calcium handling which supports the functional findings of this sudy. In support of this Bartunek *et al* (2000) demonstrated normal calcium transients in myocytes extracted from L-NAME treated hearts [199]. Similarly to the present study these investigators also found normal SERCA2a expression in LV homogenates of the same hearts.

The influence of ventricular wall thickness on chamber compliance is well described and ventricular hypertrophy in the absence of changes in lumen volume has been linked to an increase in ventricular stiffness [3]. These principles provide the best explanation of the increase in stiffness associated with chronic L-NAME treatment where the decrease in lumen volume results in a relative increase the wall thickness to lumen volume ratio (as evidenced by the preservation of LV mass). Matsubara *et al* (1998) have previously reported that the diastolic compliance of the myocardium is increased following chronic dietary supplementation of L-NAME though they could not explain how these alterations were achieved [186].

One interesting finding is that the enhanced systolic performance of L-NAME treated hearts occurs on a background of impaired coronary blood flow. Altered vascular tone (i.e. coronary vasoconstriction) resulting from the inhibition of NOS seems the most likely cause of these changes. In addition it is possible that some degree of arteriole vascular remodelling had occurred in response to the chronic elevation of blood pressure. A great number of studies in both the L-NAME induced [120] and other models of hypertension [211] have demonstrated a marked increase in arteriolar wall thickness resulting in a reduction of intra-luminal diameter. These changes have been proposed to normalise for the increase in pressure and shear stress resulting from systemic hypertension and may explain the impairment of coronary flow noted in the present study. Alternatively, the Langendorff isolated heart preparations utilised in this study were carried out under the same

perfusion pressure in control and treated hearts (80 mmHg) and as such may not truly reflect the situation in the hypertensive animals. It is possible that resetting of normal vessel tone due to a chronic increase in coronary perfusion pressure results in under perfusion in the experimental setting. The preservation of contractile performance despite a reduction of coronary flow suggests that oxgen availability is not limiting in this model although it cannot be ruled out that cardiac performance is supported by an increased degree of oxygen extraction from the perfusate therefore necessitating lower flow rates. Additionally NOS inhibition has been shown to augment the calcium-dependent contractile reserve of isolated hearts which may offer a mechanism whereby cardiac functionality can be preserved at lower rates of oxygen consumption [199]. Comparisons of performance and oxygen consumption between control and L-NAME treated animals over a range of workloads would allow for the assessment of cardiac contractile efficiency (work per unit oxygen consumption). Previous investigations have noted both increased [212] and unchanged [213] measures of cardiac efficiency in experiments of acute NOS inhibition, but no such experiments have been performed in hearts form chronically dosed animals.

Conclusion

In conclusion the initial hypothesis that chronic nitric oxide synthase inhibition would result in a model of hypertrophic growth associated with capillary rarefaction for the current conditions has been disproved. Despite this L-NAME induced hypertension resulted in pronounced ventricular remodeling which appeared to compensate for the altered ventricular wall stress experienced *in vivo* (law of LaPlace). The preservation of contractile performance with a reduced perfusion suggests that oxygen availability was not limiting to performance in this model. The lack of LV remodeling was supported by histological studies in the mouse utilising chronic L-NNA exposure. Metabolic studies were not carried out in these hearts due to the lack of alteration in ventricular capillarity.

Table 5.1. Studies demonstrating hypertrophic growth in the hearts of rats exposed to chronic L-NAME dietary supplementation.

Paper	Regime	Major findings of study
Numaguchi *et al* (1995) [197]	1.0 g/L drinking water for 8 weeks.	• L-NAME treatment associated with the development of arterial hypertension. • Hypertrophic growth of myocardium and interstitial fibrosis in treated animals. • Microvascular remodeling in treated animals (small arterioles) – increased wall/vessel lumen ratio and perivascular fiborsis. • Prevention of hypertension with hydrazaline reduced the degree of interstitial fibrosis but had no effect on cardiac hypertrophy and microvascular remodeling.
Jover *et al* (1993) [202]	20 mg/kg animal body mass/day for 25 days.	• Significant and sustained increase in arterial blood pressure after 10 days of treatment. • Significant increase in cardiac mass following treatment with L-NAME. • Comparable plasma renin activity in both control and L-NAME treatment groups but L-NAME induced hypertension and hypertrophy was prevented by treatment with Losartan (an angiotensin II receptor antagonist).
Arnal *et al* (1993) [201]	50 mg/kg animal body mass/day for 8 weeks.	• L-NAME treatment induced significant arterial hypertension in all treated animals. • Of the 25 animals used in the study hypertrophic growth of the left ventricle occurred in only 6 cases. • Systolic blood pressures, plasma renin activity and angiotensin converting enzyme activity were significantly higher in the subgroup with hypertrophy when compared to the non-hypertrophied subgroup. • Multiple regression analysis demonstrated that L-NAME administration, plasma renin activity and systolic blood pressure contributed to the increase in left ventricular weight independently of one another.
Bernatova *et al* (1999) [203]	40 mg/kg animal body mass/day for 4 weeks	• Arterial hypertension was recorded in L-NAME treated animals after 1 week of treatment and was maintained through the regime. This increase in blood pressure regressed to control values following the cessation of L-NAME treatment (3 weeks). • Addition of captopril (angiotensin converting enzyme inhibitor) to the drinking water after cessation of L-NAME dietary supplementation significantly increased the rate of recovery to 1 week. Systolic blood pressures were significantly less than control values by 3 weeks. • Significant left ventricular hypertrophy in L-NAME treated animals. Preserved following a 3 week recovery period. • Captopril therapy prevented this increase in left ventricular mass associated with L-NAME (left ventricular/body mass ratios were actually lower than control values).

Table 5.2. Studies demonstrating a non-hypertrophic growth in the hearts of rats exposed to chronic L-NAME dietary supplementation.

Paper	Regime	Major findings of study
Arnal *et al* (1993) [201]	50 mg/kg animal body mass/day for 8 weeks.	• See table 5.1.
Matsurba *et al* (1998) [200]	100 mg/kg animal body mass/day for 8 weeks.	• Systemic arterial hypertension was noted after 2 weeks of treatment and was preserved through the 6 week period. • Lisinopril prevented the increase in systolic blood pressure in L-NAME treated animals. • Left ventricular mass and myocyte cross sectional areas were comparable between control and L-NAME treated hearts. • Left ventricular lumen volumes were significant reduced in L-NAME hearts resulting in a greater LV wall to lumen ratio when compared to control hearts. • L-NAME hearts presented with preserved contractile function and greater LV compliance.
Bartunek *et al* (2000) [199]	50 mg/kg animal body mass/day for 6 weeks.	• L-NAME treated animals developed systemic arterial hypertension after 1 week which was preserved for the 6 week study period. • No hypertrophy was reported after 6 weeks when assessed in terms of total LV mass or comparison of isolated myocyte cross-sectional area. • Despite the elevated blood pressure in vivo systolic cardiac performance was preserved and associated with concentric remodeling (reduced lumen volume and increased relative wall thickness) and augmented pressure-calcium relationships in isolated heart preparations. • SERCA2a and myosin heavy chain protein expression was comparable to control hearts.

Table 5.3. Effects of L-NAME treatment on organ mass and in vivo *physiological parameters.*

	Control	***L-NAME***
Body Mass (g)	268 ± 4	224 ± 11**
Heart Mass (g)	1.04 ± 0.04	0.90 ± 0.06
Heart mass / Body Mass (mg/g)	3.87 ± 0.04	3.85 ± 0.06
LV Free Wall Mass (mg)	295 ± 15	272 ± 21
LV Free Wall mass / Body Mass Ratio (mg/g)	0.98 ± 0.07	1.02 ± 0.09
In vivo heart rate (BPM)	411 ± 8	387 ± 17
Mean arterial blood pressure (mmHg)	95 ± 4	132 ± 5*

(n=6) The effects of L-NAME treatment *p<0.05, **p<0.01

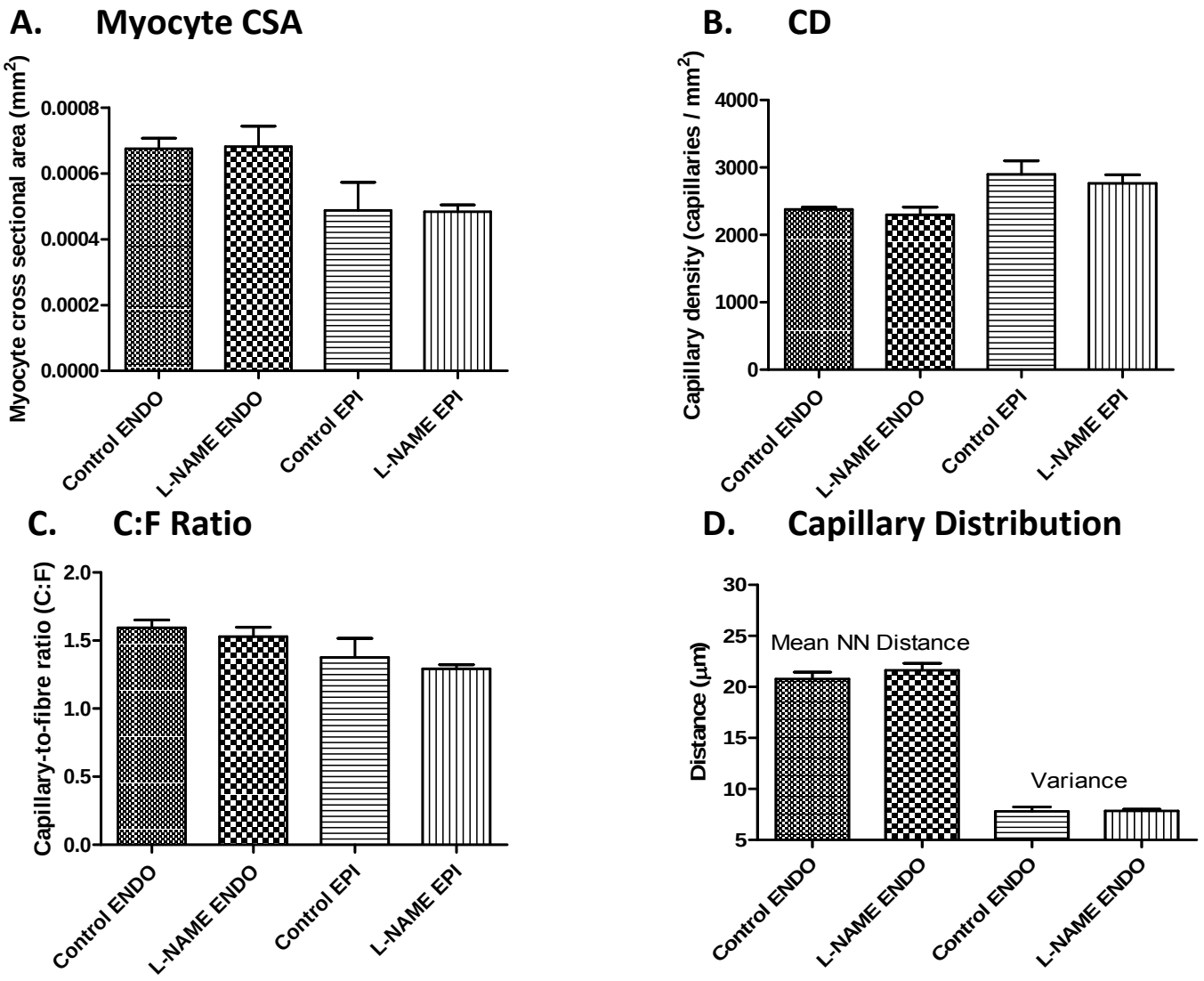

Figure 5.1. Effect of L-NAME on LV capillarity and myocyte morphology in the rat. (n=5-6)

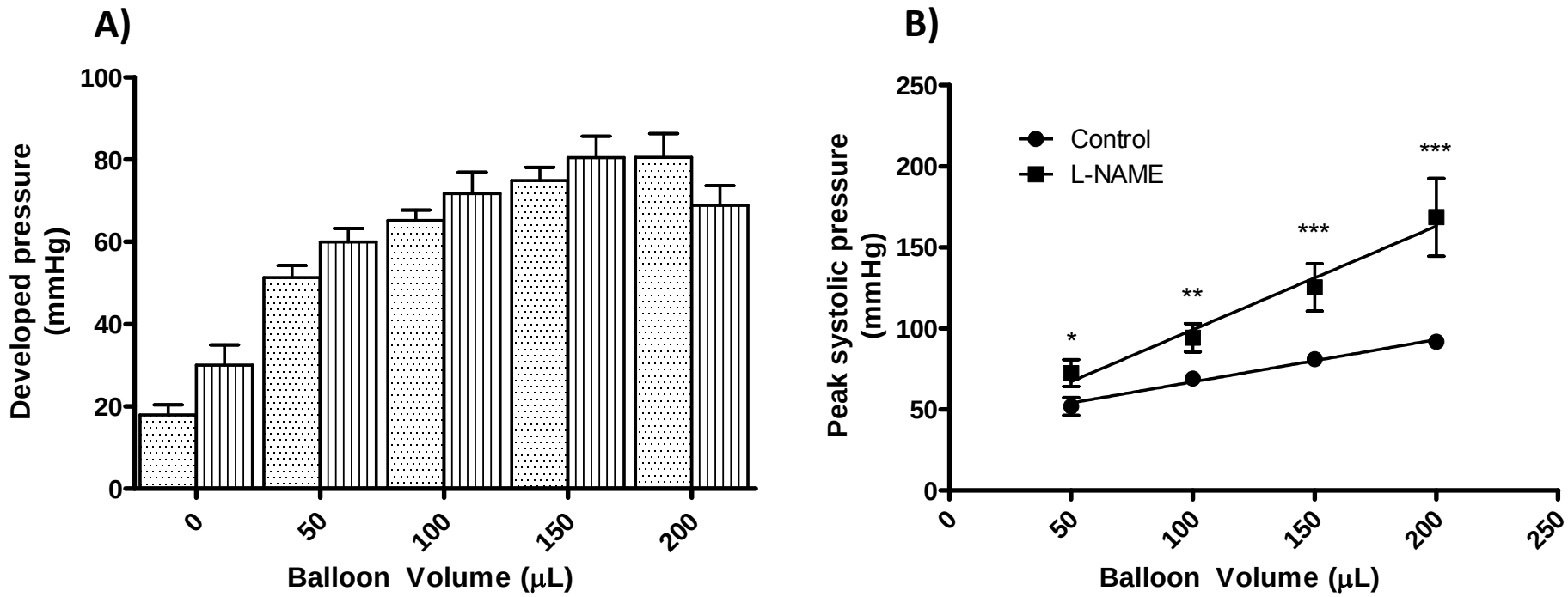

Figure 5.2 Effect of L-NAME treatment on LVDP-volume relationship (A) and peak systolic pressure (B). (n=6) The effects of L-NAME treatment; *P<0.05, **P<0.01, ***P<0.001. LEGEND: Dots = Control, Vertical stripes = L-NAME.

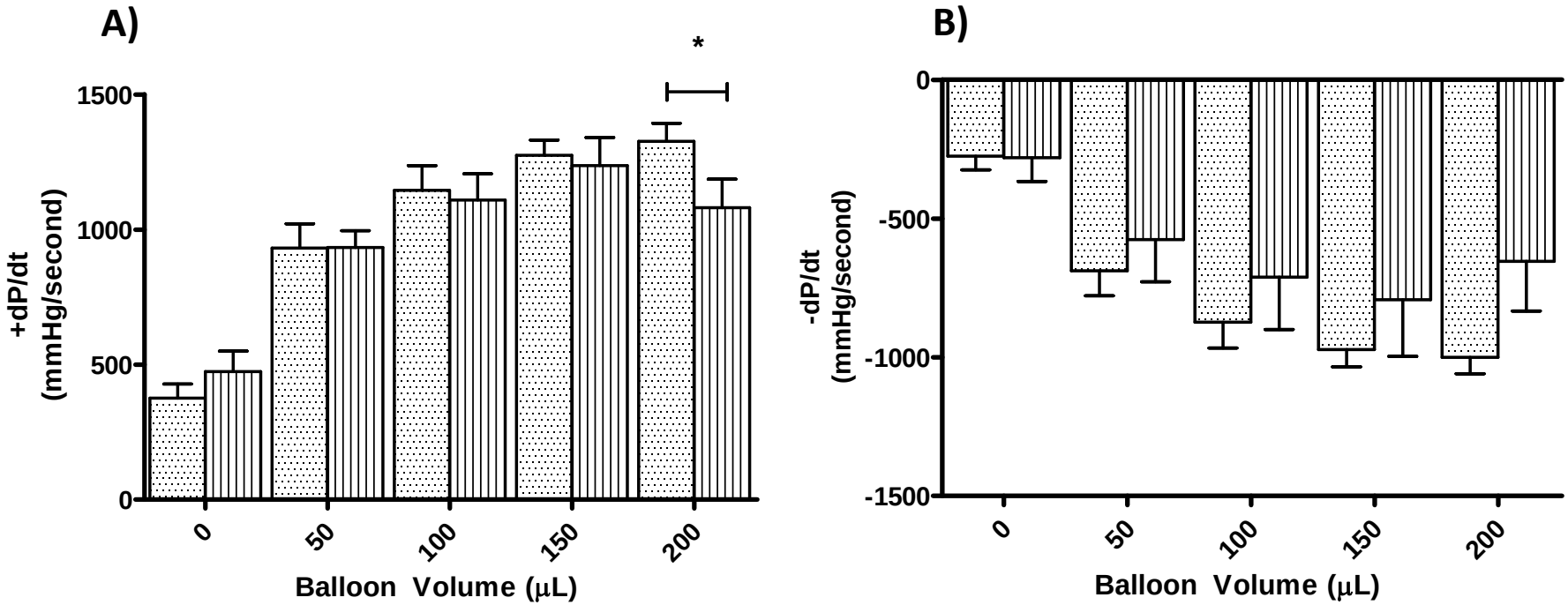

Figure 5.3 Effect of L-NAME treatment on +dPdt (A) and -dPdt (B). (n=6) The effects of L-NAME treatment; *P<0.05. LEGEND: Dots = Control, Vertical stripes = L-NAME.

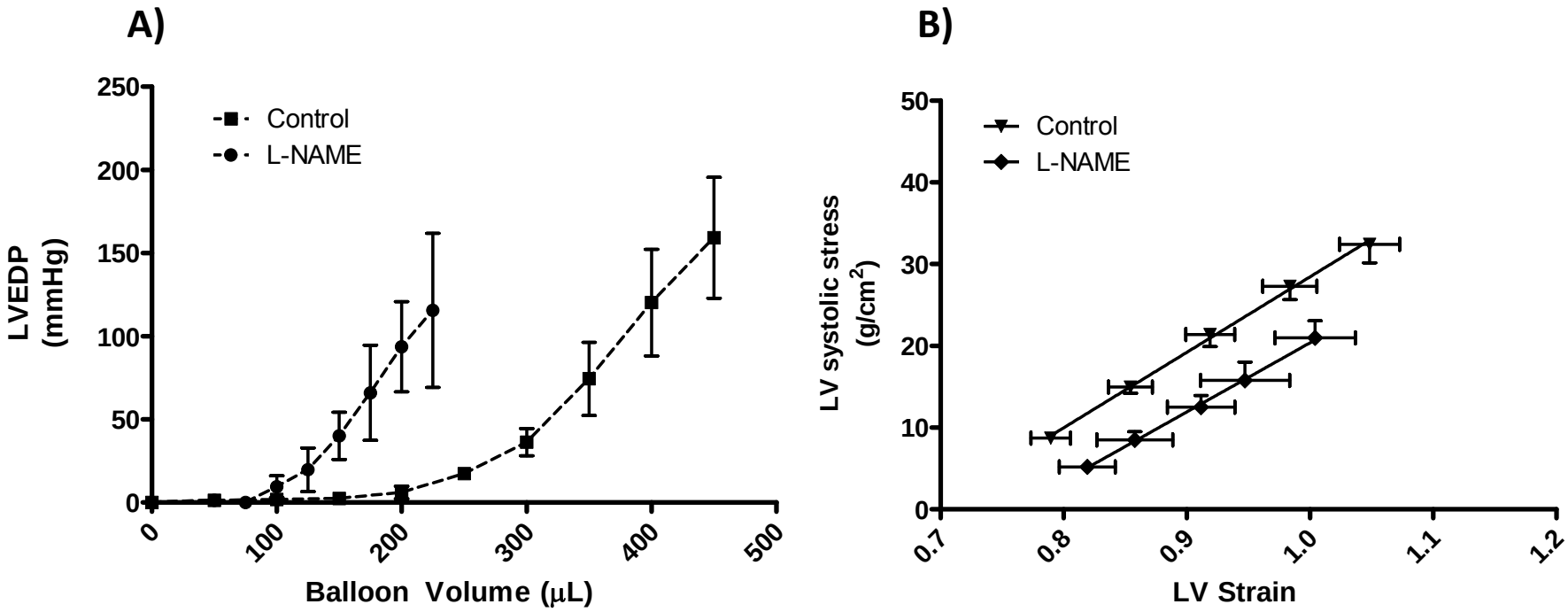

Figure 5.4 Effect of L-NAME treatment on LVEDP-volume relationship (A) and estimated LV systolic stress-strain (B). (n=6) .

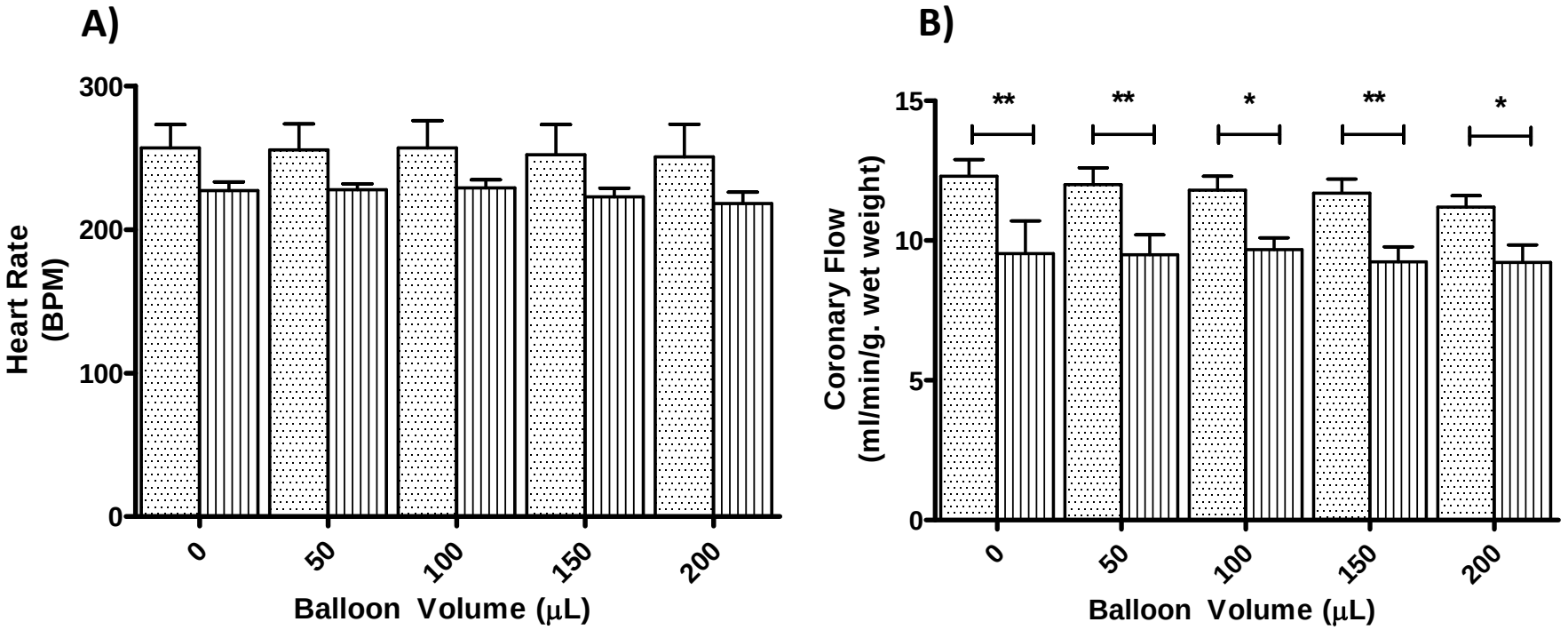

Figure 5.5. Effect of L-NAME treatment on HR (A) and CF (B). (Control n=6, 3day n=4, 10day n=4) LEGEND: Dots = Control, Vertical stripes = L-NAME.

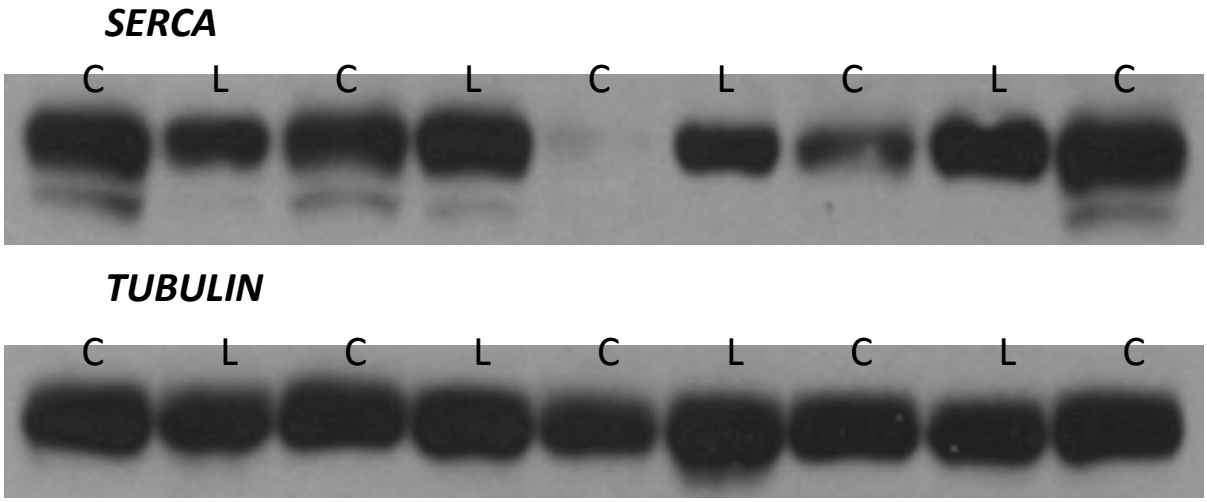

Figure 5.6. Representative western blots of SERCA2a and acylated tubulin. C = Control, L= L-NAME

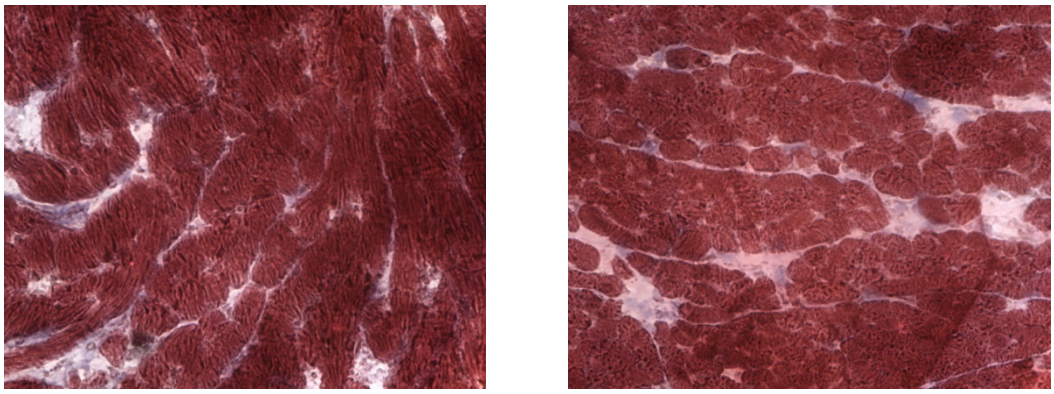

Figure 5.7. Representative images of LV subedocardial collagen content. Areas of collagen are shown in blue (see arrows). Magnification x250.

Table 5.4. Effects of L-NAME treatment on ventricular phenotype.

	Control	***L-NAME***
Estimated ventricular volume (μL)	248 ± 34	137 ± 16*
Ventricular chamber stiffness (mmHg/μL)	0.85 ± 0.19	1.61 ± 0.24*
Myocardial contractility (mmHg/ml/g. wet weight)	92 ± 2	85 ± 2
Ventricular collagen content (%)	2.54 ± 0.19	2.95 ± 0.36
SERCA2 expression (A.U)	1.00 ± 0.07	0.93 ± 0.07

(n=5-6) Estimated ventricular volume and chamber stiffness are assessed from the x intercept and slope of the linear portion of the LVEDP-volume relationship respectively. Myocardial contractility is assessed from the mean slope of the stress strain relationship. The effects of L-NAME treatment *p<0.05.

Table 5.5. Effect of dobutamine (150nM) addition on cardiac performance of control and L-NAME treated hearts.

	Control		***L-NAME***	
	Untreated	+ Dobutamine (150nM)	Untreated	+ Dobutamine (150nM)
HR (bpm)	235 ± 16	248 ± 20*	220 ± 7	253 ± 12**
Peak SP (mmHg)	100 ± 8	127 ± 6**	107 ± 8	136 ± 5***
LVDP (mmHg)	78 ± 7	103 ± 3**	86 ± 8	116 ± 9***
+ dP/dt (mmHg/sec)	1259 ± 170	2094 ± 253**	1304 ± 155	2256 ± 153***
- dP/dt (mmHg/sec)	-939 ± 142	-1431 ± 183*	-802 ± 215	-1596 ± 109**
RPP (mmHg/min)	18300 ± 1600	25500 ± 1300**	18900 ± 2000	29100 ± 2100***
% increase in RPP	-	29 ± 2	-	43 ± 3$^{\&}$

(n=5-6). The effects of dobutamine; *P<0.05, **P<0.01. The effects of L-NAME; $^{\&}$P<0.05

Chapter Six. Effects of increased capillarity on cardiac performance and metabolism. Part 1: Cold acclimation

Euthermic animals defend their core body temperature within a strict range (the hypothalamic set point) optimised for the maintenance of normal physiological function. Non-hibernating mammals acutely exposed to cold initially demonstrate shivering thermogenesis, a mechanism whereby additional heat is produced by involuntary muscle contractions [214]. Gradually this process is replaced over the following weeks by metabolic mechanisms of heat generation i.e. non-shivering thermogenesis. Hypertrophy of glycolytic skeletal muscles and accumulation of brown adipose tissue (the site of non-shivering thermogenesis) occurs in rats exposed to 5^{o}C for 8 weeks[215]. Given the extra demand for heat generation it is not surprising that exposure to cold dramatically elevates total body oxygen consumption and metabolic rate [214-216]. Increases in blood flow to the liver, kidneys, brown-adipose tissue and thyroid glands highlight the enhanced oxygen demand of these organ systems in the response to chronic cold exposure[217].

Physiological adaptation to chronic cold exposure

Chronic exposure of adult rats to a cold environment (classically 4-6^{o}C) is associated with an elevation of arterial systolic blood pressure and increased heart rate [140, 218-222]. This change in blood pressure is likely associated with the greater measures of stroke volume reported in rats exposed to these cold environments for 6 to 10 weeks [223]. A decrease in total peripheral resistance, at least partially attributable to pronounced vasodilatation in the skeletal muscles, has also been described [223]. Increased circulating concentrations of catecholamines suggest that the changes in heart rate are mediated by stimulation of the beta-adrenergic signalling pathways [224]. This conclusion is supported by studies in which cold exposed rats treated with propranolol (a non-selective β-adrenoceptor antagonist) demonstrate comparable HRs as normothermic controls [220]. The enhanced stroke volume of cold exposed rats appears to occur through ventricular chamber enlargement (though measures of the intrinsic contractility of the myocardium have not been

reported). Rats exposed to cold environments demonstrate significantly greater measures of whole heart and ventricular mass (relative to body mass) when compared to normothermic controls. Evidence from histological studies show that myocyte elongation rather than changes in cross-sectional area are responsible for these differences between groups [216]. This eccentric hypertrophy, often referred to as volume overload, is thought to underlie the physiological enlargement of the ventricle during endurance training (increased venous return and greater blood volume). Roukoyatkina *et al* (1999) demonstrated an increase in total blood volume in cold acclimated rats, suggesting that similar processes may drive the dilation of the ventricle during cold exposure [218].

Given the increase in cardiac workload (i.e. increased chamber volume and HR) associated with chronic cold exposure it is not surprising that a number of investigators have proposed that the oxygen delivery capacity of cold acclimated hearts may be modified in some manner. However, early studies by Heroux and Pierre (1957) in adult rats (5 to 6 weeks) did not demonstrate any change in the capillarity of acclimated hearts [225]. Similarly, Kayar and Banchero (1985) found no change in capillary density despite evidence of fibre hypertrophy (elongation) in comparably aged adult guinea pigs [216]. Evidence from exercise studies have suggested that very young animals have the capacity for capillary growth, while more mature animals lose the ability to respond to physiological and pathological angiogenic stimuli [80]. Acute exposure of young weaned animals animals (1 to 3 weeks of age) to cold environments (cold shock) however results in premature death. To surmount this problem, studies have been carried out in rats reared in cold environments for 68 generations [226]. This process affords some protection from the cold during weaning allowing the newborn animals to acclimate before full environmental exposure. Cold-reared rats in this setting demonstrate cardiac hypertrophy (increased myocyte cross-sectional area), greater capillary numbers and improved oxygen delivery capacity (smaller oxygen diffusion distances) providing the means to support increased cardiac workload and myocyte dimensions.

Cold acclimation of young animals

Cold acclimation describes a gradual reduction in ambient temperature and photoperiod which has been used to overcome the mortality associated with exposure of young animals to cold environments (over 4 to 8 weeks). This method has been used successfully in young rats demonstrating comparable changes to body composition and physiological parameters to those seen during chronic cold exposure [215]. Reducing the length of the photoperiod better mimics the environmental conditions during the winter season and appears to be associated with some modest physiological effects. Importantly photoperiod appears to regulate the degree of parasympathetic and sympathetic neural outflow in rodents [227] and may influence growth rates in cold exposed animals [215, 228]. Cold acclimation is associated with an increase in cardiac ventricular volume and arterial blood pressure suggesting a similar drive to increase cardiac output, and thus cardiac workload, as seen during chronic cold exposure of adult rats [228]. Preliminary evidence has suggested that cold acclimation is associated with an increase in left ventricular capillary density suggesting a significant angiogenic stimulus in younger animals (Deveci, D. PhD Thesis (1999).

Chapter Aims

Experiments were carried out to assess the impact of a reduction in environmental ambient temperature and photoperiod on ventricular capillarity and contractile performance. These were necessary before the potential exploitation of therapies to modify capillary growth in this model. Experiments were carried out in the youngest possible animals (weaning) due to evidence that age plays a role in the likelihood of new vessel growth. It was hypothesised that cold acclimation would promote capillary growth in the left ventricular free wall of treated animals supporting an increase in ventricular contractile performance.

Materials and Methods

Cold acclimation protocol

Animals were transferred to a specially designed environmental chamber. The initial air temperature was 18^{o}C and was reduced by 1^{o}C every 2 days until the ambient temperature reached 5^{o}C. Animals were kept at this temperature for a futher 4 days (31 days in total). The reduction in temperature was accompanied by a reduction in the photoperiod from a 12:12 light:dark (L:D) cycle to one hour a day by 23 days (1:23 L:D). Day length was reduced on the by 1 hour every 2 days. Figure 6.1 is a schematic representation of the acclimation process over this time period. Control animals were kept in ambient temperatures of 21 ± 1^{o}C and a daily photoperiod of 12:12 L:D. Initial rat body mass was between 60 and 90 grams representing the youngest available experimental agent (weaning). Initial mouse body masses were between 15 and 20 grams.

Results

Studies in the rat

Physiological parameters

Animal body masses were comparable between the treatment groups (303 ± 17 vs. 303 ± 8 g, n.s., Table 6.1). Cold acclimation induced cardiac hypertrophy as evidenced by an increase in cardiac mass (1.52 ± 0.06 vs. 1.72 ± 0.06 g, P<0.01, Table 6.1) and in the heart/body mass ratio (4.86 ±0.08 vs. 5.69 ± 0.10, p<0.001, Table 6.1). A modest increase in mean arterial blood pressure was noted in cold acclimated animals (100 ± 3 vs. 112 ± 3 mmHg, P<0.05, Table 6.1), with comparable heart rates between the groups (392 ± 4 vs. 384 ± 6 bpm, Table 6.1).

Capillary supply

CD (capillaries/mm^2) was unaffected by cold acclimation in both the subendocardial (2378 ± 29 vs. 2612 ± 156 capillaries/mm^2, Figure 6.1A) and subepicardial (2898 ± 201 vs. 2612 ± 156 caps/mm^2, Figure 4.1A) regions of the left ventricle. C:F ratio and myocyte CSA were comparable between groups in both ventricular regions studied (Figure 6.1B & Figure 6.1C). Delaunay triangulation assessment of capillary supply shows that mean NN distance were comparable between control and cold acclimated animals in the subendocardial (20.8 ± 0.7 vs. 19.5 ± 0.5 μm, Figure 6.1D) region of the LV. The distribution of capillaries (variance of capillary supply area) was also similar between treatment groups (Figure 6.1D).

Ex vivo contractile performance

Intrinsic HR was similar in both control and cold acclimated animals at all balloon volumes (Figure 6.6A). Pressure development increased monotonically with balloon volume up to 300 μL. Further increases in balloon volume resulted in a reduction in ventricular pressure development, associated with an increase in LVEDP and a reduction in coronary blood flow (Figure 6.3A, Figure 6.3A and

Figure 6.3B). The LVDP-volume relationship was comparable between control and cold acclimated animals at all balloon volumes (peak LVDP: 101 ± 10 vs. 86 ± 14 mmHg, Figure 6.3A). Similarly +dP/dt and –dP/dt were comparable between the two study groups (Figure 6.4A and Figure 6.4B). In keeping with this, SERCA2a protein expression was preserved (Table 6.2) and ventricular collagen content was comparable between the treatment groups (2.47 ± 0.21 vs. 2.66 ± 0.15 %, Table 6.2). Cold acclimated hearts demonstrated a significant increase in estimated LV lumen volume when compared to controls (303 ± 20 vs. 355 ± 7 μL, P>0.05, Table 6.2). This relationship is seen as a rightward shift in the LVEDP-volume relationship for cold acclimated hearts (Figure 6.3B). LV stiffness was comparable between treatment groups (0.78 ± 0.06 vs. 0.84 ± 0.04 mmHg/μL, Table 6.2). CF rates were comparable between treatment groups (Figure 6.6B). Myocardial contractility, as assessed from slope of the LV systolic stress-strain relationship, was comparable between the treatment groups (110 ±11 vs 82 ± 7 mmHg/ml/g. wet weight, Figure 6.5)

Dobutamine challenge

Addition of dobutamine to the perfusate resulted in a significant increase in SP (25 ± 9 %), LVDP (47 ± 10 %), +dP/dt (63 ± 13 %) and –dP/dt (51 ± 10 %), and RPP (39 ± 12 %) in control hearts (Table 6.3). Similar changes in contractile performance were noted in hearts from cold acclimated animals (Table 6.3)

Studies in the mouse

Cold acclimated mice failed to thrive demonstrating lower body mass (28.8 ± 0.3 vs. 25.5 ± 0.4 g. wet weight). Total heart mass (140 ± 10 vs. 190 ± 10 mg. wet weight, P<0.01) and the heart mass to body mass ratio (5.03 ± 0.35 vs. 7.72 ± 0.49, P<0.01) was significantly greater in cold acclimated animals demonstrating hypertrophy of the myocardium. In keeping with the rat there was no alteration in myocyte CSA, CD or C:F ratio in either the subendocardial (CD: 3257 ± 20 vs. 3212 ± 64 capillaries/mm^2, C:F:1.73 ± 0.03 vs. 1.77 ± 0.03, CSA: 546 ± 10 vs. 559 ± 11 μm^2) or subepicardial (CD:

3360 ± 172 vs. 3465 ± 190 capillaries/mm^2, C:F: 1.80 ± 0.02 vs. 1.80 ± 0.02 ,CSA:552 ± 24 vs. 545 ± 38 μm^2) regions of the LV free wall.

Discussion

Cold acclimation induced LV remodeling

Combined exposure of young rats to a cold environment and reduced daylight resulted in LV chamber expansion and mild hypertension. These changes were found to be in good agreement with previous studies of chronic cold exposure in both rats [140, 215, 216, 219, 220, 222] and in guinea pigs [216, 226]. Adaptation of the ventricular dimensions along with a preservation of contractile performance appears to provide a means whereby stroke volume can increase to support the global increase in metabolic rate during enhanced thermogenesis. Histological studies demonstrated no change in fibre cross-sectional area suggesting that the increase in left ventricular mass noted in the present study was a result of fibre elongation, consistent with the findings of increased lumen volume.

The stimulus for myocardial growth in response to cold exposure is unclear. Peripheral vascular resistance has been shown to fall in animals exposed to cold environments [223], at least partially attributed to the vasodilation of vessels supplying the skeletal muscles, suggesting that hypertrophy does not occur as a compensatory mechanism to overcome an increase in cardiac afterload. Moreover treatment with propranolol [220], captopril [219] or L-arginine [229], all of which significantly reduce arterial blood pressure, does not influence the cold induced increase in cardiac mass. The eccentric cardiac remodeling associated with cold acclimation has more in common with models of chronic volume load rather than pressure load (i.e. fibre elongation). Previous investigators have reported significant increases in circulating blood volume, a possible consequence of an increase in aldosterone synthesis [230]. An increase in blood volume, and thus preload, may provide a mechanical stimulus for ventricular enlargement during cold acclimation. Studies in which rats were treated with propranolol and captopril during chronic cold exposure still demonstrate a

significant increase in cardiac mass suggesting the trophic effects of catecholamines and angiotensin II may not be involved [219, 220]. Mice engineered not to express the genes encoding for angiotensinogen also demonstrate a similar phenotype to cold exposure control mice [231].

Cold cclimation and LV capillarity

In contrast to the hypothesised increase in capillarity there was no change in the capillary number, density or distribution in transverse sections of the left ventricle. This finding contrasts to the preliminary reports of increased capillary density by Deveci (Deveci, D. PhD Thesis (1999)) in rats exposed to these environmental conditions. This study however did not assess capillary number in samples where the contractile state of the myocardium was normalised (i.e. during systole or diastole) and so represents a potential source of error. Additionally the nature of the stain utilised (alkaline phosphatase) did not allow for assessment of the capillary to fibre ratio and as such it is unclear whether the reported changes were a result of true new vessel growth (angiogenesis) or changes in myocyte dimensions (i.e. a reduction in cross-sectional area). In line with the findings of the present study, Kayar and Banchero (1985) found unchanged capillary density and oxygen diffusion distances in adult guinea pigs acclimated to 4^{o}C over an 8 to 15 week period. Gao *et al* (1997) also found no influence of cold acclimation on endocardial capillarity in adult rats chronically exposed to a cold environment [226]. Similarly no growth was seen in mice exposed to the same environmental conditions. The normal distribution of capillaries in the cold acclimated heart suggests that oxygen delivery is not impaired and the lack of vessel growth suggests that the existing capillary bed is more than adequate to meet the energy/oxygen demands of the myocardium. In fact as oxygen diffusion occurs down the length of the capillary, it is possible that the eccentric remodeling associated with cold acclimation is supported by an increase in arterio-venous oxygen extraction. Simple measures of the arterio-venous oxygen difference could be used to confirm this and stereological techniques could be applied to look at capillary length as well as capillary density in the transverse plane.

A review of previous studies suggests that the angiogenic response of the adult myocardium to physiological stimuli may be somewhat limited with few investigators reporting changes in capillarity during prolonged endurance exercise or in conditions of reduced oxygen availability [80]. Hypoxia as an angiogenic stimulus seems unlikely in this modest model of ventricular adaptation and the mechanical factors of vessel stretch and shear stress are seemingly ruled out by comparable heart rates and rates of coronary blood flow demonstrated between cold acclimation and control hearts. The suggestion that capillary growth occurs more readily in younger animals is not supported by the results of the present study though no comparison between animals of different ages was made. It cannot be ruled out that cold acclimation is an insufficient angiogenic stimulus compared with the exercise regimes in which this relationship was first described.

Cold acclimation and LV contractile performance

Cardiac contractile performance was preserved in cold acclimated hearts representing a form of well adapted remodelling. It is therefore possible to predict that *in vivo* under similar loading conditions (i.e. heart rate, preload and afterload) cold acclimated hearts will eject a greater volume of blood per beat and that the increase in mean arterial blood pressure (MAP) associated with cold acclimation likely relates to an increase in the stroke volume of the myocardium (MAP = stroke volume x peripheral vascular resistance). Indeed previous investigators have noted that cardiac output is enhanced in animals exposed to cold environments for a prolonged period of time[223]. Additionally, according to the law of LaPlace, ventricular dilation without a concurrent increase in wall thickness (based on the preservation of myocyte CSA) will elevate wall stress and thus oxygen consumption, though no direct measure of oxygen consumption was made during this study.

Contractile reserve in response to β adrenoceptor stimulation was preserved in cold acclimated animals despite evidence that circulating catecholamines are elevated during exposure to cold environment [215, 220]. Previous studies have noted conflicting results with reports of both increased [232] and decreased [228] contractile responses to adrenergic agonists following prolonged periods of cold exposure. It is possible that the length of time of exposure to elevated

circulating catecholamines is an inadequate stimulus at 4 weeks to result in the desensitisation of adrenergic responses, as is seen during prolonged exposure to β adrenoceptor agonists.

Conclusion

In conclusion, the hypothesis that cold acclimation would induce left ventricular capillary growth and changes in contractile performance has been rejected. Cold acclimation is associated with ventricular luminal dilation, preserved contractile performance and a normal distribution of the ventricular capillary bed.

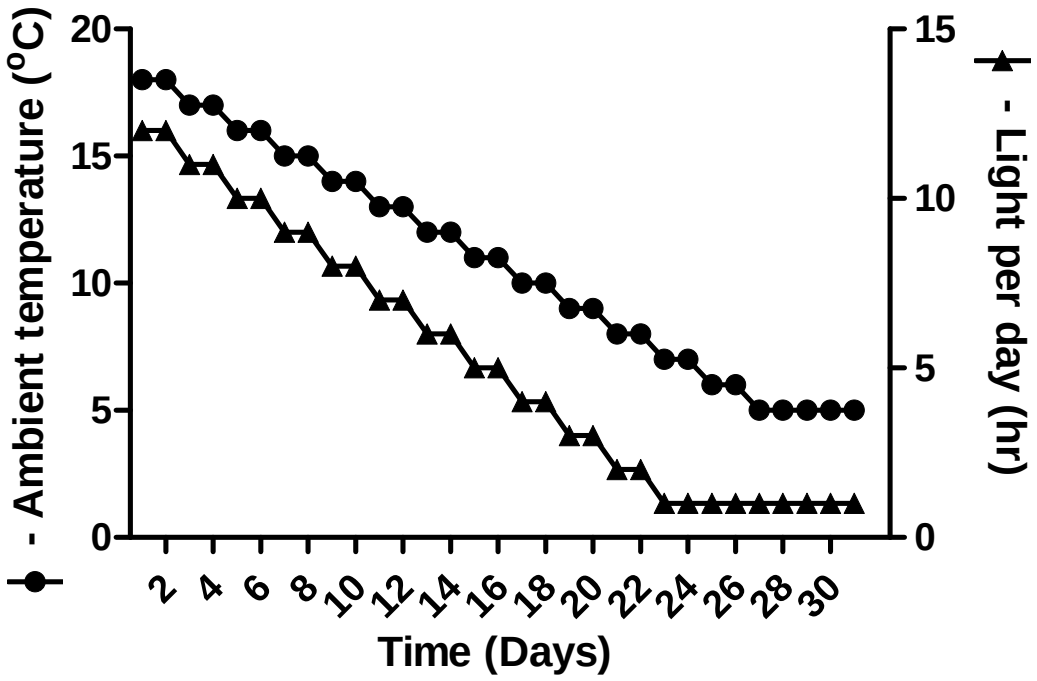

Figure 6.1. Schematic of changes in ambient temperature and hours of light per day over the 31 day cold acclimation process.

Table 6.1. Effects of cold acclimation on organ mass and in vivo physiological parameters.

	Control	***Cold Acclimated***
Body mass (g)	303 ± 16.71	303 ± 8.38
Heart mass (g)	1.52 ± 0.06	1.72 ± 0.06**
Heart mass / Body mass (mg/g)	4.86 ± 0.08	5.69 ± 0.10***
In vivo heart rate (BPM)	392 ± 4	384 ± 6
Mean arterial blood pressure (mmHg)	100 ± 3	112 ± 3*

(n=6) The effects of cold acclimation *P<0.05, **P<0.01, ***P<0.001.

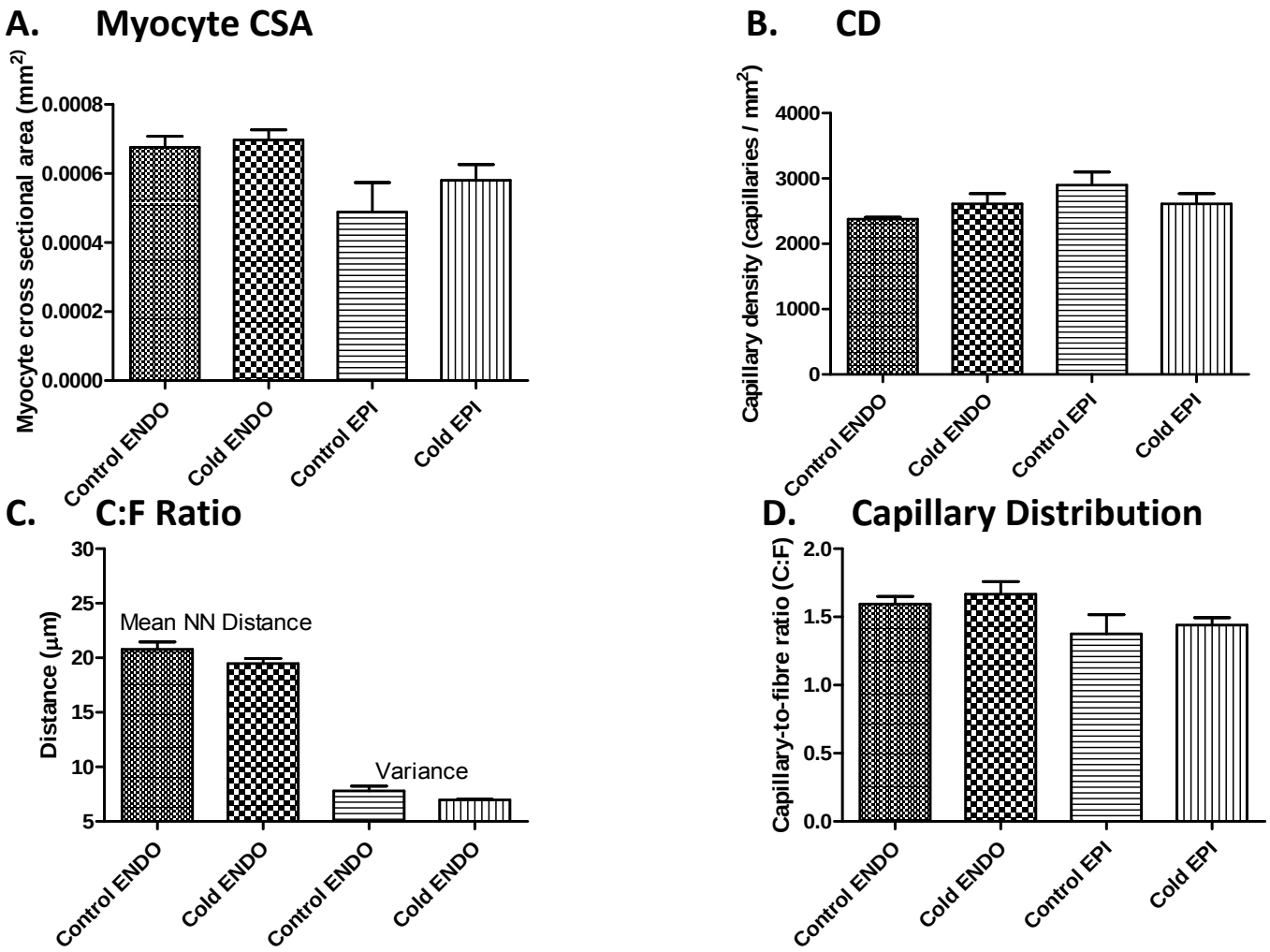

Figure 6.2. Effect of cold acclimation on LV capillarity and myocyte morphology in the rat. (n=6). Treatment vs. Control; **P<0.01, ***P<0.001

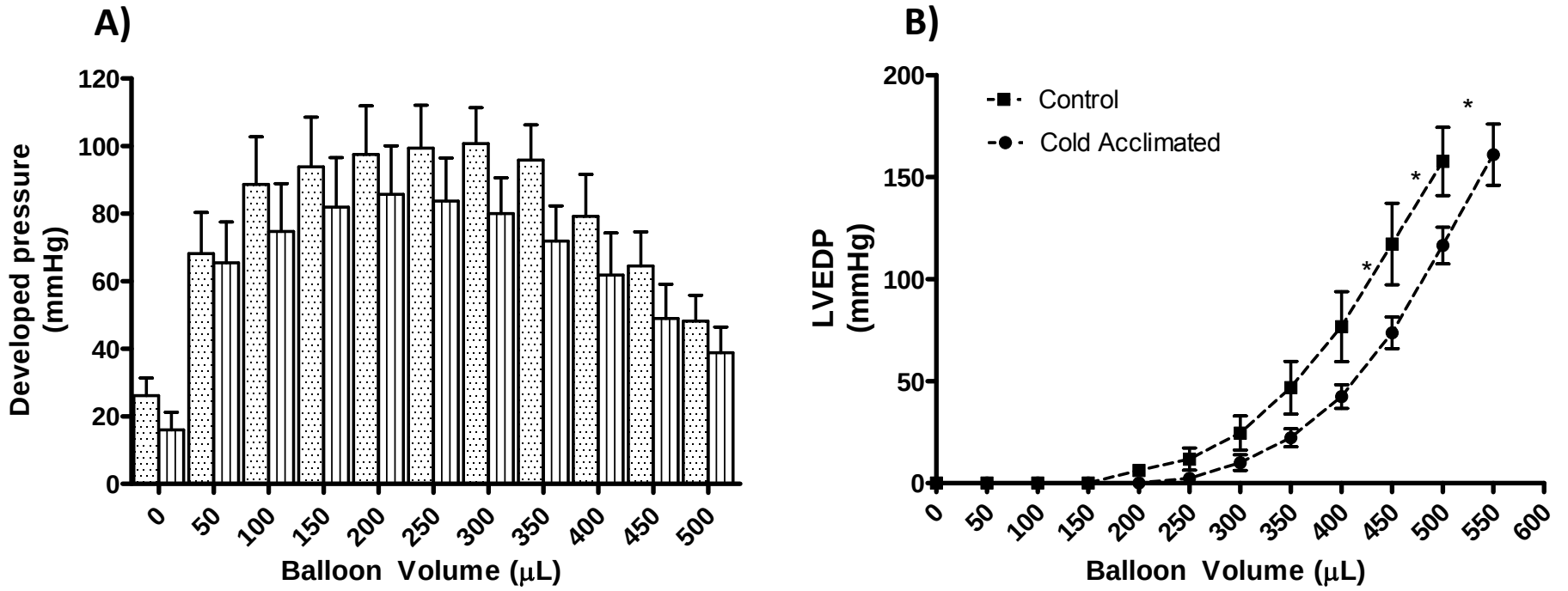

Figure 6.3. Effect of cold acclimation on LVDP-volume relationship (A) and peak systolic pressure (B). (n=6). LEGEND: Dots = Control, Vertical stripes = Cold acclimation.

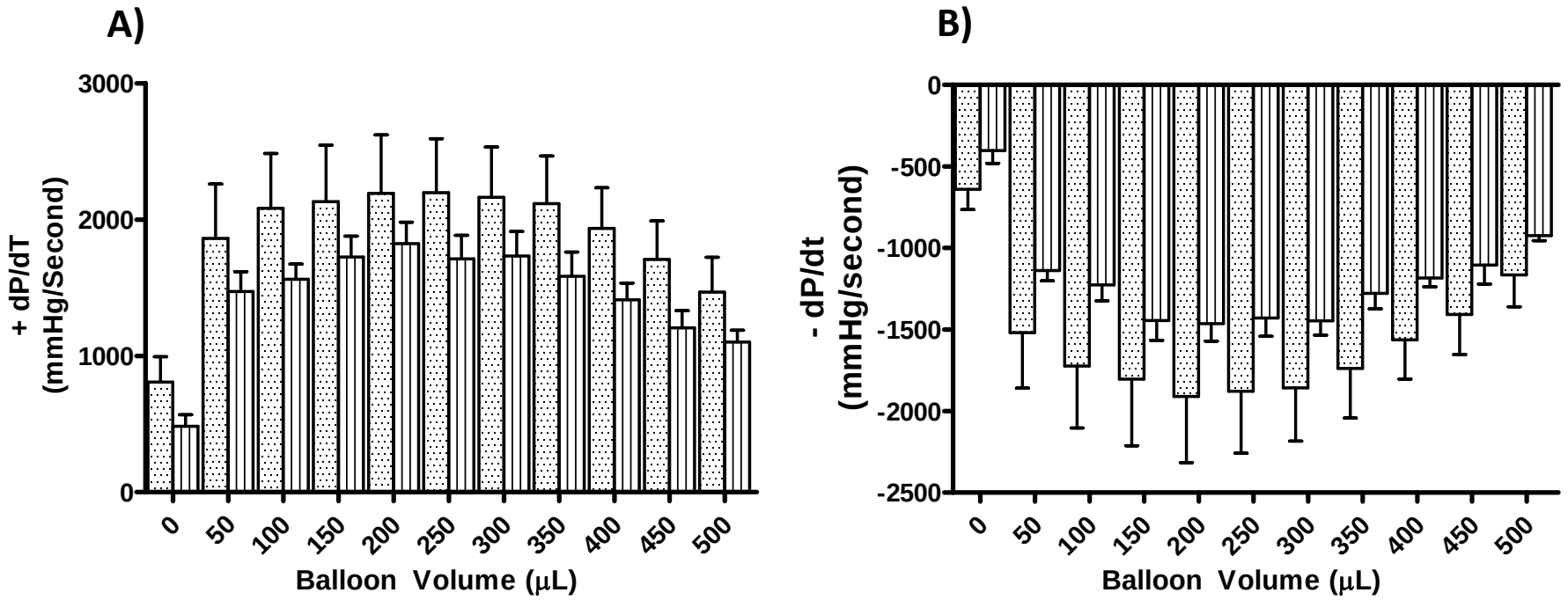

Figure 6.4. Effect of cold acclimation on +dPdt (A) and -dPdt (B). (n=6). LEGEND: Dots = Control, Vertical stripes = Cold acclimation.

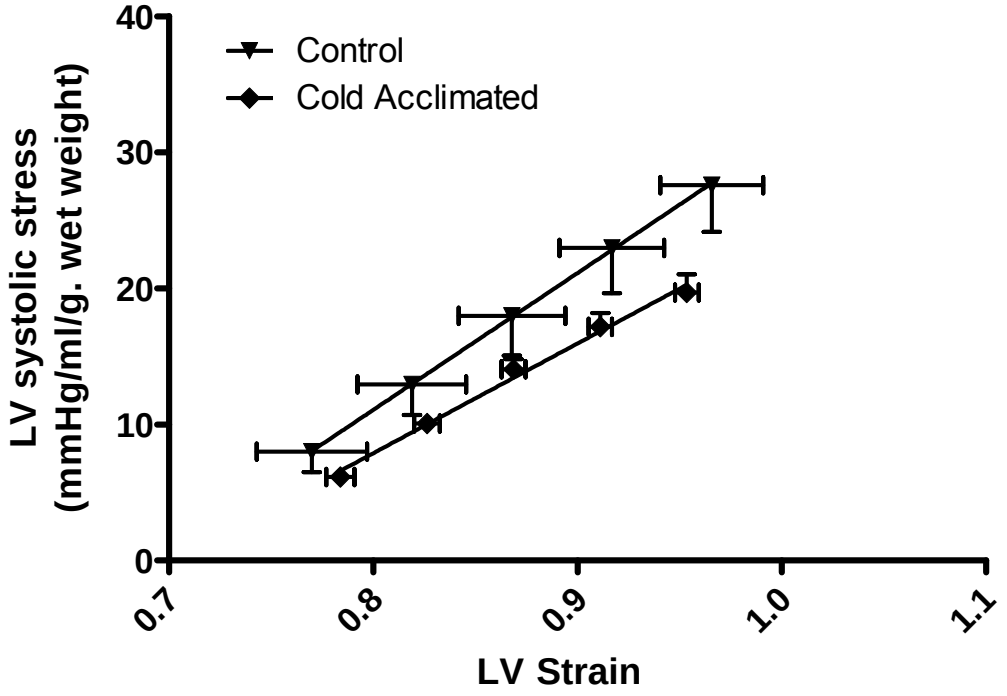

Figure 6.5. Effect of cold acclimation on estimated LV systolic stress-strain. (n=6).

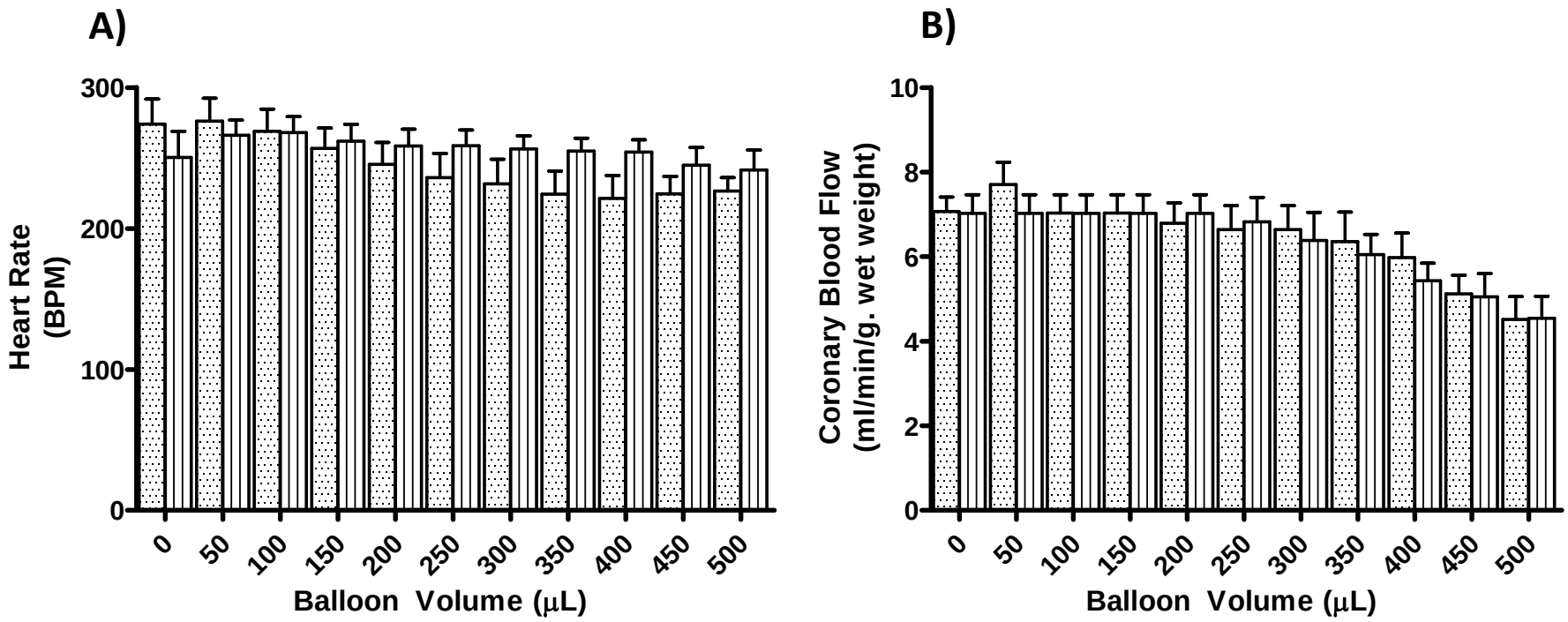

Figure 6.6. Effect of cold acclimation on HR (A) and CF (B). (n=6). LEGEND: Dots = Control, Vertical stripes = Cold acclimated.

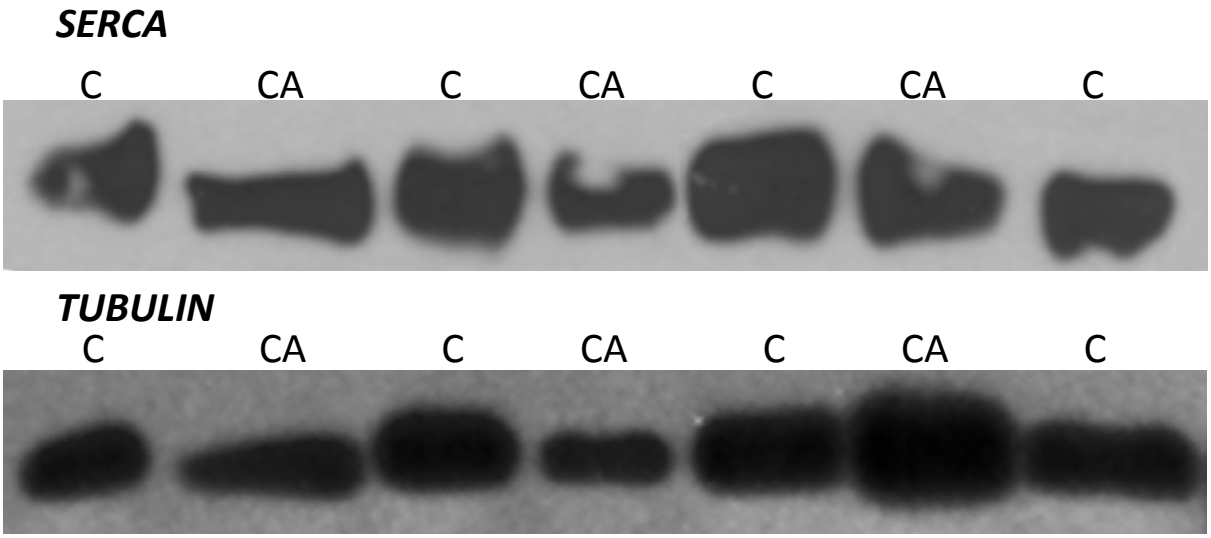

Figure 6.7. Representative western blots of SERCA2a and acylated tubulin. C = Control, CA=Cold acclimated

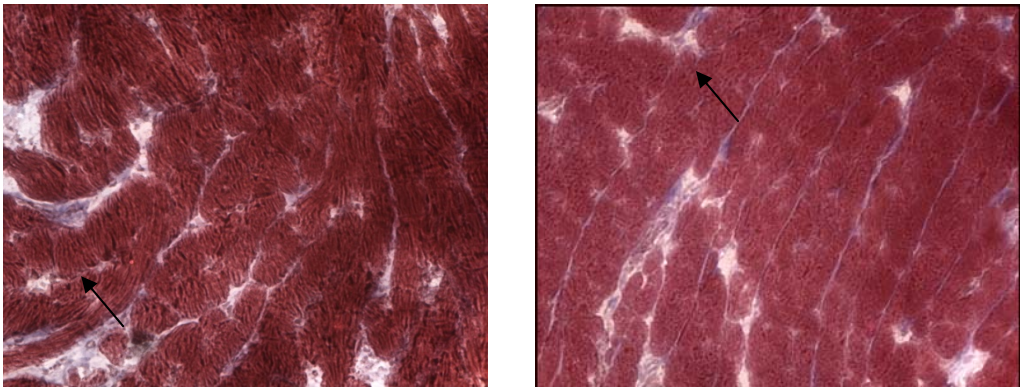

Figure 6.8. Representative images of LV subendocardial collagen content. Areas of collagen are shown in blue (see arrows). Magnification x250.

Table 6.2. Effects of cold acclimation on ventricular phenotype.

	Control	***Cold Acclimated***
Estimated ventricular volume (μL)	303 ± 21	355 ± 7*
Ventricular chamber stiffness (mmHg/μL)	0.76 ± 0.06	0.84 ± 0.04
Myocardial contractility (mmHg/ml/g. wet weight)	110 ±11	82 ± 7
Ventricular collagen content (%)	2.54 ± 0.19	2.66 ± 0.15
SERCA2 expression (A.U)	1.00 ± 0.12	1.05 ± 0.21

(n=6) The effects of cold acclimation; *p>0.05. Estimated ventricular volume and chamber stiffness are assessed from the x intercept and slope of the linear portion of the LVEDP-volume relationship respectively. Myocardial contractility is assessed from the mean slope of the stress strain relationship.

Table 6.3. Effect of dobutamine (150nM) addition on cardiac performance of control and cold acclimated hearts.

	Control		***Cold Acclimated***	
	Untreated	+ Dobutamine (150nM)	Untreated	+ Dobutamine (150nM)
HR (bpm)	229 ± 25	231 ± 32	240 ± 8	233 ± 9
Peak SP (mmHg)	96 ± 9	123 ± 14	82 ± 8	104 ± 12
LVDP (mmHg)	75 ± 10	107 ± 10***	58 ± 8	80 ± 11**
+dP/dt (mmHg/sec)	1719 ± 199	2732 ± 197***	1291 ± 210	2001 ± 325***
-dP/dt (mmHg/sec)	-1343 ± 125	-1992 ± 177**	-1190 ± 265	-1443 ± 194**
RPP (mmHg/min)	16300 ± 1000	22800 ± 1300	13600 ± 1300	18500 ± 2600
% increase in RPP	-	42 ± 11**	-	36 ± 6**

(n=5-6). The effects of dobutamine; *p<0.05 **P<0.01, ***P<0.001. The effects of cold acclimation; ^^p<0.01, ^^^p<0.001.

Chapter Seven. Effects of increased capillarity on cardiac performance and metabolism. Part 2: Atenolol

The roles of mechanical factors (shear stress, vessel wall tension and capillary stretch) in myocardial capillary growth has already been discussed in detail in the main introduction of this thesis and to avoid repetition these details have been omitted from this chapter's introductory paragraphs. Of interest to the present study is the reported improvement in cardiac performance following the induction of chronic bradycardia. Both rabbits and pigs demonstrate an improvement in stroke work and cardiac output at high workloads (demonstrated during acute pacing or adrenaline stimulation) following 60 days of bradycardic pacing [85, 86]. This improvement is unassociated with any changes in cardiac mass implying that hypertrophy of the muscle fibres (either concentric or eccentric remodeling) does not occur. Instead it has been proposed that an increase in LV capillarity allows for improved oxygen delivery, support greater performance when demand is increased. Numerous studies have also demonstrated that myocardial function is preserved in HF when chronic bradycardia is induced by the pharmacological agents (both I_f current inhibitors [89, 233, 234] and β adrenoceptor antagonists [234, 235]) and that these treatments promote ventricular capillary growth. However the role of angiogenesis in the beneficial actions of these agents is unclear as bradycardia also reduces myocardial oxygen expenditure (decreased chronotropy) and has been shown to induce favourable LV remodeling (i.e. reduced infarct size and increased LV growth) [89, 233-235].

Studies conducted to date in normal animals have relied upon *in vivo* measures of cardiac contractile performance (e.g. dilution techniques) which are influenced homeostatic, neural and hormonal mechanisms [85, 86]. In addition, these methods assess pump function rather than the instrinsic contractility of the myocardium. Isolated heart preparations are a way to assess cardiac performance and substrate metabolism away from these confounding factors and also provide a direct assessment of the true contractility of the myocardium (i.e. controlled loading conditions).

Chapter Aims

The primary aim of this chapter is to investigate the effect of improved capillarity on left ventricular performance and metabolism in the isolated heart. This study is the first to assess the impact of capillarity on the contractile function of the normal myocardium away from confounding neural, hormonal and influences. β-adrenoceptor antagonism has been selected due to its simplicity, clinical relevance, and for animal welfare reasons represented the least stress. To date there have been no studies looking at the influence of chronic bradycardia on myocardial substrate metabolism in the normal heart, which reflects a necessary 'baseline' required before exploiting bradycardia-induced angiogenesis in myocardial infarction or hypertrophy.

Materials and methods

Treatment regime

Animals were treated with atenolol, a selective β_1-adrenoceptor antagonist, *ad libitum* in drinking water at a concentration of 50 mg/L for 4 weeks, a final dose of 5mg/kg body weight/day. [236] Sucrose was added to all water based treatments at a concentration of 5 g/L drinking water (0.5% w/v) in a bid to disguise the taste of the drugs used.

Equations

The following equations have been used for the estimation of ventricle wall stretch during bradycardia. Volumes were estimated from the linear regression of the latter portion of the diastolic pressure-volume response curve and the % reduction in heart rate from *in vivo* measurements.

$$V = \frac{4}{3}\pi r^3$$

$$C = \pi 2r$$

Where V is the volume of a sphere, C the circumference of a circle and r is the radius of each respectively.

Modifications of metabolism protocol

Rates of glucose and oleate metabolism were measured according to the protocols outlined in the Chapter 2 with minor modifications. Rates of metabolism were measured at two workloads as defined by set end diastolic pressures of 20 mmHg (low) or 80 mmHg (high). These loads were defined after completion of the initial volume response curves in the two treatment groups. A set end diastolic pressure was selected to normalise ventricular wall stress in these hearts. Measurements were carried out in individual heart preparations resulting in a total of 4 experimental groups; control 20 mmHg, control 80 mmHg, atenolol 20 mmHg and atenolol 80 mmHg.

Results

Experiments in the rat

Physiological Parameters

Animal body mass (343 ± 13 vs. 330 ± 9 g. wet weight, Table 7.1), wet heart mass (1.42 ± 0.05 vs. 1.44 ± 0.19 g. wet weight, Table 7.1) and heart to body mass ratios (4.17 ± 0.19 vs. 4.35 ± 0.18, Table 7.1) were comparable between control and atenolol treated animals. Atenolol treated animals demonstrated a 10% reduction of *in vivo* heart rate at 4 weeks (411 ± 10 vs. 372 ± 8, $P<0.05$, Table 7.1). Mean arterial blood pressures were comparable between groups (95 ± 4 vs. 94 ± 1 mmHg, Table 7.1).

Capillary supply

Capillary density (number of capillaries per mm^2) was similar in the endocardial and epicardial regions of control hearts (2500 ± 27 vs 2642 ± 96 capillaries/mm^2, Figure 5.1B). Atenolol treatment did not result in any significant changes in capillary density in either the endocardial (2500 ± 27 vs. 2447 ± 185 capillaries/mm^2, Figure 5.1B) or epicardial regions (2642 ± 96 vs. 2578 ± 4, Figure 5.1B). Myocyte cross-sectional area was significantly greater in the endocardial region of atenolol treated hearts compared to controls (553 ± 10 vs. 620 ± 43μm^2, $P<0.05$, Figure 5.1A). Similarly capillary-to-fibre ratio was significantly higher in the endocardial region of atenolol treated hearts (1.37 ± 0.01 vs. 1.47 ± 0.02, $P<0.05$, Figure 5.1C). Myocyte cross-sectional areas and capillary-to-fibre ratios were similar in the epicardial region of all hearts (Figure 5.1A and Figure 5.1C). Morphometric analysis demonstrated similar values for nearest neighbour distances in the endocardial region (21.5 ± 0.1 vs. 21.9 ± 0.9, Figure 5.1D). The uniformity of capillary distribution was comparable between treatment groups in this region (Figure 5.1D).

Ex Vivo Contractile Performance

Ex vivo intrinsic heart rates were unaffected by atenolol treatment (Figure 7.5A). Pressure development increased proportionally with balloon volume until peak pressure development was

reached at 300 μL in control hearts (Peak: 65 ± 9 mmHg, Figure 7.2A). Further increases in balloon volume raised the end diastolic pressure and decreased the development of pressure in the ventricle (Figure 5.2B). Similarly pressure development in the left ventricle of hearts from atenolol treated animals increased in a manner proportional to balloon volume and was comparable to controls until balloon volumes exceeded 300 μL (Peak: 65 ± 9 mmHg, Figure 7.2A). Atenolol treated rat hearts demonstrated comparable ventricular lumen volumes (318 ± 16 vs. 333 ± 32 μL, Table 7.2) and a significant reduction in ventricular stiffness (1.07 ± 0.13 vs. 0.80 ± 0.06 mmHg/μL, P=0.06, Table 5.2) when compared to controls. LVDP was significantly greater in atenolol treated hearts at balloon volumes of 450 and 500 μL (Figure 7.2A). Similarly +dP/dt was significantly greater than control values at balloon volumes of 400-500 μL (Figure 7.3A). –dP/dt (Figure 7.3B) and CF (Figure 7.5B) were comparable between groups at all balloon volumes. Histological analysis of collagen content showed no difference between control and atenolol treated animals (2.34 ± 0.25 vs. 2.10 ± 0.26 %, Table 7.2). SERCA2a protein expression was preserved in all treatment groups (Figure 7.4 and Table 7.2).

Estimation of passive stretch during prolonged diastole

Assuming a spherical ventricle volume of 300 μL we can calculate the effect of a 10% reduction in heart rate on the stretch experienced at the ventricle wall *in vivo*.

Control

$$Vol = \frac{4}{3}\pi r^3 \quad \therefore \sqrt[3]{\frac{300}{\frac{4}{3}\pi}} = r \therefore \; r = 4.16\,\mu m$$

$$C = \pi 2r \therefore C = 26\,\mu m$$

Atenolol

$$\frac{300}{100} * 110 \; = 330\,\mu L$$

$$\sqrt[3]{\frac{330}{\frac{4}{3}\pi}} = r \therefore \; r = 4.27\,\mu m$$

$$C = \pi 2r \therefore C = 27\ \mu m$$

Therefore a 10% decrease in heart rate equates to a 3.85% increase in stretch of the ventricular wall during diastole.

Cardiac Substrate Metabolism

Contractile performance

Ex vivo heart rates were similar at both low (20mmHg) and high (80 mmHg) workloads in control and atenolol treated animals (Figure 7.9A). Left ventricular developed pressure (76 ± 7 vs. 84 ± 7 mmHg, Figure 7.9B), +dP/dt (1357 ± 107 vs. 1267 ± 66 mmHg/sec, Figure 7.9C) and -dP/dt (-1082 ± 86 vs. -1025 ± 37 mmHg/sec) were comparable between treatment groups at a set end diastolic pressure of 20 mmHg. High workloads resulted in significant reductions in LVDP (76 ± 7 vs. 54 ± 4 mmHg, $P<0.05$, Figure 7.9B), +dP/dt (1357 ± 107 vs. 875 ± 39 mmHg/sec, $P<0.001$, Figure 7.9C) and -dP/dt (-1082 ± 86 vs. -622 ± 39 mmHg/sec, $P<0.001$) in control hearts. In atenolol treated hearts the increased workload did not affect parameters of contractile function (Figure 7.9). At high workloads LVDP (54 ± 7 vs. 72 ± 6 mmHg, $P=0.06$, Figure 7.9B), +dP/dt (875 ± 39 vs. 1267 ± 67 mmHg/sec, $P<0.05$, Figure 7.9C) and -dP/dt (-622 ± 39 vs. 945 ± 91 mmHg/sec, $P<0.01$) were significantly greater than controls at the same workload. CF was comparable between all groups and workloads average 7.8 ± 0.4 ml/min/g. wet weight.

Control Metabolism

Rates of oleate oxidation were similar at both low and high workloads (62 ± 13 vs. 59 ± 9 nmoles/min/g. wet weight, Figure 7.12). Total ^{3}H labelled oleate incorporation in tissue lipids was greater in hearts performing more work and represented a significant increase of ^{3}H oleate incorporation into the triglyceride pool (1153 ± 399 vs. 2238 ± 460, $p<0.001$ nmoles/g. wet weight, Figure 7.13). Incorporation of ^{3}H Oleate into phospholipids, diacylglycerol, free FAs and cholesterol esters was comparable at both worklaods (Figure 7.13). Total tissue triglyceride content was no different between control groups (4763 ± 532 vs. 5140 ± 662 nmoles/g. wet weight). No differences

in the rates of glucose oxidation were noted between workloads in control hearts (186 ± 22 vs. 245 ± 19 nmoles/min/g. wet weight Figure 7.12). ^{14}C glucose incorporation into tissue glycogen was unaffected by workload (2227 ± 472 vs. 2238 ± 460 nmoles/g. wet weight) as was total tissue glycogen content (35800 ± 3800 vs. 34900 ± 3200 nmoles/g. wet weight).

Atenolol Metabolism

Comparable results were noted for atenolol treated hearts with no effect of workload on the rates of oleate (78 ± 6 vs. 79 ± 12 nmoles/min/g. wet weight, Figure 7.12) and glucose oxidation (178 ± 19 vs. 248 ± 32 nmoles/min/g. wet weight, Figure 7.12). Similar to control hearts the jump in workload significantly increased the incorporation of ^{3}H into the tissue lipids attributed to an increase of ^{3}H incorporation into the triglyceride pool (1554 ± 369 vs. 2637 ± 388 nmoles/g. wet weight, $P<0.001$,Figure 7.13). Incorporation of ^{3}H oleate into phospholipids, diacylglycerol, free FAs and cholesterol esters was no different at low and high workloads (Figure 7.13). No influence of workload on ^{14}C incorporation into the glycogen pool (3607 ± 835 vs. 3041 ± 609 nmoles/g. wet weight) or on total tissue glycogen content (38350 ± 3664 vs. 36932 ± 3427 nmoles/g. wet weight) was noted in atenolol treated hearts.

Control vs. Atenolol Metabolism

No differences were noted between rates of exogenous substrate oxidation, total endogenous energy stores and incorporation of exogenous tracers into these stores between treatment groups.

Experiments in the mouse

Total heart mass (144 ± 9 vs. 173 ± 11 mg. wet weight), the heart mass to body mass ratio (5.03 ± 0.35 vs. 6.16 ± 0.39) and body mass were comparable between treatment groups (28.8 ± 0.3 vs. 28.1 ± 0.6 g. wet weight). Atenolol treatment was associated with a signficiant increase in the C:F ratio in the subendocardium (1.73 ± 0.03 vs. 1.87 ± 0.03, $P<0.01$). No difference was noted in the subepicardial region of the LV free wall (1.80 ± 0.02 vs. 1.89 ± 0.04). Myocyte CSA was compabale between subendocardial and subepicardial regions. CD was comparable to controls in the

subendocardium (3257 ± 20 vs. 3339 ± 142 capillaries/mm^2) and both CD and myocyte CSA were comparable subepicardial (CD: 3360 ± 172 vs. 3462 ± 349 capillaries/mm^2, CSA:552 ± 24 vs. 574 ± 58 μm^2) region of the LV free wall.

Discussion

Bradycardia and capillarity

In keeping with the findings of previous studies in the rabbit and rat [85, 86, 237-239] chronic bradycardia stimulated capillary growth in the left ventricle of treated hearts compared with controls. The precise nature of the stimulus for angiogenic growth during bradycardia is not clear and several proposals have been made. Firstly the walls of the ventricle are exposed to greater degrees of passive stretch during the prolonged diastolic period due to the enhanced filling time. The capillaries of the myocardium are more tortuous during systole than in diastole and so will experience an increase in abluminal stretch during this period [127]. Based on the *in vivo* data, this represents a 9% increase in ventricular wall stretch during diastole in atenolol treated animals. This however seems an unlikely angiogenic stimulus in the present study as capillary growth was limited to the subendocardial region of the LV free wall. Secondly the enhancement of systolic force, due to activation of the Frank-Starling mechanism, may promote vessel growth. Previous studies in the rabbit have noted significant changes in ventricular capillarity following chronic inotropic enhancement with dobutamine [165]. However heart rate and ventricular contractility are maintained in the rat by a significant adrenergic drive from the sympathetic nervous system. Treatment with atenolol will exert negative inotropic effects through antagonism of normal sympathetic tone and so systolic forces seem an unlikely stimulus for growth in this model of chronic bradycardia. A third potential stimulus is an increase in intraluminal capillary wall stress. Capillaries have been observed to be wider during the diastolic period of the cardiac cycle and while the velocity of red blood cell flow is reduced the pressure in these vessels does not change significantly [127]. Therefore by applying LaPlace's law we can see that the tension acting at the capillary wall is much greater during diastole. These capillaries, which will be compressed during systole, will also be exposed to a greater flow, and so shear stress, when HR is reduced.

Similarly to the present study Tasgal and Williams (1981) noted capillary growth in the innermost subendocardial region of the normal rabbit myocardium during chronic treatment with propranolol

while no changes were noted in the subepicardial layers [239]. It is, however, worthy of note that significant atrophy of the ventricle was noted in this study suggesting reduction in cell size, rather than new vessel growth may explain the increase in CD (no measure of myocyte CSA or C:F ratio was presented). In keeping with the present study Ulu *et al* (2009) demonstrated a significant increase in the capillary to fibre ratio in hearts from rats with ligation induced myocardial infarction [234]. Other investigators have reported capillary growth in both subendocardial and subepicardial fields using alternative methods of chronic bradycardia [85, 86] suggesting that there may be some relationship between the pattern/degree of capillary growth and the reduction in heart rate achieved (fairly modest with β blockade (10%) when compared to pharmacological I_f current inhibition and electrical pacing induced bradycardia (25-60%)). A 6% increase in C:F ratio was achieved with atenolol induced bradycardia less than the 15% increase reported in paced rabbit hearts and in rats dosed with alinidine. Extravascular compression during systole markedly limits coronary flow and as such the majority of blood flow occurs during diastole. This extravascular compression is most pronounced in the subendocardium making this region more susceptible to ischaemia, especially at low perfusion pressures. In keeping with this during bradycardia there appears to be a redistribution of flow to the subendocardium [240]. Therefore while global coronary flow rates are comparable between groups it is possible that changes in blood flow distribution alter intra-luminal wall stress or shear stress specifically in the subendocardial vessels. It cannot be ruled out that systolic forces also play a role in capillary growth in other models of chronic bradycardia where the contractile state of the myocardium is not modified (i.e. electrical pacing or alinidine).

The increase in capillary number noted in the present study was offset by a regional increase in myocyte cross-sectional area. Such changes contrast with the earlier reports of Wright *et al* (1981) in the rabbit [85], Brown *et al* (1994) in the pig [86], Tasgal and Williams (1981) [239] in the rabbit and Brown *et al* (1990) in the rat [87] who all found significant changes in capillary density with normal measures of myocyte size and/or ventricular mass. These studies however were conducted in older animals than those used in the present study suggesting age may be an important defining factor in

the angiogenic response of the myocardium. Data from the mouse, which demonstrate a signficant increase in the C:F ratio in the subendocardial region without any change in CD, lends support to the findings in the rat.

LV mass was comparable between groups in the present study suggesting that the regional myocyte hypertrophy did not significantly alter LV wall thickness. This adaptation may be viewed as a compensation for the increase stretch of the subendocardial region during diastole. There is also evidence that angiogenesis itself may promote hypertrophy from studies utilising blood vessel growth factors in the mouse [241]. Tirzui *et al* (2007) showed that treatment of mice with VEGF or the regulatable induction of myocardial PR39 expression (a potent peptide stimulator of angiogenesis and VEGF expression [242]) promotes blood vessel growth and myocardial hypertrophy which normalises blood vessel distribution to similar values as those seen in untreated control hearts.

Bradycardia and LV contractile performance

Atenolol treatment was associated with an increase the dynamic range of LV performance allowing for greater pressure development at high intraventricular balloon volumes. This reflects a greater efficiency of performance when expressed as a ratio of CF, and was demonstrated in the two experimentally independent arms of the present study. Ventricular stiffness was lower in atenolol treated hearts and is unrelated to alterations in diastolic function (comparable -dP/dt and SERCA protein content), intra-ventricular collagen content and ventricular chamber volume. Thus an increase in ventricular compliance appears to underlie the modified performance characteristics of atenolol treated hearts. Figure 7.6 demonstrates how the shift in diastolic compliance seen in the functional arm of the present study can predict the reduction in performance between hearts at high workloads (80 mmHg) in the metabolism experiments. Several investigators have published data suggesting that ventricular compliance and estimated LV chamber diameter is increased following chronic adrenoceptor blockade with both $\beta 1$ selective [243] and non-selective beta

adrenoceptor antagonists [244, 245] without unaltered LV mass. While no alteration in LV volume was noted in the present study it is possible that the reduction in heart rate achieved (9%) was an inadequate stimulus to significantly alter LV geometry and it is some 15-20% lower than those reported in other studies [244, 245]. It seems probable that the altered ventricular compliance is a consequence of chronic stretch (i.e. volume load) during the prolonged diastolic period. Previous investigators have reported that chronic bradycardia induced by electrical pacing in rabbits and pigs is associated with an increase in cardiac output at high workloads (i.e. during dobutamine infusion and paired pacing) [85, 86]. It was concluded that, as ventricular mass was unchanged, the noted increase LV capillary content must support function by improving oxygen delivery and that this may promote a more homogenous distribution of blood flow. However given the results of the present study it is possible that these data can be explained through an increase in either LV compliance or LV chamber volume which allows for a greater stroke volume without altering mass. In support of this it has been reported that the elevation in stroke work associated with chronic bradycardia preceeds the development of new capillaries in this model [127].

It seems that LV contractile function is unaffected by modest alterations in LV chamber compliance though it is perceivable that the regional expansion of myocyte CSA in the subendocardial region represents a compensatory mechanism to maintain pressure development in these hearts (though LV free wall mass was comparable to controls). A significant alteration in ventricular compliance and LV geometry without a thickening of the ventricular wall is often associated with chamber dysfunction in accordance with the law of LaPlace (i.e. increase chamber diameter) [205-207]. In contrast with this the benefits of chronic bradycardia following ischemic injury appear to be related at least in part to a greater expansion of the ventricular dimensions.

While total LV collagen content did not differ between groups there is convincing evidence that disorganisation of the fibrillar collagen network occurs models of volume overload preceeding an expansion of the chamber volume which may have parallels with the present study where preload is

increased by a chronic reduction in HR. Alterations in collagen cross-linking could explain how this decrease in chamber stiffness is acheived. Moreover these changes are frequently associated with normal or increased myocardial collagen content in keeping with the findings of the present study. Collagen cross-linking can be assessed through a ratio of cyanogen bromide soluble and insoluble LV hydroxyproline content [101] (this hydroxylated form of proline (amino acid) is found in few proteins other than collagen [180]).

Previous studies have demonstrated that chronic treatment with atenolol promotes the growth of new arterioles (diameter 6-50 μm) in the LV free wall. While total CF was comparable between treatment groups in the present study, it is possible that arteriolar remodeling may result in a more homogenous distribution of blood flow to the subendocardial layers and that an improvement in regional oxygen delivery can support greater performance at high workloads. Arteriolar density can be assessed using simple histological techniques (i.e. α-smooth muscle actin stain). Regional blood flow could be assessed through the infusion of radio-labelled or fluorescent labeled microspheres and quantified as the total radioactivity or fluorescence in tissue homogenates excised from each region of interest.

Bradycardia and substrate metabolism

Hearts perfused with both glucose and FAs demonstrated lower CF rates than those perfused with glucose alone. This likely reflects alterations in the viscosity of the perfusate, indicating that vessel shear rate/stress and not oxygen availability are responsible for the high coronary flow rates during perfusion with crystalloid buffer solutions.

Despite the elevation of ventricular wall stress associated with an increase in LVEDP there was no increase in the rate of oxidation of either exogenous glucose or exogenous oleate. This finding contrasts with previous reports of enhanced glucose and/or oleateuptake and oxidation following an increase in perfusion pressure and ventricular afterload in isolated heart preparations [8, 23, 26, 27, 38, 105, 108]. It is, however noted that a a significant increase in ^{3}H labeled incorporation into tissue

triglycerides occurred in hearts exposed to high workloads without any change to the size of the total triglyceride pool. This suggests that hearts performing more work preferentially oxidised enogenous triglycerides to meet the increase in ATP demand and that exogenous oleate was taken up by the myocytes and desposited in the triglyceride pool preserving the content of this endogenous energy store. Goodwin *et al* (1998) have previously demonstrated that when workload is stimulated with adrenaline that rates of exogenous glucose oxidation and total β oxidation are elevated without any signficiant changes to exogenous oleate oxidation and total myocardial triglyceride content [135]. This study provides evidence that endogenous triglycerides are preferentially utilized over exogenous FAs to meet the increased ATP demand associated with an elevation of myocardial workload. At a molecular level it is known that intracellular concentrations of free FA and acyl-CoA inhibit lysosomal lipase (LAL) and hormone-sensitive lipase (HSL), the rate limiting enzymes in triglygeride breakdown [34-36]. When workload is elevated, β oxidation will increase [23] resulting in a fall of intracellular free FA and acyl-CoA removing the inhibition of TAG hydrolysis. Additional FA uptake may occur through the stimulation of CD36 translocation to the sarcolemma allowing replenishment of the endogenous triglycerides [16]. These conclusions are limited in the present study by the lack of information on the timecourse of endogenous oleate incorporation into the triglyceride pool. This could be overcome through the use of a protocol to pre-label the endogenous triglycerides with a radiolabelled FA tracer [32]. Following this 'pulse' period hearts can be perfused with a second radiolabelled FA allowing for dual measures of FA oxidation from both exogenous and endogenous sources.

While previous investigations have reported on the influence of chronic bradycardia on cardiac performance this study is the first to look at rates of substrate metabolism in hearts isolated from these animals. It was originally hypothesised that any increase in ventricular contractile performance resulting from atenolol treatment would be met through enhanced rates of substrate oxidation in keeping with the delicate balance between oxygen/substrate supply and demand. Contradictory to this, rates of exogenous and endogenous substrate oxidation were comparable between treated and

untreated animals at both workloads. Given that the performance of atenolol treated hearts was greater than that of controls, these data show an increased efficiency of contractile performance at high workloads. As discussed earlier, the altered contractile performance in this model appears to reflect changes in ventricular compliance rather than LV mass or altered myocardial contractility and as such it is conceivable that ATP consumption and so substrate utilisation was unaffected.

Caveats and future work

Only a 10% reduction of in vivo heart rate was achieved through atenolol treatment which may explain why only a modest degree of capillary growth was achieved. Previous investigators have reported heart rate reductions of 25 to 60 % using β adrenoceptor antagonists, electrical pacing strategies or the pacemaker current inhibitor alinidine and report significantly greater effects on ventricular capillary growth [85-87, 239]. The use of alternative models, which do not alter the contractile state of the myocardium, appear to be more successful in the stimulation of angiogenesis, which implies that the enhanced contraction following prolonged ventricular filling is an important stimulus for new capillary growth.

Conclusion

In conclusion chronic bradycardia induced by atenolol treatment is associated with an improvement in contractile performance which appears to be related to an increase in LV chamber compliance. Modest capillary growth was limited to the subendocardial region and any improvements in oxygen diffusion were offset by regional myocyte hypertrophy which may reflect a compensatory mechanism to maintain LV contractile function in these hearts.

Table 7.1. Effects of atenolol treatment on cardiac mass and in vivo physiological parameters.

	Control	***Atenolol***
Body Mass (g)	343 ± 13	330 ± 9
Heart Mass (mg)	1.42 ± 0.05	1.44 ± 0.19
Heart Mass / Body Mass (mg/g)	4.17 ± 0.19	4.35 ± 0.18
LV Free Wall Mass (mg)	234 ± 19	252 ± 15
LV Free Wall Mass/ Body Mass (mg/g)	0.68 ± 0.05	0.77 ± 0.06
In vivo heart rate (BPM)	411 ± 10	372 ± 8*
Mean arterial blood pressure (mmHg)	95 ± 4	94 ± 1

(n=6-10). The effects of atenolol treatment; *P<0.05, **P<0.01.

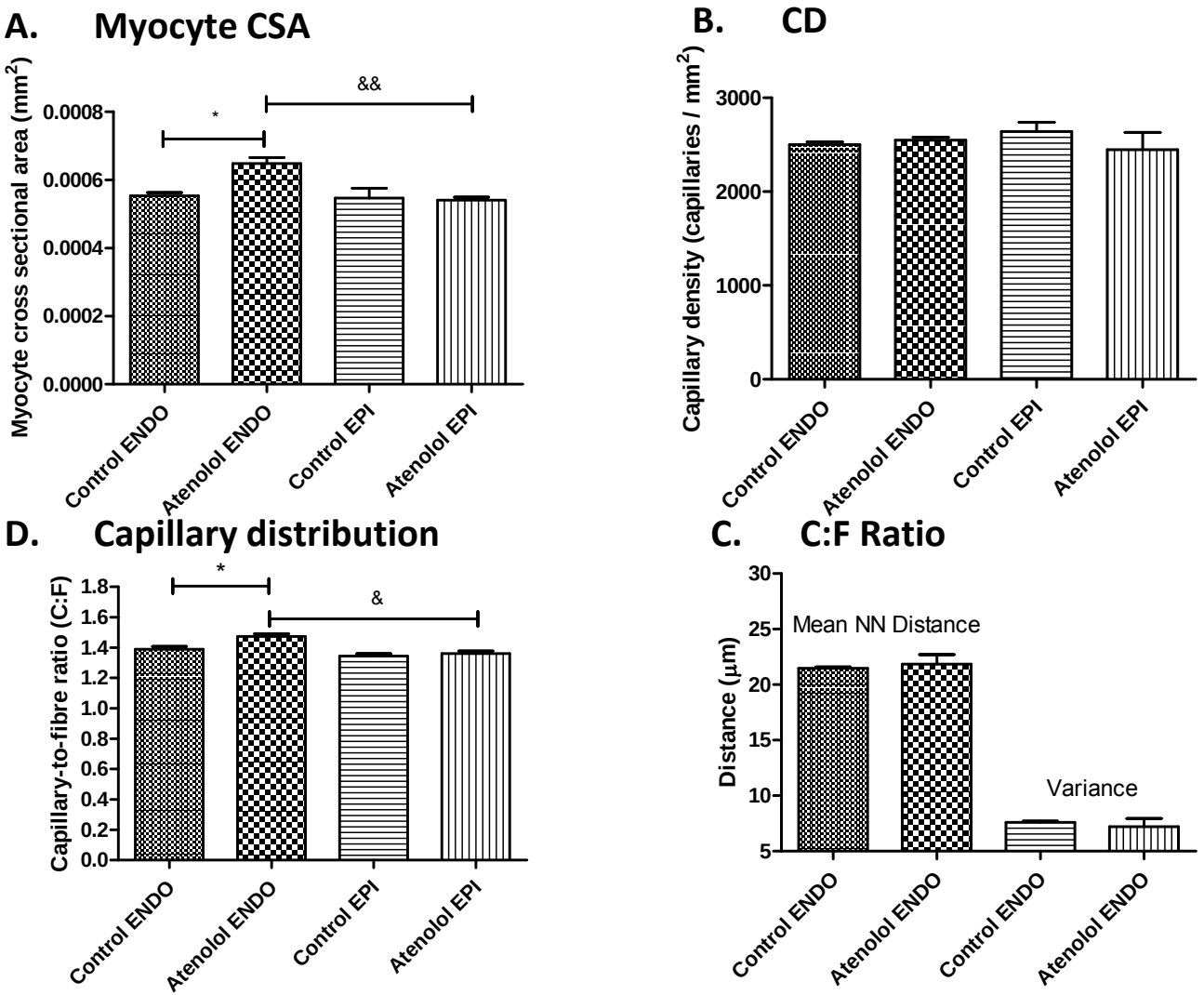

Figure 7.1. Effect of atenolol treatment on LV capillarity and myocyte morphology in the rat. (n=6) The effects of atenolol treatment; *P<0.05, **P<0.01. Endocardium vs. Epicardium; $^{\&\&}$P>0.01.

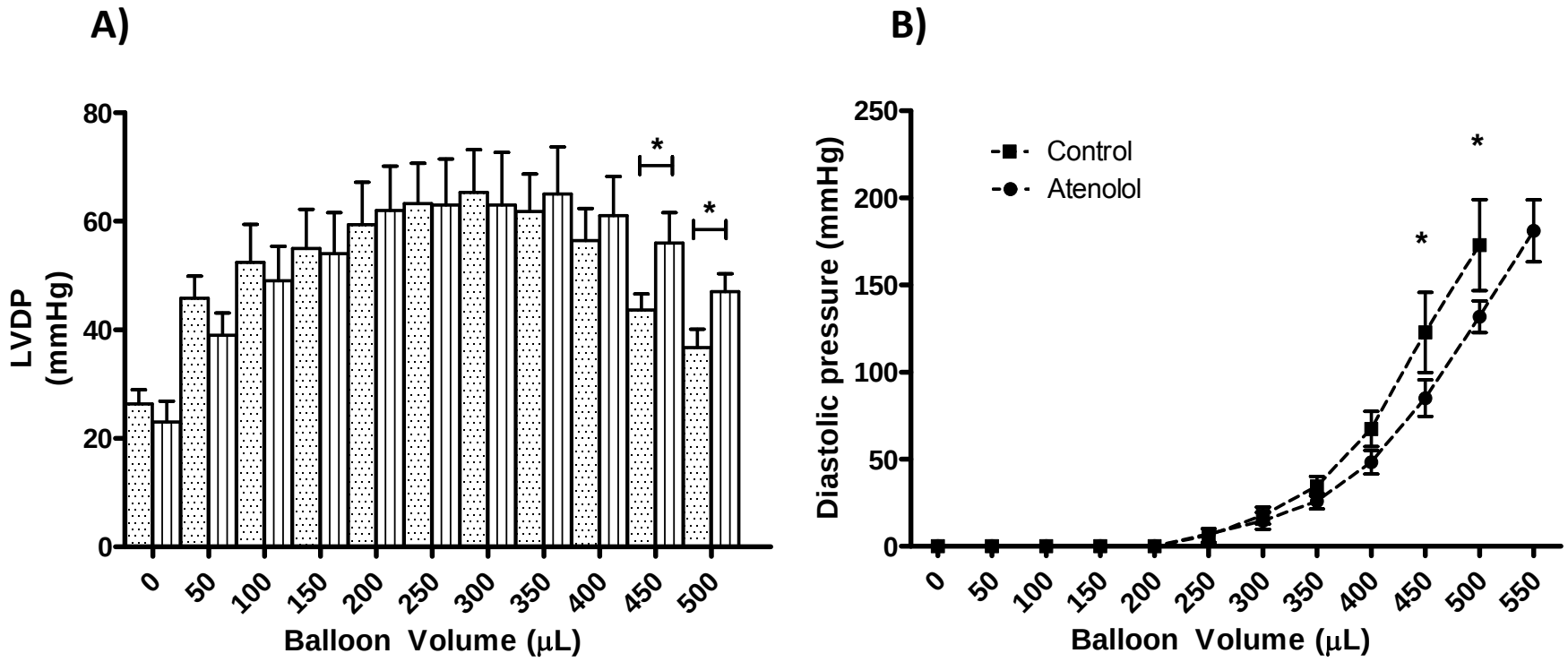

Figure 7.2 Effect of atenolol treatment on LVDP-volume relationship (A) and LVEDP-volume relationship (B). (n=6) The effects of atenolol treatment; **P<0.01. LEGEND: Dots = Control, Vertical stripes = Atenolol.

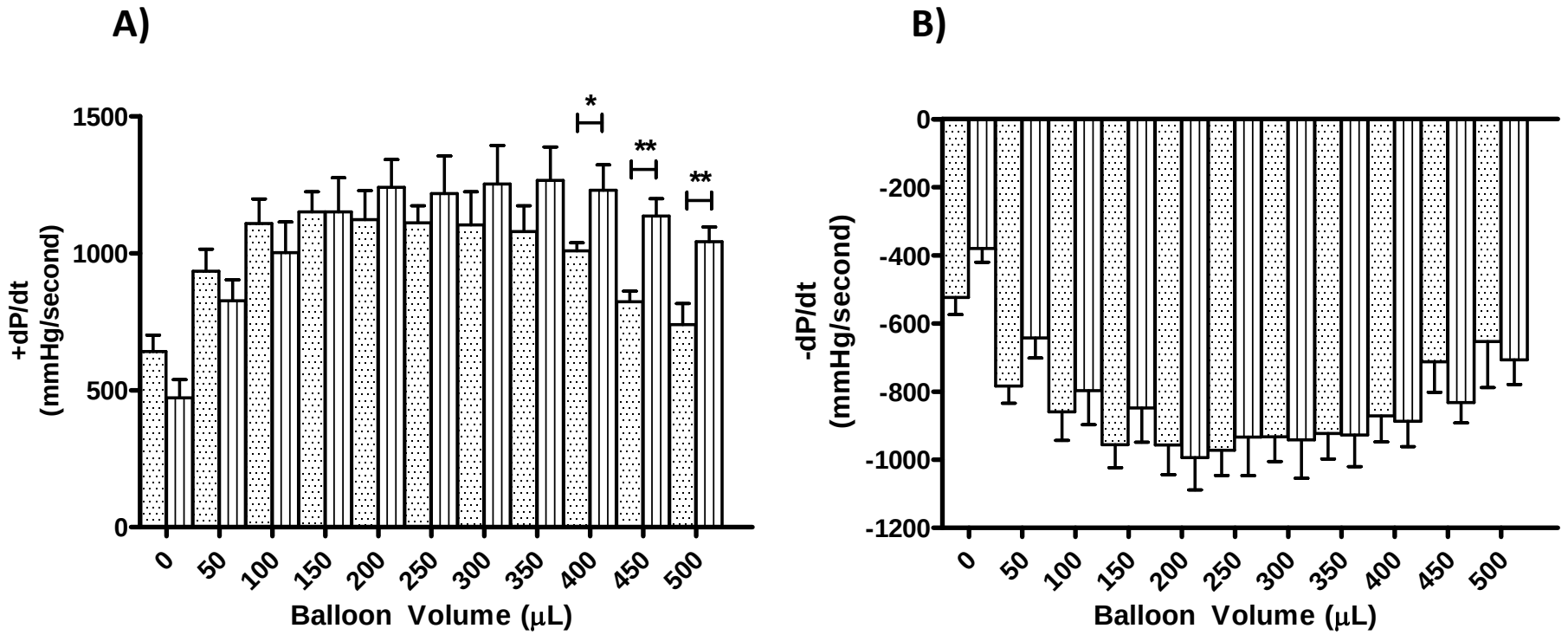

Figure 7.3 Effect of atenolol treatment on +dPdt (A) and -dPdt (B). (n=6) The effects of atenolol treatment; **P<0.01. LEGEND: Dots = Control, Vertical stripes = Atenolol.

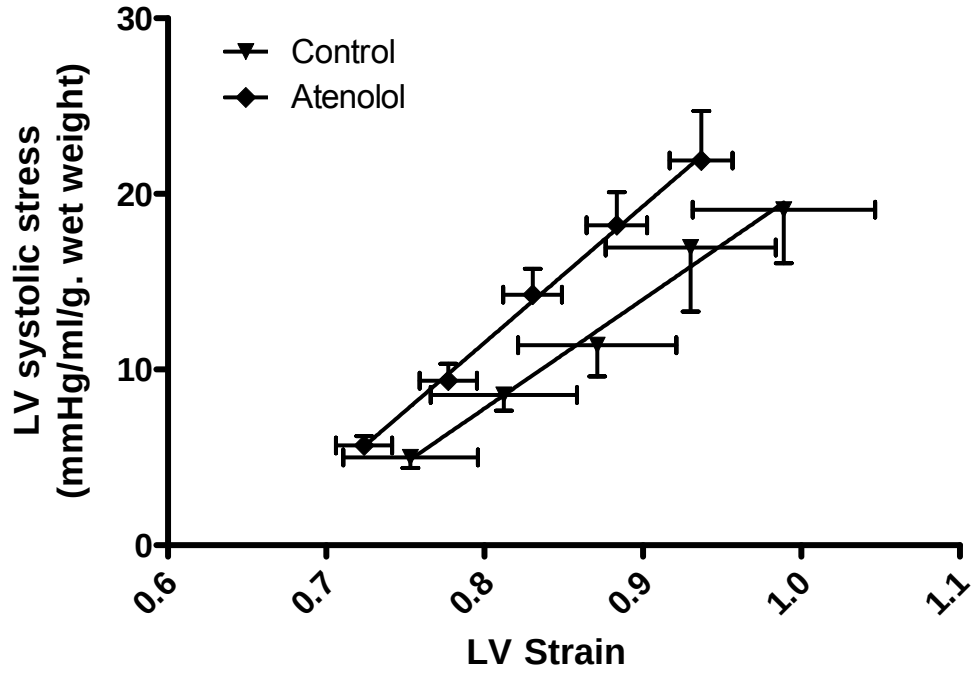

Figure 7.4 Effect of atenolol treatment on estimated LV systolic stress-strain. (n=6) The effects of atenolol treatment; *P<0.05.

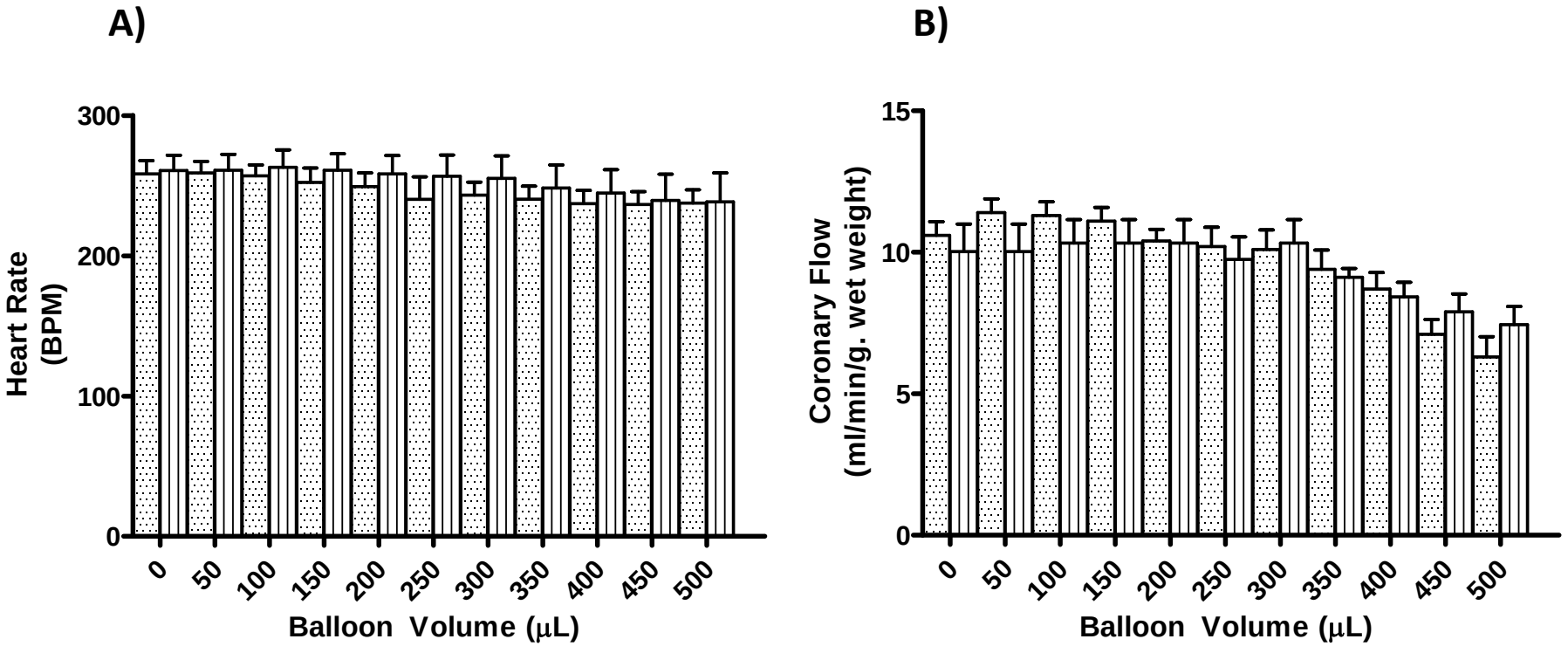

Figure 7.5 Effect of atenolol treatment on HR (A) and CF (B). (n=6) The effects of atenolol treatment; **P<0.01. LEGEND: Dots = Control, Vertical stripes = Atenolol.

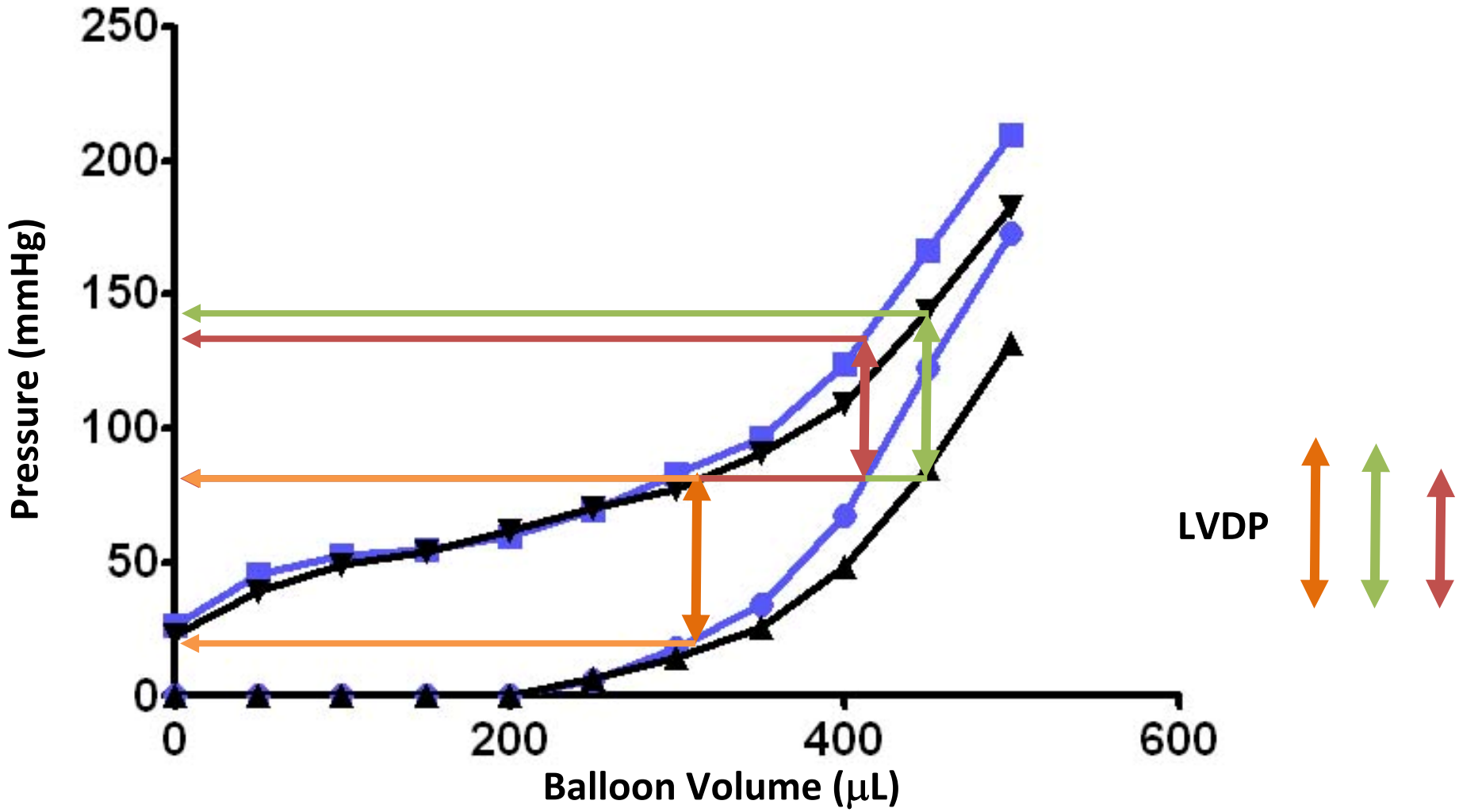

Figure 7.6. The influence of a change in ventricular compliance on pressure development at different end diastolic pressures. Blue and black represent mean diastolic and systolic pressures during the ventricular pressure-volume protocol for control and atenolol treated hearts respectively.

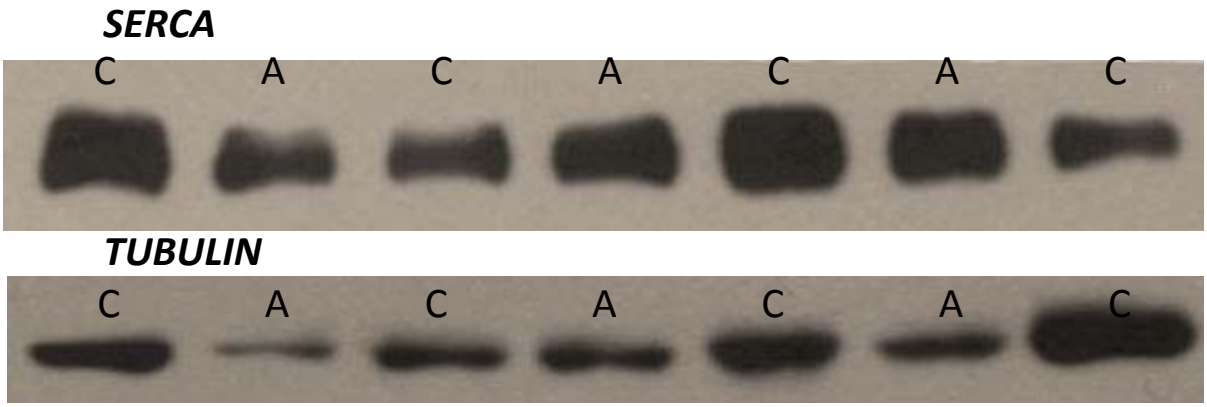

Figure 7.7. Representative western blots of SERCA2a and acylated tubulin. C = Control, A=Atenolol

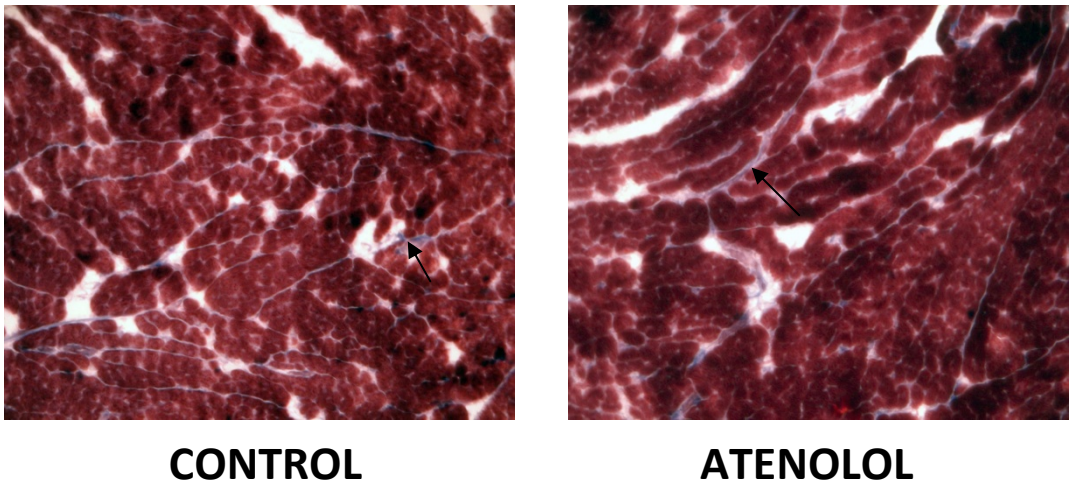

Figure 7.8. Representative images of LV subendocardial collagen content. Areas of collagen are shown in blue (see arrows). Magnification x125.

Table 7.2. Effects of atenolol treatment on ventricular phenotype.

	Control	***ATENOLOL***
Estimated ventricular volume (μL)	318 ± 16	333 ± 32
Ventricular stiffness (mmHg/ml)	1.06 ± 0.03	0.89 ± 0.04*
LV stress-strain (mmHg/ml/g. wet weight)	61 ± 13	77 ± 11
Ventricular collagen content (%)	2.34 ± 0.25	2.10 ± 0.26
SERCA2 expression (A.U)	1.00 ± 0.11	1.12 ± 0.08

(n=6) Estimated ventricular volume and chamber stiffness are assessed from the x intercept and sope of the linear portion of the LVEDP-volume relationship respectively. Myocardial contractility is assessed from the mean slope of the stress strain relationship. The effects of atenolol treatment; *P<0.05.

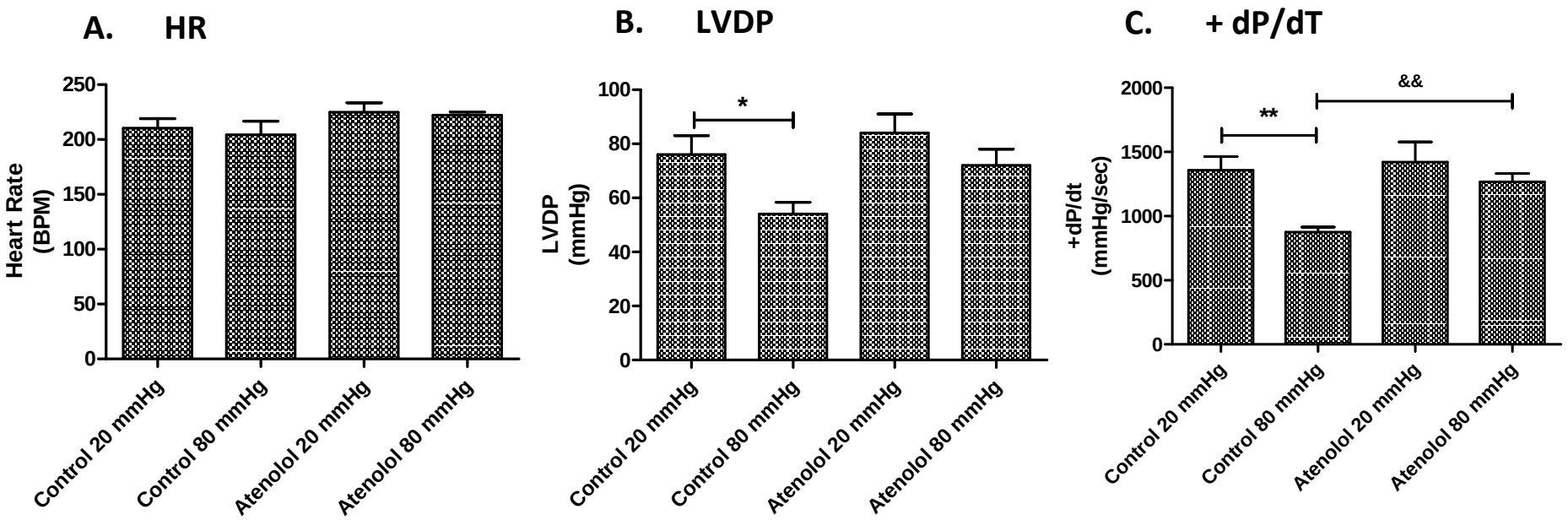

Figure 7.9. Left ventricular performance during the metabolism protocol. (n=5-6). The effects of an increase in workload; *P<0.05, **P<0.01. The effects of atenolol treatment; $^{\&\&}$P<0.01.

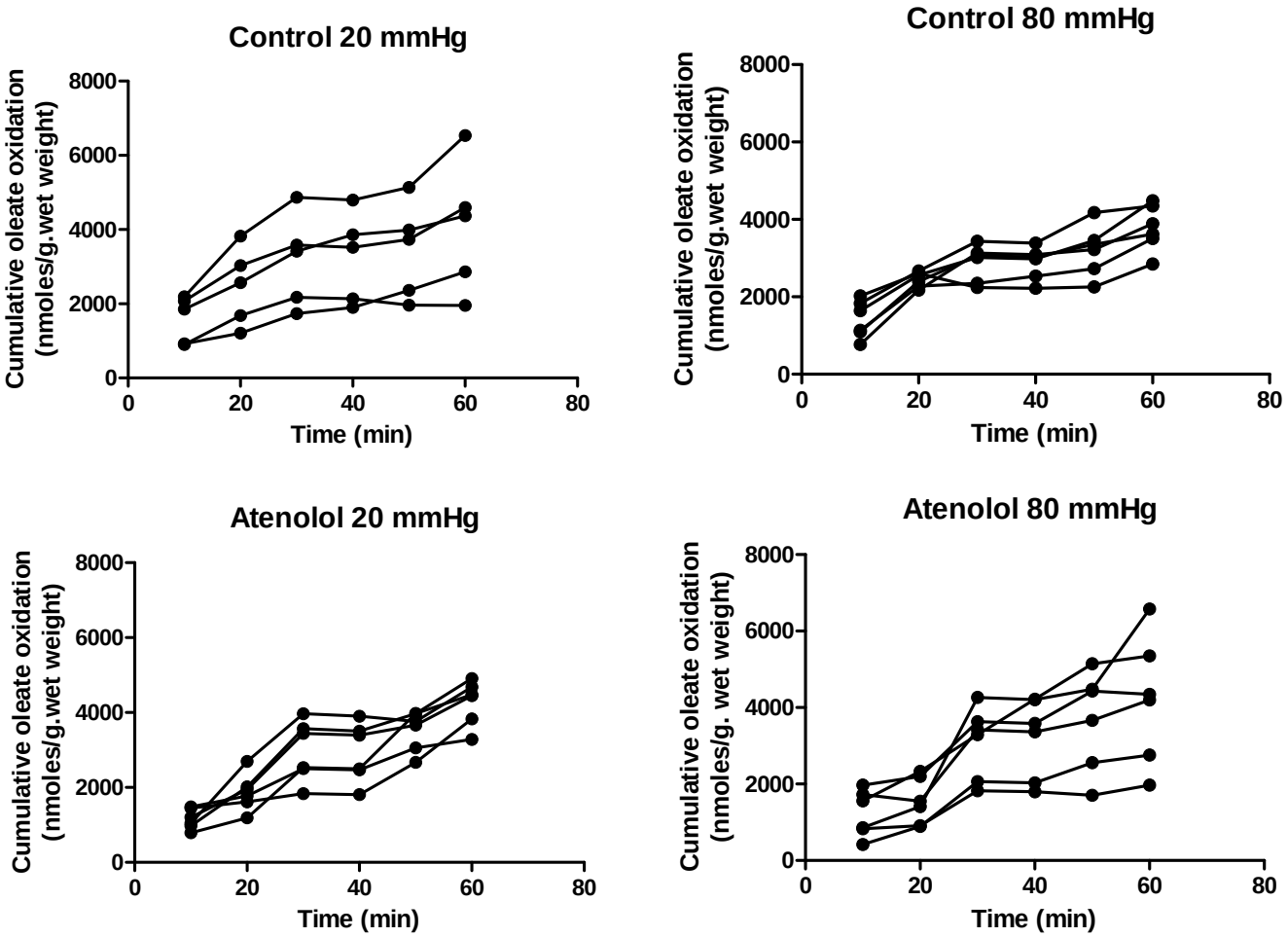

Figure 7.10. Raw data plots of oleate oxidation against time. Data demonstrate rates of oleate oxidation in all preparations used in the calculation of mean values (control 20 mmHg n=5, Control 80 mmHg n=6, Atenolol 20 mmHg n=6, Atenolol 80 mmHg n=6)

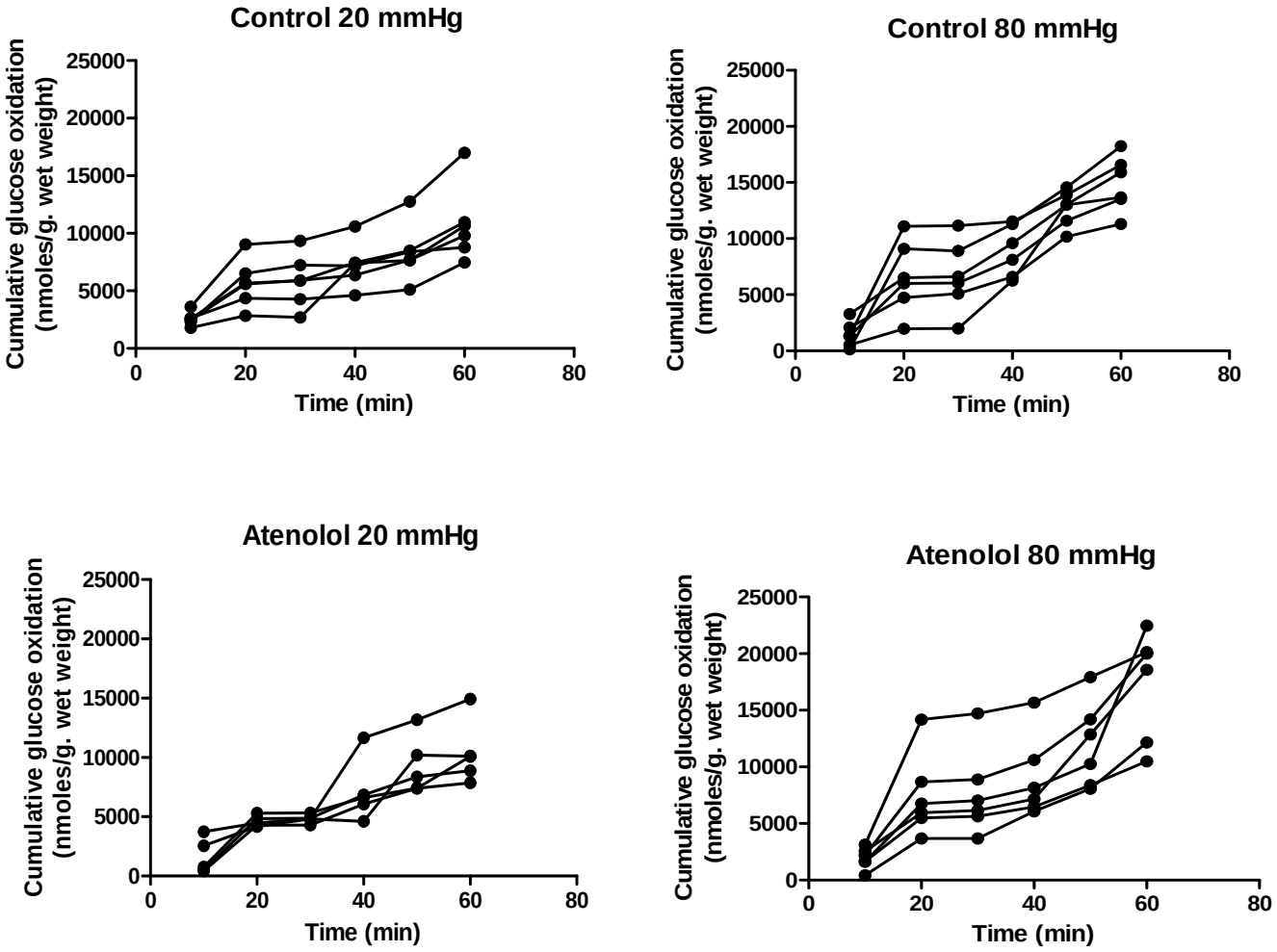

Figure 7.11. Raw data plots of glucose oxidation against time. Data demonstrate rates of glucose oxidation in all preparations used in the calculation of mean values (control 20 mmHg n=6, Control 80 mmHg n=6, Atenolol 20 mmHg n=5, Atenolol 80 mmHg n=6)

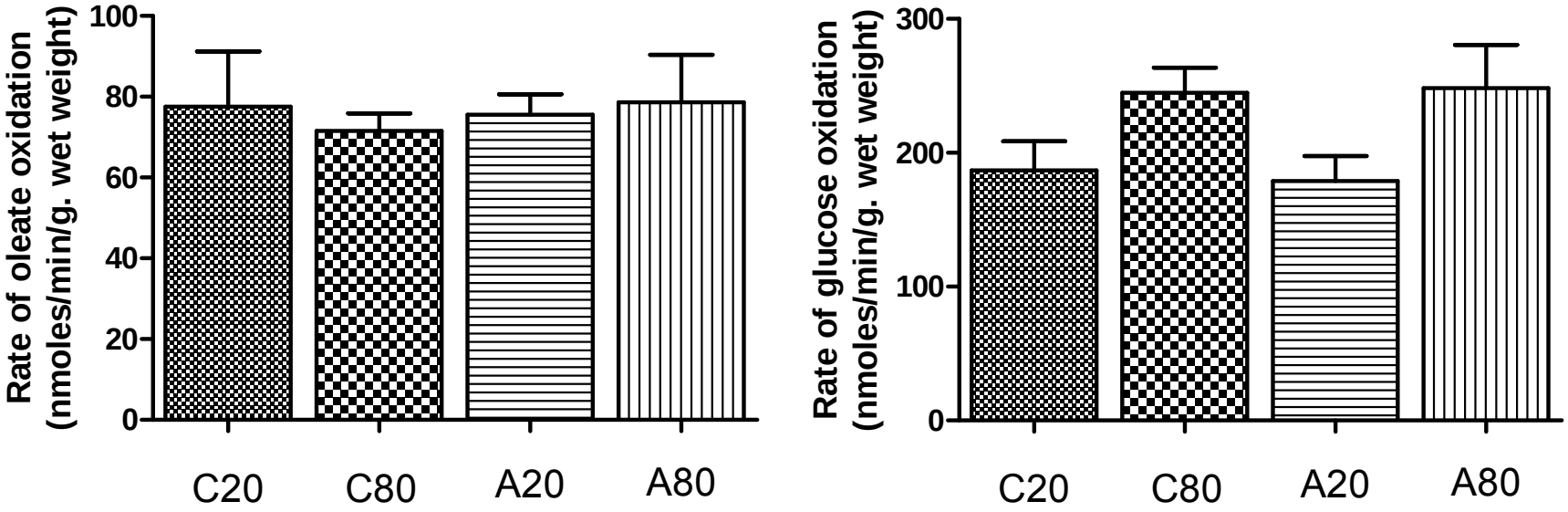

Figure 7.12. Ex vivo left ventricular substrate oxidation rates in control and atenolol treated hearts at 'low' and 'high' workloads. Legend: C20 = Control 20 mmHg, C80 = Control 80 mmHg, A20 = Atenolol 20 mmHg, A80 = Atenolol 80 mmHg. Rates were calculated from the mean gradient of the linear regression from each experiment. n=5-6.

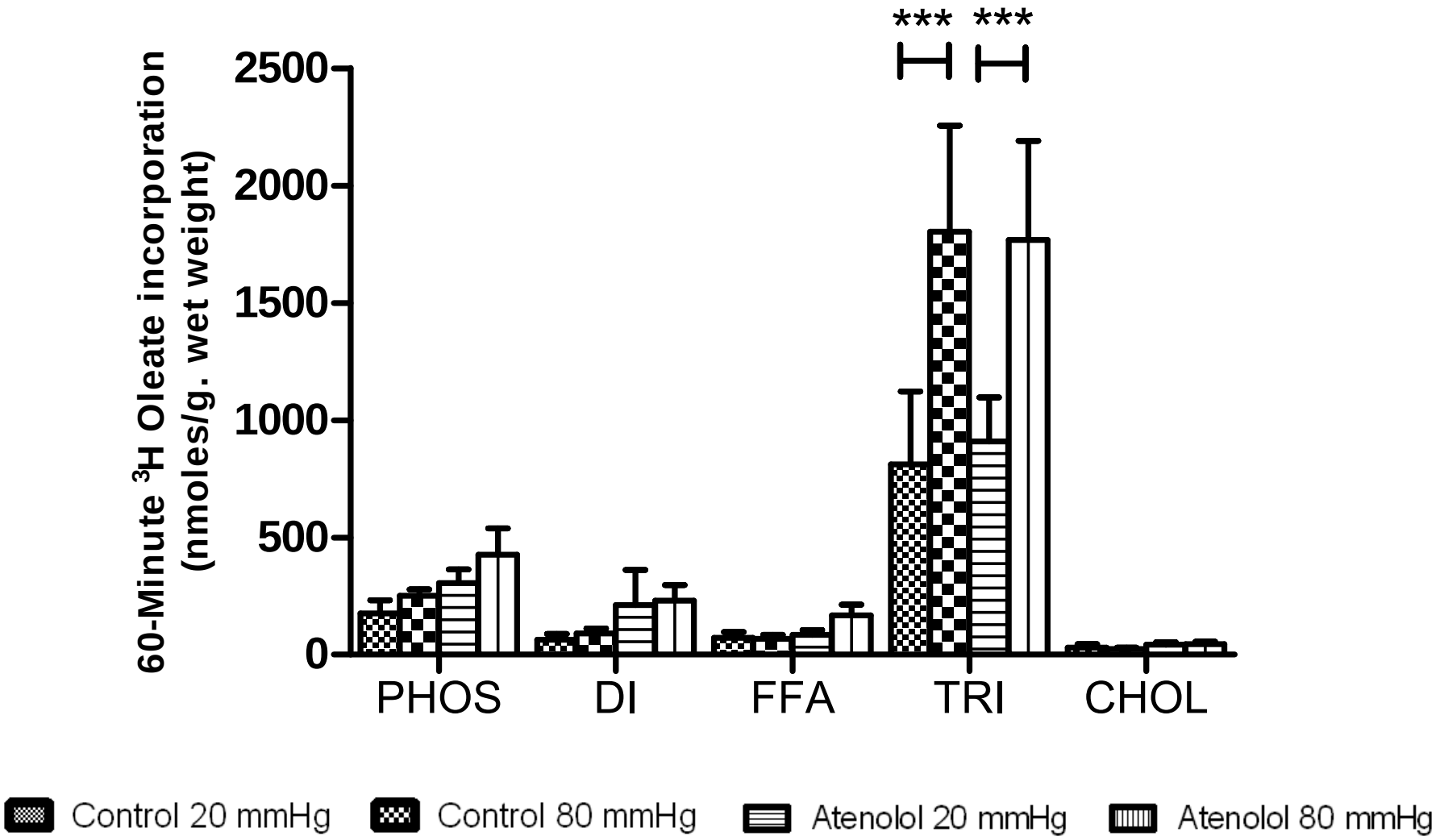

Figure 7.13. Ex vivo left ventricular metabolism in control and atenolol treated hearts at low and high workloads. (n= 5-6).The effects of workload; ***p<0.001. LEGEND: PHOS = Phospholipids, DI = Diacyglycerol, FFA = Free FAs, CHOL = Cholesterol esters.

Chapter Eight: Modifying capillary supply and substrate selection in the hypertrophied heart.

PART A. Modifying capillarity in the hypertrophied heart

Cold acclimation + Atenolol

We have previously seen that chronic bradycardia induced by atenolol induces capillary growth in the left ventricle of normal hearts and is associated with an improvement of contractile force at high workloads (Chapter 7). The aims of this work were to investigate the effects of atenolol mediated chronic bradycardia in the cold acclimated model of ventricular hypertrophy. A failure of angiogenesis has been proposed as a major factor in the progression from well compensated hypertrophy to heart failure [90, 91]. While cold acclimation represents a modest model of physiological hypertrophy it is of interest to address the ability of the cold acclimated myocardium to respond to angiogenic stimuli. Previous investigators have indicated that cold induced hypertrophy occurs independently of the activation of the sympathetic nervous system in this model therefore validating the use of atenolol as an agent in these experiments [246]. It was hypothesised, due to the physiological nature of this model, that chronic bradycardia would induce ventricular angiogenesis associated with enhanced contractile performance as previously described.

Cold acclimation + L-NAME

Chronic exposure to an elevation arterial blood pressure (i.e. increased afterload) is associated with hypertrophic growth and capillary rarefaction which over time progresses to HF[247, 248]. However hearts from L-NAME treated animals are able to normalise ventricular wall stress through a reduction in the dimension of the LV which presumably maintains cardiac output (although *in vivo* the dynamic range of these hearts may be reduced). Cold acclimation represents a well adapted form of ventricular remodelling which allows for an increase in cardiac output through eccentric remodeling of the ventricle and preserved contractile performance. The primary aim of this work was to investigate the effects of chronic increase in afterload on oxygen delivery in the cold acclimated model of hypertrophy. The aim of this study was to investigate the effects of exposure to

the combined stressors of cold acclimation and chronic pharmacological NO synthase inhibition. It was hypothesised that if the reduction in lumen dimension is aimed at reducing wall stress then the addition of a stimuli which promotes eccentric remodeling would necessitate hypertrophic wall thickening and due to the influence of L-NAME on angiogenesis (see chapter 5) that this would occur without adaptive expansion of the capillary bed.

PART B. Modifying substrate selection in the hypertrophied heart

Cold acclimation + Fibrates

The heart exhibits marked metabolic flexibility utilising any available circulating substrate to closely match energy supply and energy demand. Substrates compete with each other at various complexes of the metabolic pathways allowing energy production to proceed unabated by changes in prevailing substrate availability. Chronic alterations in substrate supply also result in adaptive changes to gene and protein expression. The peroxisomal-proliferator activated receptors (PPAR), comprising of alpha, beta and gamma isoforms, are regulated by the availability of free FA. PPAR-$\propto$ seems to be the primary regulator of cardiac lipid metabolism and has been shown to regulate expression of genes related to sarcolemmal FA uptake, FA intracellular transport, FA mitochondrial and peroxisomal uptake and β–oxidation [249, 250]. When activated PPAR-$\propto$ translocates into the nucleus where it heterodimerises with retinoid X receptor and binds to specific DNA sequences (peroxisomal proliferator hormone response elements). These sequences are usually found in the promoter regions of the genes and result in increased or decreased gene expression/transcription. Down regulation in the expression of PPAR-$\propto$ and/or RXR has been shown in both animal [251] and human [72, 252] heart failure, suggesting it has an important role in the switch towards increased carbohydrate oxidation and suppressed FA oxidation.

Incorporation of the synthetic PPAR-α fenofibrate into the standard laboratory diet of cold acclimated animals provides an opportunity to alter the balance between rates of FA and glucose

oxidation in the myocardium. Experimental evidence suggests that treatment with PPAR-∝ agonists in this manner can up-regulate proteins involved in beta-oxidation, mitochondrial energy production and FA uptake [253, 254]. Moreover direct application of PPAR-∝ agonists to myocyte cultures and chronic treatment of experimental mice with PPAR-∝ agonists enhances the rate FA oxidation and suppresses glucose oxidation [255, 256]. The efficiency of ATP production from FA in terms of O_2 used per mole ATP produced has been shown to be less than that of glucose. Therefore by forcing hearts to oxidize a greater proportion of FA the oxygen consumption per unit work/performance will be elevated. Chronic fenofibrate dietary supplementation represents a novel mechanism to increase oxygen consumption in the normal and hypertrophied heart without directly altering cardiovascular parameters (i.e. workload and contractile function) and avoiding the toxic effects of agents used to alter oxygen delivery (e.g. isoprenaline).

The aims of this work were to investigate the effects of fenofibrate on rates of metabolism and contractile performance in the cold acclimated heart. It was hypothesised that driving up rates of FA utilisation in this well adapted model of hypertrophy could push these animals into a dysfunctional state. In addition fibrates will alter whole body oxygen demand, as evidenced by an decrease in the respiratory quotient of rats treated with fibrates ($CO_{2\ eliminated}$ / $O_{2\ consumed}$), adding a further demand induced stress to the system.

Summary

The general aim of this chapter was to apply different mechanisms to change workload and/or oxygen consumption or oxygen delivery to establish whether changes can affect performance in the hypertrophied heart. Additionally experiments have looked at whether changes in workload (i.e. cold acclimation) can directly alter substrate metabolism.

Material and methods

Treatment regimes

Cold acclimation, atenolol and L-NAME

Details of the cold acclimation protocol and both the atenolol and L-NAME treatment regimens are presented in the relevant previous chapters.

Fibrates

Fenofibrate, a peroxisomal proliferator activated receptor ∝ (PPAR∝) agonist, was incorporated into standard laboratory rodent diet to give a dose of 1g/kg body mass. Based on average food intake in the rat [257] this gives a dose of 100 mg/kg/day [258]. Animals had *ad libitum* access to both diet and water during the dosing period. The fenofibrate diet was fed for a total of 7 days prior to collection of the samples.

Control data

Experiments were conducted at the same time as those presented in Chapter 5 and as such the control data shown in the present chapter is the same as that presented previously.

Chapter Legend

CON = Control, CA = Cold acclimation, CAA = Cold acclimation + Atenolol, CAL = Cold Acclimation + L-NAME, FEN= Fenofibrate, CAF = Cold acclimation + Fenofibrate.

Results

PART A. Modifying capillarity in the hypertrophied heart

Experiments in the rat

Effect of cold acclimation and L-NAME treatment on capillarity and ventricular contractile performance

CAL animals had significantly greater mean arterial blood pressures (102 ± 3 CON vs. 122 ± 5 CAL mmHg, P<0.01, Table 8.1) and comprable *in vivo* HRs (386 ± 5 CON vs. 371 ± 13 CAL bpm, Table 8.1) compared with CON. Combined chronic nitric oxide synthase inhibition and cold acclimation resulted in the development of significant systolic LV dysfunction at 4 weeks. Pressure development (Peak; 82 ± 6 vs. 57 ± 6 mmHg, P<0.05, Figure 8.2A) and +dP/dt (Peak; 1352 ± 76 CON vs. 957 ± 64 CAL mmHg/sec, P<0.01, Figure 8.3A) were significantly reduced in comparison to CON. Ventricular relaxation (-dP/dt) was also significantly impaired (Figure 8.3B). Despite an increase in cardiac mass there was a 17% reduction in LV lumen volume (335 ± 15 vs. 278 ± 6 μL, P<0.01, Figure 8.2B) and no change to the cross-sectional area of myocytes from the subendocardial (693 ± 26 CON vs. 682 ± 85 CAL μm^2, Figure 8.1A) and subepicardial (539 ± 57 CON vs. 504 ± 52 μm^2 CAL, Figure 8.1A) regions of the LV free wall. CAL animals gained weight slower that CON demonstrating a 21 % lower body weight 4 weeks from the commencement of treatment (313 ± 17 CON vs. 265 ± 8 CAL g. wet weight, P<0.05, Table 8.1). Diastolic-pressure volume relationships showed a slight leftward shift in keeping with a reduction in LV lumen dimensions (Figure 8.1B). Ventricular chamber stiffness was also similar between groups (0.84 ± 0.06 CON vs. 0.77 ± 0.06 CAL mmHg/μL, Figure 8.1B). Myocardial contractility (estimated systolic stress-strain) was unaffected by CAL treatment (85 ± 14 CON vs. 67 ± 7 CAL mmHg/ml/g. wet weight, Figure 8.4). Capillary density was similar in subendocardial (2390 ± 17 CON vs. 2274 ± 144 CAL capillaries/mm^2, Figure 8.1B) and subepicardial (2864 ± 151 CON vs. 2829 ± 269 CAL capillaries/mm^2, Figure 8.1B) regions. Capillary to fibre ratio was also no different between groups in the subendocardium (1.47 ± 0.04 CON vs. 1.53 ± 0.02 CAL, Figure 8.1C) and

subepicardium (1.42 ± 0.06 CON vs. 1.38 ± 0.02 CAL, Figure 8.1C). Despite significant systolic dysfunction the inotropic responses to dobutamine perfusion (150nM), expressed as a percentage change in RPP, were enhanced in hearts from the CAL treatment group (Table 8.3).

Effect of cold acclimation and atenolol on capillarity and ventricular contractile performance

CAA animals demonstrated similar body mass (313 ± 17 CON vs. 323 ± 16 CAA g. wet weight, Table 8.1) heart mass (1.20 ± 0.06 CON vs. 1.26 ± 0.08 CAA g. wet weight, Table 8.1) and heart to body mass ratios (3.87 ± 0.03 CON vs. 3.71 ± 0.11 CAA, Table 8.1) as CON. Capillary density, myocyte size and capillary-to-fibre ratio was comparable to CON in both the subendocardial (CD: 2390 ± 17 vs. 2274 ± 144 capillaries/mm^2, C:F: 1.42 ± 0.04 vs. 1.51 ± 0.02 MYO: 693 ± 26 vs. 684 ± 63 μm^2, Figure 8.1) and subepicardial (CD: 2864 ± 151 vs. 2616 ± 171 capillaries/mm^2, C:F: 1.42 ± 0.06 vs. 1.38 ± 0.02, MYO: 539 ± 57 vs. 595 ± 26 μm^2, Figure 8.1) regions of CAA hearts. CAA hearts demonstrated a significant rightward shift in the LVDP-volume relationship and mild impairment of systolic function at balloon volumes of 150-200 μL (Figure 8.2A). Peak pressure development was comparable between CAA and CON hearts (83 ± 8 CON vs. 75 ± 5 CAA mmHg, Figure 8.2A). CAA hearts had reduced ventricular stiffness (0.84 ± 0.06 CON vs. 0.61 ±0.05 CAA mmHg/μL, $P<0.01$, Figure 8.2) and comparable LV volume as CON (335 ± 15 CON vs. 370 ± 21 CAL μL). +dP/dt was comparable to CON at all workloads (Figure 8.3A) while –dP/dt demonstrated a slight impairment at intraventricular volumes between 100-250 μL (Figure 8.3B). The slope of the estimated systolic stress-strain relationship was similar between CON and CAA hearts (85 ± 14 CON vs. 75 ± 6 CAL mmHg/ml/g. wet weight, Figure 8.4). The inotropic responses to dobutamine perfusion were comparable to CON (Table 8.3).

Experiments in the mouse

Capillary density, myocyte size and capillary-to-fibre ratio was comparable to CON in both the subendocardial (CD: 3257 ± 19 vs. 3339 ± 147 capillaries/mm^2, C:F: 1.73 ± 0.05 vs. 1.76 ± 0.03 MYO: 546 ± 10 vs. 538 ± 30 μm^2, Figure 8.1) and subepicardial (CD: 3360 ± 172 vs. 3211 ± 203 mm^2, C:F:

1.80 ± 0.02 vs. 1.77 ± 0.04, MYO: 552 ± 24 vs. 578 ± 42, Figure 8.1) regions of CA mice treated with L-NNA.

PART B. Modifying capillarity in the cold acclimated heart

Experiments in the rat

Effect of fenofibrate on ventricular contractile performance and substrate metabolism

Plots of both oleate and glucose oxidation are presented in Figures 8.6 and 8.7 respectively. Total rates of exogenous glucose and oleate oxidation were comparable between CON (Glucose: 214 ± 32, Oleate: 71 ± 10 nmoles/min/g. wet weight), CA (Glucose: 263 ± 34, Oleate: 77 ± 12 nmoles/min/g. wet weight), FEN (Glucose: 246 ± 48, Oleate: 68 ± 14 nmoles/min/g. wet weight) and CAF (Glucose: 235 ± 55, Oleate: 90 ± 13 nmoles/min/g. wet weight) hearts (Figure 8.8). Total ^{14}C incorporation into glycogen and ^{3}H oleate incorporation into tissue lipids were unaffected by CA, FEN or the combination of both (Table 8.4 and Figure 8.9). None of the treatment regimes had any effect on animal body mass, heart mass or heart to body mass ratio (data not shown). Left ventricular contractile performance was similar in all experiments and between treatment regimes (Figure 8.10).

Experiments in the mouse

Treatment of mice with FEN caused a significant increase in liver mass (1.48 ± 0.07 vs. 2.79 ± 0.48 g. wet weight) while body mass (28.8 ± 0.3 vs. 27.8 ± 0.6 g. wet weight) and heart mass (144 ± 9 vs. 152 ± 8 mg. wet weight) were similar to CON. Similar results were seen in CA mice treated with FEN (data not shown).

Discussion

PART A. Modifying capillarity in the hypertrophied heart

Cold acclimation + Atenolol

The lack of hypertrophic growth during cold acclimation in animals dosed with atenolol implies that this remodelling is mediated in part through β1 adrenergic signaling. As previously discussed (Chapter 4) β adrenoceptor agonists have direct trophic effects on the myocardium promoting hypertrophic growth [141, 149-154]. Increased sympathetic drive associated with cold exposure therefore provides a likely stimulus for the increase in cardiac mass associated with cold acclimation (i.e. fibre elongation). These data are at odds with the report of Sun *et al* (1997) who found that hypertrophy was maintained in chronically cold exposed rats treated with propranolol [246], a difference which may reflect the method of cold exposure used i.e. animals were exposed directly to 4^{o}C for a 4 week period in contrast to the gradual acclimation procedure used in the present study. In addition to the direct influence of adrenergic stimulation an increase in sympathetic drive may increase the activity of the renin-angiotensin system (RAS), a known consequence of cold exposure [222]. Renin release from the kidney is under sympathetic control and as such chronic beta blockade may suppress the secretion of renin in during exposure to a cold environment [259]. Circulating renin cleaves angiotensinogen to angiotensin I. Angiotensin I is converted to angiotensin II by the angiotensin-converting enzymes which then binds to the AT_1 and AT_2 receptors mediating its effects on the cardiovascular system (including vasoconstriction, hypertrophic growth and modulation of myocardial angiogenesis (see below)). In addition angiotensin II may stimulate the production of aldosterone, which mediates sodium and water reabsorption in the kidneys and so regulates blood volume. Despite this, studies conducted to date suggest that the renin-angiotensin system does not contribute to the myocardial hypertrophy induced by chronic cold exposure. Experiments with combined cold exposure and captopril (an angiotensin converting enzyme inhibitor) therapy demonstrate a reduction in the cold induced increase in arterial blood pressure but no alteration in the hypertrophic response [219]. Similarly myocardial hypertrophy occurs in response to cold

acclimation in mice engineered to lack the gene encoding for angiotensinogen [231]. Experiments conducted in rats exposed to moderate cold environments (15^{o}C) for 6 weeks have shown that circulating blood aldosterone concentrations are signficantly greater than those of controls animals and that this occurs independently of any activation of the renin-angiotensin system or alterations in the hydromineral balance (i.e. blood potassium and sodium content) ref. In future work it would be necessary to measure the circulating and tissue level expression of components of the renin-angiotensin-aldosterone system to estimate its potential involvement in cold induced hypertrophy and to assess the mechanisms of action of atenolol in preventing this hypertrophy. Significant renin release may still occur during cold exposure due to catecholamine binding to the α-adrenoceptors in the kidney [260].

Despite a similar reduction in HR to that seen in the atenolol experiments, ventricular capillarity was comparable to controls in the LV free wall of CAL hearts. Previous studies utilising propranolol treatment in exercise have failed to show any changes to ventricular capillary supply [261] and parallels may be drawn between the physiological adaptation associated with exercise and cold acclimation (i.e. increased sympathetic drive). Reductions in the angiogenic capacity of the myocardium could be mediated by alterations in the renin-angiotensin-aldosterone system. Angiotensin II acts as both a promoter and inhibitor of angiogenesis in the myocardium through binding to the AT_1 and AT_2 receptors, respectively [262, 263]. Therefore it would be prudent to measure the expression of these receptors in the myocardium as well as measures of the activity of the renin-angiotensin-aldosterone system (i.e. circulating rennin, circulating and tissue AII). A more elegant experiment may be to investigate bradycardia mediated angiogenesis in AT_1 and AT_2 gene knockout mice in both normothermic and hyperthermic conditions.

Chronic bradycardia in CA animals was associated with a significant increase in ventricular compliance and a rightward shift in the LVEDP-volume relationship. This increase in ventricular compliance was greater than that seen during dosing with atenolol in normal animals (9% vs. 26%

(mean values), Table 8.2) despite a similar reduction of *in vivo* HR. It is not clear why this occurs however previous studies have demonstrated an increase in the circulating blood volume of animals exposed to cold environment for prolonged periods of time; a potential effect of an increase in circulating aldosterone in a manner independent of the activity of the renin-angiotensin system [218]. Therefore it is plausible that preload, and so ventricular stretch, is enhanced by the combined effects of increased venous return and an increase in the diastolic period of the heart beat. CAA hearts demonstrated a rightward shift in the LVDP-volume relationship with poor systolic LV performance at low intra-ventricular balloon volumes. This represents a change in the normal operating range of these hearts rather than a loss of intrinsic myocardial contractility (as evidenced by the preservation of peak LVDP and the systolic stress-strain relationship). These data appear to demonstrate a suprising adaptation to chronic volume overload independent of the well described model of eccentric hypertrophic growth. As discussed previously alterations in the volume capacity of the myocardium may underlie reports of enhanced stroke work at high workloads following chronic bradycardia in rabbits and pig [85, 86]. The lack of subendocardial hypertrophy, as seen in normal animals dosed with atenolol, provides indirect evidence that this regional myocyte expansion is linked to capillary growth.

Cold acclimation + L-NAME

The combination of CA and chronic nitric oxide synthase inhibition results in an increase in cardiac mass without any perceivable change in either myocyte cross-sectional area and a 17% reduction in ventricular chamber volume compared with controls (Table 8.2). This, at least in part, represents the combined early effects of L-NAME induced hypertension (i.e. a reduction in LV volume with no change in mass) and the eccentric remodeling associated with a gradual reduction in ambient environmental temperature and day length. L-NAME induced hypertension has been shown to occur within one week and therefore in this model the hypertensive stimulus may precede an increase in sympathetic drive resulting from the gradual reduction in ambient temperature.Therefore the eccentric remodeling associated with CA likely occurs in a heart with significantly reduced LV lumen

volume but preserved LV mass resulting in the cardiac phenotype demonstrated in the present study. However if we assume that hearts from L-NAME treated animals are representative of CAL hearts before eccentric hypertrophy occurs then we can see that the increase in the cardiac mass to body mass ratio (23%, Table 8.2) cannot account for the pronounced expansion of the ventricle lumen (102%, compared to L-NAME hearts). Whereas in normal animals the CA induced expansion of the LV volume (17%, Table 8.2) is reflected in the percentage increase in cardiac mass (13%, Table 8.2) and the cardiac mass to body mass ratio (17%, Table 18.2). Therefore CAL induced remodeling may represent a model of ventricular dilatation where there is significant expansion of the LV lumen and a dramatic thinning of the LV wall. Potentially this could occur as a net effect of myocyte elongation and cell death or as a result of myocyte slippage. The latter occurs in models of ischemic injury [205], chronic pressure [206] and chronic volume overload [207] and describes how individual fibres of groups of fibres can 'slide' in a transmural fashion to alter ventricular geometry without significantly affecting ventricular mass. This internal rearrangement of the fibres is thought to involve matrix metalloproteinases (MMPs) that degrade the extracellular matrix and whose expression is modified in experimental models of myocardial infarction [264]. Inhibitors of MMPs have been shown to prevent cardiac dilation and pump dysfunction in models of chronic pressure overload [265]. While systolic chamber function was markedly depressed estimates of true myocardial contractility (LV systolic stress-strain) were comparable between cold acclimated and control hearts. These data demonstrate that the impairment of systolic function in cold acclimated hearts treated with L-NAME is a result of geometric insufficiency (e.g. chamber dilation) rather than any alteration in the intrinsic contractile function of the myocardium. We discussed earlier (Chapter 1), through the law of LaPlace, how geometric expansion without wall thickening increases ventricular wall stress and negatively impacts upon LV contractile function. Similar impairment of systolic LV function has been demonstrated in models of chronic pressure overload and prolonged isoprenaline dosing [101, 205-207]. Nitric oxide is a regulator of β adrenergic signaling and in both L-NAME and CAL hearts resulted in an augmentation of the inotropic response to perfusion with

dobutamine. Therefore it is possible that the combination of an increase in circulating catecholamine concentrations and increased sensitivities of the β adrenergic pathway could result in myocardial damage and thus chamber remodeling.

No measure of fibrosis was made in the present study which could be used to give some indirect indication of cell death. Methods such as DNA strand breaks or caspase activation (i.e. 3, 6 and 9 – the effecter caspases which cleave other protein substrates and trigger the apoptotic process) could also be used to quantify the degree of cell death in these hearts. The transmural myocyte distribution could be assessed using low-powered electron microscopy to look the potential role of myocyte slippage in the expansion of the lumen diameter in this study.

PART B. Modifying substrate selection in the hypertrophied heart

Treatment of normothermic and CA animals with fenofibrate did not alter rates of *ex vivo* substrate oxidation in the present study. Dosing regimens were based upon those reported in previous studies and are known to have an effect on whole body FA utilisation. While no measure of the efficacy of fenofibrate treatment was made in the rat an increase in liver weight was noted in mice treated with the same regime. PPAR-α agonists are known to have pronounced effects on fatty acid uptake, synthesis and deposition in the rodent liver and an increase in liver mass in the present study likely represents a bi-product of these influences. Further to this efficacy of fenofibrate treatment could be confirmed through measurement of the respiratory quotient in a metabolic chamber (CO_2 $_{\text{eliminated}}$ / O_2 $_{\text{consumed}}$) which provides information on the contribution of substrates (i.e. carbohydrates, FAs and proteins) to ATP generation in the whole animal (a similar method could be applied to the isolated heart). A reduction in whole body RQ has been noted in humans dosed with PPAR-α agonists, indicating increased rates of FA oxidation [266]. PPAR-α mRNA expression in homogenates of cardiac tissue has also been used as a quantifiable measure of PPAR-α activation [267]. Any direct effects cardiac metabolic capacity could be assessed through measurement of the expression of genes of FA uptake and oxidation and their encoded proteins. Early reports in isolated

cardiac myocytes showed that exposure to PPAR-α agonists resulted in an increase in the expression of genes encoding CPT1, MCAD, Uncoupling protein 3 (UCP3) and LCAD [255]. Similarly several *in vivo* studies have showed that PPAR-α agonists can increase the FA oxidative capacity in the adult rodent heart [253, 254]. It is unknown whether alterations in gene and protein expression occurred in the present study but these changes were not manifested in changes to substrate selection. Substrate utilisation in the myocardium is regulated by the energetic workload of the heart, the relative availability of circulating substrates and the influence of circulating insulin and catecholamine's. Metabolic rate and flux through the individual pathways and reactions is therefore influenced by the activity of various enzymes in the metabolic pathway and is not dictated directly by gene or protein expression (unless the expression is severely altered, as occurs in HF). Previous studies have demonstrated that circulating free FA and serum triglycerides are significantly reduced in PPAR-α agonist treated rodents [267, 268] As FAs are the natural ligand activator of PPAR-α it seems is probable that in the present study there are two opposing influences on cardiac FA metabolism; 1) the supplementation of fenofibrate and 2) a potential fall in the levels of circulating lipids – though no measure of the latter was made.

There is some controversy as to whether treatment with PPAR-α agonists is able to increase rates FA oxidation in the myocardium. Direct application of PPAR-α agonists to cultured myocytes enhances the rate of FA oxidation, however these experiments remove the confounding influence of alterations in circulating substrate availability [254]. Hafstad *et al* (2009) have also demonstrated a significant increase in FA oxidation and a suppression of glucose oxidation in mice treated with the PPAR-α agonist tetradecyithioacetic acid, the only study to date to demonstrate such changes in normal animals. Other investigators have noted that PPAR-α agonists are able to prevent the substrate switch associated with aortic banding induced HF, but did not report any alteration in substrate oxidation rates in sham operated animals treated under the same dosing regimen [269, 270]. In a study in the pig Xu *et al* (2005) found that FEN had no effect of FA uptake or CPT-1β

(muscle type) expression in the myocardium [271]. Aasum et al (2005) found that the PPAR-α agonist BM 17.0744 did not alter rates of FA oxidation in the hearts of normal mice [272].

There is significant controversy as to whether reactivation of PPAR-α in models of de-compensated hypertrophy has any effect on myocardial contractile performance. Young *et al* (2001) have demonstrated that in hypertrophied hearts (induced by aortic banding) PPAR-α agonists prevented the switching of substrate utilisation associated with heart failure and resulted in rapid contractile dysfunction in the treatment group [269]. Contrary to this Labinskyy *et al* (2007) found that fenofibrate prevented the alterations in cardiac metabolic phenotype without changing the onset of de-compensation in pacing induced heart failure in dogs [270]. Myocardial contractile performance and rates of *ex vivo* substrate oxidation were comparable in CON and CA hearts in the present study. These findings are in keeping with those reported by Cheng and Hauton (2008) [140]. Fenofibrate dietary supplementation did not affect the contractile performance of CON or CA hearts which demonstrates the well compensated hypertrophic phenotype in this model (i.e. preserved contractile function and substrate selection). As PPAR-α agonists did not alter substrate oxidation rates in the present study it cannot be ruled out that an increase in the reliance upon FA oxidation could increase O_2 demand and drive this well compensated model into failure.

The use of PPAR-α-null and MHC-PPAR-α mice could provide an alternative approach to alter substrate selection in the rat heart. Experiments could be carried out to assess the response of these animals to chronic cold exposure providing a two-tailed experimental approach.

Conclusions

Attempts to alter both ventricular capillarity and myocardial substrate selection in the CA heart have been unsuccessful.

Table 8.1 Effects of treatment on in vivo physiological parameters and cardiac phenotype hearts from the cold acclimation + treatment study.

	Control	***Cold + Atenolol***	***Cold + L-NAME***
Body Mass (g)	313 ± 17	323 ± 16	265 ± 6**
Heart Mass (g)	1.20 ± 0.06	1.26 ± 0.08	1.26 ± 0.06
Heart mass / Body Mass (mg/g)	3.87 ± 0.03	3.71 ± 0.11	4.77 ± 0.26**
In vivo heart rate (BPM)	386 ± 5	339 ± 19*	357 ± 15
Mean arterial blood pressure (mmHg)	102 ± 3	103 ± 4	122 ± 5**
Estimated ventricular volume (μL)	335 ± 15	370 ± 21	278 ± 5 **
Ventricular stiffness (mmHg/ml)	0.84 ± 0.06	0.77 ± 0.06	0.61 ± 0.05**
LV systolic stress-strain (mmHg/ml/g. wet weight)	85 ±14	75 ± 6	67 ± 7

(n=5-6) Different from control; *P<0.05, **P<0.01.

Table 8.2 Summary of effect of treatment regimes on in vivo parameters and ventricular phenotype.

	Cold Acclimated	***L-NAME***	***Cold acclimation + L-NAME***	***Atenolol***	***Cold acclimation + atenolol***
Body mass	-	↑	↓	-	-
Heart mass	↑	-	*Unchanged*	-	-
Heart to body mass ratio	↑	-	↑	-	-
In vivo HR	-	-	↓	↓	↓
MAP	↑	↑↑	↑	-	-
Unstressed LV volume	↑	↓↓	↓	-	-
Ventricular stiffness	-	↑↑	-	↑	↓↓

LEGEND: - = comparable to control values, ↑ = greater than control values, ↓ = less than control values. Number of arrows indicates the degree of change associated with each treatment.

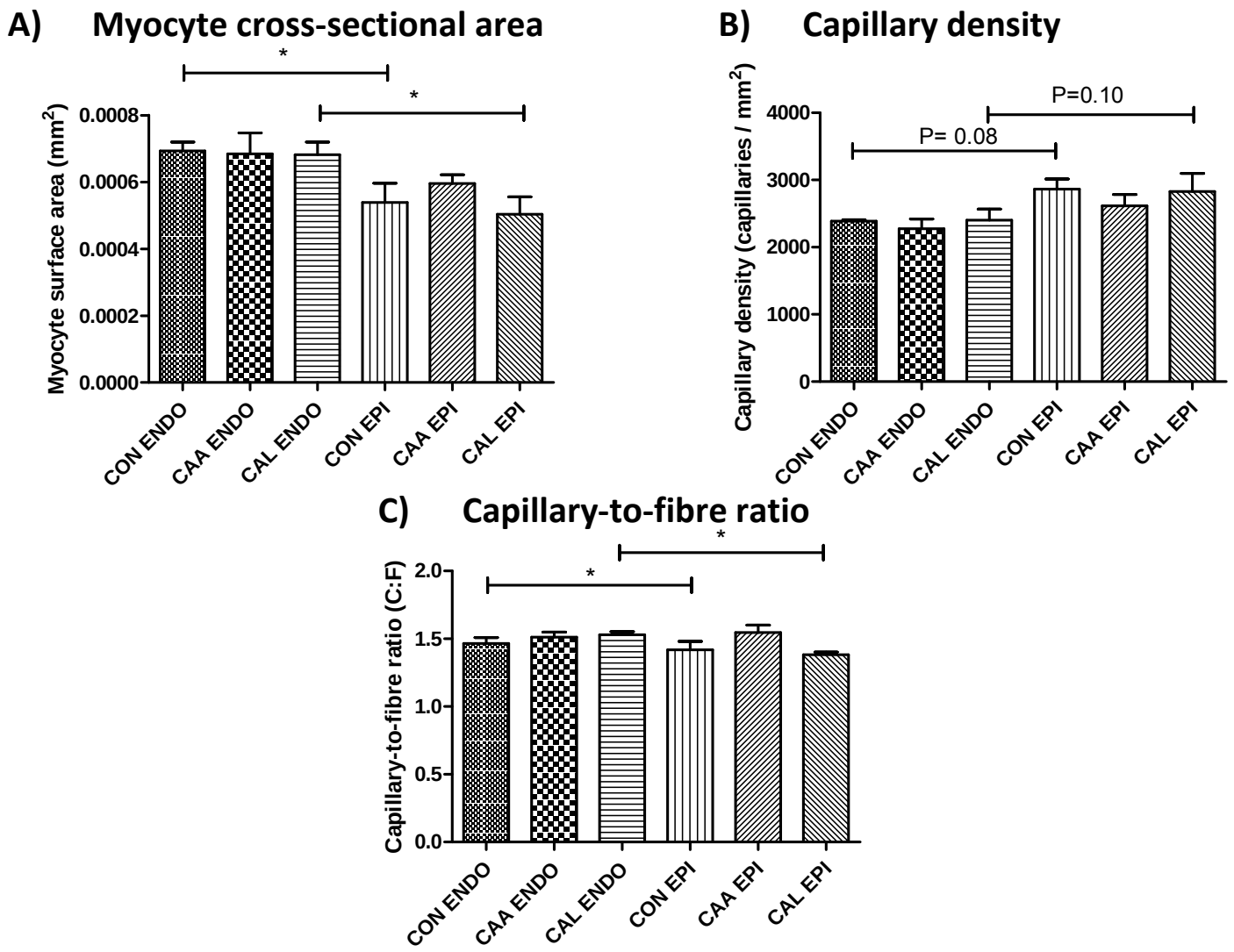

Figure 8.1. Effect of cold acclimation + treatment on LV capillarity and myocyte morphology. Legend: CON = Control, CA = Cold acclimation, CAA = Cold acclimation + Atenolol, CAL = Cold Acclimation + L-NAME

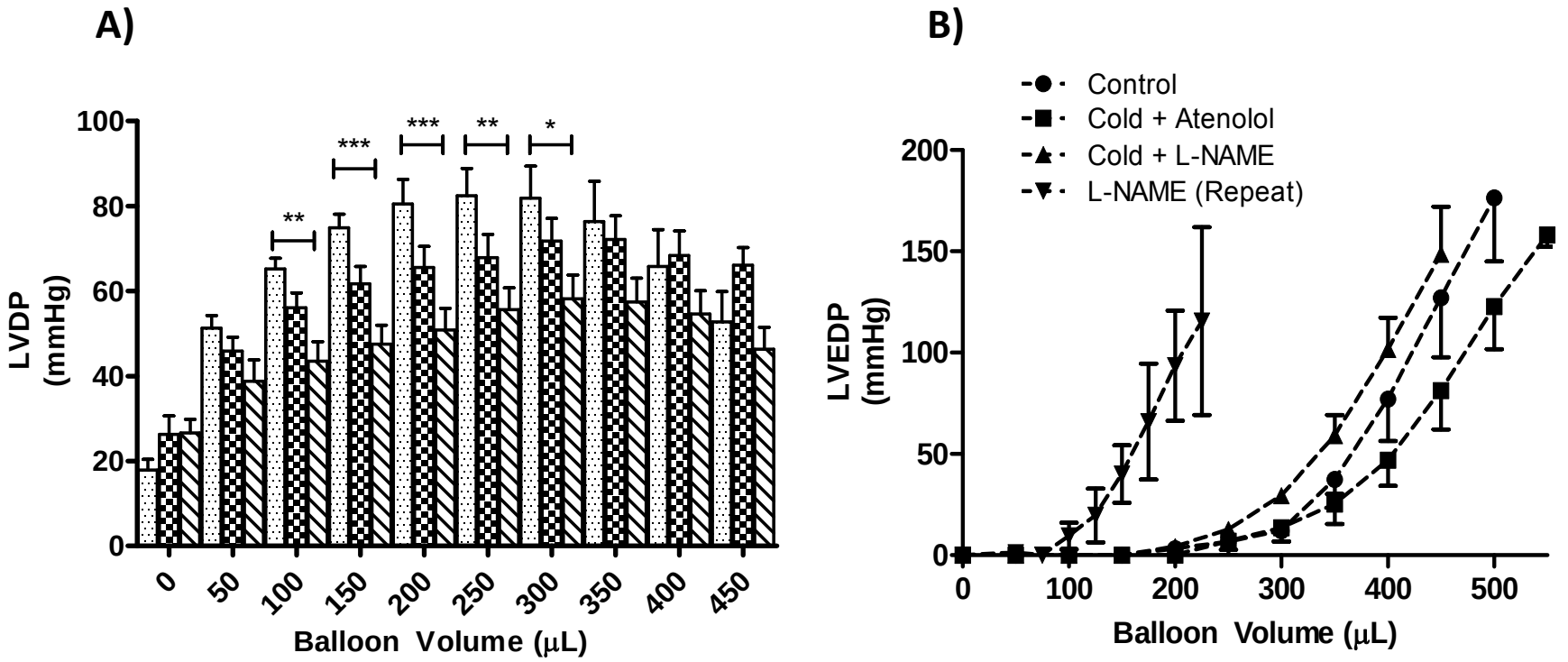

Figure 8.2 Effect of cold acclimation + treatment on LVDP-volume relationship (A) and LVEDP-volume relastionship (B). (n=6). LEGEND: Dots = Control, Squares = Cold Acclimation + Atenolol, Diagonal stripes= Cold Acclimation + L-NAME. The effects of cold + atenolol treatment; $^{\&}P<0.01$. The effects of Cold + L-NAME treatment; *P<0.05, **P<0.01, ***P<0.001

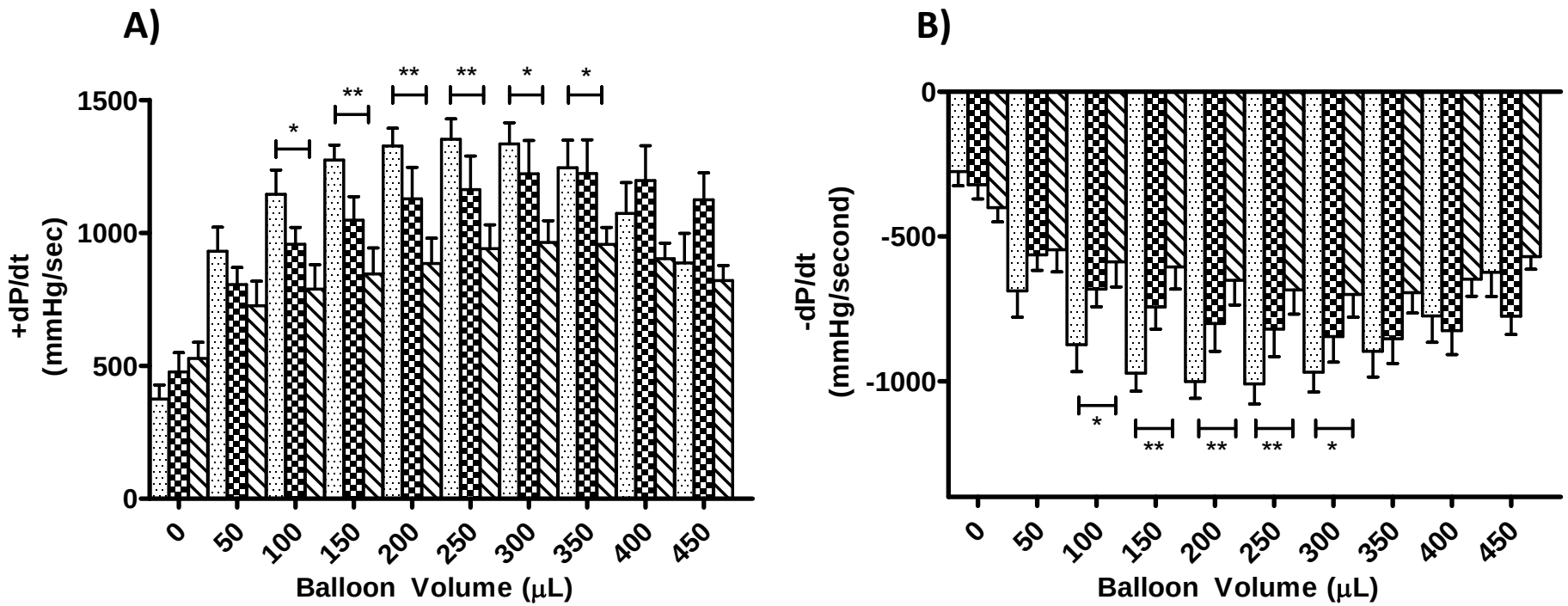

Figure 8.3 Effect of cold acclimation + treatment on +dPdt (A) and -dPdt (B). (n=6). LEGEND: Dots = Control, Squares = Cold Acclimation + Atenolol, Diagonal stripes= Cold Acclimation + L-NAME. The effects of cold + atenolol treatment; $^{\&}P<0.01$. The effects of Cold + L-NAME treatment; *P<0.05, **P<0.01.

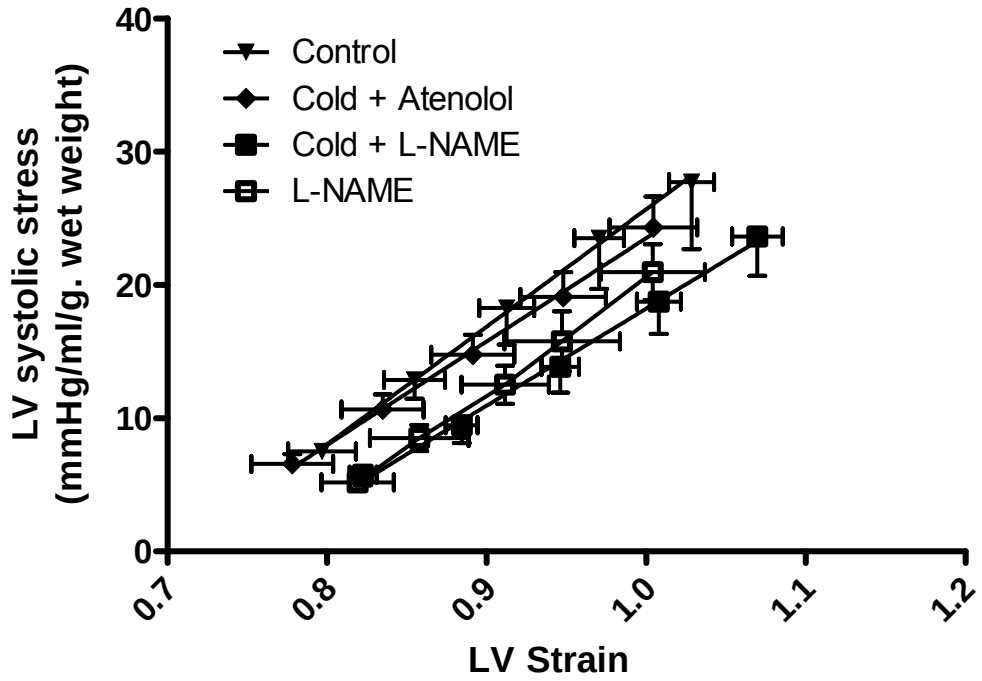

Figure 8.4 Effect of cold acclimation + treatment on LVEDP-volume relationships (A) and estimated LV stress-strain (B). (n=6) The effects of treatment; *P<0.05, **P<0.01, ***P<0.001. Legend: CON = Control, CA = Cold acclimation, CAA = Cold acclimation + Atenolol, CAL = Cold Acclimation + L-NAME.

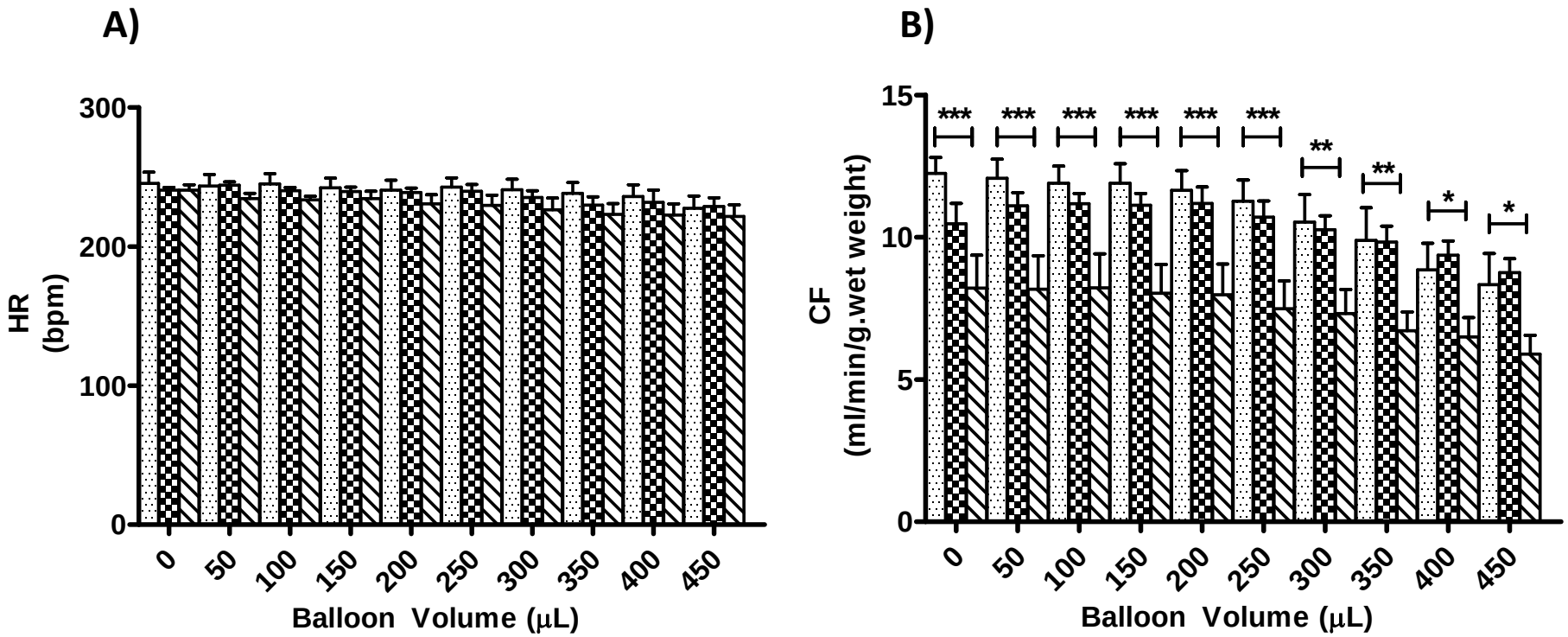

Figure 8.5 Effect of cold acclimation + treatment on HR (A) and CF (B). (n=6) LEGEND: Dots = Control, Squares = Cold Acclimation + Atenolol, Diagonal stripes= Cold Acclimation + L-NAME. The effects of treatment; *P<0.05, **P<0.01, ***P<0.001.

Table 8.3. Effect of dobutamine (150nM) perfusion on cardiac performance of control and cold + treatment hearts.

	Control		*Cold acclimation + atenolol*		*Cold acclimation + L-NAME*	
	Untreated	Dobutamine (150nM)	Untreated	Dobutamine (150nM)	Untreated	Dobutamine (150nM)
HR (bpm)	233 ± 14	245 ± 16*	200 ± 12	220 ± 8*	226 ±17	244 ± 28
Peak systolic pressure (mmHg)	99 ± 8	118 ± 10**	93 ± 9	107 ± 12*	58 ± 1$^{\&\&}$	67 ± 6$^{\&\&}$
LVDP (mmHg)	78 ± 7	96 ± 7***	79 ± 9	93 ± 12*	36 ± 2$^{\&\&\&}$	48 ± 5*$^{\&\&}$
+dP/dt (mmHg/sec)	1267 ± 179	1884 ± 287**	1162 ± 141	1776 ±243**	474 ± 26$^{\&\&}$	711 ± 36**$^{\&\&}$
-dP/dt (mmHg/sec)	-931 ± 139	-1291 ± 200**	-799 ± 94	-1194 ± 187**	-340 ± 35$^{\&\&}$	-450 ± 34**$^{\&\&}$
RPP (mmHg/min)	18000 ± 1500	23500 ± 2800**	15500 ± 1300	20200 ± 2100**	8000 ± 600$^{\&\&\&}$	11400 ± 800**$^{\&\&}$
Change in RPP (%)	-	30 ± 3	-	30 ± 4	-	42 ± 1$^{\&}$

(n=5-6). The effects of dobutamine; *p<0.05, **P<0.01, ***P<0.001. The effects of cold+L-NAME treatment; $^{\&}$p<0.05, $^{\&\&}$p<0.01, $^{\&\&\&}$p<0.001.

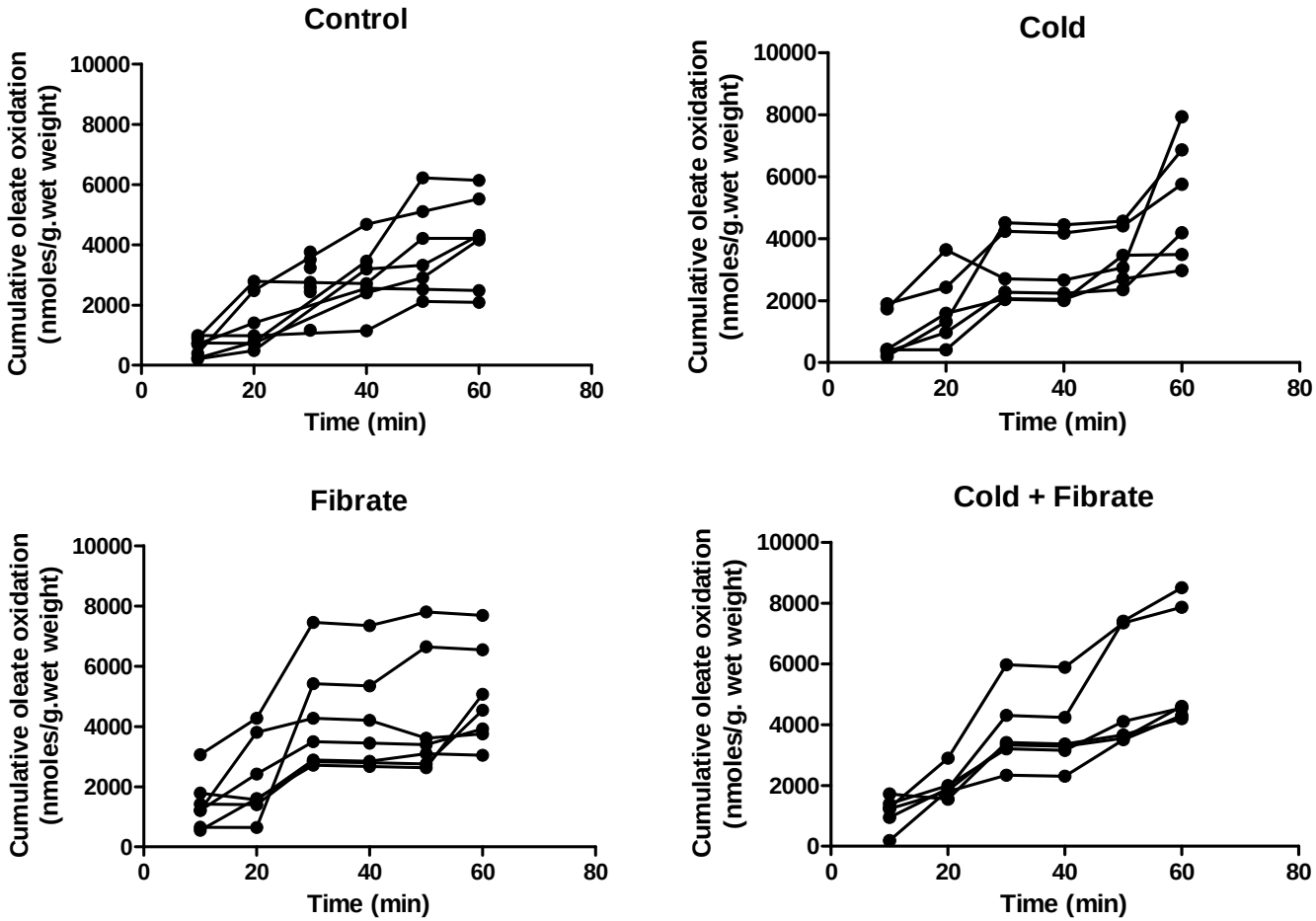

Figure 8.6. Raw data plots of oleate oxidation against time. Data demonstrate rates of oleate oxidation in all preparations used in the calculation of mean values (Control n=7, Cold n=6, Fibrate n=7, Cold + Fibrate n=6)

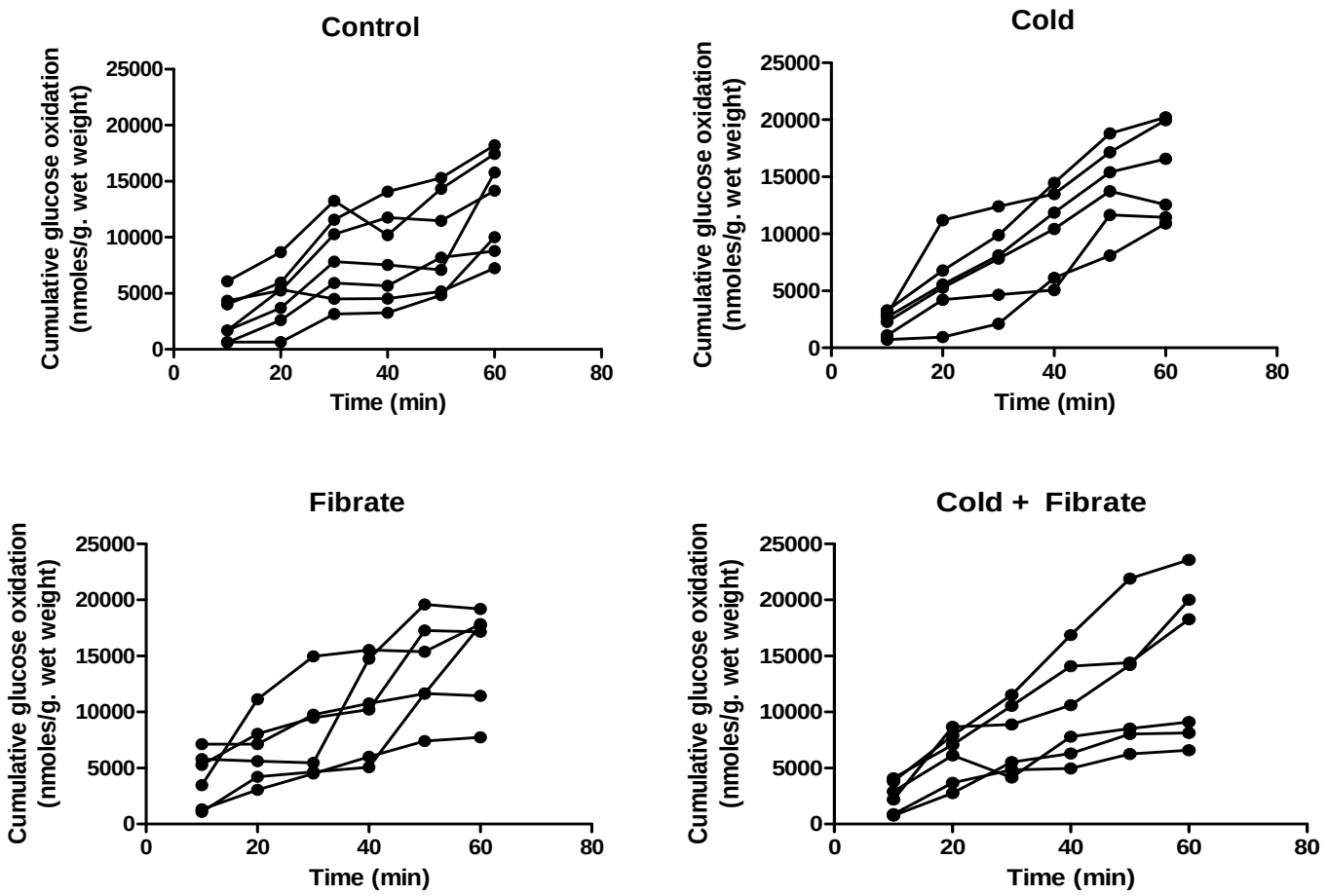

Figure 8.7. Raw data plots of glucose oxidation against time. Data demonstrate rates of glucose oxidation in all preparations used in the calculation of mean values (Control n=7, Cold n=6, Fibrate n=7, Cold + Fibrate n=6

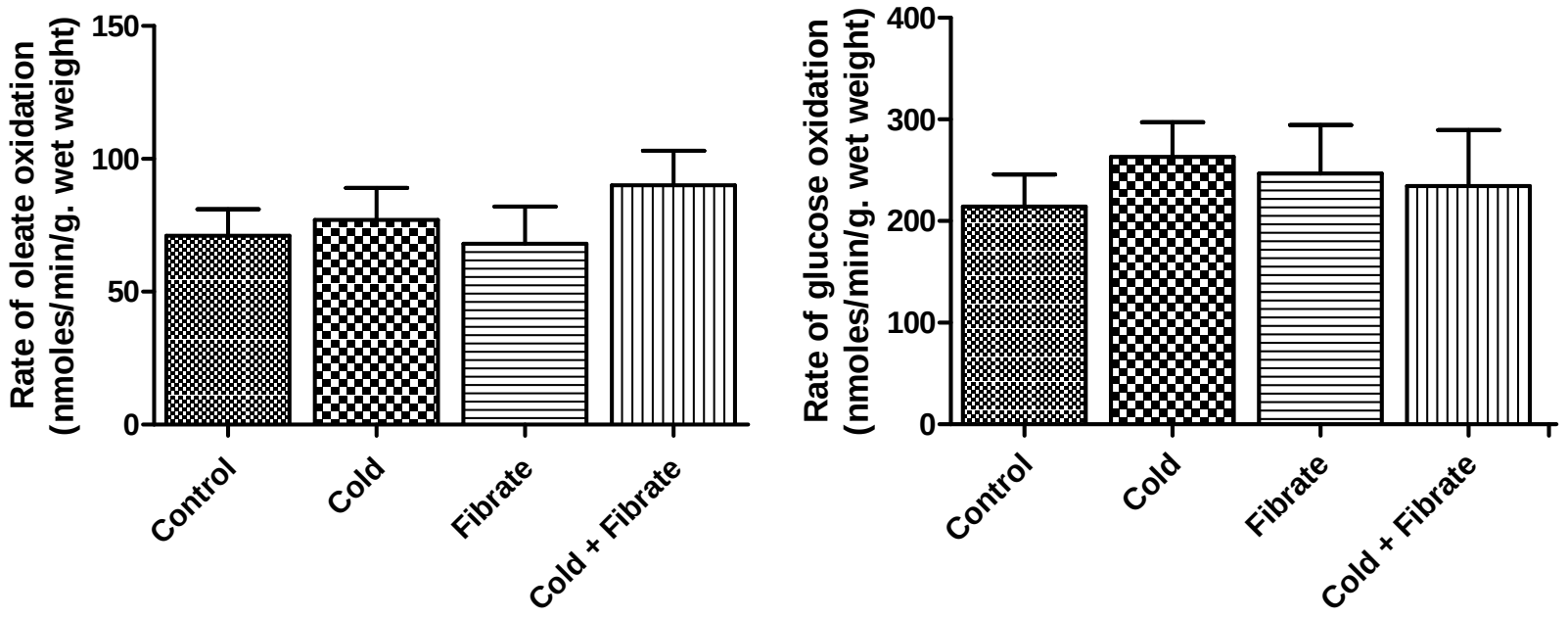

Figure 8.8. Ex vivo left ventricular substrate oxidation rates in control, cold acclimated, fenofibrate and cold acclimation + fenofibrate treated rats. (n=6-7) Rates were calculated from the gradient of linear plots of each

Table 8.4. Effect of cold acclimation and fenofibrate treatment on endogenous energy stores and labelled tracer incorporation during the 60-minute perfusion protocol.

	Control	Cold Acclimated	Fenofibrate	Cold acclimated + fenofibrate
Total tissue triglycerides (μmoles/g. wet weight)	3.91 ± 0.49	4.35 ± 0.65	5.13 ± 0.75	4.68 ± 0.51
Total tissue glycogen (μmoles/g .wet weight)	28.48 ± 2.27	33.83 ± 3.36	33.13 ± 1.97	25.36 ± 3.50
Total ^{3}H-oleate incorporation into tissue lipids (μmoles/g. wet weight)	1.02 ± 0.29	0.80 ± 0.11	1.07 ± 0.12	1.26 ± 0.25
Total ^{14}C-glucose incorporation into tissue glycogen (μmoles/g .wet weight)	4.12 ± 0.10	3.55 ± 0.45	5.22 ± 1.14	3.75 ± 0.51

(n=6-7)

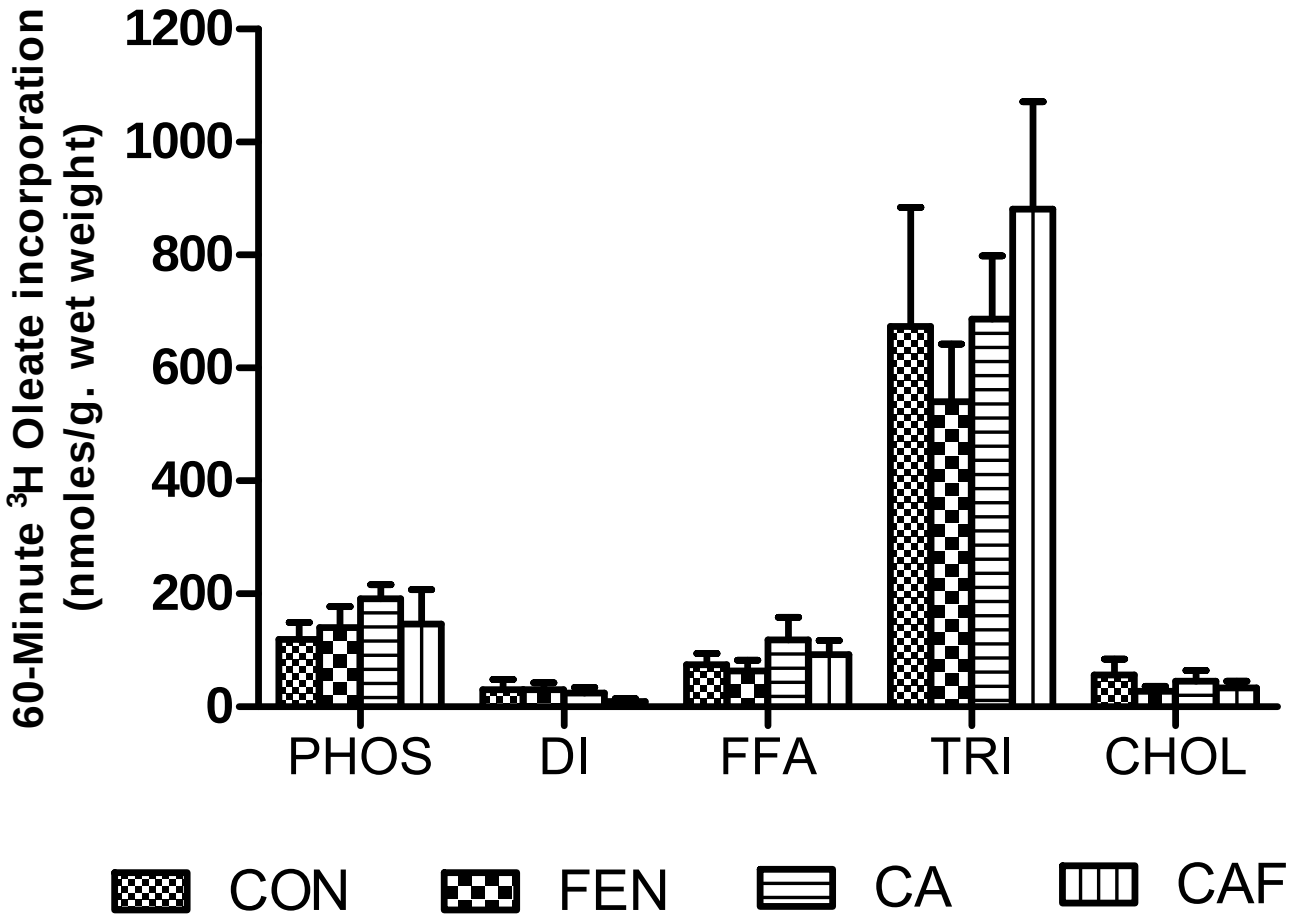

Figure 8.9. Ex vivo left ventricular metabolism in CON, FEN, CA and CAF treated hearts. (n=). LEGEND: PHOS = Phospholipids, DI = Diacyglycerol, FFA = Free FAs, CHOL = Cholesterol esters, CON = Control, FEN = Fenofibrate, CA = Cold Acclimated, CAF = Cold acclimated + Fenofibrate.

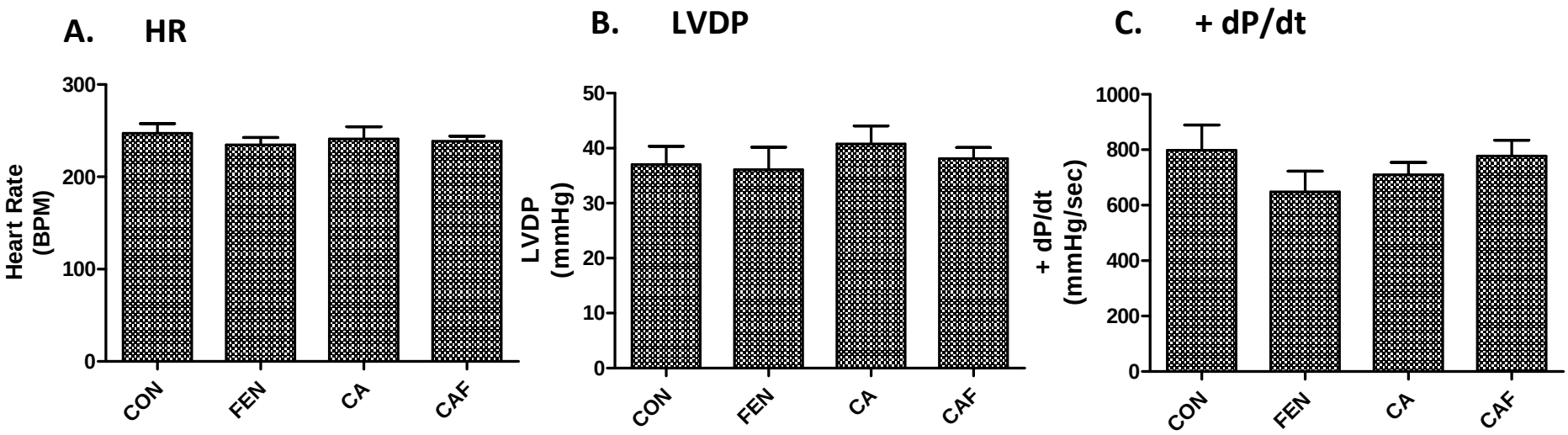

Figure 8.10. Left ventricular performance during the metabolism protocol. n=6-7

Chapter Nine: General Discussion

Summary of findings

This aims of this thesis were to investigate the influence of alterations in capillary number and distribution on ventricular contractile performance and substrate metabolism. Attempts were made to modify capillarity through prolonged exposure to physiological stressors such as elevated arterial blood pressure (L-NAME), β adrenoceptor activation (isoprenaline), prolonged exposure to a cold environment and chronic heart rate reduction (atenolol). In addition attempts were made to modify oxygen consumption through alterations in substrates selection (PPAR-α). The selection of physiologically and clinically relevant angiogenic and hypertrophic stressors represents a novel approach contrasting with previous studies utilising surgical interventions (i.e. aortic banding, electrical pacing) and genetic models (i.e. gene upregulation and downregulation). The super-physiological influence of both surgical and genetic techniques confounds any interpretation of the contribution of a failure of angiogenesis to the development of contractile dysfunction and metabolic abnormalities in HF. The present study is the first to attempt a direct comparison between alterations in ventricular capillary supply, cardiac contractile performance and substrate utilisation in the myocardium.

The myocardium demonstrates surprising plasticity in response to chronic alterations in both preload (atenolol) and afterload (L-NAME). The adaptive alteration in ventricular compliance associated with prolonged filling, during atenolol mediated bradycardia, occurs without any alteration to systolic performance. This implies that the increase in maximal stroke work evidenced in previous studies of chronic bradycardia is a result of an increased stroke volume capacity rather than improvements in myocardial oxygenation. Indeed previous investigators have noted that ventricular oxygenation does not fall to the critical level which would inhibit myocardial energetics during maximal cardiac work (i.e. stimulation with adrenaline) [95, 273]. Therefore it seems unlikely that a reduction in oxygen diffusion distances could support an improvement in function noted in

these studies [86, 87]. Chronic exposure to L-NAME was associated with a reduction in the ventricular lumen volume demonstrating that hypertrophic growth is not a necessary adaptation to preserve cardiac output in response to arterial hypertension. The preservation of LV contractile performance despite a significant reduction in coronary blood flow is a clear indication that, even in conditions of reduced oxygen content (i.e. crystalloid vs. blood perfusion), that the availability of oxygen is not limiting to performance. The contractile dysfunction noted after 10 days of isoprenaline treatment is unrelated to ventricular capillarity as a similar distribution of the capillary bed was noted in the 3 day treatment group. Inotropic responses to dobutamine were similar in all groups, implying that oxygen availability was again not limiting to performance despite pronounced concentric ventricular hypertrophy without adaptive angiogenic growth. Chronic exposure to a cold environment is associated with eccentric ventricular remodeling and the preservation of cardiac systolic performance. Despite a significant increase in cardiac workload *in vivo* there was no alteration in LV capillarity showing that hypoxia driven angiogenesis did not occur. In summary these data demonstrate that myocardial oxygenation is adequate and can support myocardial contractile function over a range of workloads and in conditions of 'reduced' oxygen availability. These data may contrast with reports in the mouse which suggest that a failure of angiogenesis to keep pace with myocardial expansion results in poor contractile performance [90, 91]. However Flanagan *et al* (1991) found that inhibition of myocardial angiogenesis with protamine in young aortic banded lambs reduced maximal LV CF but did not impair contractile performance, lending support to the findings of the present study [97]. Additionally there is no direct evidence that the failing heart is hypoxic, even at high workloads [95, 273], and it may be that the phenotypic changes associated with HF are unrelated to a lack of oxygen availability or a failure of angiogenesis to normalise oxygen delivery.

It has to been accepted that a number of the models used in the present study failed to achieve their aims of increasing (CA, atenolol, CAA) or decreasing (L-NAME and CAL) CD in the LV. This may provide evidence that capillary growth in the adult heart is somewhat limited. The death of a large

number of animals early in this project has led to restrictions on the treatment regimens that would be permitted and has somewhat limited the scope of the work. As such completion of the isoprenaline study to look at LV substrate metabolism was not possible. Additionally the use of previously described models for inducing changes in ventricular CD (alinidine (requiring injection) or electrical pacing) was unavailable (see future experiments).

Methodological considerations

SERCA activity

While normal expression levels of SERCA2a protein were demonstrated in the present study it cannot be ruled out that changes in the activity or expression of other calcium handling proteins could allow for greater calcium ion transients and augmented contractile performance. Given that phospholamban is an allosteric regulator of SERCA activity ratios of unphosphorylated and phosphorylated expression could be used in future studies to present a clearer picture of SR calcium handling in treated hearts. Fluorescent imaging techniques in the whole heart and in isolated myocytes offer an opportunity to quantify differences in the calcium transients between treatment groups.

Capillary Length

Oxygen diffusion to the tissues occurs along the length of the capillary bed and as such our methods may have failed to assess the impact of altered myocyte fibre length on oxygen delivery. Stereological modeling using a combination of longitudinal and transverse sectioning could be used to accurately account for this variable although given the nature of the lectin stain (i.e. staining both the myocyte sarcolemma and capillaries) this would require utilisation of another capillary staining method (e.g. an antibody specific marker such as CD31).

Statistical power

Several near significant trends were noted throughout this thesis which is likely the consequence of the low sample sizes in a number of experimental groups. It is probable that there was insufficient statistical power in these experiments to detect relevant trends. In future studies it would be prudent to carry out power calculations during the experimental planning stage which would set the lower limit on animal numbers required demonstrate any relevant trends within a dataset.

Future work

Alternative models for capillary growth in the rat

Chronic treatment with the I_f current blocker alinidine provides an alternative means for the induction chronic bradycardia, one which was unavailable in the present study due to the need to inject this agent. Alinidine has advantages over beta-blockers in that it does not have directly negative inotropic influences on the myocardium and induces a greater increase in capillary number than that seen during adrenergic blockade[237]. Recent advances have led to the development of ivabradine which can be incorporated into rodent chow avoiding the need for daily injections, though this agent is currently commercially unavailable [234]. Electrical pacing could also provide a means to induce myocardial angiogenesis though the procedure is invasive and has to date only been performed on larger animal species (i.e. rabbits and pigs [85, 86]).

Previous investigators have reported how alinidine induced angiogenesis in the rat could be prevented through the supplementation of these animals with VEGF blocking antibodies [237]. Such a method could be used to investigate whether changes in performance resulting from chronic bradycardia are a result of coronary angiogenesis or by alterations in ventricular compliance as suggested in the present study. Alternatively as short term isoprenaline induced hypertrophy, which did not impair contractile function, could be used to expand the cross-sectional area of myocytes (i.e. reduced CD) in alinidine treated hearts allowing comparison of the functional and metabolic characteristics of these groups.

Alternative models of hypertrophy in the rat

Spontaneously hypertensive rats present an opportunity to study the interaction between capillary growth, contractile performance and substrate utilisation in models with a well described timeline of progression from well compensated hypertrophy to HF. By utilising animals of different ages it may be possible to assess whether a failure of angiogenesis plays a role in this progression, as previously described in the mouse [90, 91]. In addition methods to induce capillary growth (i.e. bradycardia) or block any naturally occurring capillary development (e.g. VEGF blocking antibodies) could be used to modify this developmental timeline. It may therefore be possible to deduce whether a failure of angiogenesis can drive changes in substrate metabolism and whether this can be related to a change in oxygen diffusion distances/availability.

References

1. Opie, L.H., *Heart physiology. From cell to circulation.* Fourth ed. 2003: Lippincott, Williams and Wilkins. 640.
2. Katz, A.M., *Physiology of the heart.* . Fourth ed. 2005: Lippincott, Williams and Wilkins.
3. Braunwald, E., *Heart Disease. A textbook of cardiovascular medicine.* Third ed. 1988.
4. Bers, D.M., *Cardiac excitation-contraction coupling.* Nature, 2002. **415**(6868): p. 198-205.
5. Bers, D., *Excitation-Contraction Coupling and Cardiac Contractile Force*. 2 ed. 2001: Kluwer Academic Publishers. 427.
6. Brittsan, A.G. and E.G. Kranias, *Phospholamban and Cardiac Contractile Function.* J Mol Cell Cardiol, 2000. **32**(12): p. 2131-2139.
7. Sarnoff, S.J., E. Braunwald, G.H. Welch, Jr., R.B. Case, W.N. Stainsby, and R. Macruz, *Hemodynamic determinants of oxygen consumption of the heart with special reference to the tension-time index.* Am J Physiol, 1958. **192**(1): p. 148-56.
8. Neely, J.R., H. Liebermeister, E.J. Battersby, and H.E. Morgan, *Effect of pressure development on oxygen consumption by isolated rat heart.* Am J Physiol, 1967. **212**(4): p. 804-814.
9. Vasu, M.A., D.D. O'Keefe, G.Z. Kapellakis, M.P. Vezeridis, M.L. Jacobs, W.M. Daggett, and W.J. Powell, Jr., *Myocardial oxygen consumption: effects of epinephrine, isoproterenol, dopamine, norepinephrine, and dobutamine.* Am J Physiol, 1978. **235**(2): p. H237-41.
10. Feinberg, H. and L.N. Katz, *Effect of catecholamines, l-epinephrine and l-norepinephrine on coronary flow and oxygen metabolism of the myocardium.* Am J Physiol, 1958. **193**(1): p. 151-6.
11. Wiedmeier, V.T. and L.H. Spell, *Effects of catecholamines, histamine, and nitroglycerin on flow, oxygen utilization, and adenosine production in the perfused guinea pig heart.* Circ Res, 1977. **41**(4): p. 503-8.
12. Beauloye, C., A.S. Marsin, L. Bertrand, J.L. Vanoverschelde, M.H. Rider, and L. Hue, *The stimulation of heart glycolysis by increased workload does not require AMP-activated protein kinase but a wortmannin-sensitive mechanism.* FEBS Lett, 2002. **531**(2): p. 324-8.
13. Doenst, T. and H. Taegtmeyer, *{alpha}-Adrenergic Stimulation Mediates Glucose Uptake Through Phosphatidylinositol 3-Kinase in Rat Heart.* Circ Res, 1999. **84**(4): p. 467-474.
14. Egert, S., N. Nguyen, and M. Schwaiger, *Contribution of {alpha}-Adrenergic and ß-Adrenergic Stimulation to Ischemia-Induced Glucose Transporter (GLUT) 4 and GLUT1 Translocation in the Isolated Perfused Rat Heart.* Circ Res, 1999. **84**(12): p. 1407-1415.
15. Stanley, W.C., F.A. Recchia, and G.D. Lopaschuk, *Myocardial Substrate Metabolism in the Normal and Failing Heart.* Physiol Rev, 2005. **85**(3): p. 1093-1129.
16. Luiken, J.J.F.P., S.L.M. Coort, J. Willems, W.A. Coumans, A. Bonen, G.J. van der Vusse, and J.F.C. Glatz, *Contraction-Induced Fatty Acid Translocase/CD36 Translocation in Rat Cardiac Myocytes Is Mediated Through AMP-Activated Protein Kinase Signaling.* Diabetes, 2003. **52**(7): p. 1627-1634.
17. Kuang, M., M. Febbraio, C. Wagg, G.D. Lopaschuk, and J.R.B. Dyck, *Fatty Acid Translocase/CD36 Deficiency Does Not Energetically or Functionally Compromise Hearts Before or After Ischemia.* Circulation, 2004. **109**(12): p. 1550-1557.
18. Opie, L.H., K.R. Mansford, and P. Owen, *Effects of increased heart work on glycolysis and adenine nucleotides in the perfused heart of normal and diabetic rats.* Biochem J, 1971. **124**(3): p. 475-90.
19. Depre, C., M.H. Rider, K. Veitch, and L. Hue, *Role of fructose 2,6-bisphosphate in the control of heart glycolysis.* J Biol Chem, 1993. **268**(18): p. 13274-9.
20. Garland, P.B., P.J. Randle, and E.A. Newsholme, *Citrate as an Intermediary in the Inhibition of Phosphofructokinase in Rat Heart Muscle by Fatty Acids, Ketone Bodies, Pyruvate, Diabetes and Starvation.* Nature, 1963. **200**(4902): p. 169-170.

21. Philip, J.R., *Regulatory interactions between lipids and carbohydrates: the glucose fatty acid cycle after 35 years.* Diabetes Metab Rev, 1998. **14**(4): p. 263-283.
22. Kübler, W. and P.G. Spieckermann, *Regulation of glycolysis in the ischemic and the anoxic myocardium.* J Mol Cell Cardiol, 1970. **1**(4): p. 351-377.
23. Goodwin, G.W. and H. Taegtmeyer, *Regulation of fatty acid oxidation of the heart by MCD and ACC during contractile stimulation.* Am J Physiol Endocrinol Metab, 1999. **277**(4): p. E772-777.
24. Collins-Nakai, R.L., D. Noseworthy, and G.D. Lopaschuk, *Epinephrine increases ATP production in hearts by preferentially increasing glucose metabolism.* Am J Physiol Heart Circ Physiol, 1994. **267**(5): p. H1862-1871.
25. Hinkle, P.C., M.A. Kumar, A. Resetar, and D.L. Harris, *Mechanistic stoichiometry of mitochondrial oxidative phosphorylation.* Biochemistry, 1991. **30**(14): p. 3576-3582.
26. Neely, J.R., M. Whitmer, and S. Mochizuki, *Effects of mechanical activity and hormones on myocardial glucose and fatty acid utilization.* Circ Res, 1976. **38**(5 Suppl 1): p. I22-30.
27. Neely, JR, R. Bowman, and H. Morgan, *Effects of ventricular pressure development and palmitate on glucose transport.* Am J Physiol, 1969. **216**(4): p. 804-811.
28. Meyer, R.A., H.L. Sweeney, and M.J. Kushmerick, *A simple analysis of the "phosphocreatine shuttle".* Am J Physiol Cell Physiol, 1984. **246**(5): p. C365-377.
29. Dzeja, P.P. and A. Terzic, *Phosphotransfer networks and cellular energetics.* J Exp Biol, 2003. **206**(12): p. 2039-2047.
30. Henning, S.L., R.B. Wambolt, B.O. Schonekess, G.D. Lopaschuk, and M.F. Allard, *Contribution of Glycogen to Aerobic Myocardial Glucose Utilization*. 1996. p. 1549-1555.
31. Goldfarb, A.H., J.F. Bruno, and P.J. Buckenmeyer, *Intensity and duration effects of exercise on heart cAMP, phosphorylase, and glycogen*. 1986. p. 1268-1273.
32. Saddik, M. and G.D. Lopaschuk, *Myocardial triglyceride turnover and contribution to energy substrate utilization in isolated working rat hearts.* J Biol Chem, 1991. **266**(13): p. 8162-8170.
33. Lewin, T.M. and R.A. Coleman, *Regulation of myocardial triacylglycerol synthesis and metabolism.* Biochimica et Biophysica Acta (BBA) - Molecular and Cell Biology of Lipids, 2003. **1634**(3): p. 63-75.
34. Stam, H. and W.C. Hasslemann, *Regulation of lipases involved in the supply of substrate fatty acids for the heart.* European Heart Journal, 1985. **6**(2): p. 158-167.
35. Severson, D.L. and B. Hurley, *Regulation of rat heart triacylglycerol ester hydrolases by free fatty acids, fatty acyl CoA and fatty acyl carnitine.* J Mol Cell Cardiol, 1982. **14**(8): p. 467-474.
36. McDonough, K.H. and J.R. Neely, *Inhibition of myocardial lipase by palmityl CoA.* J Mol Cell Cardiol, 1988. **20**(Supplement 2): p. 31-39.
37. Grossman, W., D. Jones, and L.P. McLaurin, *Wall stress and patterns of hypertrophy in the human left ventricle.* The Journal of Clinical Investigation, 1975. **56**(1): p. 56-64.
38. Allard, M.F., B.O. Schonekess, S.L. Henning, D.R. English, and G.D. Lopaschuk, *Contribution of oxidative metabolism and glycolysis to ATP production in hypertrophied hearts.* Am J Physiol Heart Circ Physiol, 1994. **267**(2): p. H742-750.
39. Allard, M.F., R.B. Wambolt, S.L. Longnus, M. Grist, C.P. Lydell, H.L. Parsons, B. Rodrigues, J.L. Hall, W.C. Stanley, and G.P. Bondy, *Hypertrophied rat hearts are less responsive to the metabolic and functional effects of insulin.* Am J Physiol Endocrinol Metab, 2000. **279**(3): p. E487-493.
40. Doenst, T., G.W. Goodwin, A.M. Cedars, M. Wang, S. Stepkowski, and H. Taegtmeyer, *Load-induced changes in vivo alter substrate fluxes and insulin responsiveness of rat heart in vitro.* Metabolism, 2001. **50**(9): p. 1083-1090.
41. Alexander, N., T. Goldfarb, D.R. Drury, and D. With the Technical Assistance of Marjorie, *Cardiac Performance of Hypertensive Aorta-Constricted Rabbits.* Circ Res, 1962. **10**(1): p. 11-16.

42. el Alaoui-Talibi, Z., S. Landormy, A. Loireau, and J. Moravec, *Fatty acid oxidation and mechanical performance of volume-overloaded rat hearts.* Am J Physiol Heart Circ Physiol, 1992. **262**(4): p. H1068-1074.
43. Batra, S. and K. Rakusan, *Geometry of capillary networks in volume overloaded rat heart.* Microvasc Res, 1991. **42**(1): p. 39-50.
44. de la Bastie, D., D. Levitsky, L. Rappaport, J.J. Mercadier, F. Marotte, C. Wisnewsky, V. Brovkovich, K. Schwartz, and A.M. Lompre, *Function of the sarcoplasmic reticulum and expression of its Ca2(+)-ATPase gene in pressure overload-induced cardiac hypertrophy in the rat.* Circ Res, 1990. **66**(2): p. 554-64.
45. Meyer, M., W. Schillinger, B. Pieske, C. Holubarsch, C. Heilmann, H. Posival, G. Kuwajima, K. Mikoshiba, H. Just, and G. Hasenfuss, *Alterations of Sarcoplasmic Reticulum Proteins in Failing Human Dilated Cardiomyopathy.* Circulation, 1995. **92**(4): p. 778-784.
46. Hasenfuss, G., H. Reinecke, R. Studer, M. Meyer, B. Pieske, J. Holtz, C. Holubarsch, H. Posival, H. Just, and H. Drexler, *Relation between myocardial function and expression of sarcoplasmic reticulum Ca(2+)-ATPase in failing and nonfailing human myocardium.* Circ Res, 1994. **75**(3): p. 434-442.
47. Schwinger, R.H.G., M. Bohm, U. Schmidt, P. Karczewski, U. Bavendiek, M. Flesch, E.-G. Krause, and E. Erdmann, *Unchanged Protein Levels of SERCA II and Phospholamban but Reduced Ca2+ Uptake and Ca2+-ATPase Activity of Cardiac Sarcoplasmic Reticulum From Dilated Cardiomyopathy Patients Compared With Patients With Nonfailing Hearts.* Circulation, 1995. **92**(11): p. 3220-3228.
48. Limas, C.J., M.-T. Olivari, I.F. Goldenberg, T.B. Levine, D.G. Benditt, and A. Simon, *Calcium uptake by cardiac sarcoplasmic reticulum in human dilated cardiomyopathy.* Cardiovasc Res, 1987. **21**(8): p. 601-605.
49. Schwinger, R.H.G., G. Münch, B. Bölck, P. Karczewski, E.-G. Krause, and E. Erdmann, *Reduced Ca2+-Sensitivity of SERCA 2a in Failing Human Myocardium due to Reduced Serin-16 Phospholamban Phoshorylation.* J Mol Cell Cardiol, 1999. **31**(3): p. 479-491.
50. Miyamoto, M.I., F. del Monte, U. Schmidt, T.S. DiSalvo, Z.B. Kang, T. Matsui, J.L. Guerrero, J.K. Gwathmey, A. Rosenzweig, and R.J. Hajjar, *Adenoviral gene transfer of SERCA2a improves left-ventricular function in aortic-banded rats in transition to heart failure.* Proceedings of the National Academy of Sciences of the United States of America, 2000. **97**(2): p. 793-798.
51. Studer, R., H. Reinecke, J. Bilger, T. Eschenhagen, M. Bohm, G. Hasenfuss, H. Just, J. Holtz, and H. Drexler, *Gene expression of the cardiac Na(+)-Ca2+ exchanger in end-stage human heart failure.* Circ Res, 1994. **75**(3): p. 443-453.
52. Flesch, M., R.H.G. Schwinger, F. Schiffer, K. Frank, M. Sudkamp, F. Kuhn-Regnier, G. Arnold, and M. Bohm, *Evidence for Functional Relevance of an Enhanced Expression of the Na+-Ca2+ Exchanger in Failing Human Myocardium.* Circulation, 1996. **94**(5): p. 992-1002.
53. Reinecke, H., R. Studer, R. Vetter, J.r. Holtz, and H. Drexler, *Cardiac Na+/Ca2+ exchange activity in patients with end-stage heart failure.* Cardiovasc Res, 1996. **31**(1): p. 48-54.
54. Starling, R.C., D.F. Hammer, and R.A. Altschuld, *Human myocardial ATP content and in vivo contractile function.* Mol Cell Biochem, 1998. **180**(1-2): p. 171-7.
55. Beer, M., T. Seyfarth, J.o. Sandstede, W. Landschutz, C. Lipke, H. Kostler, M. von Kienlin, K. Harre, D. Hahn, and S. Neubauer, *Absolute concentrations of high-energy phosphate metabolites in normal, hypertrophied, and failing human myocardium measured noninvasively with 31P-SLOOP magnetic resonance spectroscopy.* J Am Coll Cardiol, 2002. **40**(7): p. 1267-1274.
56. Shen, W., K. Asai, M. Uechi, M.A. Mathier, R.P. Shannon, S.F. Vatner, and J.S. Ingwall, *Progressive Loss of Myocardial ATP Due to a Loss of Total Purines During the Development of Heart Failure in Dogs : A Compensatory Role for the Parallel Loss of Creatine.* Circulation, 1999. **100**(20): p. 2113-2118.

57. Ingwall, J.S., M.F. Kramer, M.A. Fifer, B.H. Lorell, R. Shemin, W. Grossman, and P.D. Allen, *The creatine kinase system in normal and diseased human myocardium.* N Engl J Med, 1985. **313**(17): p. 1050-4.
58. Arnold, M.K., *Is the failing heart energy depleted?* Cardiology clinics, 1998. **16**(4): p. 633-644.
59. Nakae, I., K. Mitsunami, T. Omura, T. Yabe, T. Tsutamoto, S. Matsuo, M. Takahashi, S. Morikawa, T. Inubushi, Y. Nakamura, M. Kinoshita, and M. Horie, *Proton magnetic resonance spectroscopy can detect creatine depletion associated with the progression of heart failure in cardiomyopathy.* J Am Coll Cardiol, 2003. **42**(9): p. 1587-1593.
60. Conway, M.A., J. Allis, R. Ouwerkerk, T. Niioka, B. Rajagopalan, and G.K. Radda, *Detection of low phosphocreatine to ATP ratio in failing hypertrophied human myocardium by 31P magnetic resonance spectroscopy.* Lancet, 1991. **338**(8773): p. 973-6.
61. de Roos, A., J. Doornbos, P.R. Luyten, L.J. Oosterwaal, E.E. van der Wall, and J.A. den Hollander, *Cardiac metabolism in patients with dilated and hypertrophic cardiomyopathy: assessment with proton-decoupled P-31 MR spectroscopy.* J Magn Reson Imaging, 1992. **2**(6): p. 711-9.
62. Ingwall, J.S. and R.G. Weiss, *Is the Failing Heart Energy Starved?: On Using Chemical Energy to Support Cardiac Function.* Circ Res, 2004. **95**(2): p. 135-145.
63. Chandler, M.P., J. Kerner, H. Huang, E. Vazquez, A. Reszko, W.Z. Martini, C.L. Hoppel, M. Imai, S. Rastogi, H.N. Sabbah, and W.C. Stanley, *Moderate severity heart failure does not involve a downregulation of myocardial fatty acid oxidation.* Am J Physiol Heart Circ Physiol, 2004. **287**(4): p. H1538-43.
64. Recchia, F.A., P.I. McConnell, R.D. Bernstein, T.R. Vogel, X. Xu, and T.H. Hintze, *Reduced Nitric Oxide Production and Altered Myocardial Metabolism During the Decompensation of Pacing-Induced Heart Failure in the Conscious Dog.* Circ Res, 1998. **83**(10): p. 969-979.
65. Christe, M.E. and R.L. Rodgers, *Altered Glucose and Fatty Acid Oxidation in Hearts of the Spontaneously Hypertensive Rat.* J Mol Cell Cardiol, 1994. **26**(10): p. 1371-1375.
66. Lei, B., V. Lionetti, M.E. Young, M.P. Chandler, C. d' Agostino, E. Kang, M. Altarejos, K. Matsuo, T.H. Hintze, W.C. Stanley, and F.A. Recchia, *Paradoxical downregulation of the glucose oxidation pathway despite enhanced flux in severe heart failure.* J Mol Cell Cardiol, 2004. **36**(4): p. 567-576.
67. Leong, H.S., M. Grist, H. Parsons, R.B. Wambolt, G.D. Lopaschuk, R. Brownsey, and M.F. Allard, *Accelerated rates of glycolysis in the hypertrophied heart: are they a methodological artifact?* Am J Physiol Endocrinol Metab, 2002. **282**(5): p. E1039-1045.
68. Taylor, M., T.R. Wallhaus, T.R. DeGrado, D.C. Russell, P. Stanko, R.J. Nickles, and C.K. Stone, *An Evaluation of Myocardial Fatty Acid and Glucose Uptake Using PET with [18F]Fluoro-6-Thia-Heptadecanoic Acid and [18F]FDG in Patients with Congestive Heart Failure.* J Nucl Med, 2001. **42**(1): p. 55-62.
69. Davila-Roman, V.i.G., G. Vedala, P. Herrero, L. de las Fuentes, J.G. Rogers, D.P. Kelly, and R.J. Gropler, *Altered myocardial fatty acid and glucose metabolism in idiopathic dilated cardiomyopathy.* J Am Coll Cardiol, 2002. **40**(2): p. 271-277.
70. Taegtmeyer, H. and M.L. Overturf, *Effects of moderate hypertension on cardiac function and metabolism in the rabbit.* Hypertension, 1988. **11**(5): p. 416-26.
71. Razeghi, P., M.E. Young, J.L. Alcorn, C.S. Moravec, O.H. Frazier, and H. Taegtmeyer, *Metabolic Gene Expression in Fetal and Failing Human Heart.* Circulation, 2001. **104**(24): p. 2923-2931.
72. Sack, M.N., T.A. Rader, S. Park, J. Bastin, S.A. McCune, and D.P. Kelly, *Fatty Acid Oxidation Enzyme Gene Expression Is Downregulated in the Failing Heart.* Circulation, 1996. **94**(11): p. 2837-2842.
73. Osorio, J.C., W.C. Stanley, A. Linke, M. Castellari, Q.N. Diep, A.R. Panchal, T.H. Hintze, G.D. Lopaschuk, and F.A. Recchia, *Impaired Myocardial Fatty Acid Oxidation and Reduced Protein*

Expression of Retinoid X Receptor-{alpha} in Pacing-Induced Heart Failure. Circulation, 2002. **106**(5): p. 606-612.
74. Laughlin, M.H. and R.M. McAllister, *Exercise training-induced coronary vascular adaptation.* J Appl Physiol, 1992. **73**(6): p. 2209-25.
75. Hudlicka, O., M. Brown, and S. Egginton, *Angiogenesis in skeletal and cardiac muscle*. Phys Rev, 1992. 72(2):p. 369-417.
76. Robert, J.T., *Effects of age and exercise on the extent of the myocardial capillary bed.* The Anatomical Record, 1970. **167**(1): p. 55-62.
77. Tomanek, R.J., *Exercise-induced coronary angiogenesis: a review.* Med Sci Sports Exerc, 1994. **26**(10): p. 1245-51.
78. Mandache, E., G. Unge, L.E. Appelgren, and A. Ljungqvist, *The proliferative activity of the heart tissues in various forms of experimental cardiac hypertrophy studied by electron microscope autoradiography.* Virchows Archiv B Cell Pathology Zell-pathologie, 1972. **12**(1): p. 112-122.
79. Choi, Y.H., D.B. Cowan, M. Nathan, D. Poutias, C. Stamm, P.J. del Nido, and F.X. McGowan, Jr., *Myocardial hypertrophy overrides the angiogenic response to hypoxia.* PLoS ONE, 2008. **3**(12): p. e4042.
80. Koyama, T., Z. Xie, M. Gao, J. Suzuki, and S. Batra, *Adaptive changes in the capillary network in the left ventricle of rat heart.* The Japanese journal of physiology, 1998. **48**(4): p. 229-41.
81. Ziada, A.M., O. Hudlicka, K.R. Tyler, and A.J. Wright, *The effect of long-term vasodilatation on capillary growth and performance in rabbit heart and skeletal muscle.* Cardiovasc Res, 1984. **18**(12): p. 724-32.
82. Tornling, G., *Capillary neoformation in the heart of dipyridamole-treated rats.* Acta Pathol Microbiol Immunol Scand A, 1982. **90**(4): p. 269-71.
83. Tornling, G., *Capillary neoformation in the heart and skeletal muscle during dipyridamole--treatment and exercise.* Acta Pathol Microbiol Immunol Scand Suppl, 1982. **278**: p. 1-63.
84. Zhou, A., S. Egginton, O. Hudlicka, and M.D. Brown, *Internal division of capillaries in rat skeletal muscle in response to chronic vasodilator treatment with alpha1-antagonist prazosin.* Cell Tissue Res, 1998. **293**(2): p. 293-303.
85. Wright, A. and O. Hudlicka, *Capillary growth and changes in heart performance induced by chronic bradycardial pacing in the rabbit.* Circ Res, 1981. **49**(2): p. 469-478.
86. Brown, M.D., M.K. Davies, and O. Hudlicka, *The effect of long-term bradycardia on heart microvascular supply and performance.* Cell Mol Biol Res, 1994. **40**(2): p. 137-42.
87. Brown, M.D., M.J. Cleasby, and O. Hudlicka, *Capillary Supply of Hypertrophied Rat Hearts after Chronic Treatment with the Bradycardic Agent Alinidine.* Journal of Physiology-London, 1990. **427**: p. P40-P40.
88. Zhou, A.L., S. Egginton, M.D. Brown, and O. Hudlicka, *Capillary growth in overloaded, hypertrophic adult rat skeletal muscle: an ultrastructural study.* Anat Rec, 1998. **252**(1): p. 49-63.
89. Lei, L., R. Zhou, W. Zheng, L.P. Christensen, R.M. Weiss, and R.J. Tomanek, *Bradycardia Induces Angiogenesis, Increases Coronary Reserve, and Preserves Function of the Postinfarcted Heart.* Circulation, 2004. **110**(7): p. 796-802.
90. Shiojima, I., K. Sato, Y. Izumiya, S. Schiekofer, M. Ito, R. Liao, W.S. Colucci, and K. Walsh, *Disruption of coordinated cardiac hypertrophy and angiogenesis contributes to the transition to heart failure.* The Journal of Clinical Investigation, 2005. **115**(8): p. 2108-2118.
91. Sano, M., T. Minamino, H. Toko, H. Miyauchi, M. Orimo, Y. Qin, H. Akazawa, K. Tateno, Y. Kayama, M. Harada, I. Shimizu, T. Asahara, H. Hamada, S. Tomita, J.D. Molkentin, Y. Zou, and I. Komuro, *p53-induced inhibition of Hif-1 causes cardiac dysfunction during pressure overload.* Nature, 2007. **446**(7134): p. 444-448.
92. Jaakkola, P., D.R. Mole, Y.-M. Tian, M.I. Wilson, J. Gielbert, S.J. Gaskell, A.v. Kriegsheim, H.F. Hebestreit, M. Mukherji, C.J. Schofield, P.H. Maxwell, C.W. Pugh, and P.J. Ratcliffe, *Targeting*

of HIF-alpha to the von Hippel-Lindau Ubiquitylation Complex by O2-Regulated Prolyl Hydroxylation. Science, 2001. **292**(5516): p. 468-472.
93. Ivan, M., K. Kondo, H. Yang, W. Kim, J. Valiando, M. Ohh, A. Salic, J.M. Asara, W.S. Lane, and W.G. Kaelin, Jr., *HIFalpha Targeted for VHL-Mediated Destruction by Proline Hydroxylation: Implications for O_2 Sensing.* Science, 2001. **292**(5516): p. 464-468.
94. Chun, Y.S., M.S. Kim, and J.W. Park, *Oxygen-dependent and -independent regulation of HIF-1alpha.* J Korean Med Sci, 2002. **17**(5): p. 581-8.
95. Bache, R.J., J. Zhang, Y. Murakami, Y. Zhang, Y.K. Cho, H. Merkle, G. Gong, A.H.L. From, and K. Ugurbil, *Myocardial oxygenation at high workstates in hearts with left ventricular hypertrophy.* Cardiovasc Res, 1999. **42**(3): p. 616-626.
96. Rakusan, K., L. Hoofd, and Z. Turek, *The effect of cell size and capillary spacing on myocardial oxygen supply.* Adv Exp Med Biol, 1984. **180**: p. 463-75.
97. Flanagan, M., A. Fujii, S. Colan, R. Flanagan, and J. Lock, *Myocardial angiogenesis and coronary perfusion in left ventricular pressure-overload hypertrophy in the young lamb. Evidence for inhibition with chronic protamine administration.* Circ Res, 1991. **68**(5): p. 1458-1470.
98. Kim, C.-H., Y.-S. Cho, Y.-S. Chun, J.-W. Park, and M.-S. Kim, *Early Expression of Myocardial HIF-1{alpha} in Response to Mechanical Stresses: Regulation by Stretch-Activated Channels and the Phosphatidylinositol 3-Kinase Signaling Pathway.* Circ Res, 2002. **90**(2): p. e25-33.
99. Bachmanov, A.A., D.R. Reed, G.K. Beauchamp, and M.G. Tordoff, *Food intake, water intake, and drinking spout side preference of 28 mouse strains.* Behav Genet, 2002. **32**(6): p. 435-43.
100. Kristal, M.B. and R.S. Wampler, *Food and water intake prior to parturition in the rat*. Phys Psy. 1973, 1(3) p. 297-300.
101. Woodiwiss, A.J., O.J. Tsotetsi, S. Sprott, E.J. Lancaster, T. Mela, E.S. Chung, T.E. Meyer, and G.R. Norton, *Reduction in Myocardial Collagen Cross-Linking Parallels Left Ventricular Dilatation in Rat Models of Systolic Chamber Dysfunction.* Circulation, 2001. **103**(1): p. 155-160.
102. Nahrendorf, M., F. Wiesmann, K.-H. Hiller, K. Hu, C. Waller, J. Ruff, T.E. Lanz, S. Neubauer, A. Haase, G. Ertl, and W.R. Bauer, *Serial cine-magnetic resonance imaging of left ventricular remodeling after myocardial infarction in rats.* J Magn Reson Imaging, 2001. **14**(5): p. 547-555.
103. Weber, K., J. Janicki, S. Shroff, R. Pick, R. Chen, and R. Bashey, *Collagen remodeling of the pressure-overloaded, hypertrophied nonhuman primate myocardium.* Circ Res, 1988. **62**(4): p. 757-765.
104. Taegtmeyer, H., R. Hems, and H.A. Krebs, *Utilization Of Energy-Providing Substrates In The Isolated Working Rat-Heart.* Biochemical Journal, 1980. **186**(3): p. 701-711.
105. Goodwin, G.W., C.S. Taylor, and H. Taegtmeyer, *Regulation of energy metabolism of the heart during acute increase in heart work.* J Biol Chem, 1998. **273**(45): p. 29530-9.
106. Kobayashi, K. and J. Neely, *Control of maximum rates of glycolysis in rat cardiac muscle.* Circ Res, 1979. **44**(2): p. 166-175.
107. Bennett, M.J., D. Hauton, D.G. Hole, and R.D. Evans, *Preparation of radiolabelled very-low-density lipoprotein in high yield by extended rat liver perfusion.* Biotechnology Letters, 2000. **22**(4): p. 301-306.
108. Neely, J.R., R.M. Denton, P.J. England, and P.J. Randle, *The effects of increased heart work on the tricarboxylate cycle and its interactions with glycolysis in the perfused rat heart.* Biochem J, 1972. **128**(1): p. 147-59.
109. Liu, Y.-H., J. Xu, X.-P. Yang, F. Yang, E. Shesely, and O.A. Carretero, *Effect of ACE Inhibitors and Angiotensin II Type 1 Receptor Antagonists on Endothelial NO Synthase Knockout Mice With Heart Failure.* Hypertension, 2002. **39**(2): p. 375-381.
110. Gundersen, H.J.G., *Notes on estimation of numerical density of arbitrary profiles - edge effect.* J Microsc-Oxf, 1977. **111**(NOV): p. 219-223.

111. Katz, L.N. and H. Feinberg, *The relation of cardiac effort to myocardial oxygen consumption and coronary flow.* Circ Res, 1958. **6**(5): p. 656-69.
112. Camici, P.G. and F. Crea, *Coronary microvascular dysfunction.* N Engl J Med, 2007. **356**(8): p. 830-40.
113. Chilian, W.M., *Coronary microcirculation in health and disease. Summary of an NHLBI workshop.* Circulation, 1997. **95**(2): p. 522-8.
114. Lim, H.E., W.J. Shim, H. Rhee, S.M. Kim, G.S. Hwang, Y.H. Kim, H.S. Seo, D.J. Oh, and Y.M. Ro, *Assessment of coronary flow reserve with transthoracic Doppler echocardiography: comparison among adenosine, standard-dose dipyridamole, and high-dose dipyridamole.* J Am Soc Echocardiogr, 2000. **13**(4): p. 264-70.
115. Davis, C.P., P.F. Liu, M. Hauser, S.C. Gohde, G.K. von Schulthess, and J.F. Debatin, *Coronary flow and coronary flow reserve measurements in humans with breath-held magnetic resonance phase contrast velocity mapping.* Magn Reson Med, 1997. **37**(4): p. 537-44.
116. Mouren, S.p., E. Vicaut, L. Lamhaut, B. Riou, and A. Ouattara, *Crystalloid versus red blood cell-containing medium in the Langendorff-perfused isolated heart preparation.* Eur J of Anaesthesiol. **27**(9): p. 780-787.
117. Matsumoto, T., H. Tachibana, T. Asano, M. Takemoto, Y. Ogasawara, K. Umetani, and F. Kajiya, *Pattern differences between distributions of microregional myocardial flows in crystalloid- and blood-perfused rat hearts.* Am J Physiol Heart Circ Physiol, 2004. **286**(4): p. H1331-1338.
118. Alessia, G., S.-E. Jan, N. Danilo, S. Gianmario, G. Assuero, B. Giovanni, P. Guido, P. Roberto, and P. Oberdan, *Homogeneously Reduced Versus Regionally Impaired Myocardial Blood Flow in Hypertensive Patients: Two Different Patterns of Myocardial Perfusion Associated With Degree of Hypertrophy.* JACC, 1998. **31**(2): p. 366-373.
119. Brilla, C.G., J.S. Janicki, and K.T. Weber, *Impaired diastolic function and coronary reserve in genetic hypertension. Role of interstitial fibrosis and medial thickening of intramyocardial coronary arteries.* Circ Res, 1991. **69**(1): p. 107-15.
120. Numaguchi, K., K. Egashira, M. Takemoto, T. Kadokami, H. Shimokawa, K. Sueishi, and A. Takeshita, *Chronic Inhibition of Nitric Oxide Synthesis Causes Coronary Microvascular Remodeling in Rats.* Hypertension, 1995. **26**(6): p. 957-962.
121. Marcus, M.L., D.G. Harrison, W.M. Chilian, S. Koyanagi, T. Inou, R.J. Tomanek, J.B. Martins, C.L. Eastham, and L.F. Hiratzka, *Alterations in the coronary circulation in hypertrophied ventricles.* Circulation, 1987. **75**(1 Pt 2): p. I19-25.
122. Kalkman, E.A., Y.M. Bilgin, P. van Haren, R.J. van Suylen, P.R. Saxena, and R.G. Schoemaker, *Determinants of coronary reserve in rats subjected to coronary artery ligation or aortic banding.* Cardiovasc Res, 1996. **32**(6): p. 1088-95.
123. Cecchi, F., A. Sgalambro, M. Baldi, B. Sotgia, D. Antoniucci, P. Camici, R. Sciagrà, and I. Olivotto, *Microvascular Dysfunction, Myocardial Ischemia, and Progression to Heart Failure in Patients with Hypertrophic Cardiomyopathy.* J Cardiovasc Transl Res, 2009. **2**(4): p. 452-461.
124. Cross, H.R., L.H. Opie, G.K. Radda, and K. Clarke, *Is a High Glycogen Content Beneficial or Detrimental to the Ischemic Rat Heart? : A Controversy Resolved.* Circ Res, 1996. **78**(3): p. 482-491.
125. Fraser, H., G.D. Lopaschuk, and A.S. Clanachan, *Assessment of glycogen turnover in aerobic, ischemic, and reperfused working rat hearts.* Am J Physiol Heart Circ Physiol, 1998. **275**(5): p. H1533-1541.
126. Whitmer, J.T., J.A. Idell-Wenger, M.J. Rovetto, and J.R. Neely, *Control of fatty acid metabolism in ischemic and hypoxic hearts.* J Biol Chem, 1978. **253**(12): p. 4305-4309.
127. Hudlická, O., M.D. Brown, H. Walter, J.B. Weiss, and A. Bate, *Factors involved in capillary growth in the heart.* Mol Cell Biochem, 1995. **147**(1): p. 57-68.

128. Russell, R.R., III, R. Bergeron, G.I. Shulman, and L.H. Young, *Translocation of myocardial GLUT-4 and increased glucose uptake through activation of AMPK by AICAR.* Am J Physiol Heart Circ Physiol, 1999. **277**(2): p. H643-649.
129. Marsin, A.S., L. Bertrand, M.H. Rider, J. Deprez, C. Beauloye, M.F. Vincent, G. Van den Berghe, D. Carling, and L. Hue, *Phosphorylation and activation of heart PFK-2 by AMPK has a role in the stimulation of glycolysis during ischaemia.* Current Biology, 2000. **10**(20): p. 1247-1255.
130. Goodwin, G.W., F. Ahmad, and H. Taegtmeyer, *Preferential oxidation of glycogen in isolated working rat heart.* J Clin Invest, 1996. **97**(6): p. 1409-16.
131. Habets, D.D.J., W.A. Coumans, P.J. Voshol, M.A.M. den Boer, M. Febbraio, A. Bonen, J.F.C. Glatz, and J.J.F.P. Luiken, *AMPK-mediated increase in myocardial long-chain fatty acid uptake critically depends on sarcolemmal CD36.* Biochem Biophys Res Commun, 2007. **355**(1): p. 204-210.
132. Kudo, N., A.J. Barr, R.L. Barr, S. Desai, and G.D. Lopaschuk, *High Rates of Fatty Acid Oxidation during Reperfusion of Ischemic Hearts Are Associated with a Decrease in Malonyl-CoA Levels Due to an Increase in 5â€²-AMP-activated Protein Kinase Inhibition of Acetyl-CoA Carboxylase.* J Biol Chem, 1995. **270**(29): p. 17513-17520.
133. Viollet, B., F. Andreelli, S.B. Jorgensen, C. Perrin, D. Flamez, J. Mu, J.F. Wojtaszewski, F.C. Schuit, M. Birnbaum, E. Richter, R. Burcelin, and S. Vaulont, *Physiological role of AMP-activated protein kinase (AMPK): insights from knockout mouse models.* Biochem Soc Trans, 2003. **31**(Pt 1): p. 216-9.
134. Goodwin, G.W., F. Ahmad, T. Doenst, and H. Taegtmeyer, *Energy provision from glycogen, glucose, and fatty acids on adrenergic stimulation of isolated working rat hearts.* Am J Physiol, 1998. **274**(4 Pt 2): p. H1239-47.
135. Goodwin, G.W., C.S. Taylor, and H. Taegtmeyer, *Regulation of Energy Metabolism of the Heart during Acute Increase in Heart Work.* J Biol Chem, 1998. **273**(45): p. 29530-29539.
136. Buser, P.T., S.A. Camacho, S.T. Wu, C.B. Higgins, G. Jasmin, W.W. Parmley, and J. Wikman-Coffelt, *The effect of dobutamine on myocardial performance and high-energy phosphate metabolism at different stages of heart failure in cardiomyopathic hamsters: A 31P MRS study.* American Heart Journal, 1989. **118**(1): p. 86-91.
137. Sabri, A., J.-L. Samuel, F. Marotte, P. Poitevin, L. Rappaport, and B.I. Levy, *Microvasculature in Angiotensin II–Dependent Cardiac Hypertrophy in the Rat.* Hypertension, 1998. **32**(2): p. 371-375.
138. Rakusan, K. and P. Wicker, *Morphometry of the small arteries and arterioles in the rat heart: effects of chronic hypertension and exercise.* Cardiovasc Res, 1990. **24**(4): p. 278-84.
139. Mihl, C., W.R. Dassen, and H. Kuipers, *Cardiac remodelling: concentric versus eccentric hypertrophy in strength and endurance athletes.* Neth Heart J, 2008. **16**(4): p. 129-33.
140. Cheng, Y. and D. Hauton, *Cold acclimation induces physiological cardiac hypertrophy and increases assimilation of triacylglycerol metabolism through lipoprotein lipase.* Biochim Biophys Acta, 2008. **1781**(10): p. 618-26.
141. Rona, G., *CITATION CLASSIC - AN INFARCT-LIKE MYOCARDIAL LESION AND OTHER TOXIC MANIFESTATIONS PRODUCED BY ISOPROTERENOL IN THE RAT.* An infarct-like myocardial lesion and other toxic consequences produced by isoproterenol in the rat. AMA Arch Pathol, 1959 **67**(4): p. 443-455.
142. Rona, G., *Catecholamine cardiotoxicity.* J Mol Cell Cardiol, 1985. **17**(4): p. 291-306.
143. Handforth, C.P., *Isoproterenol-induced myocardial infarction in animals.* Arch Pathol, 1962. **73**: p. 161-5.
144. Maruffo, C.A., *Fine structural study of myocardial changes induced by isoproterenol in rhesus monkeys. (Macaca mulatta).* Am J Pathol, 1967. **50**(1): p. 27-37.

145. Saito, S., Y. Hiroi, Y. Zou, R. Aikawa, H. Toko, F. Shibasaki, Y. Yazaki, R. Nagai, and I. Komuro, *beta-Adrenergic pathway induces apoptosis through calcineurin activation in cardiac myocytes.* J Biol Chem, 2000. **275**(44): p. 34528-33.
146. Weinberg, J.M., *Lipotoxicity.* Kidney Int, 2006. **70**(9): p. 1560-6.
147. Borradaile, N.M. and J.E. Schaffer, *Lipotoxicity in the heart.* Curr Hypertens Rep, 2005. **7**(6): p. 412-7.
148. Zou, Y., I. Komuro, T. Yamazaki, S. Kudoh, H. Uozumi, T. Kadowaki, and Y. Yazaki, *Both Gs and Gi Proteins Are Critically Involved in Isoproterenol-induced Cardiomyocyte Hypertrophy.* J Biol Chem, 1999. **274:**: p. 9760-9770.
149. Morisco, C., D.C. Zebrowski, D.E. Vatner, S.F. Vatner, and J. Sadoshima, *Beta-adrenergic cardiac hypertrophy is mediated primarily by the beta(1)-subtype in the rat heart.* J Mol Cell Cardiol, 2001. **33**(3): p. 561-73.
150. Zhang, G.X., S. Kimura, A. Nishiyama, T. Shokoji, M. Rahman, L. Yao, Y. Nagai, Y. Fujisawa, A. Miyatake, and Y. Abe, *Cardiac oxidative stress in acute and chronic isoproterenol-infused rats.* Cardiovasc Res, 2005. **65**(1): p. 230-8.
151. Takeshita, D., J. Shimizu, Y. Kitagawa, D. Yamashita, K. Tohne, C. Nakajima-Takenaka, H. Ito, and M. Takaki, *Isoproterenol-Induced Hypertrophied Rat Hearts: Does Short-Term Treatment Correspond to Long-Term Treatment?* J Physiol Sci, 2008. **58**(3): p. 179-188.
152. Benjamin, I.J., J.E. Jalil, L.B. Tan, K. Cho, K.T. Weber, and W.A. Clark, *Isoproterenol-induced myocardial fibrosis in relation to myocyte necrosis.* Circ Res, 1989. **65**(3): p. 657-70.
153. Ennis, I.L., E.M. Escudero, G.M. Console, G. Camihort, C.G. Dumm, R.W. Seidler, M.C. Camilion de Hurtado, and H.E. Cingolani, *Regression of Isoproterenol-Induced Cardiac Hypertrophy by Na+/H+ Exchanger Inhibition*. Hypertension, 2003.**41**(6) p. 1324-1329.
154. Kitagawa, Y., D. Yamashita, H. Ito, and M. Takaki, *Reversible effects of isoproterenol-induced hypertrophy on in situ left ventricular function in rat hearts.* Am J Physiol Heart Circ Physiol, 2004. **287**(1): p. H277-85.
155. Gillis, A.M., H.J. Mathison, C. Patel, and W.M. Lester, *Quinidine Pharmacodynamics in Normal and Isoproterenol-Induced Hypertrophied Blood-Perfused Working Rabbit Hearts.* Journal of Cardiovascular Pharmacology, 1996. **27**(6): p. 916-926.
156. Maisel, A., C. Phillips, M. Michel, M. Ziegler, and S. Carter, *Regulation of cardiac beta-adrenergic receptors by captopril. Implications for congestive heart failure.* Circulation, 1989. **80**(3): p. 669-675.
157. Berg, R.A., J. Moss, B.J. Baum, and R.G. Crystal, *Regulation of collagen production by the beta-adrenergic system.* J Clin Invest, 1981. **67**(5): p. 1457-62.
158. Osadchii, O.E., *Cardiac hypertrophy induced by sustained beta-adrenoreceptor activation: pathophysiological aspects.* Heart Fail Rev, 2007. **12**(1): p. 66-86.
159. Golomb, E., Z.A. Abassi, G. Cuda, M. Stylianou, V.R. Panchal, D. Trachewsky, and H.R. Keiser, *Angiotensin II maintains, but does not mediate, isoproterenol-induced cardiac hypertrophy in rats.* Am J Physiol, 1994. **267**(4 Pt 2): p. H1496-506.
160. Nakajima-Takenaka, C., G.X. Zhang, K. Obata, K. Tohne, H. Matsuyoshi, Y. Nagai, A. Nishiyama, and M. Takaki, *Left ventricular function of isoproterenol-induced hypertrophied rat hearts perfused with blood: mechanical work and energetics.* Am J Physiol Heart Circ Physiol, 2009. **297**(5): p. H1736-43.
161. Linck, B., P. Boknik, H.A. Baba, T. Eschenhagen, U. Haverkamp, E. Jackel, L.R. Jones, U. Kirchhefer, J. Knapp, S. Laer, F.U. Muller, W. Schmitz, H. Scholz, A. Syska, U. Vahlensieck, and J. Neumann, *Long-term beta adrenoceptor-mediated alteration in contractility and expression of phospholamban and sarcoplasmic reticulum Ca(++)-ATPase in mammalian ventricle.* J Pharmacol Exp Ther, 1998. **286**(1): p. 531-8.
162. Leenen, F.H., R. White, and B. Yuan, *Isoproterenol-induced cardiac hypertrophy: role of circulatory versus cardiac renin-angiotensin system.* Am J Physiol Heart Circ Physiol, 2001. **281**(6): p. H2410-6.

163. Williams, J.L., D. Cartland, A. Hussain, and S. Egginton, *A differential role for nitric oxide in two forms of physiological angiogenesis in mouse*. J Physiol, 2006. **1(**570(Part 3));p. 445-454.
164. Williams, J.L., A. Weichert, A. Zakrzewicz, L. Da Silva-Azevedo, A.R. Pries, O. Baum, and S. Egginton, *Differential gene and protein expression in abluminal sprouting and intraluminal splitting forms of angiogenesis.* Clinical Science, 2006. **110**(5): p. 587-595.
165. Brown, M.D. and O. Hudlicka, *Capillary supply and cardiac performance in the rabbit after chronic dobutamine treatment.* Cardiovasc Res, 1991. **25**(11): p. 909-915.
166. Grimm, D., D. Elsner, H. Schunkert, M. Pfeifer, D. Griese, G.n. Bruckschlegel, F. Muders, G.n.A.J. Riegger, and E.P. Kromer, *Development of heart failure following isoproterenol administration in the rat: role of the renin-angiotensin system.* Cardiovasc Res, 1998. **37**(1): p. 91-100.
167. Kung, H.F. and M. Blau, *Subcutaneous Isoproterenol: A Convenient Rat Model for Early Detection of Myocardial Necrosis.* J Nucl Med, 1978. **19**(8): p. 948-951.
168. Chang, H.Y., R.M. Klein, and G. Kunos, *Selective desensitization of cardiac beta adrenoceptors by prolonged in vivo infusion of catecholamines in rats.* J Pharmacol Exp Ther, 1982. **221**(3): p. 784-9.
169. Osadchii, O., A. Woodiwiss, N. Alves, and G. Norton, *Mechanisms of preserved baseline cardiac systolic function in rats with adrenergic inotropic downregulation.* Life Sci, 2005. **78**(4): p. 366-75.
170. Ferreira, A.J., T.L. Oliveira, M.C. Castro, A.P. Almeida, C.H. Castro, M.V. Caliari, E. Gava, G.T. Kitten, and R.A. Santos, *Isoproterenol-induced impairment of heart function and remodeling are attenuated by the nonpeptide angiotensin-(1-7) analogue AVE 0991.* Life Sci, 2007. **81**(11): p. 916-23.
171. Heathier, L.C., D.J. Catchpolel, M.A. Stuckey, M.A. Cole, C.A. Carr, and K. Clarke, *Isoproterenol induces in vivo functional and metabolic abnormalities: similar to those found in the infarcted rat heart.* Journal of physiology and pharmacology : an official journal of the Polish Physiological Society, 2009. **60**(3): p. 31-39.
172. Pirolo, J.S., G.M. Hutchins, and G.W. Moore, *Infarct expansion: pathologic analysis of 204 patients with a single myocardial infarct.* J Am Coll Cardiol, 1986. **7**(2): p. 349-54.
173. Gunja-Smith, Z., A. Morales, R. Romanelli, and J. Woessner, Jr, *Remodeling of human myocardial collagen in idiopathic dilated cardiomyopathy. Role of metalloproteinases and pyridinoline cross-links.* Am J Pathol, 1996. **148**(5): p. 1639-1648.
174. Stefano, L.M.D., L.S. Matsubara, and B.B. Matsubara, *Myocardial dysfunction with increased ventricular compliance in volume overload hypertrophy.* Eur J Heart Fail, 2006. **8**(8): p. 784-789.
175. Spinale, F.G., J.L. Zellner, W.S. Johnson, D.M. Eble, and P.D. Munyer, *Cellular and Extracellular Remodeling with the Development and Recovery from Tachycardia-induced Cardiomyopathy: Changes in Fibrillar Collagen, Myocyte Adhesion Capacity and Proteoglycans.* J Mol Cell Cardiol, 1996. **28**(8): p. 1591-1608.
176. Olivetti, G., J. Capasso, L. Meggs, E. Sonnenblick, and P. Anversa, *Cellular basis of chronic ventricular remodeling after myocardial infarction in rats.* Circ Res, 1991. **68**(3): p. 856-869.
177. Miyata, S., W. Minobe, M.R. Bristow, and L.A. Leinwand, *Myosin Heavy Chain Isoform Expression in the Failing and Nonfailing Human Heart.* Circ Res, 2000. **86**(4): p. 386-390.
178. Movsesian, M., M. Karimi, K. Green, and L. Jones, *Ca(2+)-transporting ATPase, phospholamban, and calsequestrin levels in nonfailing and failing human myocardium.* Circulation, 1994. **90**(2): p. 653-657.
179. Tang, Q. and P.B. Taylor, *Regression of isoproterenol-induced cardiac hypertrophy.* Can J Physiol Pharmacol, 1984. **62**(9): p. 1141-6.
180. Neuman, R.E. and M.A. Logan, *The determination of hydroxyproline.* J Biol Chem, 1950. **184**(1): p. 299-306.

181. Engelhardt, S., L. Hein, F. Wiesmann, and M.J. Lohse, *Progressive hypertrophy and heart failure in beta1-adrenergic receptor transgenic mice.* Proc Natl Acad Sci U S A, 1999. **96**(12): p. 7059-64.
182. Barouch, L.A., R.W. Harrison, M.W. Skaf, G.O. Rosas, T.P. Cappola, Z.A. Kobeissi, I.A. Hobai, C.A. Lemmon, A.L. Burnett, B. O'Rourke, E.R. Rodriguez, P.L. Huang, J.A. Lima, D.E. Berkowitz, and J.M. Hare, *Nitric oxide regulates the heart by spatial confinement of nitric oxide synthase isoforms.* Nature, 2002. **416**(6878): p. 337-9.
183. Khan, S.A., M.W. Skaf, R.W. Harrison, K. Lee, K.M. Minhas, A. Kumar, M. Fradley, A.A. Shoukas, D.E. Berkowitz, and J.M. Hare, *Nitric oxide regulation of myocardial contractility and calcium cycling: independent impact of neuronal and endothelial nitric oxide synthases.* Circ Res, 2003. **92**(12): p. 1322-9.
184. Sears, C.E., S.M. Bryant, E.A. Ashley, C.A. Lygate, S. Rakovic, H.L. Wallis, S. Neubauer, D.A. Terrar, and B. Casadei, *Cardiac neuronal nitric oxide synthase isoform regulates myocardial contraction and calcium handling.* Circ Res, 2003. **92**(5): p. e52-9.
185. Ziolo, M.T. and D.M. Bers, *The real estate of NOS signaling: location, location, location.* Circ Res, 2003. **92**(12): p. 1279-81.
186. Brunner, F., P. Andrew, G. Wolkart, R. Zechner, and B. Mayer, *Myocardial contractile function and heart rate in mice with myocyte-specific overexpression of endothelial nitric oxide synthase.* Circulation, 2001. **104**(25): p. 3097-102.
187. Robert, F.F., *Endothelium-Derived Relaxing Factor: Discovery, Early Studies, and Identifcation as Nitric Oxide (Nobel Lecture).* Angewandte Chemie International Edition, 1999. **38**(13-14): p. 1870-1880.
188. Huang, P.L., *Neuronal and endothelial nitric oxide synthase gene knockout mice.* Braz J Med Biol Res, 1999. **32**(11): p. 1353-9.
189. Yang, X.P., Y.H. Liu, E.G. Shesely, M. Bulagannawar, F. Liu, and O.A. Carretero, *Endothelial nitric oxide gene knockout mice: cardiac phenotypes and the effect of angiotensin-converting enzyme inhibitor on myocardial ischemia/reperfusion injury.* Hypertension, 1999. **34**(1): p. 24-30.
190. Kubis, N., S. Besnard, J.S. Silvestre, M. Feletou, P.L. Huang, B.I. Levy, and A. Tedgui, *Decreased arteriolar density in endothelial nitric oxide synthase knockout mice is due to hypertension, not to the constitutive defect in endothelial nitric oxide synthase enzyme.* J Hypertens, 2002. **20**(2): p. 273-80.
191. Hood, J.D., C.J. Meininger, M. Ziche, and H.J. Granger, *VEGF upregulates ecNOS message, protein, and NO production in human endothelial cells.* Am J Physiol, 1998. **274**(3 Pt 2): p. H1054-8.
192. van der Zee, R., T. Murohara, Z. Luo, F. Zollmann, J. Passeri, C. Lekutat, and J.M. Isner, *Vascular endothelial growth factor/vascular permeability factor augments nitric oxide release from quiescent rabbit and human vascular endothelium.* Circulation, 1997. **95**(4): p. 1030-7.
193. Babaei, S., K. Teichert-Kuliszewska, J.C. Monge, F. Mohamed, M.P. Bendeck, and D.J. Stewart, *Role of nitric oxide in the angiogenic response in vitro to basic fibroblast growth factor.* Circ Res, 1998. **82**(9): p. 1007-15.
194. Ziche, M., L. Morbidelli, R. Choudhuri, H.T. Zhang, S. Donnini, H.J. Granger, and R. Bicknell, *Nitric oxide synthase lies downstream from vascular endothelial growth factor-induced but not basic fibroblast growth factor-induced angiogenesis.* J Clin Invest, 1997. **99**(11): p. 2625-34.
195. Zhao, X., X. Lu, and Q. Feng, *Deficiency in endothelial nitric oxide synthase impairs myocardial angiogenesis.* Am J Physiol Heart Circ Physiol, 2002. **283**(6): p. H2371-8.
196. Jozkowicz, A., J.P. Cooke, I. Guevara, I. Huk, P. Funovics, O. Pachinger, F. Weidinger, and J. Dulak, *Genetic augmentation of nitric oxide synthase increases the vascular generation of VEGF.* Cardiovasc Res, 2001. **51**(4): p. 773-83.

197. Numaguchi, K., K. Egashira, M. Takemoto, T. Kadokami, H. Shimokawa, K. Sueishi, and A. Takeshita, *Chronic inhibition of nitric oxide synthesis causes coronary microvascular remodeling in rats.* Hypertension, 1995. **26**(6 Pt 1): p. 957-62.
198. Bern·tov·, I., O.g. Pech·nov·, V.c. Pelouch, and F. Simko, *Regression of Chronic -NAME-Treatment-induced Left Ventricular Hypertrophy: Effect of Captopril.* J Mol Cell Cardiol, 2000. **32**(2): p. 177-185.
199. Bartunek, J., E.O. Weinberg, M. Tajima, S. Rohrbach, S.E. Katz, P.S. Douglas, and B.H. Lorell, *Chronic N(G)-nitro-L-arginine methyl ester-induced hypertension : novel molecular adaptation to systolic load in absence of hypertrophy.* Circulation, 2000. **101**(4): p. 423-9.
200. Matsubara, B.B., L.S. Matsubara, L.A. Zornoff, M. Franco, and J.S. Janicki, *Left ventricular adaptation to chronic pressure overload induced by inhibition of nitric oxide synthase in rats.* Basic Res Cardiol, 1998. **93**(3): p. 173-81.
201. Arnal, J.F., A.I. el Amrani, G. Chatellier, J. Menard, and J.B. Michel, *Cardiac weight in hypertension induced by nitric oxide synthase blockade.* Hypertension, 1993. **22**(3): p. 380-7.
202. Jover, B., A. Herizi, F. Ventre, M. Dupont, and A. Mimran, *Sodium and angiotensin in hypertension induced by long-term nitric oxide blockade.* Hypertension, 1993. **21**(6 Pt 2): p. 944-8.
203. Bernatova, I., O. Pechanova, V. Pelouch, and F. Simko, *Regression of chronic L -NAME-treatment-induced left ventricular hypertrophy: effect of captopril.* J Mol Cell Cardiol, 2000. **32**(2): p. 177-85.
204. Vandsburger, M., B.A. French, R.J. Roy, C.M. Kramer, and F.H. Epstein, *Abstract 766: Cardiac MRI Phenotyping of nNOS Knockout Mice In Vivo Demonstrates Attenuated Contractile Response to Dobutamine and Normal Perfusion Reserve.* Circulation, 2006. **114**(18_MeetingAbstracts): p. II_132-d-133.
205. Olivetti, G., J.M. Capasso, E.H. Sonnenblick, and P. Anversa, *Side-to-side slippage of myocytes participates in ventricular wall remodeling acutely after myocardial infarction in rats.* Circ Res, 1990. **67**(1): p. 23-34.
206. Vitali-Mazza, L., P. Anversa, F. Tedeschi, R. Mastandrea, V. Mavilla, and O. Visioli, *Ultrastructural basis of acute left ventricular failure from severe acute aortic stenosis in the rabbit.* J Mol Cell Cardiol, 1972. **4**(6): p. 661-665.
207. Ross, J., Jr., E.H. Sonnenblick, R.R. Taylor, H.M. Spotnitz, and J.W. Covell, *Diastolic Geometry and Sarcomere Lengths in the Chronically Dilated Canine Left Ventricle.* Circ Res, 1971. **28**(1): p. 49-61.
208. Moreno, H., K. Metze, A.C. Bento, E. Antunes, R. Zatz, and G. Nucci, *Chronic nitric oxide inhibition as a model of hypertensive heart muscle disease.* Basic Research in Cardiology, 1996. **91**(3): p. 248-255.
209. Frey, N., H.A. Katus, E.N. Olson, and J.A. Hill, *Hypertrophy of the Heart: A New Therapeutic Target?* Circulation, 2004. **109**(13): p. 1580-1589.
210. Hill, J.A., M. Karimi, W. Kutschke, R.L. Davisson, K. Zimmerman, Z. Wang, R.E. Kerber, and R.M. Weiss, *Cardiac Hypertrophy Is Not a Required Compensatory Response to Short-Term Pressure Overload.* Circulation, 2000. **101**(24): p. 2863-2869.
211. Tomanek, R.J., P.J. Palmer, G.L. Peiffer, K.L. Schreiber, C.L. Eastham, and M.L. Marcus, *Morphometry of canine coronary arteries, arterioles, and capillaries during hypertension and left ventricular hypertrophy.* Circ Res, 1986. **58**(1): p. 38-46.
212. Reller, M.D., M.A. Burson, J.L. Lohr, M.J. Morton, and K.L. Thornburg, *Nitric oxide is an important determinant of coronary flow at rest and during hypoxemic stress in fetal lambs.* Am J Physiol Heart Circ Physiol, 1995. **269**(6): p. H2074-2081.
213. Suto, N., A. Mikuniya, T. Okubo, H. Hanada, N. Shinozaki, and K. Okumura, *Nitric oxide modulates cardiac contractility and oxygen consumption without changing contractile efficiency.* Am J Physiol Heart Circ Physiol, 1998. **275**(1): p. H41-49.

214. Sellers, E.A., J.W. Scott, and N. Thomas, *Electrical Activity of Skeletal Muscle of Normal and Acclimatized Rats on Exposure to Cold.* Am J Physiol, 1954. **177**(3): p. 372-376.
215. Deveci, D. and S. Egginton, *The effects of reduced temperature and photoperiod on body composition in hibernator and non-hibernator rodents.* Journal of Thermal Biology, 2002. **27**(6): p. 467-478.
216. Kayar, S.R. and N. Banchero, *Volume overload hypertrophy elicited by cold and its effects on myocardial capillarity.* Respir Physiol, 1985. **59**(1): p. 1-14.
217. Jansky, L., *Non-shivering thermogenesis and its thermoregulatory significance.* Biol Rev Camb Philos Soc, 1973. **48**(1): p. 85-132.
218. Roukoyatkina, N.I., S.I. Chefer, J. Rifkind, R. Ajmani, and M.I. Talan, *Cold acclimation-induced increase of systolic blood pressure in rats is associated with volume expansion.* Am J Hypertens, 1999. **12**(1 Pt 1): p. 54-62.
219. Shechtman, O., M.J. Fregly, P. van Bergen, and P.E. Papanek, *Prevention of cold-induced increase in blood pressure of rats by captopril.* Hypertension, 1991. **17**(6 Pt 1): p. 763-70.
220. Sun, Z., J.R. Cade, M.J. Fregly, and N.E. Rowland, *Effect of chronic treatment with propranolol on the cardiovascular responses to chronic cold exposure.* Physiol Behav, 1997. **62**(2): p. 379-84.
221. Fregly, M.J., D.C. Kikta, R.M. Threatte, J.L. Torres, and C.C. Barney, *Development of hypertension in rats during chronic exposure to cold.* J Appl Physiol, 1989. **66**(2): p. 741-9.
222. Sun, Z., R. Cade, Z. Zhang, J. Alouidor, and H. Van, *Angiotensinogen gene knockout delays and attenuates cold-induced hypertension.* Hypertension, 2003. **41**(2): p. 322-7.
223. Chiu, D.T.J. and K.K. Cheng, *CIRCULATORY CHANGES IN COLD-ACCLIMATION AND COLD STRESS.* Clinical and Experimental Pharmacology and Physiology, 1976. **3**(5): p. 449-452.
224. Leduc, J., *Catecholamine production and release in exposure and acclimation to cold.* Acta Physiol Scand Suppl, 1961. **183**: p. 1-101.
225. Heroux, O. and J. St. Pierre, *Effect of Cold Acclimation on Vascularization of Ears, Heart, Liver and Muscles of White Rats.* Am J Physiol, 1956. **188**(1): p. 163-168.
226. Gao, M., S. Batra, T. Koyama, T. Yahata, and A. Kuroshima, *The capillarity of the subendocardium of left ventricle in rats reared at a low temperature for many generations.* Acta Physiol Scand, 1997. **160**(1): p. 67-70.
227. Weil, Z.M., G.J. Norman, A.C. DeVries, G.G. Berntson, and R.J. Nelson, *Photoperiod alters autonomic regulation of the heart.* Proceedings of the National Academy of Sciences, 2009. **106**(11): p. 4525-4530.
228. Cheng, Y. and D. Hauton, *Cold acclimation induces physiological cardiac hypertrophy and increases assimilation of triacylglycerol metabolism through lipoprotein lipase.* Biochimica et Biophysica Acta (BBA) - Molecular and Cell Biology of Lipids, 2008. **1781**(10): p. 618-626.
229. Fregly, M.J., F. Rossi, Z. Sun, N. Tumer, J.R. Cade, D. Hegland, and M. Yurekli, *Effect of chronic treatment with prazosin and L-arginine on the elevation of blood pressure during cold exposure.* Pharmacology, 1994. **49**(6): p. 351-62.
230. Cassis, L., A. Laughter, M. Fettinger, S. Akers, R. Speth, G. Burke, V. King, and L. Dwoskin, *Cold exposure regulates the renin-angiotensin system.* J Pharmacol Exp Ther, 1998. **286**(2): p. 718-26.
231. Sun, Z., R. Cade, Z. Zhang, J. Alouidor, and H. Van, *Angiotensinogen Gene Knockout Delays and Attenuates Cold-Induced Hypertension.* Hypertension, 2003. **41**(2): p. 322-327.
232. Barney, C.C., M.J. Katovich, M.J. Fregly, and P.E. Tyler, *Changes in beta-adrenergic responsiveness of rats during chronic cold exposure.* J Appl Physiol, 1980. **49**(6): p. 923-929.
233. Mulder, P., S. Barbier, A. Chagraoui, V. Richard, J.P. Henry, F. Lallemand, S. Renet, G. Lerebours, F. Mahlberg-Gaudin, and C. Thuillez, *Long-Term Heart Rate Reduction Induced by the Selective If Current Inhibitor Ivabradine Improves Left Ventricular Function and Intrinsic Myocardial Structure in Congestive Heart Failure.* Circulation, 2004. **109**(13): p. 1674-1679.

234. Ulu, N., R.H. Henning, M. Goris, R.G. Schoemaker, and W.H. van Gilst, *Effects of ivabradine and metoprolol on cardiac angiogenesis and endothelial dysfunction in rats with heart failure.* J Cardiovasc Pharmacol, 2009. **53**(1): p. 9-17.
235. Bristow, M.R., *Mechanism of action of beta-blocking agents in heart failure.* Am J Cardiol, 1997. **80**(11A): p. 26L-40L.
236. Widdop, R.E., S.M. Gardiner, P.A. Kemp, and T. Bennett, *The influence of atropine and atenolol on the cardiac haemodynamic effects of NG-nitro-L-arginine methyl ester in conscious, Long Evans rats.* Br J Pharmacol, 1992. **105**(3): p. 653-6.
237. Zheng, W., M.D. Brown, T.A. Brock, R.J. Bjercke, and R.J. Tomanek, *Bradycardia-Induced Coronary Angiogenesis Is Dependent on Vascular Endothelial Growth Factor.* Circ Res, 1999. **85**(2): p. 192-198.
238. Lei, L., R. Zhou, W. Zheng, L.P. Christensen, R.M. Weiss, and R.J. Tomanek, *Bradycardia Induces Angiogenesis, Increases Coronary Reserve, and Preserves Function of the Postinfarcted Heart.* Circulation, 2004: p. 01.CIR.0000138933.85923.36.
239. Tasgal, J. and E.M. Williams, *The effect of prolonged propranolol administration on myocardial transmural capillary density in young rabbits.* J Physiol, 1981. **315**: p. 353-67.
240. Berdaux, A., J.R. Bossier, and J.F. Giudicelli, *Effects of atenolol on regional myocardial blood flow and ST segment elevation in the canine myocardium.* Br J Pharmacol, 1977. **60**(3): p. 433-9.
241. Tirziu, D., E. Chorianopoulos, K.L. Moodie, R.T. Palac, Z.W. Zhuang, M. Tjwa, C. Roncal, U. Eriksson, Q. Fu, A. Elfenbein, A.E. Hall, P. Carmeliet, L. Moons, and M. Simons, *Myocardial hypertrophy in the absence of external stimuli is induced by angiogenesis in mice.* The Journal of Clinical Investigation, 2007. **117**(11): p. 3188-3197.
242. Li, J., M. Post, R. Volk, Y. Gao, M. Li, C. Metais, K. Sato, J. Tsai, W. Aird, R.D. Rosenberg, T.G. Hampton, J. Li, F. Sellke, P. Carmeliet, and M. Simons, *PR39, a peptide regulator of angiogenesis.* Nat Med, 2000. **6**(1): p. 49-55.
243. Hu, K., P. Gaudron, and G. Ertl, *Long-Term Effects of Beta-Adrenergic Blocking Agent Treatment on Hemodynamic Function and Left Ventricular Remodeling in Rats With Experimental Myocardial Infarction: Importance of Timing of Treatment and Infarct Size.* Journal of the American College of Cardiology, 1998. **31**(3): p. 692-700.
244. Fishbein, M.C., L.Q. Lei, and S.A. Rubin, *Long-term propranolol administration alters myocyte and ventricular geometry in rat hearts with and without infarction.* Circulation, 1988. **78**(2): p. 369-375.
245. Oh, B.H., S. Ono, E. Gilpin, and J. Ross, Jr., *Altered left ventricular remodeling with beta-adrenergic blockade and exercise after coronary reperfusion in rats.* Circulation, 1993. **87**(2): p. 608-616.
246. Sun, Z., J.R. Cade, M.J. Fregly, and N.E. Rowland, *Effect of Chronic Treatment with Propranolol on the Cardiovascular Responses to Chronic Cold Exposure.* Physiology & Behavior, 1997. **62**(2): p. 379-384.
247. Conrad, C.H., W.W. Brooks, K.G. Robinson, and O.H. Bing, *Impaired myocardial function in spontaneously hypertensive rats with heart failure.* Am J Physiol Heart Circ Physiol, 1991. **260**(1): p. H136-145.
248. Doi, R., T. Masuyama, K. Yamamoto, Y. Doi, T. Mano, Y. Sakata, K. Ono, T. Kuzuya, S. Hirota, T. Koyama, T. Miwa, and M. Hori, *Development of different phenotypes of hypertensive heart failure: systolic versus diastolic failure in Dahl salt-sensitive rats.* J Hypertens, 2000. **18**(1): p. 111-120.
249. Cariello, N.F., E.H. Romach, H.M. Colton, H. Ni, L. Yoon, J.G. Falls, W. Casey, D. Creech, S.P. Anderson, G.R. Benavides, D.J. Hoivik, R. Brown, and R.T. Miller, *Gene expression profiling of the PPAR-alpha agonist ciprofibrate in the cynomolgus monkey liver.* Toxicol Sci, 2005. **88**(1): p. 250-64.

250. Mandard, S., M. Muller, and S. Kersten, *Peroxisome proliferator-activated receptor alpha target genes.* Cell Mol Life Sci, 2004. **61**(4): p. 393-416.
251. Barger, P.M., J.M. Brandt, T.C. Leone, C.J. Weinheimer, and D.P. Kelly, *Deactivation of peroxisome proliferatorâ€"activated receptor-Î± during cardiac hypertrophic growth.* The Journal of Clinical Investigation, 2000. **105**(12): p. 1723-1730.
252. Karbowska, J., Z. Kochan, and R.T. Smolenski, *Peroxisome proliferator-activated receptor alpha is downregulated in the failing human heart.* Cell Mol Biol Lett, 2003. **8**(1): p. 49-53.
253. Morgan, E.E., J.H. Rennison, M.E. Young, T.A. McElfresh, T.A. Kung, K.-Y. Tserng, B.D. Hoit, W.C. Stanley, and M.P. Chandler, *Effects of chronic activation of peroxisome proliferator-activated receptor-{alpha} or high-fat feeding in a rat infarct model of heart failure.* Am J Physiol Heart Circ Physiol, 2006. **290**(5): p. H1899-1904.
254. YOUNG, M.E., S. PATIL, J. YING, C. DEPRE, H.S. AHUJA, G.L. SHIPLEY, S.M. STEPKOWSKI, P.J.A. DAVIES, and H. TAEGTMEYER, *Uncoupling protein 3 transcription is regulated by peroxisome proliferator-activated receptor {alpha} in the adult rodent heart.* FASEB J, 2001. **15**(3): p. 833-845.
255. Gilde, A.J., K.A.J.M. van der Lee, P.H.M. Willemsen, G. Chinetti, F.R. van der Leij, G.J. van der Vusse, B. Staels, and M. van Bilsen, *Peroxisome Proliferator-Activated Receptor (PPAR) {alpha} and PPAR{beta}/{delta}, but not PPAR{gamma}, Modulate the Expression of Genes Involved in Cardiac Lipid Metabolism.* Circ Res, 2003. **92**(5): p. 518-524.
256. Hafstad, A.D., A.M. Khalid, M. Hagve, T. Lund, T.S. Larsen, D.L. Severson, K. Clarke, R.K. Berge, and E. Aasum, *Cardiac peroxisome proliferator-activated receptor-Î± activation causes increased fatty acid oxidation, reducing efficiency and post-ischaemic functional loss.* Cardiovasc Res, 2009. **83**(3): p. 519-526.
257. Berg, B.N., *Nutrition and Longevity in the Rat: I. Food Intake in Relation to Size, Health and Fertility.* J Nutr, 1960. **71**(3): p. 242-254.
258. Chaput, E., R. Saladin, M. Silvestre, and A.D. Edgar, *Fenofibrate and Rosiglitazone Lower Serum Triglycerides with Opposing Effects on Body Weight.* Biochemical and Biophysical Research Communications, 2000. **271**(2): p. 445-450.
259. Schweda, F., U. Friis, C. Wagner, O. Skott, and A. Kurtz, *Renin release.* Physiology (Bethesda), 2007. **22**: p. 310-9.
260. Blair, M.L., *Stimulation of renin secretion by alpha-adrenoceptor agonists.* Am J Physiol Endocrinol Metab, 1983. **244**(1): p. E37-44.
261. Thomas, D.P., K.M. McCormick, and R.R. Jenkins, *Effects of beta-adrenergic blockade on training-induced structural adaptations in rat left ventricle.* Eur J Appl Physiol Occup Physiol, 1988. **57**(6): p. 671-6.
262. Ichiki, T., *Role of Renin Angiotensin System in Angiogenesis: It Is Still Elusive.* Arterioscler Thromb Vasc Biol, 2004. **24**(4): p. 622-624.
263. Munzenmaier, D.H. and A.S. Greene, *Opposing actions of angiotensin II on microvascular growth and arterial blood pressure.* Hypertension, 1996. **27**(3 Pt 2): p. 760-5.
264. Romanic, A.M., C.L. Burns-Kurtis, B. Gout, I. Berrebi-Bertrand, and E.H. Ohlstein, *Matrix metalloproteinase expression in cardiac myocytes following myocardial infarction in the rabbit.* Life Sciences, 2001. **68**(7): p. 799-814.
265. Heymans, S., F. Lupu, S. Terclavers, B. Vanwetswinkel, J.-M. Herbert, A. Baker, D. Collen, P. Carmeliet, and L. Moons, *Loss or Inhibition of uPA or MMP-9 Attenuates LV Remodeling and Dysfunction after Acute Pressure Overload in Mice.* Am J Pathol, 2005. **166**(1): p. 15-25.
266. Arioglu, E., J. Duncan-Morin, N. Sebring, K.I. Rother, N. Gottlieb, J. Lieberman, D. Herion, D.E. Kleiner, J. Reynolds, A. Premkumar, A.E. Sumner, J. Hoofnagle, M.L. Reitman, and S.I. Taylor, *Efficacy and Safety of Troglitazone in the Treatment of Lipodystrophy Syndromes.* Annals of Internal Medicine, 2000. **133**(4): p. 263-274.
267. Xu, Y., L. Lu, C. Greyson, M. Rizeq, K. Nunley, B. Wyatt, M.R. Bristow, C.S. Long, and G.G. Schwartz, *The PPAR-{alpha} activator fenofibrate fails to provide myocardial protection in*

ischemia and reperfusion in pigs. Am J Physiol Heart Circ Physiol, 2006. **290**(5): p. H1798-1807.

268. Hafstad, A.D., A.M. Khalid, M. Hagve, T. Lund, T.S. Larsen, D.L. Severson, K. Clarke, R.K. Berge, and E. Aasum, *Cardiac peroxisome proliferator-activated receptor-α activation causes increased fatty acid oxidation, reducing efficiency and post-ischaemic functional loss.* Cardiovasc Res, 2009. **83**(3): p. 519-526.
269. Young, M.E., F.A. Laws, G.W. Goodwin, and H. Taegtmeyer, *Reactivation of Peroxisome Proliferator-activated Receptor alpha Is Associated with Contractile Dysfunction in Hypertrophied Rat Heart.* J Biol Chem, 2001. **276**(48): p. 44390-44395.
270. Labinskyy, V., M. Bellomo, M.P. Chandler, M.E. Young, V. Lionetti, K. Qanud, F. Bigazzi, T. Sampietro, W.C. Stanley, and F.A. Recchia, *Chronic activation of peroxisome proliferator-activated receptor-alpha with fenofibrate prevents alterations in cardiac metabolic phenotype without changing the onset of decompensation in pacing-induced heart failure.* J Pharmacol Exp Ther, 2007. **321**(1): p. 165-71.
271. Xu, Y., L. Lu, C. Greyson, M. Rizeq, K. Nunley, B. Wyatt, M.R. Bristow, C.S. Long, and G.G. Schwartz, *The PPAR-alpha activator fenofibrate fails to provide myocardial protection in ischemia and reperfusion in pigs.* Am J Physiol Heart Circ Physiol, 2006. **290**(5): p. H1798-807.
272. Aasum, E., M. Cooper, L. Severson David, and S. Larsen Terje, *Effect of BM 17.0744, a PPARalpha ligand, on the metabolism of perfused hearts from control and diabetic mice.* Canadian Journal of Physiology and Pharmacology, 2005. **83**: p. 183-190.
273. Choi, Y.-H., D.B. Cowan, M. Nathan, D. Poutias, C. Stamm, P.J. del Nido, and F.X. McGowan, Jr., *Myocardial Hypertrophy Overrides the Angiogenic Response to Hypoxia.* PLoS ONE, 2008. **3**(12): p. e4042.